National Library
of Canada

Canadian Theses Service

Ottawa, Canada
K1A 0N4

Bibliothèque nationale
du Canada

Service des thèses canadiennes

NOTICE

The quality of this microform is heavily dependent upon the quality of the original thesis submitted for microfilming. Every effort has been made to ensure the highest quality of reproduction possible.

If pages are missing, contact the university which granted the degree.

Some pages may have indistinct print especially if the original pages were typed with a poor typewriter ribbon or if the university sent us an inferior photocopy.

Reproduction in full or in part of this microform is governed by the Canadian Copyright Act, R.S.C. 1970, c. C-30, and subsequent amendments.

AVIS

La qualité de cette microforme dépend grandement de la qualité de la thèse soumise au microfilmage. Nous avons tout fait pour assurer une qualité supérieure de reproduction.

S'il manque des pages, veuillez communiquer avec l'université qui a conféré le grade.

La qualité d'impression de certaines pages peut laisser à désirer, surtout si les pages originales ont été dactylographiées à l'aide d'un ruban usé ou si l'université nous a fait parvenir une photocopie de qualité inférieure.

La reproduction, même partielle, de cette microforme est soumise à la Loi canadienne sur le droit d'auteur, SRC 1970, c. C-30, et ses amendements subséquents.

NL-339 (r. 88/04) c

Canada

UNIVERSITY OF ALBERTA

MODELLING MASS TRANSPORT IN FRACTURED ROCKS USING TRANSFER FUNCTIONS

BY

© JOÃO ALFREDO KÜPPER

A THESIS
SUBMITTED TO THE FACULTY OF GRADUATE STUDIES AND RESEARCH
IN PARTIAL FULFILLMENT OF THE REQUIREMENTS FOR THE DEGREE
OF DOCTOR OF PHILOSOPHY

DEPARTMENT OF CIVIL ENGINEERING

EDMONTON, ALBERTA
SPRING 1990

National Library of Canada
Bibliothèque nationale du Canada

Canadian Theses Service
Service des thèses canadiennes

Ottawa, Canada
K1A 0N4

NOTICE

The quality of this microform is heavily dependent upon the quality of the original thesis submitted for microfilming. Every effort has been made to ensure the highest quality of reproduction possible.

If pages are missing, contact the university which granted the degree.

Some pages may have indistinct print especially if the original pages were typed with a poor typewriter ribbon or if the university sent us an inferior photocopy.

Reproduction in full or in part of this microform is governed by the Canadian Copyright Act, R.S.C. 1970, c. C-30, and subsequent amendments.

AVIS

La qualité de cette microforme dépend grandement de la qualité de la thèse soumise au microfilmage. Nous avons tout fait pour assurer une qualité supérieure de reproduction.

S'il manque des pages, veuillez communiquer avec l'université qui a conféré le grade.

La qualité d'impression de certaines pages peut laisser à désirer, surtout si les pages originales ont été dactylographiées à l'aide d'un ruban usé ou si l'université nous a fait parvenir une photocopie de qualité inférieure.

La reproduction, même partielle, de cette microforme est soumise à la Loi canadienne sur le droit d'auteur, SRC 1970, c. C-30, et ses amendements subséquents.

ISBN 0-315-60395-X

NL-339 (r. 88/04) c

Canada

UNIVERSITY OF ALBERTA

RELEASE FORM

NAME OF AUTHOR: JOÃO ALFREDO KÜPPER

TITLE OF THESIS: MODELLING MASS TRANSPORT IN FRACTURED ROCKS USING TRANSFER FUNCTIONS

DEGREE : DOCTOR OF PHILOSOPHY

YEAR THIS DEGREE GRANTED: SPRING 1990

PERMISSION IS HEREBY GRANTED TO THE UNIVERSITY OF ALBERTA LIBRARY TO REPRODUCE SINGLE COPIES OF THIS THESIS AND TO LEND OR SELL SUCH COPIES FOR PRIVATE, SCHOLARLY OR SCIENTIFIC RESEARCH PURPOSES ONLY.

THE AUTHOR RESERVES OTHER PUBLICATION RIGHTS, AND NEITHER THE THESIS NOR EXTENSIVE EXTRACTS FROM IT MAY BE PRINTED OR OTHERWISE REPRODUCED WITHOUT THE AUTHOR'S WRITTEN PERMISSION.

Permanent address:

Rua Caboquenas, 167
04090 São Paulo SP
BRASIL

Date: April 1, 1990

UNIVERSITY OF ALBERTA

FACULTY OF GRADUATE STUDIES AND RESEARCH

THE UNDERSIGNED CERTIFY THAT THEY HAVE READ, AND RECOMMEND TO THE FACULTY OF GRADUATE STUDIES AND RESEARCH FOR ACCEPTANCE, A THESIS ENTITLED *MODELLING MASS TRANSPORT IN FRACTURED ROCKS USING TRANSFER FUNCTIONS* SUBMITTED BY *JOÃO ALFREDO KÜPPER* IN PARTIAL FULFILLMENT OF THE REQUIREMENTS FOR THE DEGREE OF DOCTOR OF PHILOSOPHY.

Dr. P. M. Steffler (co-supervisor)

Frank W. Schwartz

Dr. F. W. Schwartz (co-supervisor)

Dr. N. Rajaratnam

Dr. D. C. Sego

Dr. J. Tóth

Dr. E. A. Sudicky

Date: January 26, 1990

ABSTRACT

The process of matrix diffusion plays an important role in controlling mass transport in fractured media. However, discrete fracture models that address geometries other than sets of parallel fractures have not been extended to include matrix diffusion until very recently. The model developed in this thesis extends the present capabilities in modelling mass transport in complex fracture networks subject to matrix diffusion. Based on systems analysis, this model uses the concept of transfer functions to consider not only physical and chemical transport in the network, but also diffusion and kinetic decay in the matrix blocks, with considerable reduction in the fracture and matrix discretization. The fracture network is seen as a large system constituted of, basically, two different types of components: the fracture segments and the intersections. If the transfer function is known for each component, the response of the system can be evaluated by considering the interactions of all the components. In this work the fracture component is approximated by the single fracture model, while the intersection component is approximated by either the complete mixing or the streamline routing model. In essence, the model is a com-bination of numerical and analytical approaches at the fracture scale, where mass is routed successively through fracture segments and intersections. The model can handle efficiently heterogeneous systems as well as compute exceedingly low concentrations accurately, what is important for many organic compounds that have drinking water standards in the PPB range.

Verification of the approach has come through a comparison of predicted concentrations with analytical solutions for simple fracture networks. A series of applications involved the analysis of the relative importance of the mixing models for the

fracture intersections, the role of diffusion in regional scale transport and the potential impact of matrix diffusion on the interpretation of tracer tests. In general, the results have shown that mass transport in discrete fracture networks is strongly dependent on the flow field developed within the network. Estimated parameters from tracer tests may not represent an average for the fracture system surrounding the wells, but a specific test dependent situation. The results also suggest that even short tracer tests may be influenced by diffusive effects, especially if instantaneous injection is considered.

TO

Angela,
Arthur,
Suzana

ACKNOWLEDGEMENTS

I am deeply grateful to Drs. Frank W. Schwartz and Peter M. Steffler for their continuous support, guidance and enthusiasm throughout this work. Their ideas, discussions and suggestions were invaluable for the accomplishment of this research.

The financial support provide by CAPES-Coordenação de Aperfeiçoamento de Pessoal de Nível Superior is gratefully acknowledged. The research was also supported by grants from the National Sciences and Engineering Research Council of Canada to Drs. F.W. Schwartz and Peter M. Steffler.

During the course of this work many people have contributed to its development. Prof. N. Rajaratnam helped define a cooperation program between the Departments of Geology and Civil Engineering, making this research feasible. Prof. J. Toth motivated enlightening discussions on several topics during field trips. I also thank Allan Fryar, Rob Schincariol and Allan Crowe for valuable discussions in the subject.

Finally, I thank my family for their never-ending support.

TABLE OF CONTENTS

1. INTRODUCTION 1

1.1 Background 3

2. METHODOLOGY 10

2.1 Introduction 10

2.2 The Concepts of System and Transfer Functions 13

2.3 Application to a Fracture Network 18

2.3.1 Fracture component 20

2.3.2 Intersection component - complete mixing 24

2.3.3 Intersection component - streamline routing 25

2.3.4 Intersection component - transfer function matrix 29

2.3.5 Selection of mixing models 32

2.4 Analytical Solution for a Simple Fracture Network 34

2.5 Behaviour and Limitations of the Response Functions 38

2.5.1 Dimensionless analysis 39

2.5.2 Limitations of the response function 47

3. NUMERICAL IMPLEMENTATION 50

3.1 Fracture Network Generation 50

3.2 Flow Modelling 52

3.3 Transport Modelling 57

3.3.1 Discretization of the input function 58

3.3.2 Location in time of the output function 60

3.3.3 Description of the procedure for a fracture network 63

3.4 Verification of the Transport Model 69
3.4.1 Single fracture problem 70
3.4.2 Fracture network problem 78
3.4.3 Discussion 83

4. APPLICATIONS OF THE TRANSFER FUNCTION MODEL 84
4.1 The Effect of the Intersection Mixing Models on the Overall Response of a Discrete Fracture System 85
4.1.1 Regionally uniform flow field 86
4.1.2 Regionally divergent-convergent flow field 104
4.1.3 Discussion 116
4.2 The Effects of Diffusion into Matrix on the Overall Response of Discrete Fracture Networks 121
4.2.1 Regular fracture network 121
4.2.2 Complex fracture network 123
4.2.3 Discussion 128
4.3 Mass Transport Behaviour for a Two Well System in Discrete Fracture Networks 130
4.3.1 Distinct paths within fracture networks 131
4.3.2 Effects of different injection conditions 138
4.3.3 Effects of different fracture densities 145
4.3.4 Discussion 156

5. CONCLUSIONS 159

REFERENCES 165
APPENDIX A. ANALYTICAL SOLUTIONS FOR A SIMPLE FRACTURE NETWORK 172

LIST OF TABLES

Table 2.1 Some analytical solutions for mass transport in fractured porous media, considering either a constant or a decaying step for the inlet boundary condition........ 21

Table 4.1 Data used for the regionally uniform flow field case........ 90

Table 4.2 Recovery for different region sizes........ 106

Table 4.3 Coefficients of variation for the aperture distribution........ 109

Table 4.4 Data used for fracture generation........ 126

Table 4.5 Sequence of segments for each path........ 134

Table 4.6 Parameters for each path shown in Table 4.5........ 136

Table 4.7 Data used for the generation of fracture networks with different densities........ 145

LIST OF FIGURES

Fig. 2.1 System representation 14

Fig. 2.2 Analysis of two subsystems in series, showing the input and output functions for each subsystem 16

Fig. 2.3 Definition of the components for a fracture system 19

Fig. 2.4 Representation of the complete mixing model 25

Fig. 2.5 Possible flow patterns at a fourway intersection 26

Fig. 2.6 Possible streamline distributions for a continuous intersection 28

Fig. 2.7 (a) Two-input, two-output process; (b) block diagram for the transfer function matrix 30

Fig. 2.8 Limiting conditions for the mixing models (modified after Hull et al., 1987) 33

Fig. 2.9 Simple fracture system consisting of three segments and four nodes (a) and equivalent system representation (b) 34

Fig. 2.10 Breakthrough curves for the unit step response function as a function of the matrix parameter δ ($\boldsymbol{Pe} = \infty$ and $\Lambda = 0.0$) 41

Fig. 2.11 Breakthrough curves for the unit step response function, considering the influence of both the matrix parameter δ and the dispersion parameter $\boldsymbol{Pe}$, for $\Lambda = 0.0$ 43

Fig. 2.12 Breakthrough curves for the unit step response function, considering the influence of both the matrix parameter δ and the dispersion parameter $\boldsymbol{Pe}$, for $\Lambda = 0.1$ 44

Fig. 2.13 Breakthrough curves for the unit step response function, considering the influence of both the matrix parameter δ and the dispersion parameter $\boldsymbol{Pe}$, for $\Lambda = 1.0$ 45

Fig. 2.14 Breakthrough curves for the unit step response function, considering the influence of both the matrix parameter δ and the dispersion parameter $\boldsymbol{Pe}$, for $\Lambda = 5.0$ 46

Fig. 3.1 Simple fracture network to exemplify the flow modelling procedure 54

Fig. 3.2 Definition of boundary conditions for the flow modelling procedure 56

Fig. 3.3 Discretization of the input function for a fracture segment 59

Fig. 3.4 Location in time of the discretized concentration steps 61

Fig. 3.5 Program flow chart 64

Fig. 3.6 Key concentration points and respective time points for the redistribution of the time sampling points 67

Fig. 3.7 Breakthrough curves obtained at the end of different segments, for a linear succession of segments. (a) advection dominated (b) diffusion dominated 71

Fig. 3.8 Influence of the number of discretized concentration steps (NC) on the accuracy of the numerical solution for the breakthrough curve at the end of the last segment. (a) advection dominated (b) diffusion dominated. 73

Fig. 3.9 Breakthrough curves obtained at the end of different segments, for a linear succession of segments. (a) advection dominated (b) diffusion dominated 74

Fig. 3.10 Influence of the parameter NTP on the accuracy of the numerical solution for NC = 500. Advection dominated. 75

Fig. 3.11 Influence of the parameter NTP on the accuracy of the numerical solution for NC = 500. Diffusion dominated. 76

Fig. 3.12 Verification of the accuracy of the numerical solution when dispersion in the fracture is also considered. Results obtained for the diffusion dominated case. 77

Fig. 3.13 Fracture nework and fracture parameters used to verify the accuracy of the model for a general network. 79

Fig. 3.14 Breakthrough curves obtained at all exit nodes showing the influence of the parameter NC on the accuracy of the numerical solution. Complete mixing model for mass distribution at intersections. 81

Fig. 3.15 Breakthrough curves obtained at all exit nodes showing the influence of the parameter NC on the accuracy of the numerical solution. Streamline routing model for mass distribution at intersections. 82

Fig. 4.1a Sparse fracture network (Δl = 127.28 m). 87

Fig. 4.1b Intermediate fracture network (Δl = 23.14 m). 88

Fig. 4.1c Incomplete fracture network (Δl = 23.14 m). 89

Fig. 4.2 Maximum relative concentration distribution at the exit boundary for trials 1 and 2. 91

Fig. 4.3 Comparison of the effects of the mixing models on the normalized breakthrough curves for the centerline outlets (x=300 m, y=300 m). 92

Fig. 4.4 Comparison of the normalized breakthrough curves for all the outlets at the exit (x=300 m) boundary. 92

Fig. 4.5 Complete network with ∇h at 34° and uniform aperture distribution.
(a) Maximum concentration distribution at exit boundary.
(b) Selected breakthrough curves at exit boundary.
(c) Selected breakthrough curves at exit boundary.
(d) Correspondent normalized breakthrough curves. 94

Fig. 4.6 Complete network with ∇h at 34° and random aperture distribution.
(a) Maximum concentration distribution at exit boundary.
(b) Selected breakthrough curves at exit boundary.
(c) Selected breakthrough curves at exit boundary. 97

Fig. 4.7 Incomplete network with ∇h at 34° and uniform aperture distribution.
(a) Maximum concentration distribution at exit boundary.
(b) Selected breakthrough curves at exit boundary.
(c) Selected breakthrough curves at exit boundary. 100

Fig. 4.8 Incomplete network with ∇h at 34° and random aperture distribution.
(a) Maximum concentration distribution at exit boundary.
(b) Selected breakthrough curves at exit boundary.
(c) Selected breakthrough curves at exit boundary. 102

Fig. 4.9 Fracture networks for the two well system, showing the direction of groundwater movement. (a) 100 x 100 m (b) 380 x 380 m. 105

Fig. 4.10 Breakthrough curves at the pumping well for different region sizes (complete mixing model). 108

Fig. 4.11 Comparison of the effects of the two mixing models on the breakthrough curves at the pumping well for Trial 7. 108

Fig. 4.12 Comparison of the effects of the two mixing models on the breakthrough curves at the pumping well for Trial 8. 111

Fig. 4.13 Comparison of the effects of the two mixing models on the breakthrough curves at the pumping well for Trial 9. 112

Fig. 4.14 Random fracture network, considering variations in both fracture position and fracture length. 113

Fig. 4.15 Comparison of the effects of the mixing models on the breakthrough curve at the pumping well for Trial 10. 113

Fig. 4.16 Comparison of the effects of the mixing models on the breakthrough curve at the pumping well for Trial 11. 114

Fig. 4.17 Comparison of the effects of the mixing models on the breakthrough curve at the pumping well for Trial 12. 115

Fig. 4.18 Possible flow patterns at a fourway intersection. 116

Fig. 4.19 Fracture networks considered by Krizek et al. (1973). 118

Fig. 4.20 Fracture network considered by Hull et al. (1987). 118

Fig. 4.21 Effect of the diffusion coefficient on the breakthrough curves for the network analysed in Trial 4. (a) D_m = 1.6x10^{-10} m^2/s (b) D_m = 1.6x10^{-12} m^2/s. 122

Fig. 4.22 Complex fracture network, showing the position of the pumping well and the injection nodes. 124

Fig. 4.23 Correspondent flow field obtained for the complex fracture network. 125

Fig. 4.24 Verification of the numerical model accuracy for the complex fracture network. 127

Fig. 4.25 Effect of the diffusion coefficient on the breakthrough curves obtained at the pumping well, for the complex fracture network. 127

Fig. 4.26 Hypothetical regular fracture network, showing the different apertures for each fracture and the position of the wells. 132

Fig. 4.27 Breakthrough curve obtained at the pumping well for a continuous injection. 133

Fig. 4.28 Relative contribution of the different paths. 134

Fig. 4.29 Breakthrough curves obtained at the pumping well for an injection/withdrawal rate Q=3.128×10^{-5} $m^2/s/m$. (a) continuous injection. (b) instantaneous injection. 140

Fig. 4.30 Breakthrough curves obtained at the pumping well for an injection/withdrawal rate Q=3.128×10^{-5} $m^2/s/m$. (a) continuous injection. (b) instantaneous injection. 141

Fig. 4.31 Breakthrough curves obtained at the pumping well for a injectio/withdrawal rate Q=3.128×10^{-7} $m^2/s/m$. (a) continuous injection. (b) instantaneous injection. 142

Fig. 4.32 Breakthrough curves obtained at the pumping well for an injection/withdrawal rate Q=3.128×10^{-8} $m^2/s/m$. Instantaneous injection. 144

Fig. 4.33 Sparse fracture network, showing the position of the wells and the flow field obtained. 146

Fig. 4.34 Intermediate fracture network, showing the position of the wells and the flow field obtained. 147

Fig. 4.35 Dense fracture network, showing the position of the wells and the flow field obtained. 148

Fig. 4.36 Effect of different fracture densities on the mass transport by advection only ($D_m = 0.0$). Breakthrough curves obtained at the pumping well for continuous injection. 150

Fig. 4.37 Effect of different fracture densities on the mass transport by advection, when diffusion into matrix is significant ($D_m = 1.6 \times 10^{-10}$ m²/s). Breakthrough curves obtained at the pumping well for continuous injection.. ... 150

Fig. 4.38 Effect of different fracture densities on the breakthrough curves obtained for an instantaneous injection.($D_m = 1.6 \times 10^{-14}$ m²/s). 152

Fig. 4.39 Effect of different fracture densities on the breakthrough curves obtained for an instantaneous injection.($D_m = 1.6 \times 10^{-12}$ m²/s). 153

Fig. 4.40 Effect of different fracture densities on the breakthrough curves obtained for an instantaneous injection.($D_m = 1.6 \times 10^{-11}$ m²/s). 154

Fig. 4.41 Effect of different fracture densities on the breakthrough curves obtained for an instantaneous injection.($D_m = 1.6 \times 10^{-10}$ m²/s). 155

Fig. 4.42 Combined effect of different fracture densities and diffusion coefficients on the breakthrough curves obtained for an instantaneous injection. 158

Fig. A.1 Fracture nework and fracture parameters used to calculate the analytical solution.......... 173

1. INTRODUCTION

The process of diffusion into the matrix plays an important role in controlling mass transport in fractured rock systems (Neretnieks, 1980; Grisak and Pickens, 1980a; Tang et al. 1981). Early studies have essentially considered the interactions between a single fracture and its surrounding matrix, aiming to gain insight into the mass transport behaviour. Grisak and Pickens (1980a) examined the problem from a numerical point of view. Their model included advection and diffusion into the matrix and considered both the fracture and the matrix as a single continuum. Tang et al. (1981) presented a more complete analysis for the same problem. They derived an analytical solution for mass transport in a single fracture that included the processes of radioactive decay, advection, dispersion in the fracture, diffusion into the matrix and adsorption in both fracture and matrix. Later works have contributed to the understanding of the transport phenomena by treating the fractured media as double continuum media (e.g., Bibby, 1981; Rasmuson, 1984, 1985a; Neretnieks and Rasmuson,1984; Huyakorn, 1983a, 1983b; Hopkirk and Gilby, 1984).

Modelling of matrix diffusion in fracture networks with geometries other than parallel fractures have not being addressed until very recently. All previous works on fracture networks were concerned with transport in the network itself and completely neglected diffusion into the matrix (e.g., Schwartz et al., 1983; Smith and Schwartz, 1984; Robinson, 1984). One of the first attempts to account for diffusion into the matrix in a fracture network was carried out by Germain (1988). That work considered an orthogonal system of fractures with variable aperture and used an analytical approach for dealing with diffusion into the matrix, which was coupled to a numerical scheme for treating mass transport in the fractures. More recently, Sudicky (1989b) presented a numerical scheme based on the Laplace Transform Galerkin Technique (Sudicky, 1989a) which handles matrix diffusion during mass transport through an orthogonal fracture network and also allows for mass advection in the matrix.

The model that is developed in this thesis is designed to extend the present capabilities in modelling mass transport analytically in fracture networks subject to matrix diffusion. Flow in the matrix is, however, neglected. One of the main motivations for undertaking this present study was the realization that in many cases (e.g., nuclear waste repositories, geothermal reservoirs), fractures can be sparse and poorly connected (Marsily, 1985a; Neretnieks, 1987) and the matrix permeability is often low. The models currently available are not adequate to efficiently model such systems in an analytic fashion, when matrix diffusion is an important process.

An important goal of this study is to apply the model to better understand mass transport processes in fracture networks. Works on the single fracture modelling suggest that diffusion into the matrix is an important process that may have to be considered in the interpretation of tracer tests (Neretnieks, 1983; Jensen, 1983). Different mixing models have been considered for mass distribution at fracture intersections (e.g., Castillo et al., 1972; Hull and Koslow, 1986), but no definite guideline is available for their selection. Another important issue, that is yet poorly understood, is the effect of channeling on mass transport in the fracture plane. The model that is developed in this thesis provides a useful tool to resolve these issues.

With these overall goals in mind, the specific objectives of this thesis are: (1) to develop a discrete fracture model not only involving transport in the network, but also diffusion into the matrix; (2) to consider different mixing models for the mass distribution at the intersections; (3) to verify this model using analytical solutions; and (4) to apply this model to study the relative importance of fracture intersection mixing models, the role of diffusion in regional scale transport and the potential impact of matrix diffusion on the interpretation of tracer tests.

The thesis is organized in five chapters. As part of the introduction, an overview of the present techniques for modelling mass transport in fracture networks is presented. Chapter 2 considers the theoretical background necessary for the development of the model. Chapter 3 discusses the numerical implementation of the model and its verification against known analytical solutions. Chapter 4 introduces the model applications and Chapter 5 presents the conclusions and recommendations.

1.1 Background

For the last decade, there has been considerable interest in the problems of flow and mass transport in fractured rocks. In countries around the world deep low permeability rocks have been considered as potential sites for the disposal and isolation of high level nuclear waste. In most instances, these rocks are fractured and an understanding of the transport mechanisms is required in order to correctly evaluate the risks associated with a possible failure of the repositories.

High level nuclear waste is generated mainly from the reprocessing of spent nuclear fuel (Cohen, 1977). It contains many long-lived fission products that need to be isolated for a very long period of time, 1000 to 10000 years (NRC, 1983), to allow the radionuclides to decay to safe levels. The burial of waste in deep underground repositories seems to provide sufficient isolation. The Swedish (Neretnieks and Rasmuson, 1984) and American (Cohen, 1977) repository concepts, for instance, place the repository at depths of 500 - 600 m, which provides enough protection against the degradation processes of the surface.

Potential sites are being located in geologically stable formations to minimize the possibility of new fracture pathways to the biosphere.

The geosphere is, therefore, considered to be part of a succession of engineered and natural barriers to confine the wastes to the vicinity of the repositories. Groundwater flow is the major natural agent in the geosphere that could transport the radionuclides from the repositories to some accessible point in the environment. The integrity of the engineered barriers, however, may be compromised due to the presence of groundwater in the the rock and the long period of isolation. The possible degradation of engineered barriers (e.g., break up of concrete liners and corrosion of metal canisters) would allow groundwater to come in contact with the buried wastes, to leach them into solution and to carry them away. Once the radionuclides enter the groundwater system, their mobility is controlled by the pH and Eh of the water and they may experience a variety of geochemical processes during transport from the repository. If the rocks are dense with very low permeability, the flux of groundwater will be extremely slow, allowing enough time for some of the contaminants to decay to safe levels, before reaching the biosphere.

It happens, however, that rocks often are fractured, even at great depth (Neretnieks, 1985), or may become fractured in the future due to tectonic forces (Tewley, 1977, in Moench,1984; Stein and Yeats,1989) and their presence may increase considerably the overall permeability of the rock (Neretnieks, 1985). In addition, it may create preferential pathways that decrease the residence time of the radionuclides, increasing the chances of waste migration to the biosphere.

There are several factors that influence transport and residence time of the radionuclides in fractured rocks. The basic factors are those related to the geometry and structure of the fractures that ultimately control the velocity field of groundwater flow, under a prescribed hydraulic gradient. They are fracture dimensions, aperture, orientation, density and connectivity. There is some uncertainty about the geometrical form of actual fractures. Some researchers consider them to be rectangular planes (e.g., Smith et al., 1985a), while others (e.g., Long, 1985) consider them to be circular in shape. Although fractures are usually modelled as parallel plates, the actual fracture surfaces are irregular, with many contact points (or areas) and, therefore, the fracture aperture is not constant throughout. Flow can take place only through those areas that are open and, consequently, it is not uniformly distributed along the fracture plane, tending to concentrate in specific paths and also forming some pockets and dead-end zones. This phenomenon is called "channelling" and in some cases 5-20% of the fracture plane may carry more than 90% of the flow (Rasmuson and Neretnieks, 1986). This kind of transport behaviour can adversely affect the safety of nuclear repositories, because fast channels tend to shorten even more the residence time of radionuclides in the geosphere.

Connectivity is an important parameter related to the fracture arrangement in the three-dimensional space, because it defines how fluid flows through the fracture system. The intersections of finite length fractures from different sets can produce a connected series of pathways through the rock that is referred to as a network. It is important to realize that, although rocks are fractured, the network may not be percolating. A so-called critical density of fractures must be achieved before the fracture network becomes conductive (Robinson, 1984).

Many different processes can influence mass transport in a fracture network. The most important ones include advection, dispersion in the fracture, diffusion into the rock matrix, sorption on the fracture surfaces and within the matrix and radioactive decay (Neretnieks, 1980; Tang et al., 1981). One of the most important contributions to the study of mass transport in fractured rock systems has been the recognition of the importance of diffusion into the matrix (Neretnieks, 1980; Tang et al., 1981; Grisak and Pickens, 1981). This process effectively makes the storage volume inside the rock matrix accessible to the radionuclides. Sorption on the internal surface of the porous matrix enhances even more the storage capacity, contributing significantly to the retardation of the radionuclides.

Mass transport in fractured rocks has been modelled with either the continuum or the discrete approach. In the first approach, the fractures are assumed to be so abundant that they can be represented using equivalent continuum properties of the rock (e.g., permeability, porosity, dispersivities and so on). In the discrete approach, each fracture is explicitly considered at a smaller scale, and the properties for the individual fractures and intersections must be specified.

In the continuum approach, modelling is just an extension of the methods currently available for porous media (e.g., Robertson, 1974; Mercer and Faust, 1979; Fryar and Domenico, 1989). When the interactions with the porous matrix are important, the concept of double porosity (or double continuum), as proposed by Barenblatt et al. (1960), is used (Narasimham, 1982; Rasmuson et al., 1982; Huyakorn et al., 1983a, 1983b). For fluid flow the continuum approach has worked extremely well for many naturally fractured reservoirs in the areas of oil fields, geothermal reservoirs and aquifers, but it may not work as well for mass transport problems. One reason is that the continuum approach does not fully represent the complexity of transport that can occur in fractured media (Schwartz and Smith, 1988). A second reason is that sparsely fractured media may not be describable through a representative elementary volume (REV, Bear, 1972), an essential requirement for the continuum approach to be valid.

The transport of mass is much more selective than the flow of the natural fluid. The effects of channelling and poor connectivity of the fracture network can make the flow paths very tortuous and two adjacent streamlines in the repository may take the radionuclides to very different places (a porous medium example is given by Freeze and Witherspoon, 1967). The immediate consequence is that mass being transported samples a smaller area, thus requiring a larger volume of rock, perhaps as large as the study region, before homogenization takes place. In this case the continuum approach may be totally inappropriate (Endo et al., 1984; Robinson, 1984).

The discrete approach, in contraposition, does not require assumptions about REV's and overall provides a more realistic description of the transport process. As a consequence, it can be applied to a much wider range of problems. Its main limitations, however, are the larger number of parameters required to fully describe the network and the computational effort that is required to model networks of even moderate size.

Two basic methodologies have been used in modelling transport through networks, particle tracking and conventional finite elements and finite differences. Particle tracking models have been successful in simulating advection and dispersion in fractured networks (e.g., Schwartz et al., 1983; Smith and Schwartz, 1984; Robinson, 1984; Smith et al., 1985b; Rouleau, 1987), but they are incapable of incorporating diffusion into the matrix, a process that cannot really be ignored in real systems. The finite element method (FEM) and the integrated finite difference method (IFDM) are almost equivalent in terms of capability, being different in the way they work with the governing equations (Narasimham, 1982). Both methods usually require refined discretizations, especially in the matrix blocks due to the high concentration gradients between fracture and matrix at early times. The fracture discretization and the time step are also constrained due to the ill-behaviour of the advection term. The finite element models developed by Grisak and Pickens (1981) and Noorishad and Mehran (1982) and the integrated finite difference model of Narasinham et al. (1982) discretize both matrix and fractures. More recently, Germain (1988) developed a model that does not require discretization of the matrix. Instead, it uses an analytical solution to account for the mass diffusion into the blocks. It also employs a different approach, in which the governing equations and corresponding boundary and initial conditions are rewritten in the Laplace domain and solved using traditional FEM (Sudicky, 1989a). The advantage is that the usual problems related to the time discretizations are eliminated. A numerical inversion gives the solution in the real domain. The drawbacks of this model are that it is restricted to orthogonal fractures and that the numerical Laplace inversion methods may not be sufficiently robust to converge to the correct solution (Robinson, 1984).

One of the requirements for all discrete representations of networks is a mixing model that describes how mass reaching a fracture intersection is partitioned among the fractures receiving flow. Work to date has modelled mixing with what is known as the complete mixing model, which is discussed in detail in Chapter 2. There is, however, experimental evidence that this may not be always the case and, in fact, mass would be transported along streamlines with very little interference between adjacent streamlines at the intersections (e.g., Wilson and Witherspoon, 1976; Hull and Koslow, 1986; Robinson and Gale, 1988). The choice of the mixing model, however, is dependent on the fluid residence time at the intersection and also on the diffusive properties of the mass being transported.

A few attempts have been made to incorporate streamline routing through intersections into numerical models. Endo et al. (1984) simulated mechanical transport in a fracture network based on a detailed description of the movement of the fluid within the fractures. They considered the two-dimensional character of the velocity profile within a fracture and developed a model that tracked down streamtubes from inlets to outlets. By calculating residence times for each streamtube it was possible to obtain the distribution of residence times for the system.

Hull et al.(1987) developed a more complete model that considered not only the velocity distribution within individual fractures but also transverse molecular diffusion within the fracture system (including intersections). Their model used the particle tracking technique (Ahlstrom et al., 1978) with a deterministic motion (advection) added to a random motion (diffusion) as the particles moved along the system.

Robinson and Gale (1988) used the finite element method to discretize the fracture system. At the fourway intersections they had to uncouple and recouple the finite element nodes in order to properly assign concentrations to each fracture element (equivalent to considering the intersection as an immaterial element with four nodes). Their model considered advection and dispersion along the fractures and streamline routing at intersections, but no diffusion between streamlines at intersections.

2. METHODOLOGY

2.1 Introduction

Of the possible approaches for modelling mass transport in a fractured rock system, which can account for realistic geometries and matrix diffusion, only numerical methods are applicable. It is possible to represent the entire system (fractures and matrix) either as a single continuum or as a double continuum. In the single continuum approach fractures are assumed to represent a heterogeneity within the matrix domain with different flow and transport characteristics. This procedure was implemented by Grisak and Pickens (1980a) and Noorishad and Mehran (1982) for a system of parallel fractures.

In the double continuum approach the fracture and the porous matrix systems are considered as two distinct and overlapping media that are related to each other through a source/sink term. Huyakorn et al. (1983a) discusses the formulation of this approach and describes how both systems can be discretized and the resultant equations solved simultaneously. One can potentially avoid the discretization of the matrix, however, by using an analytical solution to express the mass transfer between the fracture and the matrix. Bibby (1981) derived his source/sink term based on a simple solution for a system of parallel fractures and expressed the mass flux as a function of the average concentration inside the block matrix. Hopkirk and Gilby (1984) preferred to characterize the mass distribution inside the porous matrix (idealized as slabs or spheres) through an analytical solution whose coefficients had to be fitted at the end of each time interval.

Although the single continuum approach may rely on few simplifying assumptions, it requires a refined discretization for the matrix because of high concentration gradients at the fracture/matrix interface. For large realistic three-dimensional systems, this approach becomes impracticable. In the double continuum approach, the physical quantities (e.g., permeability, dispersivity and so on) represent an average over sufficiently large blocks of rock that contain many fractures (the representative elementary volume, REV, as defined by Bear, 1972). For nuclear waste repository sites, for instance, the fracture network may be sparse and poorly connected and, consequentely, the size of the REV may become large, perhaps as large as the study area, making the double continuum approach inappropriate on theoretical grounds.

Another approach in modelling mass transport is to consider the system at the fracture scale, with both fracture and matrix blocks treated separately. Germain (1988) developed a model in which diffusion into the matrix is accounted for by using an analytical solution. The matrix domain, however, is assumed to consist of rectangular blocks and the mass flux is a function of the fracture concentration at the boundary of the blocks. Although the fractures must still be individually discretized, the use of an analytical solution may enable larger systems to be treated with the same computational effort. Similar concepts have also been used for flow modelling in multilayered aquifers (e.g., Herrera and Yates, 1977; Huyakorn, 1986).

In this work a somewhat different procedure is considered. It is also a combination of numerical and analytical approaches at the fracture scale, but, unlike Germain's (1988), it does not involve a complete discretization of the fractures. The idea is to regard each fracture segment between intersections and the intersections themselves as components of a large system, for which the laws governing the mass transport are known. By appropriate calculations, the interactions among all the components can be found, leading to the evaluation of the breakthrough curves at specific outlets.

Ross and Koplick (1979) used a similar technique to model transport in porous media. The steady-state flow field is approximated by a network of streamtubes, within which transport is assumed to be unidimensional. Knowing the impulse response (Green's function) for a generic streamtube, it is possible to calculate sequentially the mass transport along the streamtube network by using the convolution theorem. Following the same technique, Gureghian and Jansen (1985) derived an analytical solution that can account for the transport of a three-member decay chain in a multilayered medium. They assume the radionuclides will be confined to a streamtube, which can be subdivided into several segments, according to the geologic unit they belong to. Each streamtube segment can be assigned different properties and the convolution theorem is used to sequentially calculate the mass transport along each segment.

Although not explicitly mentioned, these techniques represent an application of a quite general methodology, systems analysis, where the behavior of the system as a whole can be characterized by an appropriate transfer function that relates the output functions to the input functions. There are several advantages in using such an approach for modelling mass transport in fractured media. First, it minimizes the fracture and matrix discretization involved and, consequently, a greater number of fractures can be considered for the same computational effort. Second, it can realistically account for the fracture distribution when the REV becomes large. Third, it can efficiently handle heterogeneous systems. And fourth, most important of all, the traditional problems involved with the solution of the transport equation, such as numerical dispersion and oscillations, are completely eliminated.

There are, however, some limitations. As with most other approaches, it assumes steady-state flow of groundwater in the fractures and neglects flow in the matrix. It also assumes that the mass penetration depth into the matrix is small compared to the distance between fractures. By considering the fracture segment and surrouding matrix as a component, one is implicitly assuming that the knowledge of mass distribution inside the matrix is not important for the overall mass transport through the fractures, where the matrix acts as a buffer for the mass being transported. This model is primarily applied to two-dimensional fracture networks, because of the nature of the transfer functions employed. It is difficult to extended the model to three dimensions, by assuming a plane or disc shaped fracture. The model is, however, readily extensible to three-dimensional systems, when one considers a more realistic fracture representation that includes the effects of channeling.

The transfer function approach, unlike all the other approaches, does not need to explicitly solve a partial differential equation. It assumes that a solution is already known or that it can be found based on the knowledge of the input and output functions. The convolution integral is then used to account for the relations of several components in a system (Wylie, 1966; McGillem and Cooper, 1984).

In the next section, the concepts of system and transfer function will be discussed and it will be shown how these concepts can be applied to the problem of mass transport in fractured rocks.

2.2 The Concepts of System and Transfer Function

A system, represented as a black box model (Figure 2.1), in its most basic form consists of an input function (external stimulus or excitation), an output function (response) and an operation function that relates the input to the output. This operation function, which represents the fundamental behaviour of the system, is called the transfer function.

The complexity of the transfer function depends on the nature of the components involved with the system. It might accomplish a simple scaling, or a complicated non-linear mapping of one function into another (McGillen and Cooper, 1984).

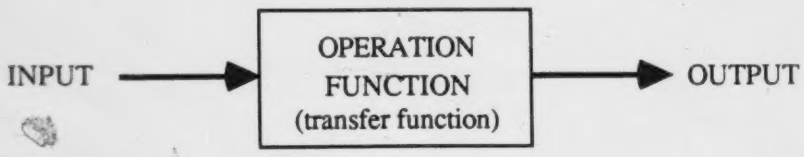

Figure 2.1 System Representation

The system in Figure 2.1 could represent mass transport in a single fracture, with a transfer function characterizing the transport processes. The input could be a variable-in-time release of radionuclides and the output would be the breakthrough curve at the end of the fracture. Generally, the transfer function is defined in the Laplace domain, as the ratio of the transforms of the output and the input functions, when the initial conditions are zero. If the input is *i(t)* and the output is *o(t)*, then the transfer function *H(s)* is given by

$$H(s) = \frac{L\{o(t)\}}{L\{i(t)\}} = \frac{O(s)}{I(s)} \tag{2.1}$$

where $L\{\}$ is the Laplace operator, defined as $L\{f(t)\} = \int_0^\infty f(t)\, e^{-st}\, dt$, $O(s)$ is the Laplace transform of the output, $I(s)$ is the Laplace transform of the input and s is the Laplace variable.

In many situations, the internal processes operating in the system are unknown and the problem consists of just determining the system transfer function (e.g., Jury, 1982; White et al., 1986). A simple way to obtain the transfer function is to set the input as the unit impulse function and the output of the system, called the unit impulse response function, will coincide with the transfer function (Himmelblau and Bischoff, 1968). If the input is given, instead, by the unit step function, the output is the integral of the transfer function and is called the unit step response function or the indicial admittance function (Wylie,1966). In concept, both functions are equivalent and it is simple to go from one function to the other. In fact, it is easier to find the transfer function from the unit step response function, because only a differentiation is involved. In this study, the unit step response function is used to characterize the system response because it has certain advantages in numerically implementing the method (as discussed in Chapter 3).

In the approach used here, the fracture system is a combination of many segments and intersections that can be thought as individual components or subsystems within the global system. If the unit step response function is known for each of these components, then the response of the system can be found by means of the convolution integral. The procedure that leads to the convolution integral can be exemplified by a simple system consisting of m subsystems in series. Each subsystem is characterized by its own unit step response function. Figure 2.2a depicts the first subsystem subjected to a step input of magnitude c_0. The output is shown as the S-shaped curve $c_1(t)$, which would coincide with the unit step response function $f_1(t)$, except for the scaling factor c_0. Therefore

$$c_1(t) = c_0 f_1(t) \tag{2.2}$$

The output of the first subsystem becomes, now, the input for the second subsystem. Because this input is a continuous function, it has to be discretized in a series of steps to allow the use of the known unit step response function. Figure 2.2b shows the input curve discretized in three steps Δc_i, with the respective time τ_i that each step occurs.

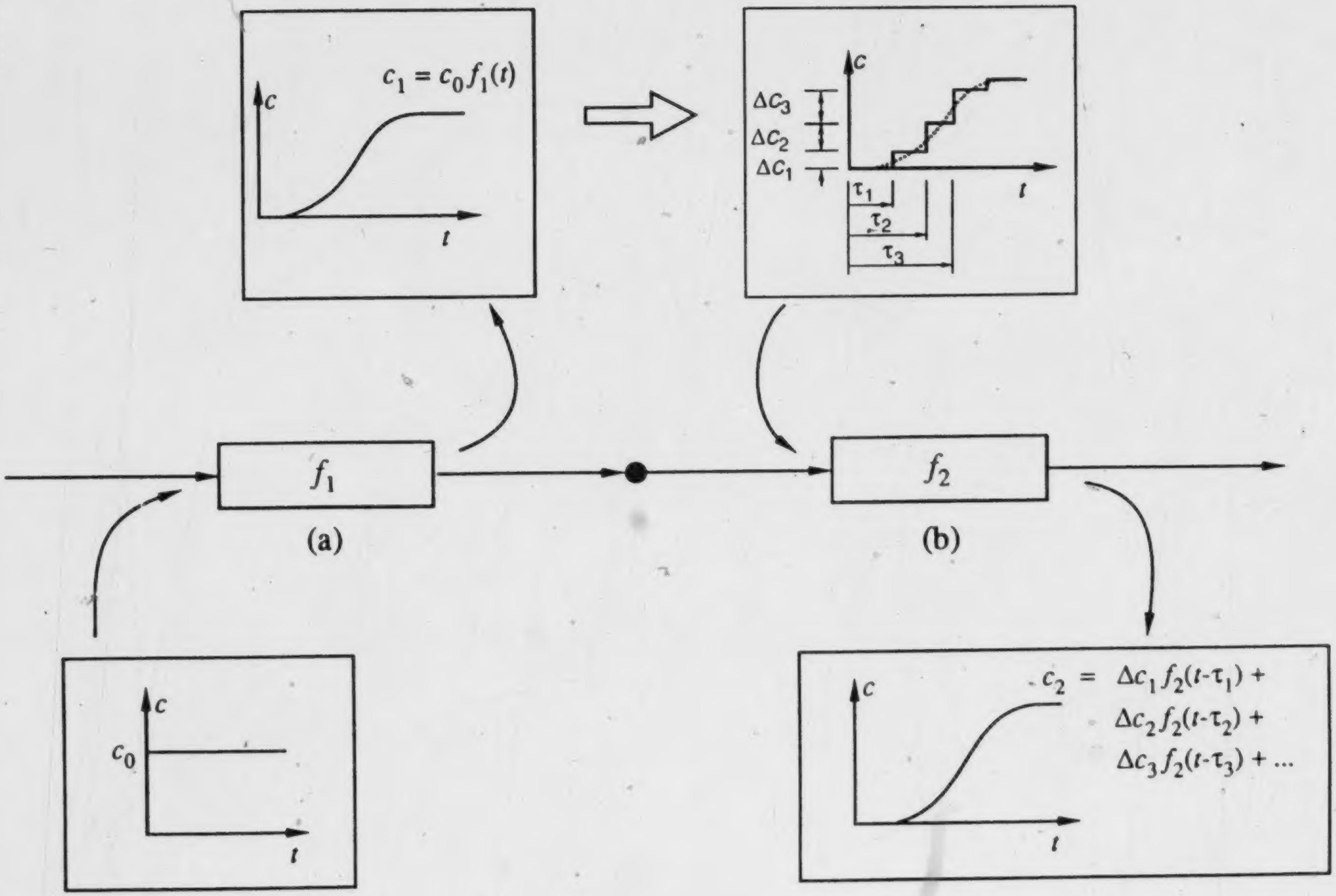
$c_1 = c_0 f_1(t)$
c
t
Δc_3
Δc_2
Δc_1
c
t
τ_1
τ_2
τ_3
f_1
(a)
f_2
(b)
c
c_0
t
c
$c_2 = \Delta c_1 f_2(t-\tau_1) + \Delta c_2 f_2(t-\tau_2) + \Delta c_3 f_2(t-\tau_3) + \ldots$
t

Fig. 2.2 Analysis of two subsystems in series, showing the input and output functions for each subsystem.

Assuming that the behaviour for each subsystem is linear, the output for the second subsystem is the summation of all the elementary step responses, that in a general form is given by

$$\begin{aligned} c_2(t) \;=\; & \Delta c_1 f_2(t-\tau_1) + \Delta c_2 f_2(t-\tau_2) + \cdots \\ & \ldots + \Delta c_{n-1} f_2(t-\tau_{n-1}) + \Delta c_n f_2(t-\tau_n) \end{aligned} \tag{2.3}$$

which can be put in the form,

$$c_2(t) = \sum_{i=1}^{n} \Delta c_i f_2(t-\tau_i) \tag{2.4}$$

where Δc_i represents the discretized steps of the input. By substituting

$$\Delta c_i = \frac{\partial}{\partial \tau}(c_1(\tau))\bigg|_{\tau=\tau_i} \Delta \tau_i \tag{2.5}$$

into equation (2.4), one obtains

$$c_2(t) = \sum_{i=1}^{n} \frac{\partial c_1(\tau)}{\partial \tau}\bigg|_{\tau=\tau_i} \Delta \tau_i f_2(t-\tau_i) \tag{2.6}$$

Taking $n \rightarrow \infty$ and $\Delta\tau_i \rightarrow 0$, equation (2.6) becomes

$$c_2(t) = \int_0^t \frac{\partial c_1(\tau)}{\partial \tau} f_2(t-\tau)\, d\tau \tag{2.7}$$

and finally, generalizing for any subsystem, one obtains

$$c_m(t) = \int_0^t \frac{\partial c_{m-1}(\tau)}{\partial \tau} f_m(t-\tau)\, d\tau \tag{2.8}$$

This equation, often referred to as Duhamel's formula, represents the convolution between the derivative of the input function and the unit step response function, for the mth

subsystem. In other words, it expresses the response of a system to a general driving force $c_{m-1}(t)$ in terms of the experimentally accessible response $f_m(t)$ to a unit step function. In the Laplace domain, equation (2.8) becomes:

$$C_m(s) = s\, C_{m-1}(s)\, F_m(s) \tag{2.9}$$

where $F(s)$ is known as the indicial admittance function (Wylie, 1966). It is important to note that equation (2.9) contains only multiplications of the Laplace transforms, which makes it very simple to derive the response of almost any system. The difficult part might be finding the equivalent real solution. Fortunately, for transport in fracture networks the solutions in the Laplace domain are given by simple expressions, making it possible to find analytical solutions for simple fracture networks.

2.3 Application to a Fracture Network

The concept of transfer function provides a useful way of modelling mass transport in a complex fracture system. Jury (1982) and Jury et al.(1986), for instance, developed a transfer function model for mass transport in unsaturated soils. Their model did not explicitly account for the details of mass transport within the soil. Instead, all the unknown transport mechanisms were lumped together into the transfer function derived from measurable parameters, the net amount of water entering the soil and the breakthrough curve at a depth L.

The approach in this study is the opposite. It is assumed that the transfer function or the unit step response function is known for each component of the system. The objective is, therefore, to evaluate the response of the system considering the interactions of all the components. For a complex fracture system, two different types of components are considered: the fracture segment and the intersection (Figure 2.3). The first component, responsible for all the physical processes involved, can be approximated by the single fracture model. The second component is just a connecting device with no physical size. Its purpose is to properly distribute the incoming discharges into the exit segments. The attractiveness of the transfer function method is that each type of component obeys the same processes, while parameters for each component can vary.

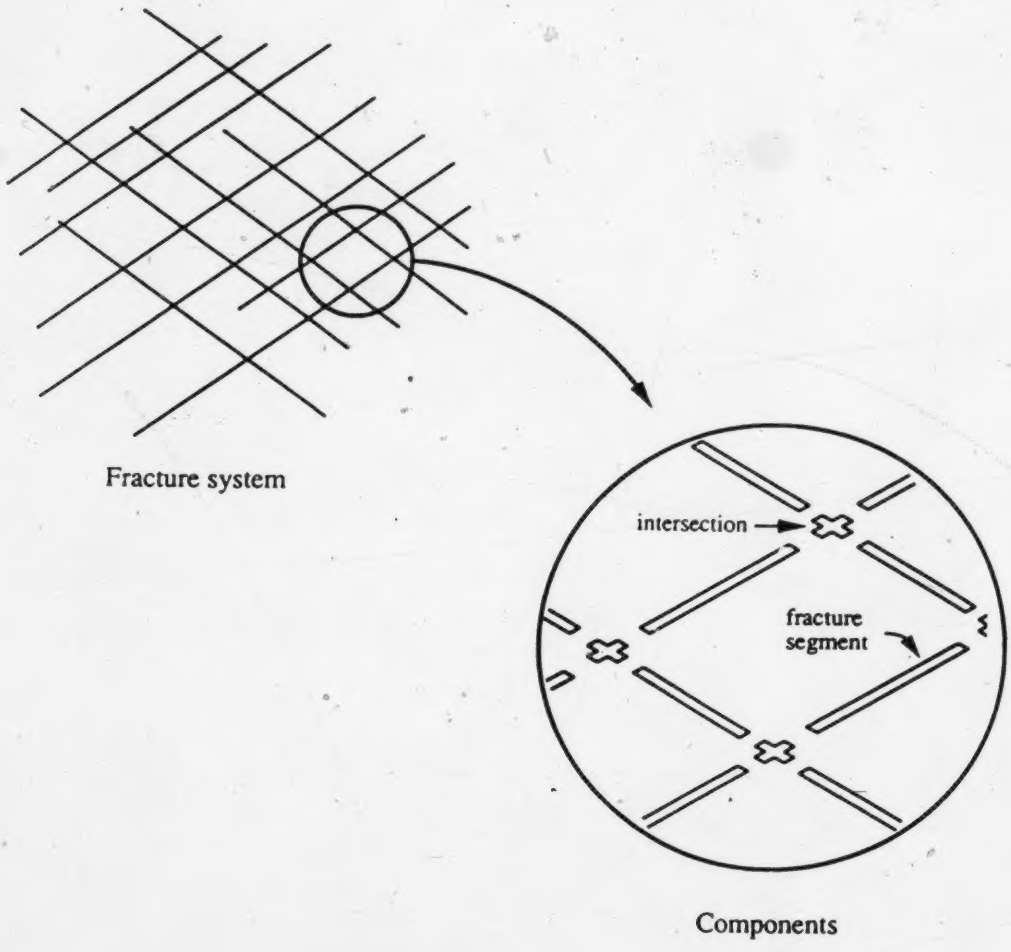

Fig. 2.3 Definition of the components for a fracture system.

2.3.1 Fracture component

The appropriate unit step response function for the fracture segment can be developed from well-known analytical solutions for mass transport in single fractures. In general, fractures are idealized as two smooth parallel plates. Fluid flow is assumed to be laminar and transport is controlled by advection, dispersion along the fracture, diffusion into the matrix, radioactive decay, and adsorption in the fracture and inside the matrix. The following system of linear partial differential equations describe the phenomena for a single fracture in a porous rock (Tang et al., 1981),

$$\left\{ \begin{aligned} & \frac{D}{R_f}\frac{\partial^2 c}{\partial z^2} - \frac{V}{R_f}\frac{\partial c}{\partial z} = \frac{\partial c}{\partial t} + \lambda c + \frac{q}{bR_f} \\ & \frac{D_m}{R_m}\frac{\partial^2 c_m}{\partial x^2} = \frac{\partial c_m}{\partial t} + \lambda c_m \\ & q = -\theta D_m \left.\frac{\partial c_m}{\partial x}\right|_{x=b} \end{aligned} \right. \tag{2.10}$$

where,

c - concentration in the fracture,
c_m - concentration in the matrix,
V - groundwater velocity in the fracture,
D - dispersion coefficient,
λ - decay coefficient equal to $(ln2)/t_{1/2}$,
$t_{1/2}$ - half-life,
θ - matrix porosity,
D_m - effective diffusion coefficient for the matrix,
R_f - retardation coefficient for the fracture,
R_m - retardation coefficient for the matrix,
$2b$ - fracture aperture,
z - distance along the fracture axis, and
t - time.

Table 2.1 Some analytical solutions for mass transport in fractured porous media, considering either a constant or a decaying step for the inlet boundary condition

Reference	Block matrix model	Inlet boundary condition	Dispersion in the fracture	Radioactive decay	Notes
Neretnieks (1980)	infinite	$c = c_0\ e^{-\lambda t}$	no	yes	discrete fracture
Rasmuson and Neretnieks (1981)	spheres	$c = c_0\ e^{-\lambda t}$	yes	yes	fractured medium
Grisak and Pickens (1981)	infinite	$c = c_0$	no	no	discrete fracture
Tang et al. (1981)	infinite	$c = c_0$	yes	yes	single fracture
Barker (1982)	slabs	generic	yes	yes	fractured medium
Sudicky and Frind (1982)	slabs	$c = c_0$	yes	yes	discrete fracture
Sudicky and Frind (1984)	infinite	$c = c_0$	no	yes	discrete fracture two member decay
Rasmuson (1984)	spheres slabs	$c = c_0$	yes	yes	fractured medium film resistance
van Genuchten et al. (1984)	infinite	$c = c_0$	yes	no	cylindrical macropore
Rasmuson (1985a)	various block geometries	$c = c_0$	yes	no	fractured medium film resistance
Rasmuson (1985b)	various block geometries	$c = c_0$	yes	no	fractured medium film resistance
Moreno and Rasmuson (1986)	infinite	$Wc_0 = Wc - D\dfrac{\partial c}{\partial z}$	yes	no	single fracture

Several solutions have been obtained for the system of equations (2.10), considering different boundary and initial conditions. Table 2.1 presents a summary of the available solutions with the respective boundary conditions and simplifying assumptions. The solution by Tang et al. (1981) is most appropriate for this study, because of its simplicity. Their general analytical solution for the concentration in the fracture is given by equation (2.11),

$$\frac{c}{c_0} = \frac{1}{\sqrt{\pi}} \, exp\left(\frac{Vz}{2D}\right) \int_l^{\infty} exp\left(-\xi^2 - \frac{V^2 z^2}{16 D \xi^2} - \eta z^2\right) \cdot$$

$$\cdot \left\{ exp\left(-\lambda^{0.5} Y\right) \cdot erfc\left(\frac{Y}{2T} - \lambda^{2} T\right) + \right.$$

$$\left. + \; exp\left(+\lambda^{0.5} Y\right) \cdot erfc\left(\frac{Y}{2T} + \lambda^{2} T\right)\right\} d\xi \qquad (2.11)$$

while equation (2.12) presents the simplified solution for the case of no-dispersion.

$$\frac{c}{c_0} = \frac{1}{2} \, exp\left(-\frac{\lambda R_f z}{V}\right) \cdot \left[exp\left(-\lambda^{0.5} Y'\right) \cdot erfc\left(\frac{Y'}{2T'} - \lambda^{0.5} T'\right)\right.$$

$$\left. + \; exp\left(+\lambda^{0.5} Y'\right) \cdot erfc\left(\frac{Y'}{2T'} + \lambda^{0.5} T'\right)\right] \qquad (2.12)$$

where,

$$\eta = \frac{\lambda R_f}{4 D \xi^2} \qquad Y = \frac{\theta (R_m D_m)^{0.5} z^2}{4 D b \xi^2} \qquad Y' = \frac{\theta (R_m D_m)^{0.5} z}{V b}$$

$$l = \left(\frac{R_f z^2}{4 D t}\right)^{0.5} \qquad T = \left(t - \frac{R_f z^2}{4 D \xi^2}\right)^{0.5} \qquad T' = \left(t - \frac{R_f z}{V}\right)^{0.5}$$

If $c_0 = 1.0$ and $z = L$ is the length of the segment between fracture intersections, then the solutions presented by equations (2.11) and (2.12) are the unit step response functions. In the Laplace domain these functions become (Tang et al., 1981), respectively,

$$F = \frac{1}{s} exp\left(\frac{VL}{2D}\right) exp\left[-\frac{VL}{2D}\left\{1 + \frac{4RD}{V^2}\left(\frac{\theta(R_m D_m)^{0.5}}{bR} \cdot (s+\lambda)^{0.5} + (s+\lambda)\right)\right\}^{0.5}\right] \qquad (2.13)$$

$$F = \frac{1}{s} exp\left[-\left(\frac{\theta(R_m D_m)^{0.5} L}{Vb} \cdot (s+\lambda)^{0.5} + \frac{RL}{V} \cdot (s+\lambda)\right)\right] \qquad (2.14)$$

where F has been substituted for C to stress the fact that it represents the unit step response function (in the Laplace domain), and L is the segment length. The transfer function in the Laplace domain is obtained by simply multiplying equations (2.13) and (2.14) by the Laplace variable s (Wylie, 1966).

There is an important difference between these two equations. Equation (2.12), for the general case, has a square root in the argument of the exponential function. This non-linearity makes it impossible to relate the convolution form in the Laplace domain with the expression in the Real domain. This means that the inverse Laplace transform is necessary in order to find an analytical solution for any complex system. In the simplified case, equation (2.13), it is easy to find the relationship between the Laplace transform and the expression in the Real domain, to avoid the inverse transform. To explain this point, consider, for instance, two fracture segments in series. If the input for the first one is a step function, the breakthrough curve at the end of the first segment is the step response function as given by either equation (2.11) or (2.12). The response of the second segment can be found by using equation (2.9). Thus the convolution process in the Laplace domain leads to the multiplication of two exponential terms and, consequently, to the addition of the arguments. If equation (2.11) were used to represent the fracture segment, the addition of arguments in the Laplace domain would lead to the addition of the corresponding arguments in the Real domain. This procedure is illustrated in section 2.5, where an analytical solution for a simple fracture network is derived. This rather simple procedure, however, cannot be used for the general case (equation 2.10) and the convolution integral has to be evaluated either analytically or numerically.

2.3.2 Intersection component = Complete mixing

Having found an appropriate response function for the fracture, it is necessary to consider the second type of component, the intersection. Although the intersection is a simple component, it may have several inputs and outputs. The description of the transfer function becomes more complicated, because any output may depend on many inputs, giving rise to a transfer function matrix. The derivation of the transfer function matrix becomes simple if we derive first the response of the component based only on physical considerations, i.e. continuity equation.

The intersection specifies how the incoming mass is distributed among the outgoing fluxes. There are two basic models describing mass mixing at intersections: complete mixing and streamline routing.

The complete mixing model assumes that the incoming mass is completely mixed at the intersection and the concentration leaving the node is the same for any segment. This is the equivalent of the completely stirred tank model in chemical engineering (Stephanopoulos, 1984).

Mathematically, a very simple mass balance equation can define the outgoing concentration. If Q_3 and Q_4 are the incoming volumetric discharges with respective mass concentration c_3 and c_4, as shown in Figure 2.4, then the outgoing concentration c, valid at any instant, is given by

$$c = \frac{c_3 Q_3 + c_4 Q_4}{Q_3 + Q_4} \quad (2.15)$$

When there is more than two incoming segments, equation (2.15) can be generalized to

$$c = \frac{\left(\sum_{i=1}^{n} c_i Q_i\right)}{\left(\sum_{i=1}^{n} Q_i\right)} \quad (2.16)$$

where the subscript i represents any of the n incoming segments.

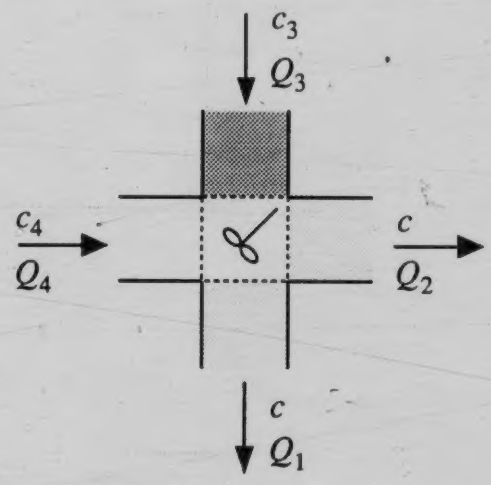

Fig. 2.4 Complete mixing model representation.

2.3.3 Intersection Component - Streamline Routing

In the streamline routing model, mass follows the streamlines at the intersection and no mixing occurs between different streamlines, while in the intersection (Hull and Koslow, 1986). Unlike the complete mixing model, the concentration leaving the node differs for each exiting segment, depending on the specific streamlines that converge to each one. This partitioning makes the problem more complex and two mass balance equations become necessary to define the outgoing concentration. Once the mass has entered any of the exiting segments, it is assumed that the segment is long enough so that diffusion in the fracture can homogenize the concentration over the cross section (Taylor, 1955).

In the streamline routing the relative position of the nodes at the intersection is of fundamental importance. In this study it is assumed that only two fractures can intersect at a point, leading to four basic flow patterns (Figure 2.5): (a) one incoming segment; (b) one outgoing segment; (c) discontinuous intersection; and (d) continuous intersection. The terms discontinuous and continuous intersections were suggested by Hull and Koslow (1986).

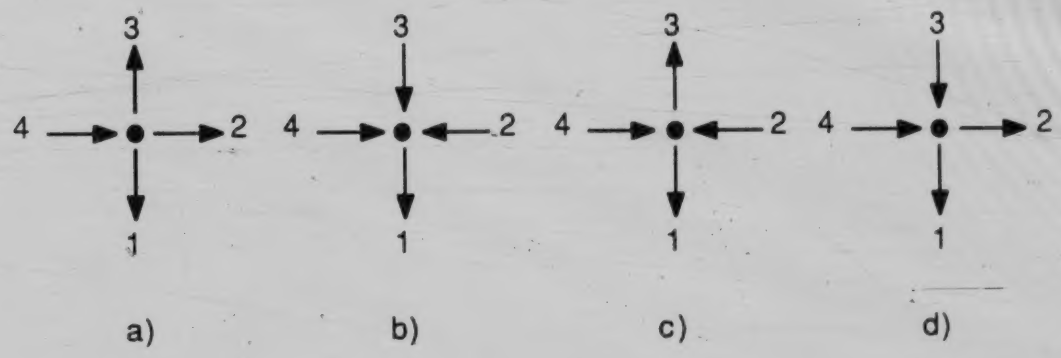

Fig. 2.5 Possible flow patterns at a fourway intersection

Case (a) has only one incoming segment and, therefore, the concentration will be the same for any of the other three exiting segments,

$$\text{case } (a) \qquad c_1 = c_2 = c_3 = c_4 \tag{2.17}$$

In case (b) there is only one exiting segment and, consequently, there will be a forced mixing of the three incoming fluxes after they enter the exiting segment. Although no mixing occurs at the intersection, case (b) is mathematically equivalent to the complete mixing model and can be described by

$$\text{case } (b) \qquad c_1 = \frac{c_2Q_2 + c_3Q_3 + c_4Q_4}{Q_2 + Q_3 + Q_4} \tag{2.18}$$

Both cases (c) and (d) were analyzed by Hull and Koslow (1986) and their routing procedure has been termed proportional routing (Philip, 1988). Essentially, the outgoing concentration is weighed in proportion to the concentration carried by the different streamlines that arrive at one specific exiting segment.

In case (c), discontinuous intersection, proportional routing leads to the same concentration for both outlets, although no mixing occurs in the intersection. The outgoing concentrations are given by:

$$\text{case } (c) \qquad c_1 = c_3 = \frac{c_2Q_2 + c_4Q_4}{Q_2 + Q_4} \tag{2.19}$$

Philip (1988) pointed out that the use of proportional routing in case (c) introduces significant errors when the following three conditions are met simultaneously: (1) there are great differences between the incoming fluxes; (2) there are great differences between the outgoing fluxes; and (3) the smaller incoming flux carries the majority of the tracer arriving at the intersection. These restrictions, however, represent only a small number of all possible situations in a intersection and their overall effect in a network can be considered negligible (in most cases).

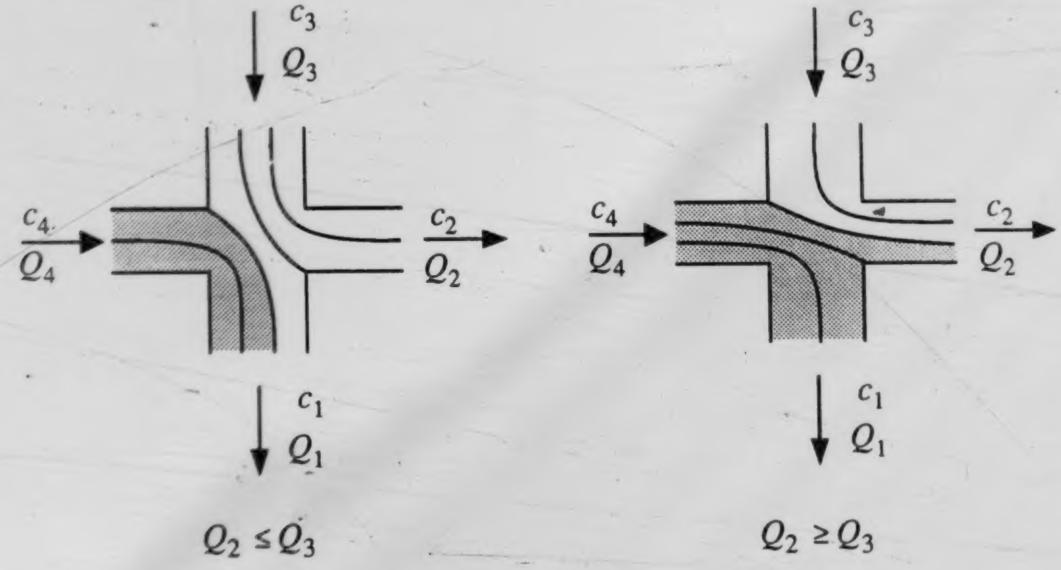

Fig. 2.6 Possible streamline distributions for a continuous intersection.

In case (d), continuous intersection, the partition of the streamlines is a function of the discharges Q_2 and Q_3. If, according to Figure 2.6, $Q_2 \le Q_3$, then the streamlines arriving at segment 2 will all come from segment 3 and the concentration at 2 will equal the concentration at 3. The concentration at 1 is then given by a weighted average of the mass fluxes coming from segments 3 and 4. In the case $Q_2 \ge Q_3$ the converse is true and the concentration at 1 equals the concentration at 4, and the concentration at 2 is a weighted average of the mass fluxes coming from 3 and 4. Mathematically, this condition is translated as case (d)

$$Q_2 \leq Q_3 \qquad \begin{cases} c_2 = c_3 \\ c_1 = \dfrac{c_3(Q_1 - Q_4) + c_4 Q_4}{Q_1} \end{cases} \qquad (2.20a)$$

$$Q_2 \geq Q_3 \qquad \begin{cases} c_1 = c_4 \\ c_2 = \dfrac{c_4(Q_2 - Q_3) + c_3 Q_3}{Q_2} \end{cases} \qquad (2.20b)$$

The proportional routing in cases (a), (b) and (c) leads to the same type of equations as the complete mixing model, but there is no actual mixing at the intersection. Another important point concerns the distribution of concentration over a cross section just at the beginning of the exit segments. In all cases but (a), the concentration is not uniform over the cross section. If the segment is long enough, diffusion in the fracture will homogenize the concentration over the cross section (Taylor, 1954). For modelling purposes, it is assumed, however, that homogenization takes place at the beginning of the segment.

2.3.4 Intersection Component – Transfer Function Matrix

Once the response functions for the intersection have been derived, the concept of transfer function matrix becomes rather intuitive. Consider the system depicted in Figure 2.7, which corresponds to case (d). In the general case, each output may be dependent on both inputs and one may write (capital letters indicate the Laplace transform),

$$\begin{cases} O_1 = H_{11} I_1 + H_{12} I_2 \\ O_2 = H_{21} I_1 + H_{22} I_2 \end{cases} \qquad (2.21)$$

or, in matrix notation

$$\begin{Bmatrix} O_1 \\ O_2 \end{Bmatrix} = \begin{bmatrix} H_{11} & H_{12} \\ H_{21} & H_{22} \end{bmatrix} \begin{Bmatrix} I_1 \\ I_2 \end{Bmatrix} \qquad (2.22)$$

where O is the output Laplace transform matrix, I is the input Laplace transform matrix and H is the transfer function matrix. In the general case H is a $m \times n$ matrix, where m is the number of outputs and n is the number of inputs.

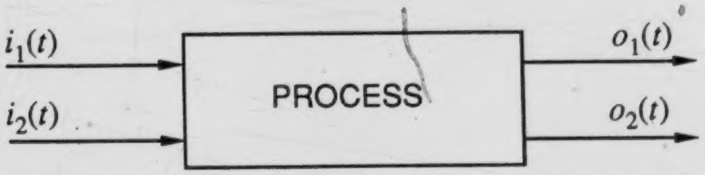
$i_1(t)$
$i_2(t)$
PROCESS
$o_1(t)$
$o_2(t)$

(a)

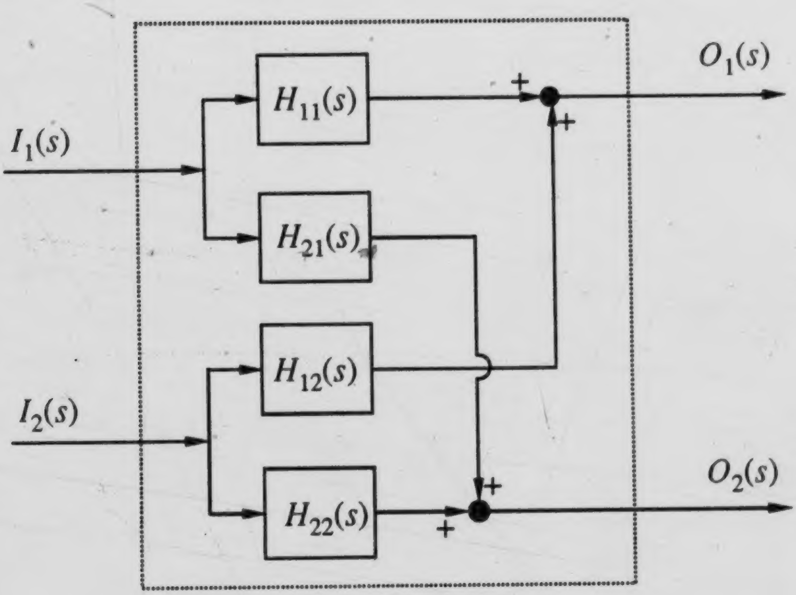
$H_{11}(s)$
$H_{21}(s)$
$H_{12}(s)$
$H_{22}(s)$
$I_1(s)$
$I_2(s)$
$O_1(s)$
$O_2(s)$
+
+
+
+

(b)

Fig. 2.7 (a) Two-input, two-output process.
(b) block diagram for the transfer function matrix.

The transfer function matrix is dependent on the flow pattern at the intersection and for the cases illustrated in Figure 2.5 it can be written as:

(a) Only one inlet

$$\begin{Bmatrix} O_1 \\ O_2 \\ O_3 \end{Bmatrix} = \begin{bmatrix} H_{11} \\ H_{21} \\ H_{31} \end{bmatrix} \{I_1\} \quad \Rightarrow \quad \begin{Bmatrix} C_1 \\ C_2 \\ C_3 \end{Bmatrix} = \begin{bmatrix} 1 \\ 1 \\ 1 \end{bmatrix} \{C_4\} \tag{2.23}$$

(b) Only one outlet

$$\{O_1\} = \begin{bmatrix} H_{11} & H_{12} & H_{13} \end{bmatrix} \begin{Bmatrix} I_1 \\ I_2 \\ I_3 \end{Bmatrix} \quad \Rightarrow \quad \{C_1\} = \frac{1}{Q_1} \begin{bmatrix} Q_2 & Q_3 & Q_4 \end{bmatrix} \begin{Bmatrix} C_2 \\ C_3 \\ C_4 \end{Bmatrix} \tag{2.24}$$

(c) discontinuous intersection

$$\begin{Bmatrix} O_1 \\ O_2 \end{Bmatrix} = \begin{bmatrix} H_{11} & H_{12} \\ H_{21} & H_{22} \end{bmatrix} \begin{Bmatrix} I_1 \\ I_2 \end{Bmatrix} \quad \Rightarrow \quad \begin{Bmatrix} C_1 \\ C_3 \end{Bmatrix} = \frac{1}{Q_2 + Q_4} \begin{bmatrix} Q_2 & Q_4 \\ Q_2 & Q_4 \end{bmatrix} \begin{Bmatrix} C_2 \\ C_4 \end{Bmatrix} \tag{2.25}$$

(d1) continuous intersection - complete mixing model

$$\begin{Bmatrix} O_1 \\ O_2 \end{Bmatrix} = \begin{bmatrix} H_{11} & H_{12} \\ H_{21} & H_{22} \end{bmatrix} \begin{Bmatrix} I_1 \\ I_2 \end{Bmatrix} \quad \Rightarrow \quad \begin{Bmatrix} C_1 \\ C_2 \end{Bmatrix} = \frac{1}{Q_3 + Q_4} \begin{bmatrix} Q_3 & Q_4 \\ Q_3 & Q_4 \end{bmatrix} \begin{Bmatrix} C_3 \\ C_4 \end{Bmatrix} \tag{2.26}$$

(d2) continuous intersection - streamline routing model

$$\begin{Bmatrix} O_1 \\ O_2 \end{Bmatrix} = \begin{bmatrix} H_{11} & H_{12} \\ H_{21} & H_{22} \end{bmatrix} \begin{Bmatrix} I_1 \\ I_2 \end{Bmatrix} \quad \Rightarrow$$

$$\Rightarrow \left| \begin{array}{lll} \begin{Bmatrix} C_1 \\ C_2 \end{Bmatrix} = \dfrac{1}{Q_1} \begin{bmatrix} Q_1 - Q_4 & Q_4 \\ Q_1 & 0 \end{bmatrix} \begin{Bmatrix} C_3 \\ C_4 \end{Bmatrix} & \quad \textit{for} \quad Q_2 \leq Q_3 & \quad (2.27\text{a}) \\ \begin{Bmatrix} C_1 \\ C_2 \end{Bmatrix} = \dfrac{1}{Q_2} \begin{bmatrix} 0 & Q_2 \\ Q_3 & Q_2 - Q_3 \end{bmatrix} \begin{Bmatrix} C_3 \\ C_4 \end{Bmatrix} & \quad \textit{for} \quad Q_2 \geq Q_3 & \quad (2.27\text{b}) \end{array} \right.$$

The transfer function matrix provides a convenient way to represent the mass distribution at the intersection. In this particular case, all the elements of the matrix are constants. Consequently, the structure of the expressions in both Real and Laplace domain are completely similar and the advantages gained by using the Laplace transform are minimal. In the general case, however, equivalent expressions in the Real domain are more complex, because the convolution integral is involved. Then, the Laplace transform is much more advantageous, because the convolution integral becomes a multiplication of two functions (refer to equation (2.9))

2.3.5 Selection of Mixing Models

The advantage of the complete mixing model is its simplicity. The early studies of Castillo et al. (1972) and Krizek et al. (1972) led to the conclusion that the complete mixing model was valid for laminar flow through intersections. The experimental work of Krizek et al. (1972), however, was not conclusive, because the intersection was limited to only one inlet and all the outlets had nearly identical discharges. Later experimental work has shown that in many situations mass followed the streamlines with very little mixing at the intersections (Wilson and Witherspoon, 1976; Hull and Koslow, 1986).

The proper choice of a mixing model is strongly dependent on the flow characteristics at the intersection and also on the diffusion properties of the mass being transported. Hull et al. (1987) presented a simplified analysis regarding the applicability of the two extreme mixing models. They considered the relation between the intersection residence time, $2b/V$, and the diffusion characteristic time, $(2b)^2/D_0$. Based on simple analytical solutions for the diffusion equation they concluded that the complete mixing model is valid for

$$\frac{(2b)}{V} > 0.5\frac{(2b)^2}{D_0} \qquad \text{or} \qquad V < 2\frac{D_0}{(2b)}$$

and the streamline routing model for

$$\frac{(2b)}{V} < 0.003\frac{(2b)^2}{D_0} \qquad \text{or} \qquad V > 333.\frac{D_0}{(2b)}$$

where $2b$ is the fracture aperture, V is the fluid velocity in the fracture and D_0 is the diffusion coefficient in pure fluid.

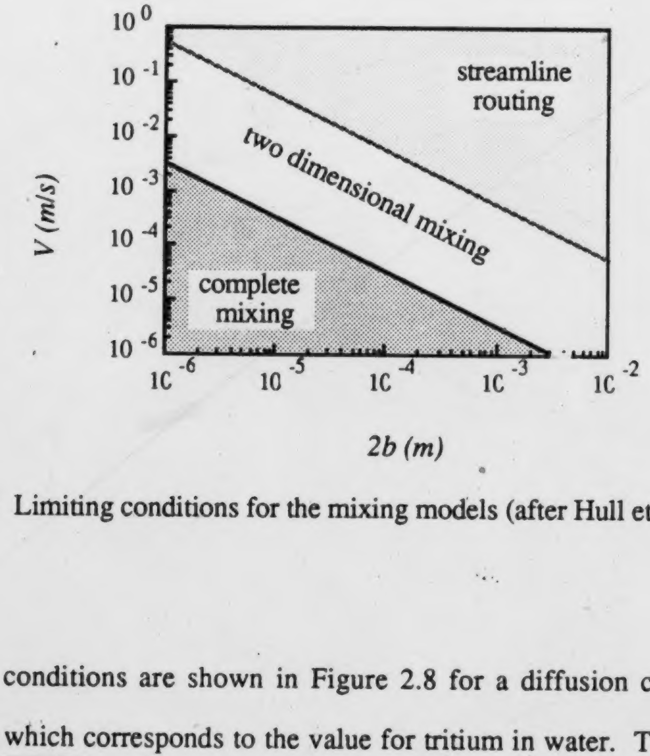

Fig. 2.8 Limiting conditions for the mixing models (after Hull et al., 1987)

These limiting conditions are shown in Figure 2.8 for a diffusion coefficient $D_0 = 1.67\times10^{-9}$ m^2/s, which corresponds to the value for tritium in water. The two ranges of representative fracture apertures used by Hull et al. (1987) are also included in Figure 2.8.

It is interesting to note that for crystalline repositories, characterized by small fracture apertures and low velocities, the complete mixing model may be a reasonable approximation, while for geothermal reservoirs, with large fracture apertures and relatively high velocities, the streamline routing may be more appropriate. Although these limits do not consider the mechanics of transport within the intersections, they give a good indication that both models are valid.

2.4 Analytical Solution for a Simple Fracture Network

This section presents an application of the analytical procedure for a simple fracture network. Because of the simplicity of the transfer function matrix for the intersection, it is preferable to use the physical approach, continuity equation, rather than the mathematical approach to evaluate the mass distribution at the intersection.

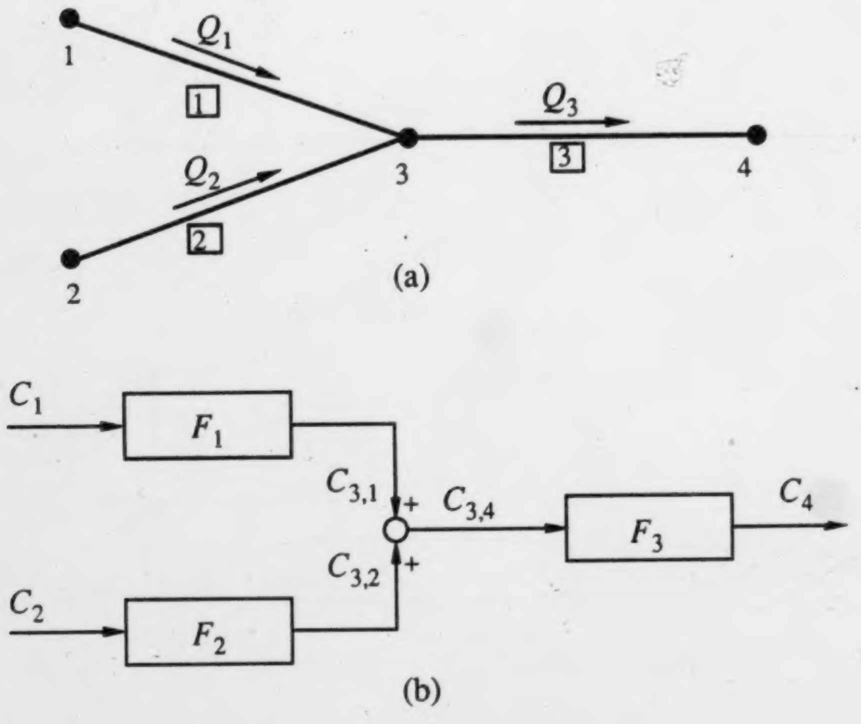

Fig. 2.9 Simple fracture system consisting of three segments and four nodes (a), and equivalent system representation (b).

Although the transfer function approach can provide analytical solutions for many fracture systems, the solutions for the simplified no-dispersion case can be easily obtained. For the general case, however, it is not possible to avoid the evaluation of the convolution integral. This will be made clear through the following example.

Figure 2.9a shows a simple system, consisting of three segments and four nodes. Assume that nodes 1 and 2 are the inlets and node 4 is the outlet. The problem is to find the breakthrough curve at node 4, given the inlet breakthrough curves at nodes 1 and 2. Figure 2.9b shows the equivalent system representation, with four subsystems. The functions F_1, F_2 and F_3 are the Laplace transforms of the unit step response function for each segment. According to equation (2.9), the output for the segment one is:

$$C_{3,1}(s) = C_1(s)\,F_1(s)\,s \tag{2.28}$$

and similarly for segment two:

$$C_{3,2}(s) = C_2(s)\,F_2(s)\,s \tag{2.29}$$

The outputs $C_{3,1}$ and $C_{3,2}$ become the inputs for the intersection subsystem. Using equation (2.24), the output $C_{3,4}$ is given by:

$$C_{3,4}(s) = \frac{Q_1}{Q_3}\,C_{3,1}(s) + \frac{Q_2}{Q_3}\,C_{3,2}(s) \tag{2.30}$$

If $\eta_{1,3} = Q_1/Q_3$ and $\eta_{2,3} = Q_2/Q_3$ are introduced, then the input for segment three is given by:

$$C_{3,4}(s) = \eta_{1,3}\,C_1(s)\,F_1(s)\,s + \eta_{2,3}\,C_2(s)\,F_2(s)\,s \tag{2.31}$$

By using equation (2.9) again, the output for segment three is given by:

$$C_4(s) = [\eta_{1,3}\, C_1(s)\, F_1(s)\, s + \eta_{2,3}\, C_2(s)\, F_2(s)\, s\,]\, F_3(s)\, s \tag{2.32}$$

or,

$$C_4(s) = \eta_{1,3}\, C_1(s)\, F_1(s)\, F_3(s)\, s^2 + \eta_{2,3}\, C_2(s)\, F_2(s)\, F_3(s)\, s^2 \tag{2.33}$$

Equation (2.33) is valid for any unit step response function. For the simplified no-dispersion solution, its Laplace transform can be put into the form:

$$F(s) = \frac{1}{s}\, exp\left[-\left\{A\left(s+\lambda\right)^{0.5} + B\left(s+\lambda\right)\right\}\right] \tag{2.34}$$

where the constants A and B are defined as

$$A = \frac{\theta\,(R_m\, D_m)^{0.5}\, L}{V\, b} \tag{2.35a}$$

$$B = \frac{R_f\, L}{V} \tag{2.35b}$$

Substituting equation (2.34) into equation (2.33) and simplifying, one obtains:

$$C_4(s) = \eta_{1,3}\, C_1(s)\, exp\left[-\left\{(A_1+A_3)\left(s+\lambda\right)^{0.5} + (B_1+B_3)\left(s+\lambda\right)\right\}\right] + \eta_{2,3}\, C_2(s)\, exp\left[-\left\{(A_2+A_3)\left(s+\lambda\right)^{0.5} + (B_2+B_3)\left(s+\lambda\right)\right\}\right] \tag{2.36}$$

The input functions c_1 and c_2 can be given, without loss of generality, by the unit step function, whose Laplace transform is $1/s$ (Abramowitz and Stegun, 1967). Equation (2.36) is then given by:

$$C_4(s) = \eta_{1,3}\, \frac{1}{s}\, exp\left[-\left\{(A_1+A_3)\left(s+\lambda\right)^{0.5} + (B_1+B_3)\left(s+\lambda\right)\right\}\right] + \eta_{2,3}\, \frac{1}{s}\, exp\left[-\left\{(A_2+A_3)\left(s+\lambda\right)^{0.5} + (B_2+B_3)\left(s+\lambda\right)\right\}\right] \tag{2.37}$$

Equation (2.37) has two components on the right hand side that have exactly the same form as equation (2.34). Therefore, the solution for c_4 , in the Real domain, can be obtained through a linear combination of solutions given by equation (2.11). The constants A and B, as defined by equation (2.35), represent now a summation of the contributions of two segments and must be replaced by their equivalents in equation (2.37).

If the general solution is now considered, its Laplace transform can be written as

$$F(s) = \frac{1}{s} exp\left[E - E\left\{1 + \frac{A}{E}\left(s + \lambda\right)^{0.5} + \frac{B}{E}\left(s + \lambda\right)\right\}^{0.5}\right] \tag{2.38}$$

where A and B are given by equation (2.35) and $E = (VL)/D$. Following the same procedure, the output for segment three is given by

$$\begin{aligned} C_4(s) = \; & \eta_{1,3} \frac{1}{s} exp\left[(E_1 + E_3) - E_1\left\{1 + \frac{A_1}{E_1}(s+\lambda)^{0.5} + \frac{B_1}{E_1}(s+\lambda)\right\}^{0.5} \right. \\ & \left. - E_3\left\{1 + \frac{A_3}{E_3}(s+\lambda)^{0.5} + \frac{B_3}{E_3}(s+\lambda)\right\}^{0.5}\right] + \\ & \eta_{2,3} \frac{1}{s} exp\left[(E_2 + E_3) - E_2\left\{1 + \frac{A_2}{E_2}(s+\lambda)^{0.5} + \frac{B_2}{E_2}(s+\lambda)\right\}^{0.5} \right. \\ & \left. - E_3\left\{1 + \frac{A_3}{E_3}(s+\lambda)^{0.5} + \frac{B_3}{E_3}(s+\lambda)\right\}^{0.5}\right] \end{aligned} \tag{2.39}$$

Equation (2.39), however, does not lead to an equivalent form of equation (2.38), as in the no-dispersion case, and there is no alternative but to perform the inverse Laplace transform, either analytically or numerically.

In more complex fracture networks, the application of this procedure to successive nodes allows the calculation of the breakthrough curve for every node (refer to Appendix A, where a complete derivation for a simple fracture network is presented). The number of components present in the solution for a node is directly related to the number of independent paths the contaminant can follow from the source(s) to that particular node. This number can be very large. As an example, assume that, on average, two segments arrive at a node and two leave it. If the contaminant source is represented by only one node, then the first downstream nodes connected to it will have only one component in their solution. The second series of nodes may have a maximum of two components in each solution, the third series may have a maximum of four, the fourth series may have a maximum of eight and so on. For this particular source arrangement the maximum number of components in a solution will be $2^{(n-1)}$, where n represents the order of the node ($n = 1$ represents the first nodes, $n = 2$, the second series and so on). In a particular series of nodes of order n, only one or two may have the maximum number of components in their solution (regular mesh with fractures of infinite length), but this is enough to show how difficult the task of finding analytical solutions can be.

2.5 Behaviour and Limitations of the Response Functions

Once a unit step response function has been selected for the fracture segment, it is important to understand how the different variables influence the behaviour of the response function and what limitations are involved. The behaviour of the response function can be analyzed by introducing appropriate dimensionless parameters that reduce the number of variables and relate different transport processes. The limitations of the response functions are mainly concerned with the assumption of infinite matrix used by Tang et al. (1981) in their derivations of the analytical solutions.

2.5.1 Dimensionless analysis

Although the analytical solutions derived by Tang et al. (1981) include all the important transport processes and have a fairly simple form, the relative importance of the processes is not clearly perceived. This situation is largely due to the number of variables involved. A way to overcome this problem is to introduce dimensionless parameters that group the variables together. In general, two processes are usually represented in one parameter and its numerical value is a measure of the relative importance of one process to the other. The analysis of these dimensionless parameters may help understand the behaviour of the response functions.

Based on the Buckingham's π-theorem (Streeter and Wylie, 1970) and following Ogata and Banks (1961) and Rasmuson (1984), four dimensionless parameters may be derived, considering advection as the basic process:

$$\begin{aligned} &\text{Time Parameter:} && \tau = \frac{V\,t}{R_f\,L} \\ &\text{Matrix Parameter:} && \delta = \frac{\theta\,(R_m\,D_m)^{0.5}}{bR_f}\left(\frac{R_f\,L}{V}\right)^{0.5} \\ &\text{Decay Parameter:} && \Lambda = \frac{\lambda R_f\,L}{V} \\ &\text{Dispersion Parameter:} && \mathbf{Pe} = \frac{V\,L}{D} \end{aligned} \tag{2.40}$$

The time parameter is a dimensionless time, whose reference is the time advection takes to travel a length L in the fracture. The other three parameters can be thought as being a relation between the characteristic time for the process involved (radioactive decay, diffusion into the matrix or dispersion) and the advection time. For instance, in the matrix parameter, if the advection time is greater than the diffusion time, then diffusion into matrix becomes important. The dispersion parameter is usually referred in the literature as the Peclet number. The use of these dimensionless parameters is convenient because it simplifies the notation of the response functions and equations (2.11) and (2.12) become:

(a) General solution

$$\frac{c}{c_0} = \frac{exp(Pe/4)}{\sqrt{\pi}} \int_{l}^{\infty} exp\left(-\xi^2 - \frac{(Pe)^2}{4\xi^2} - \frac{\Lambda Pe}{4\xi^2}\right) \cdot$$

$$\left\{ + exp\left[-\Lambda^{0.5}\delta\frac{Pe}{4\xi^2}\right] \cdot erfc\left[\frac{\left(\delta\frac{Pe}{4\xi^2}\right)}{2\left(\tau - \frac{Pe}{4\xi^2}\right)^{0.5}} - \Lambda^{0.5}\left(\tau - \frac{Pe}{4\xi^2}\right)^{0.5}\right] + \right.$$

$$\left. + exp\left[+\Lambda^{0.5}\delta\frac{Pe}{4\xi^2}\right] \cdot erfc\left[\frac{\left(\delta\frac{Pe}{4\xi^2}\right)}{2\left(\tau - \frac{Pe}{4\xi^2}\right)^{0.5}} + \Lambda^{0.5}\left(\tau - \frac{Pe}{4\xi^2}\right)^{0.5}\right]\right\} d\xi \qquad (2.41)$$

(b) Simplified no-dispersion solution

$$\frac{c}{c_0} = \frac{1}{2}\, exp\left(-\Lambda\right) \cdot$$

$$\left\{ + exp\left[-\Lambda^{0.5}\delta\right] \cdot erfc\left[\frac{\delta}{2(\tau-1)^{0.5}} - \Lambda^{0.5}(\tau-1)^{0.5}\right] + \right.$$

$$\left. + exp\left[+\Lambda^{0.5}\delta\right] \cdot erfc\left[\frac{\delta}{2(\tau-1)^{0.5}} + \Lambda^{0.5}(\tau-1)^{0.5}\right]\right\} \qquad (2.42)$$

Figures 2.10 to 2.14 show solutions of the above equations under different conditions, in order to illustrate the relative importance of each process. In Figure 2.10 only the effect of the matrix parameter is considered. It shows three distinct regions: for $\delta \leq 0.1$ matrix diffusion is negligible; for $0.1 \leq \delta \leq 10$ there is a transition zone from advection dominated to diffusion dominated transport; and for $\delta \geq 10$ diffusion into the matrix is fully dominant and the breakthrough curves become self-similar, meaning that a variation in δ implies only in a scaled variation in τ (shifting property).

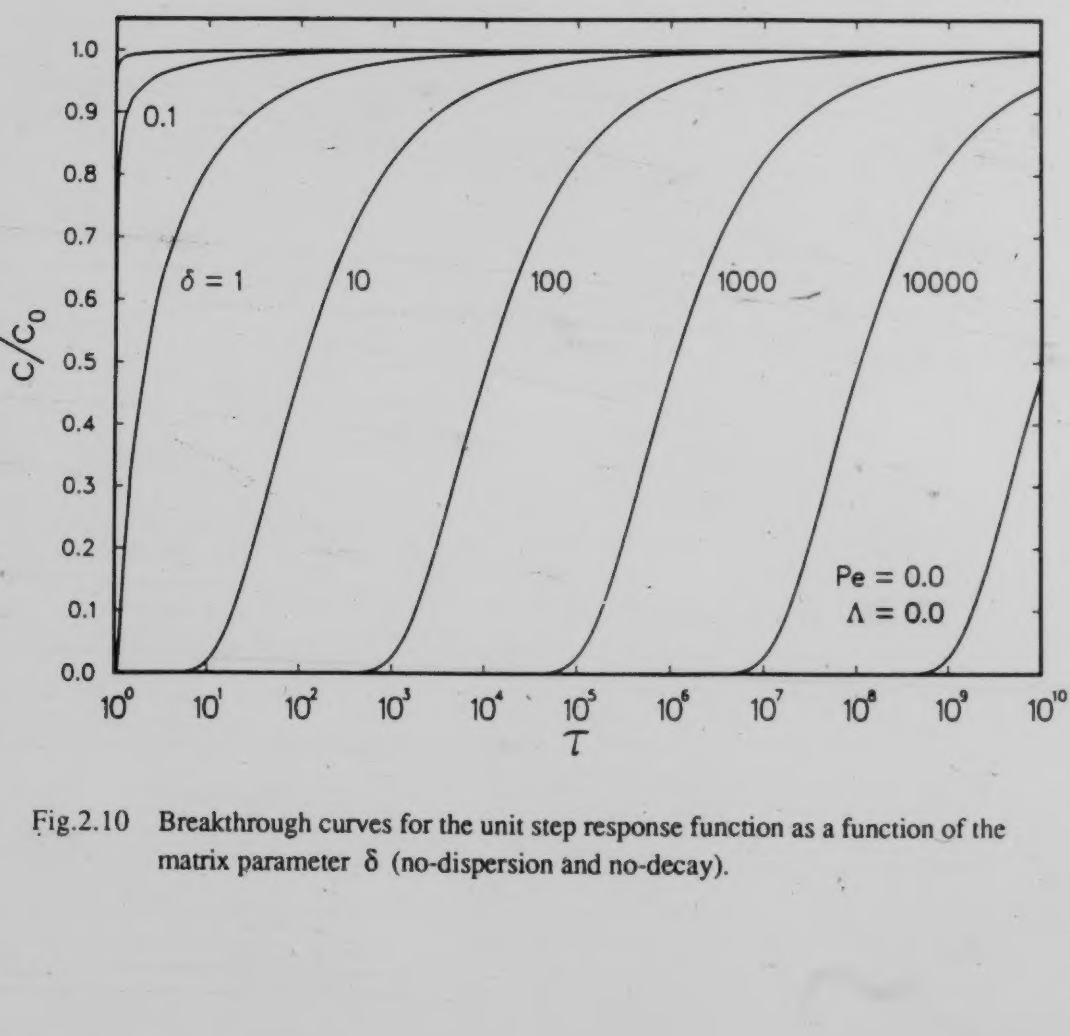

Fig.2.10 Breakthrough curves for the unit step response function as a function of the matrix parameter δ (no-dispersion and no-decay).

When dispersion is introduced, the breakthrough curve starts to happen earlier. The smaller the Peclet number the earlier it happens. For **Pe** ≥ 100, the effects of dispersion are negligible. For **Pe** ≤ 0.1 dispersion becomes so important, that it would apply only to the regions very close to the source, under very high concentration gradients. Actually, in this case diffusion in the fracture, rather than dispersion, would be the dominant process (recall that $D = \alpha V + D_0$, where α is the dispersivity and D_0 is the diffusion coefficient in the fracture). Figure 2.11 shows the results for three different values of the matrix parameter. From this Figure it is very clear that the simplified equation for no-dispersion can be safely used for **Pe** ≥ 100 .

When radioactive decay is introduced, care must be taken when choosing one of the two solutions. Dispersion increases the amount of mass that arrives early, producing a higher steady-state value than the simplified no-dispersion solution would. Figures 2.12 to 2.14 suggest that the early arrival is not sensitive to variations in either the decay parameter or the matrix parameter for **Pe** ≤ 1.0 , reinforcing the point that **Pe** ≤ 0.1 applies only to the region close to the source. For $\Lambda \geq 5.0$, the concentration falls to very small levels, and its importance is a function of the current safety levels adopted.

The importance of the above analysis is to determine the range in which each process is important. As a general rule it may be concluded that dispersion is important in the range $1.0 \leq$ **Pe** ≤ 100. For **Pe** ≥ 100 the simplified solution for no-dispersion can be used without introducing significant errors. The matrix parameter has an important effect when $\delta \geq 0.1$. The importance of the decay parameter is related to the safety levels required for a particular contaminant and a preliminary range could be $0.0 \leq \Lambda \leq 10.0$.

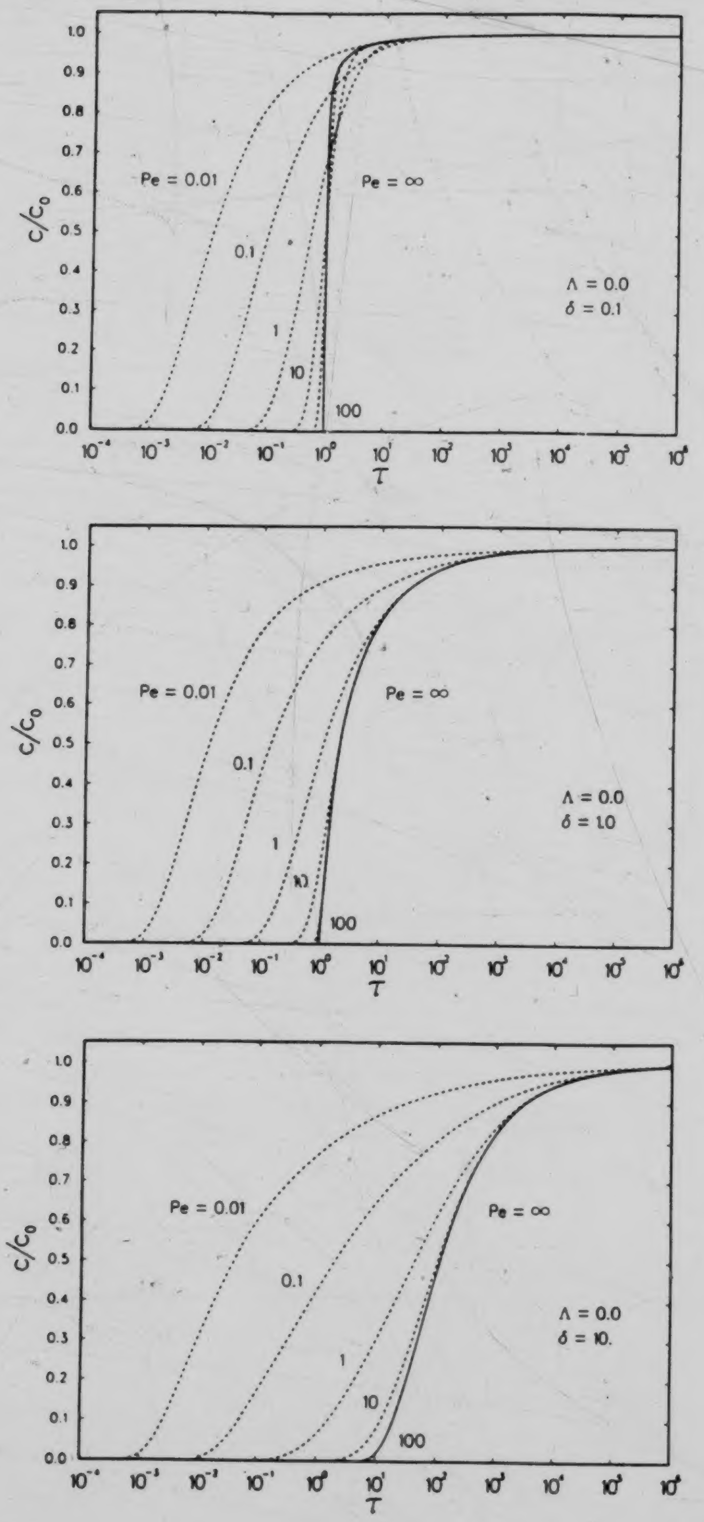

Fig. 2.11 Breakthrough curves for the unit step response function, considering the influence of both the matrix parameter δ and the dispersion parameter ***Pe***, for Λ = 0.0.

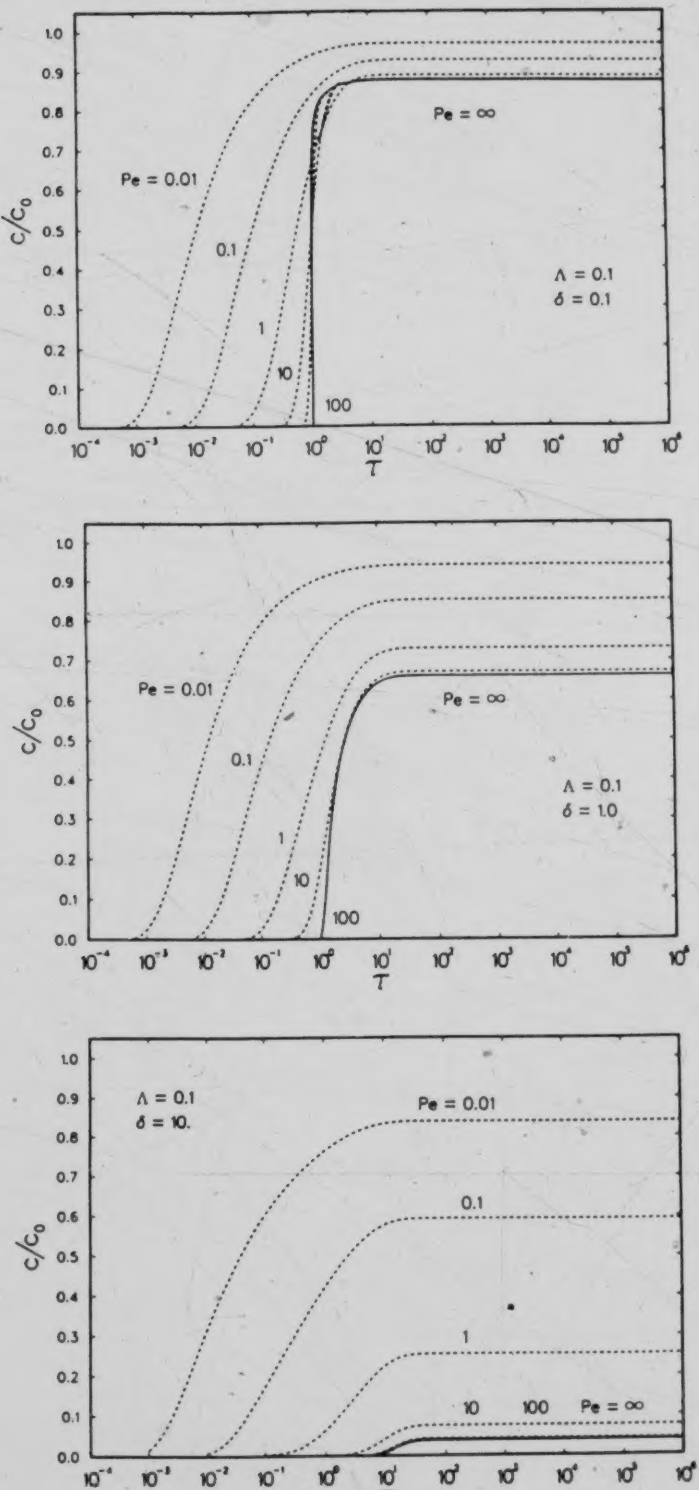

Fig. 2.12 Breakthrough curves for the unit step response function, considering the influence of both the matrix parameter δ and the dispersion parameter ***Pe***, for $\Lambda = 0.1$.

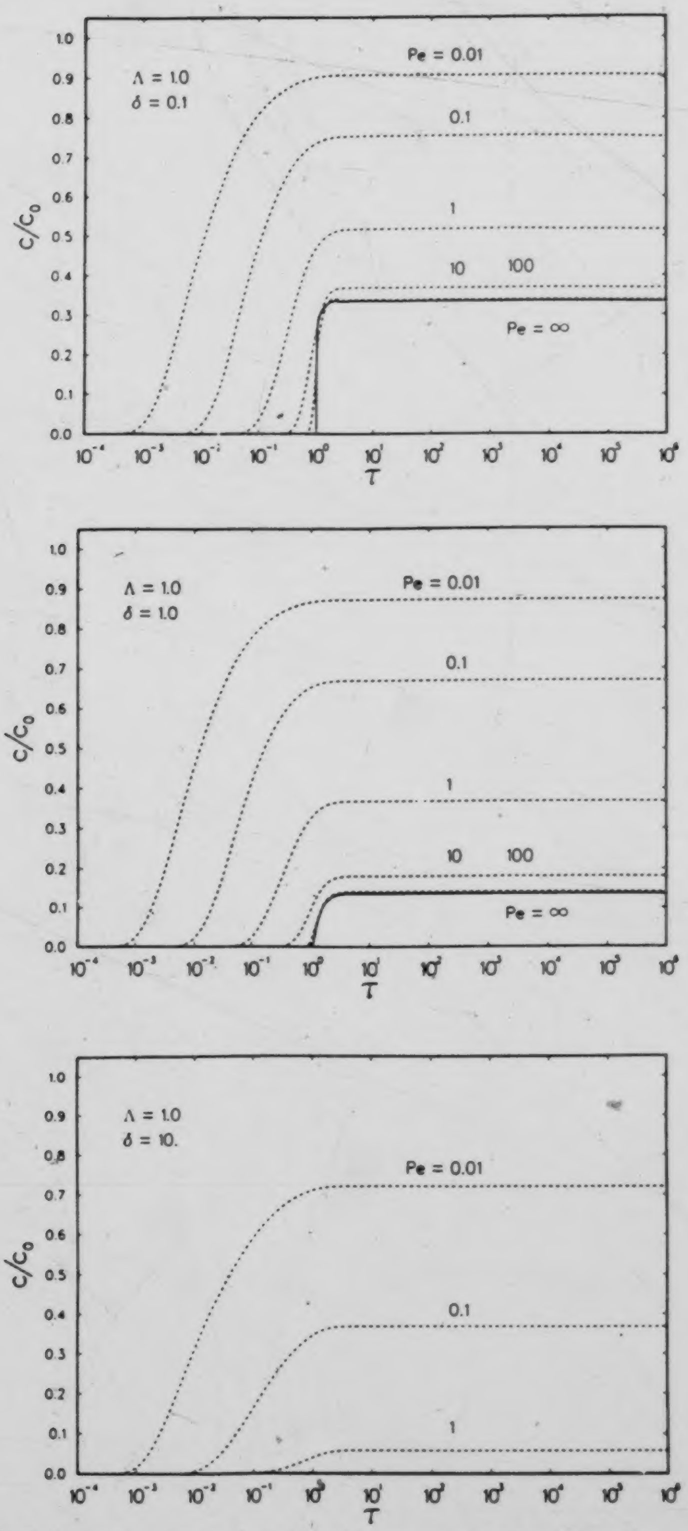

Fig. 2.13 Breakthrough curves for the unit step response function, considering the influence of both the matrix parameter δ and the dispersion parameter $\boldsymbol{Pe}$, for $\Lambda = 1.0$.

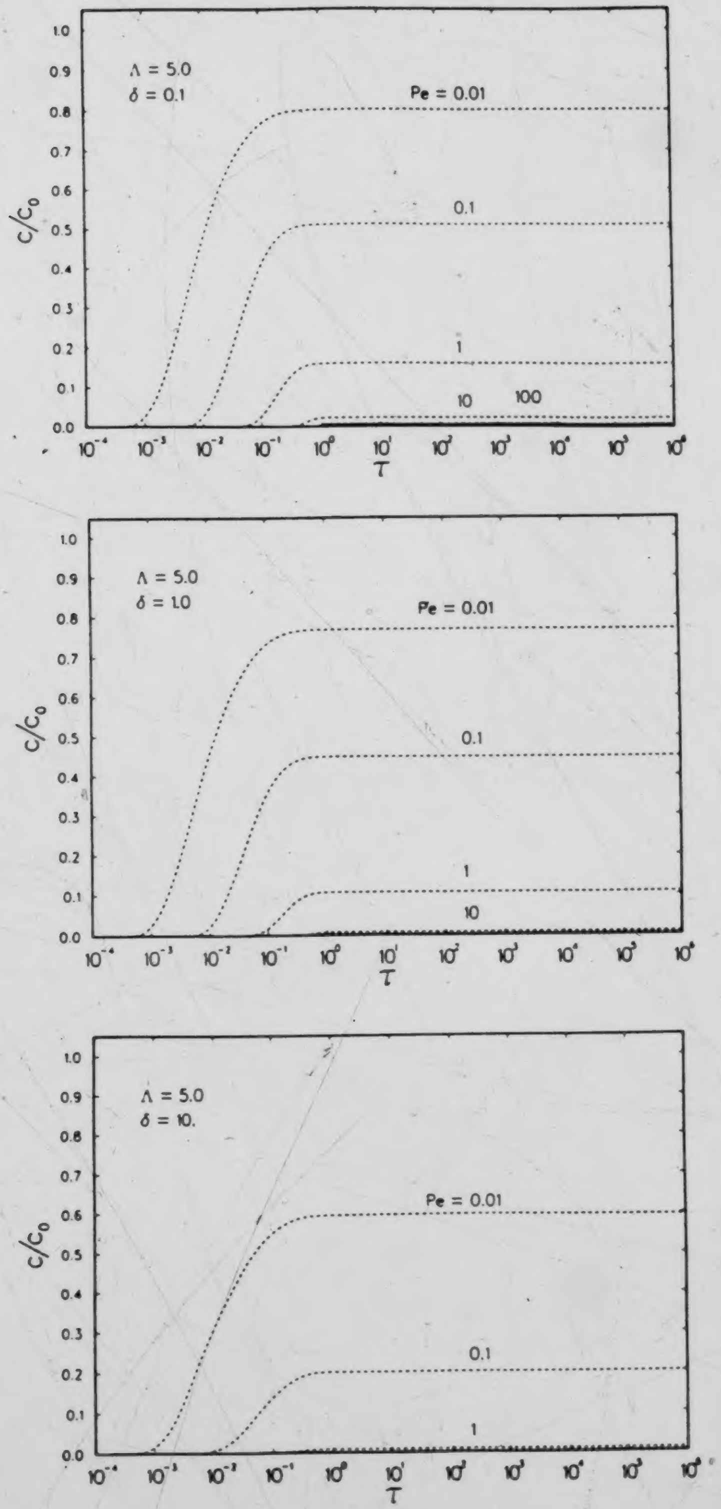

Fig. 2.14 Breakthrough curves for the unit step response function, considering the influence of both the matrix parameter δ and the dispersion parameter Pe, for $\Lambda = 5.0$.

2.5.2 Limitations of the response function

Tang et al. (1981) have considered an infinite matrix as boundary condition for the diffusion into the matrix. For a fractured rock system, this may impose some restrictions, once the solution for both the fracture and the matrix will be valid while the concentration front does not reach the block centerline. For radionuclides the maximum depth of penetration can be estimated from the steady state equation for the concentration in the matrix (Tang et al., 1981),

$$\frac{c_m}{c_0} = exp\left\{ L\left[\frac{V}{2D} - \left(\frac{V^2}{4D^2} + \frac{\lambda R_f}{D} + \frac{\theta\,(R_m\,D_m)^{0.5}}{b\,D}\right)\right]^{0.5}\right\} \cdot$$

$$\cdot\ exp\left\{ - \left(\frac{\lambda R_m}{D_m}\right)^{0.5} \cdot (x-b)\right\} \qquad (2.43)$$

The maximum depth of penetration, for a constant strength source, occurs at the origin and can be obtained by setting $L = 0$ in equation (2.43),

$$(x-b)_{max} = ln\left(\frac{c_0}{c_m}\right) \cdot \left[\frac{D_m\,t_{1/2}}{ln(2)\,R_m}\right]^{0.5} \qquad (2.44)$$

The concentration front, however, is not well defined. There is not a "zero" concentration front and some concentration level must be set arbitrarily in order to define the depth of penetration. Fortunately, the variation in the $ln(c_0/c_m)$ is not very large for detection limits c_m/c_0 between 0.01 and 0.001 ($4.61 \leq ln(c_0/c_m) \leq 6.91$) and meaningful estimates of the penetration depth can be obtained. For a detection limit $c_m/c_0 = 0.005$, equation (2.44) becomes

$$(x-b)_{max} = 5.3 \cdot \left[\frac{D_m\,t_{1/2}}{ln(2)\,R_m}\right]^{0.5} \qquad (2.45)$$

Since the maximum depth of penetration is proportional to the radionuclide half-life, long lived radionuclides, of which neptunium (^{237}Np) is an example, will pose the severest constraint. The neptunium half-life is $t_{1/2} = 2.14\times10^{6}$ years and both the diffusion and the retardation coefficients can be estimated from the Swedish KBS-3 study for crystalline rocks (Rasmuson and Neretnieks, 1986) . Therefore, $D_m = 1.0\times10^{-11}$ m^2/s and $R_m = 2.0\times10^{6}$ (strongly sorbing), for a rock porosity of $\theta = 0.5\%$ (Neretnieks, 1980). By substituting these values into equation (2.45), the maximum depth of penetration for ^{237}Np can be estimated as,

$$(x - b)_{max} = 5.3 \cdot \left[\frac{1.0\times10^{-11} \cdot 2.14\times10^{6} \cdot (365\cdot 86400)}{ln(2) \cdot 2.0\times10^{6}}\right]^{0.5} \approx 0.12 \text{ m} \qquad (2.46)$$

If the radionuclide is, instead, intermediately sorbing with $R_m = 2.0\times10^{4}$ (Neretnieks, 1980), then the maximum depth of penetration becomes $(x-b)_{max} = 1.2$ m. It is seen, therefore, that the infinite matrix limitation is not severe at all. For intermediately sorbing radionuclides this would imply a fracture spacing of 2.5 m, what is much less than expected for nuclear repository sites [50 – 100m before reaching a major pathway (Neretnieks and Rasmuson, 1984; Rasmuson and Neretnieks, 1986)].

If it happens that the maximum depth of penetration is greater than half the fracture spacing, then a response function based on an analytical solution for finite blocks idealized as slabs or spheres could be used (e.g., Sudicky and Frind, 1982; Rasmuson, 1984, 1985a).

For stable species the depth of penetration can be estimated from the simplified solution for the concentration in the matrix, given by Tang et al. (1981) as,

$$\frac{c_m}{c_0} = erfc\left\{\frac{1}{2}\left[\frac{L\,\theta\,(R_m D_m)^{0.5}}{V\,b} + \left(\frac{R_m}{D_m}\right)^{0.5}\cdot(x-b)\right]\cdot\left[t-\frac{R_f\,L}{V}\right]^{-0.5}\right\} \tag{2.47}$$

By setting $L = 0$ (greatest penetration occurs at the source and is independent of dispersion), one obtains

$$\frac{c_m}{c_0} = erfc\left[\frac{1}{2}\left(\frac{R_m}{D_m\cdot t}\right)^{0.5}\cdot(x-b)\right] \tag{2.48}$$

The depth of penetration is then given by

$$(x-b) = 2\,erfc^{-1}\left(\frac{c_m}{c_0}\right)\cdot\left(\frac{D_m\,t}{R_m}\right)^{0.5} \tag{2.49}$$

Using the same reasoning as before, it can be shown that the variation in $erfc^{-1}\,(c_m/c_0)$ is relatively small for $0.001 \leq (c_m/c_0) \leq 0.01$ ($2.32 \geq erfc^{-1}\,(c_m/c_0) \geq 1.82$). Adopting for the concentration front the level $(c_m/c_0) = 0.005$, one obtains for the penetration depth,

$$(x-b) = 4\cdot\left(\frac{D_m\,t}{R_m}\right)^{0.5} \tag{2.50}$$

Equation (2.50) is unbounded, what means that there is no maximum penetration depth. The penetration depth is a function of time, and the response functions will only apply for a limited time range, for non-sorbing or weakly sorbing, non-decaying solutes. This time range is dependent on the fracture spacing and on the matrix diffusion coefficient. Accurate estimates, however, can be obtained for the early part of the breakthrough curves, which are not influenced by the finite matrix block size, because mass transport in the fracture is, usually, much faster than mass transport in the matrix (Neretnieks et al., 1980; Tang et al., 1981; Rasmuson, 1984, 1985a, 1985b; Moreno and Rasmuson, 1986).

3. NUMERICAL IMPLEMENTATION

The simulation of contaminant transport in a fracture network can be divided into three parts: fracture network generation, flow modelling and transport modelling. The first two parts have been extensively treated in the literature (Long et al., 1982; Schwartz et al. 1983; Robinson, 1984; among others) and only a brief description is presented here. The transport modelling involves a completely new method and will be considered in detail. The theoretical approach described in chapter 2 is implemented in two computer codes, the first involved with fracture generation and flow modelling and the second involved with solving the mass transport problem. These codes are verified against known analytical solutions for a single fracture and simple fracture networks.

3.1 Fracture Network Generation

Fractures in the real systems have very complex surfaces, with variable shapes and sizes. Their aperture can be variable due to the inherent roughness of the fracture surfaces. Subsequent changes due to stress or mineral deposition can close original openings in the fracture plane. Following conventional practice, fractures are idealized by representing their surfaces as planes and their aperture as constant throughout. In this work, it is further assumed that fractures can be modelled in a two-dimensional system, where only the traces of the fracture planes on an intersecting plane are considered. Fractures are thus represented by straight lines with four characteristic parameters: the location in space of their midpoints, their orientation with respect to the coordinate axis, their length and their aperture.

These four parameters are a function of the type of rock and exhibit great variability due to the different physical processes to which the rock mass has been subjected. They are considered random variables and may be described by appropriate probability distributions. The description of the fractures is simplified by grouping into sets, fractures that have the same trend in the orientation. Generally, fractures within a given set are thought to be formed by the same mechanisms and consequently the parameters associated with fractures from a set are considered to be similar. Several sets may be present in the rock mass, but in many situations four orientations often predominate and are usually consistent over large areas (Price, 1974; Mollard, 1988).

The approach for generating the fractures is based on commonly used conceptualizations of real fracture systems. It has been assumed that: 1) the fracture orientation is constant for a given set (Price, 1974; Bridges, 1975; Mollard, 1988); 2) the fracture spacing is determined by the location of the fracture midpoints, which are selected from a uniform distribution; 3) the fracture length obeys an exponential distribution (Cruden, 1977), where only the tail is sampled, in order to produce a reasonable degree of connectivity (Schwartz et al., 1983); and 4) the fracture aperture is given by a log-normal distribution (Snow, 1970).

Following Long et al. (1982) and Schwartz and Smith (1988), fractures are generated in a rectangular region that is larger than the actual flow region, in order to maintain appropriate fracture densities close to the boundaries. Both regions are concentric and the generating region is double the size of the actual region. Each fracture set is generated independently and the total number of fractures in each set must be specified. Individual fractures within a set are generated sequentially in three basic steps (Long et al., 1982): 1) sampling of the fracture midpoint position; 2) sampling of the fracture length; and 3) sampling of the fracture aperture. After the fracture has been defined, the code checks its position in relation to the actual flow region and only the portion that falls into it is saved.

When all sets have been generated, the intersections are calculated and numbered. The resulting fracture segments are identified, numbered and associated with the intersections at their ends. In this work intersections are also referred to as nodes and both are used interchangeably throughout the text. A connectivity table is prepared for every node, relating all the adjacent nodes and respective segments connected to it. This table is used later in the mass transport program.

The generation of fractures is not restricted to orthogonal sets. Any orientation and any number of sets can be accommodated. The only restriction, due to numerical limitations, is that only two fractures can intersect at a point. In order to simplify the solution for the head distribution, all dead end and isolated fractures are removed from the network (Schwartz et al., 1983; Robinson, 1984).

3.2 Flow Modelling

The flow of a viscous, incompressible fluid through a fracture is often idealized with the parallel plate model. For a laminar steady flow, velocity can be related to hydraulic gradient by an equation very similar to Darcy's equation (Marsily, 1986):

$$V = \frac{g}{12\nu}(2b)^2\frac{\Delta H}{L} = K_f\frac{\Delta H}{L} \tag{3.1}$$

where $\Delta H/L$ is the hydraulic gradient (ΔH being the drop in hydraulic head over a distance L), $2b$ is the fracture aperture, g is gravity, ν is the kinematic viscosity, V is the fracture mean velocity and K_f is the fracture hydraulic conductivity. The discharge per unit width is given by:

$$Q = \frac{g}{12\nu}(2b)^3 \frac{\Delta H}{L} \tag{3.2}$$

The parallel plate model of a discrete fracture has formed the basis of several different flow models (e.g., Long et al., 1982; Robinson, 1984; Rouleau, 1984; Schwartz and Smith, 1983; Hopkirk and Gilby, 1984; among others). Experimental work (e.g., Witherspoon et al., 1980) has shown that equation (3.2) can be applied irrespective of the rock type and is valid whether the fractures are fully open or partially closed due to stress. Conditions, however, do exist when this model may not hold (Gale, 1982). Deviations from the ideal parallel plate model, due to the roughness of the adjoining fracture surfaces, tend to reduce the flow and they may be accounted for by introducing a correction factor $1/f$ into equations (3.1) and (3.2). In the investigations of Whiterspoon et al. (1980), f varied between 1.04 and 1.65, representing up to 15% decrease in the fracture aperture (smaller effective aperture). In cases where fracture surfaces are in contact, this correction alone may not be adequate to describe the flow properly.

Having developed a flow equation for an idealized fracture, the next step in modelling is to solve the flow through a fracture network subjected to different boundary conditions. The procedure adopted in this work uses the concepts of pipe network analysis, as described by Jeppson (1976). A general framework for this class of problems can be found in Strang (1988). First, continuity equations are written for each fracture intersection (node). The discharges per unit width, as given by equation (3.2), are then substituted by the unknown nodal heads. The resulting system of linear equations is symmetric and can be solved simultaneously for the unknown head values.

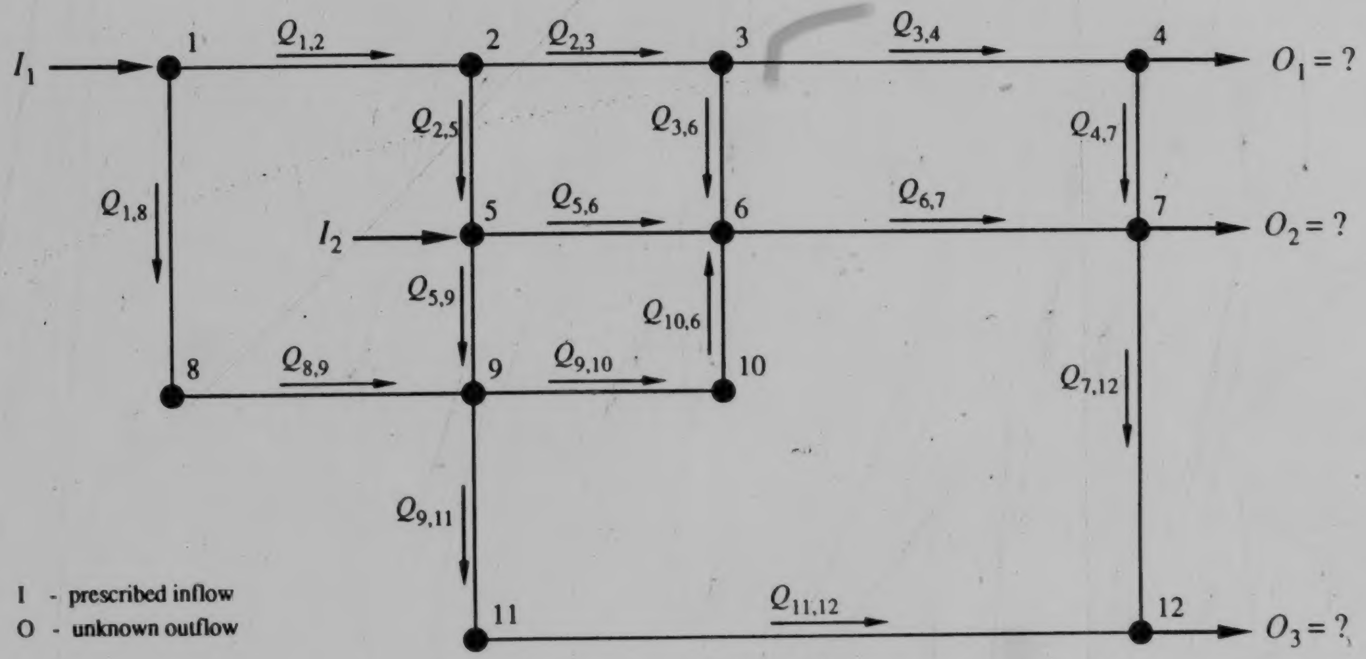
I_1
1
$Q_{1,2}$
2
$Q_{2,3}$
3
$Q_{3,4}$
4
$O_1 = ?$
$Q_{1,8}$
$Q_{2,5}$
$Q_{3,6}$
$Q_{4,7}$
I_2
5
$Q_{5,6}$
6
$Q_{6,7}$
7
$O_2 = ?$
$Q_{5,9}$
$Q_{10,6}$
8
$Q_{8,9}$
9
$Q_{9,10}$
10
$Q_{7,12}$
$Q_{9,11}$
I - prescribed inflow
O - unknown outflow
11
$Q_{11,12}$
12
$O_3 = ?$

Fig. 3.1 Simple fracture network to exemplify the flow modelling procedure

Consider, for instance, the simple fracture network depicted in Figure 3.1. The continuity equation for node 5 is given by:

$$I_2 + Q_{2,5} = Q_{5,6} + Q_{5,9} \tag{3.3}$$

where $Q_{i,j}$ represents the discharge from node i to node j and I_2 is a possible well recharge/discharge. Using equation (3.2) and substituting discharges for hydraulic heads, one obtains

$$I_2 + \beta_{2,5}(H_2 - H_5) = \beta_{5,6}(H_5 - H_6) + \beta_{5,9}(H_5 - H_9) \tag{3.4}$$

where $\beta_{i,j}$ represents the characteristics of the fracture segment between nodes i and j and is given by

$$\beta_{i,j} = \left(\frac{g}{12\nu}\frac{(2b)^3}{L}\right)_{i,j} \tag{3.5}$$

Rearranging equation (3.4), one obtains

$$-\beta_{2,5}H_2 + \left(\beta_{2,5} + \beta_{5,6} + \beta_{5,9}\right)H_5 - \beta_{5,6}H_6 - \beta_{5,9}H_9 = I_2 \tag{3.6}$$

This equation has only the heads as unknowns. By writing similar continuity equations for all the nodes, a system of linear equations is obtained which can be solved simultaneously for the unknown head values.

In this procedure, boundary conditions can include both prescribed head and flow values. Prescribed flow values are simply introduced into the I_2 term for the corresponding boundary node. Prescribed head nodes are dealt with by a variant of the "penalty" method: the continuity equation for the node with known head is not eliminated from the system of equations, instead, it is reformulated such that the diagonal coefficient is set to one and all others to zero; the RHS contains then the appropriate prescribed head value for that node. The final system of linear equations is solved by the Gauss elimination method, using bandwith storage for a symmetrical matrix.

In the code developed, boundary conditions are defined in terms of prescribed head values which are assigned to the node boundaries according to the procedure used by Long et al. (1982) and Schwartz and Smith (1988). First, values of hydraulic head are specified at all four corners of the rectangular area (Figure 3.2). By linear interpolation it is possible to use these values at the corners to define the hydraulic head at nodes along the side boundaries. This approach allows one to fix the regional hydraulic gradient at any desired orientation, when the anisotropic behaviour of the fracture system is under consideration. Internal wells and prescribed flux boundaries can also be specified.

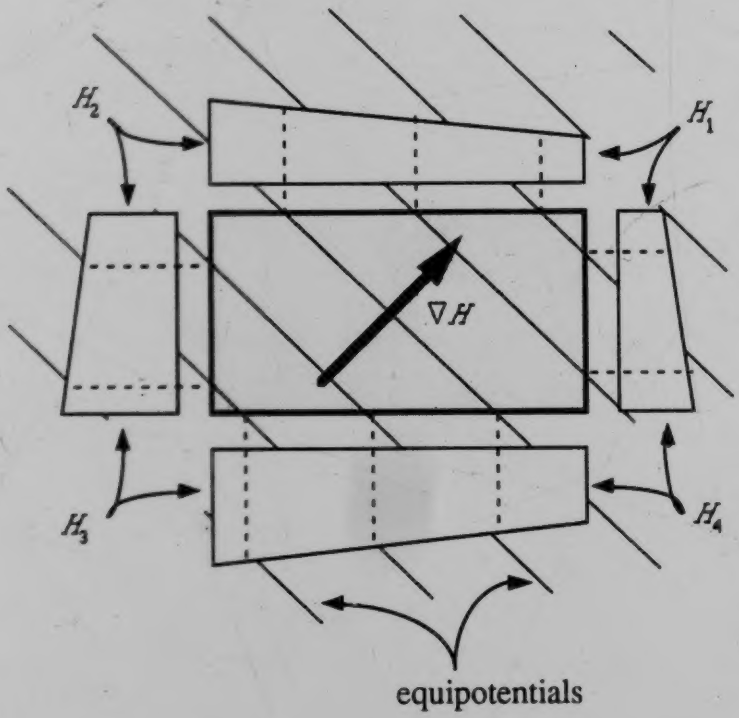

Fig. 3.2 Definition of boundary conditions for the flow modelling procedure.

3.3 Transport Modelling

For modelling mass transport in a fracture network, it is assumed that the network consists of two basic components, the fracture segment and the fracture intersection. The fracture segment is responsible for all the physical processes happening in a fracture, while the intersection (or node) is responsible for the appropriate linking between the segments by distributing the incoming mass into the outgoing segments.

In the fracture segment, there is no consideration of spatial variations and the intervening mass transport processes are lumped together into a unit step response function that is characteristic of each segment. By knowing the response function and the variation with time of the concentration at the input end of the fracture segment, it is possible to calculate the breakthrough curve at the output end of the segment through the convolution integral, as given by equation (2.8).

Mass distribution at intersections can be treated by either the complete mixing or the streamline routing model. The complete mixing model, as pointed out in section 2.3, is very simple and requires only one equation to describe the mass balance at the node. Concentration can be associated with the nodes, requiring less computer memory for storage of the breakthrough curves, because there are, in general, fewer nodes than segments. The streamline routing model, however, is more complex and requires that concentration be associated with the segments leaving the node. In this case, the segments have associated with them their input concentration. In the code developed, both mixing models were implemented, but the description that follows considers only the streamline routing model, because the complete mixing model can be regarded as a special case of the streamline routing model (refer to section 2.3).

The discrete form of the convolution integral (equation 2.5) is used to numerically calculate the mass transport through a fracture segment. The convolution equation, as derived in section 2.2, assumes that the response of the system is due to a unit step excitation and, therefore, any general input function has to be discretized into a series of steps in order to apply the transfer function method. To numerically evaluate the breakthrough curve at the end of the segment, three important factors must be considered: (1) the unit step response function itself; (2) the discretization of the complex input function; and (3) the time points for the evaluations of the output function.

The unit step response function has been treated at length in Chapter 2 and it is assumed that an efficient code is available for it. The discretization of the input function and the definition of the time points to evaluate the output function are discussed, respectively, in sections 3.3.1 and 3.3.2. Once the basic procedure for calculating the breakthrough curve at the end of a segment is known, it is then possible to describe the implementation to a fracture network. This is done in section 3.3.3.

3.3.1 Discretization of the input function

In general, the input function is complex and has to be discretized in a series of steps to allow proper evaluation of the output function. Two parameters are necessary to define the steps: their magnitude and their location in time. The concentration steps Δc_i, as shown in Figure 3.3, can have any magnitude, but it is preferable to make them equal to simplify calculations. Equation (2.5) becomes then a summation of delayed values of the unit step response function,

$$c_m(t) = \Delta c \sum_{i=1}^{n} f_m(t - \tau_i) \qquad (3.7)$$

where c_m is the relative concentration (c/c_{max}), $\Delta c = 1/n$, f_m is the unit step response function for the mth segment and τ_i is the time associated with the i^{th} concentration step (vide Figure 3.3). Accuracy of the numerical procedure is primarily dependent on the number of subdivisions n that discretizes the input function. The greater the number, the better the accuracy.

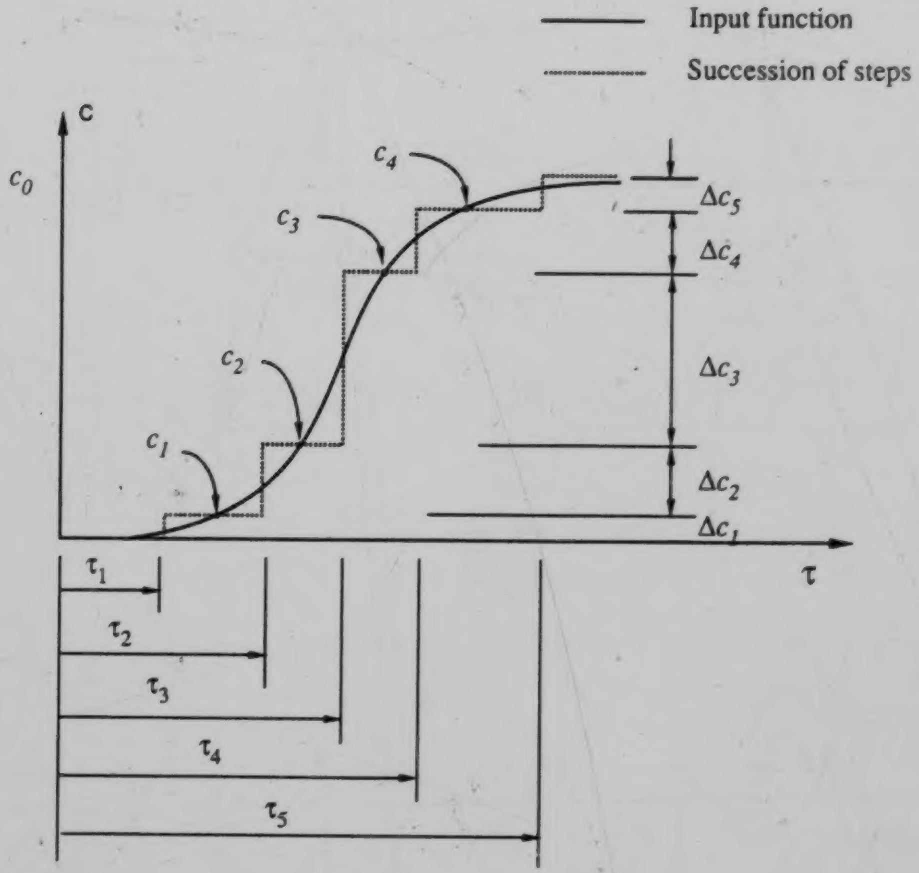
Input function
Succession of steps
c
c_0
c_4
c_3
c_2
c_1
Δc_5
Δc_4
Δc_3
Δc_2
Δc_1
τ
τ_1
τ_2
τ_3
τ_4
τ_5

Fig. 3.3 Discretization of the input function for a fracture segment.

Once the magnitude of the concentration steps has been defined, it is possible to define their location in time. Figure 3.4 presents the scheme adopted for the definition of the time τ_i that is related to the concentration step Δc_i. Any intermediate i^{th} step should increase the input concentration from the $(i-1)\Delta c$ level to the $i\Delta c$ level. If the time values for these two concentration levels are known (t^*_{i-1} and t^*_i), then the time τ_i will be given by the average of these two time values.

For the first and last concentration step another procedure has to be devised, because the intervals $[0, \Delta c]$ and $[(n-1)\Delta c, 1]$ are not closed: according to the analytical solutions, the relative concentration is never zero or one. The solution is to associate the time τ_i with a certain concentration level within the discretized step. This is accomplished by introducing two user defined parameters, ε_1 and ε_2, such that τ_1 is the time corresponding to the $\varepsilon_1\Delta c$ concentration level and τ_n is the time corresponding to the $(1 - \varepsilon_2\Delta c)$ concentration level (refer to Figure 3.4). The natural choice for these parameters is 0.5, the middle of the concentration interval. This value is used for the first interval, but $\varepsilon_2 = 0.3$ is used for the last interval. Initially, it was thought that $\varepsilon_2 = 0.3$ would give a better approximation for the long tail, but preliminary tests showed no significant difference between $\varepsilon_2 = 0.3$ and $\varepsilon_2 = 0.5$ The accuracy of the approximation is mostly controlled by the number of discretization steps, as explained in section 3.5, and variations in either ε_1 or ε_2 will have negligible effect on the accuracy, as n gets large.

3.3.2 Location in time of the output function

The calculation of the breakthrough curve at the end of the segment requires the definition of discrete time points as basic data. There are, however, some difficulties in defining these time points. Although the convolution equation can be evaluated at any

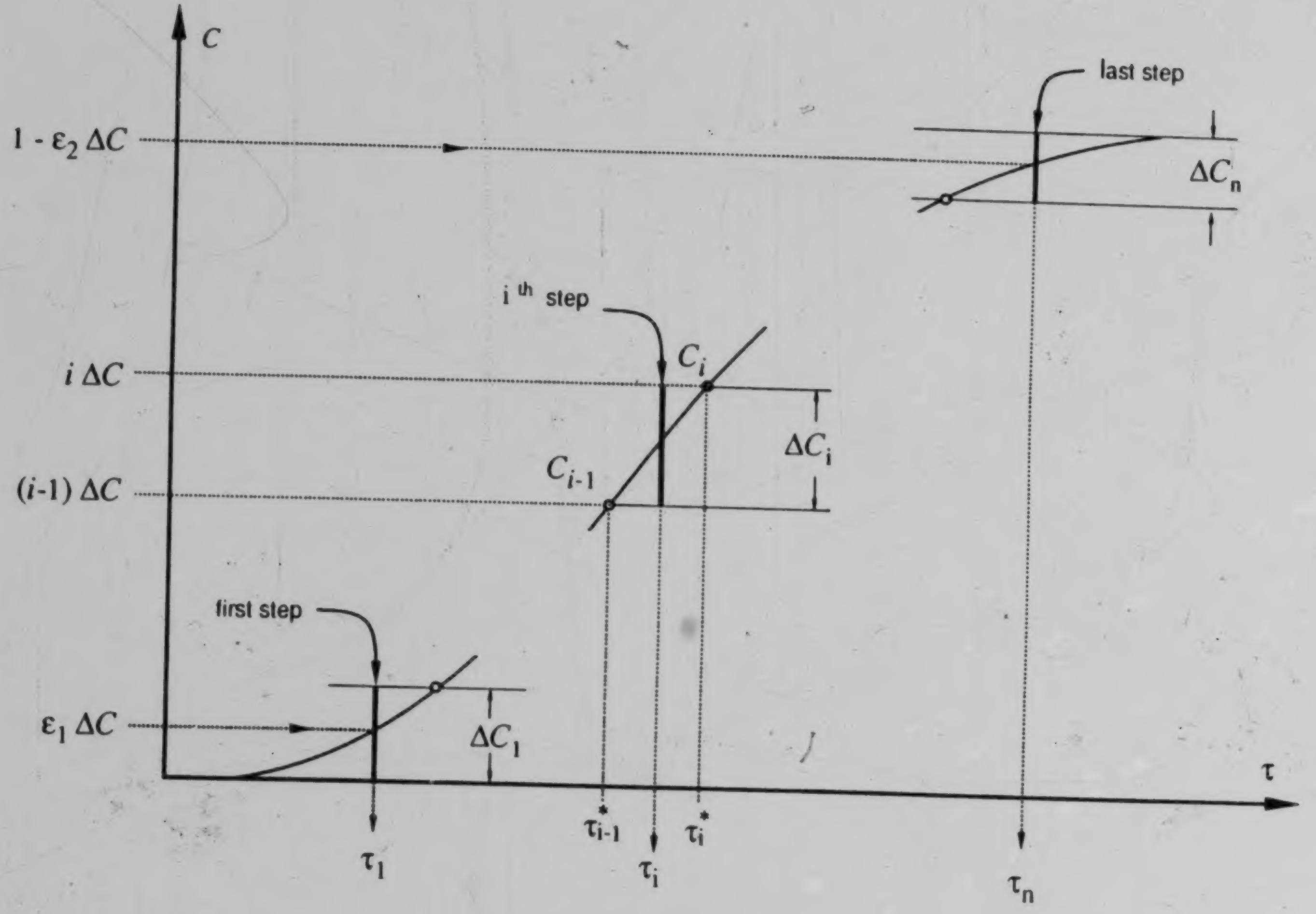
C
τ
$1 - \varepsilon_2 \Delta C$
$i \Delta C$
$(i\text{-}1) \Delta C$
$\varepsilon_1 \Delta C$
first step
i^{th} step
last step
C_i
C_{i-1}
ΔC_1
ΔC_i
ΔC_n
τ_1
τ^*_{i-1}
τ_i
τ^*_i
τ_n

Fig. 3.4 Location in time of the discretized concentration steps.

point, the location in time of the breakthrough curve is not known a priori and many function evaluations may be necessary to fully describe it. In addition, the breakthrough curve has a characteristic mathematical behaviour: it is bounded in terms of concentration, but it is not in terms of time. This means that although the concentration tends to zero at small times or to a maximum value at large times, it will never, mathematically speaking, reach these values. A natural solution to this problem would be to solve equation (3.7) inversely for time values, given concentration values. But this is not feasible, because of the many components present in the convolution equation. The only solution is then to solve equation (3.7) directly for concentration, given the time values.

Therefore, it is necessary to properly estimate the time range within which the breakthrough curve is contained. Here, it has been assumed that the time range corresponds to the time required for the relative concentration (c/c_{max}) at a point to increase from 0.005 to 0.995. These time end points are denoted, respectively, $t_{.005}$ and $t_{.995}$.

If the input function were given by only one step, then the time range would be just $[t^1_{.005}, t^1_{.995}]$, where $t^1_{.005}$ and $t^1_{.995}$ are obtained by inversely solving the unit step response function for the particular segment. For a multi-step input function the time range is estimated by $[\tau_1 + t^1_{.005}, \tau_n + t^1_{.995}]$, where τ_1 and τ_n are the times associated, respectively, with the first and last discretized concentration steps. Naturally, the time range obtained in this way is larger than the actual time range for the breakthrough curve and it is dependent on the discretization of the input function, the finer the discretization, the larger the time range. Care must then be taken with the discrete distribution of points in this time range in order to ensure that the breakthrough curve is well described.

This procedure for the estimation of the time range leads to the consideration of the predictor-corrector method for evaluating the breakthrough curve. Initially, a rough estimate of the breakthrough curve is made based on a large time range and few discrete time points. Then the time range is properly "accessed" and a finer distribution of discrete time points is used to obtain a better representation of the breakthrough curve. This procedure is discussed in detail in the next section.

3.3.3 Description of the procedure for a fracture network

For a fracture network, the breakthrough curves are calculated sequentially, node by node, from the source point to the outlets. For the breakthrough curves at a node to be calculated, all upstream breakthrough curves must have already been calculated in order to determine the mass transfer along the connecting segments. The objective of the calculations at the node is to determine the breakthrough curves of the incoming segments and the appropriate input function for each outgoing segment. The procedure is similar to that described in sections 3.3.1 and 3.3.2. The difference now is that the time range should be large enough to contain all the incoming breakthrough curves, and that an appropriate routing procedure has to be incorporated into the calculations.

Figure 3.5 illustrates the flow chart for the mass transport code. Once the basic input data are read, the program processes all the nodes present in the network, in order of decreasing hydraulic head. This ensures that upstream nodes will have already being calculated, when a specific node is under calculation. Due to the nature of the fracture network, it is possible that mass may not be transported through major pieces of the fracture network. Provisions have been taken to avoid calculations for the corresponding nodes.

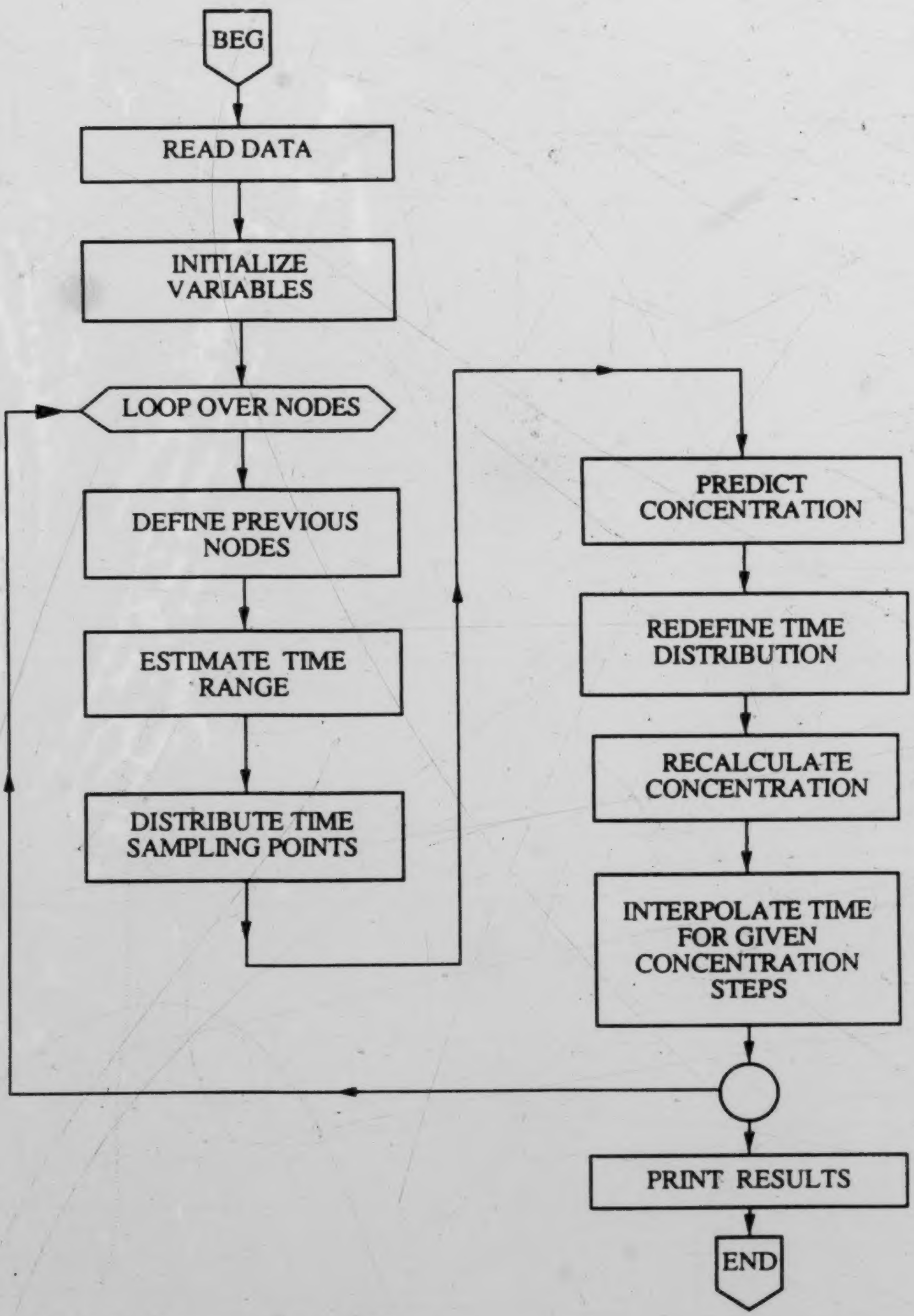
BEG
READ DATA
INITIALIZE VARIABLES
LOOP OVER NODES
DEFINE PREVIOUS NODES
ESTIMATE TIME RANGE
DISTRIBUTE TIME SAMPLING POINTS
PREDICT CONCENTRATION
REDEFINE TIME DISTRIBUTION
RECALCULATE CONCENTRATION
INTERPOLATE TIME FOR GIVEN CONCENTRATION STEPS
PRINT RESULTS
END

Fig. 3.5 Program flow chart

At node level, a basic predictor-corrector scheme is used to evaluate the input function for the outgoing segments. Initially, a rough estimate of the node output breakthrough curves is made. In a second stage, this estimate is refined to ensure better description of the curves.

a) first stage: prediction

The prediction stage provides an initial estimate of the node output breakthrough curves. It has to consider the mass transfer through the node incoming segments and the appropriate mass distribution to the output segments. For this initial estimate, the time range may not be well defined and few time points are used to evaluate the breakthrough curve. The prediction basically involves three steps.

First, the upstream segments connected to the node being evaluated are identified and an estimate of the time range for each incoming breakthrough curves is made, as explained in section 3.3.1. Because time ranges for each segment may overlap each other, a global time range for the node, containing all the individual breakthrough curves that arrive at the node, is defined.

The second step is to distribute time sampling points within the global time range. From the behaviour of the unit step response function (Figure 2.7), the maximum time range (for one segment) spans over five orders of magnitude. An educated guess suggested that 5 points per log-cycle would give a reasonable density of points to represent the estimated breakthrough curve. In this way, 25 points are logarithmically distributed within the time range and four points are added to each side of the time range, in order to include the extremes of the curve. Depending on the delay experienced by the different paths that arrive at a particular node, the time range may, actually, span over more than five orders of magnitude. This fact, however, does not invalidate the procedure, because the main concern, at this point, is only to define the time spaned by the breakthrough curve.

In the third step, the routing procedure is defined, according to the magnitude of the discharges and to the relative position of the segments (Hull and Koslow, 1986). The breakthrough curves leaving the node are then evaluated for all time sampling points by using equation (3.7) and equations (2.15) to (2.19).

Because the time range is "large" enough to contain all the time ranges for each arriving segment, the estimated breakthrough curve may not be very well defined, due to the lack of points. To get a better description of the breakthrough curve, concentrations should be recalculated, based on a corrected and possibly refined distribution of the time sampling points. At the end of this stage, the relative position in time of the breakthrough curves is known. The next section explains how a better description of the breakthrough curve can be obtained, by refining and redistributing the time sampling points.

b) second stage: correction

For the second stage, the relative position of the breakthrough curves is already known, although its description may be poor. The objective is then to improve the description of the output breakthrough curves, by increasing the number of time points and redistributing them in a better defined time range.

The redistribution of time points can be understood with reference to Figure 3.6, which shows a completely developed breakthrough curve with a long tail. Eleven key concentration points, taken as the nine deciles of the relative concentration plus the two extreme concentration levels 0.005 and 0.995, are also plotted along the curve.

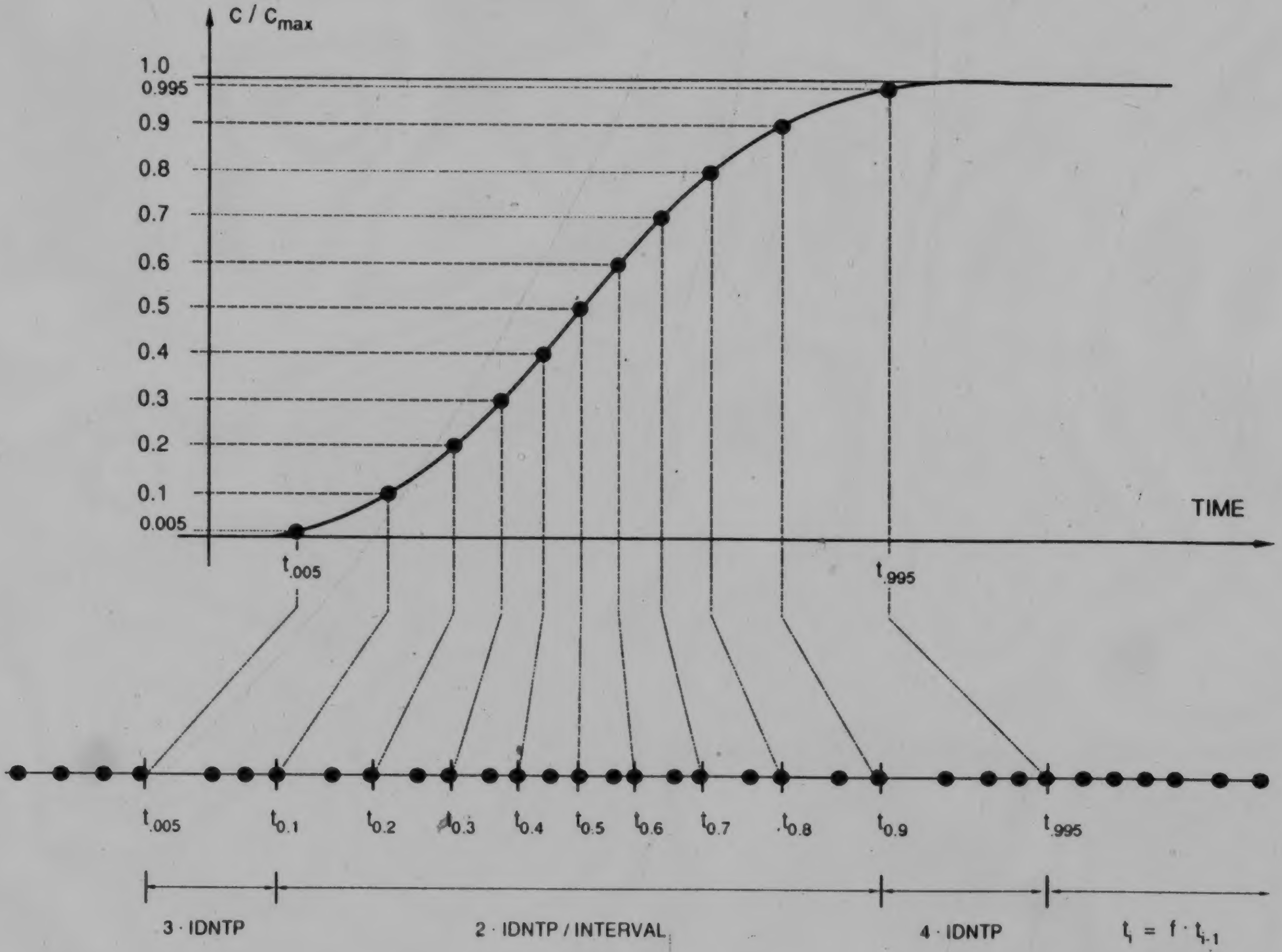
C / C_{max}
1.0
0.995
0.9
0.8
0.7
0.6
0.5
0.4
0.3
0.2
0.1
0.005
TIME
$t_{.005}$
$t_{.995}$
$t_{.005}$
$t_{0.1}$
$t_{0.2}$
$t_{0.3}$
$t_{0.4}$
$t_{0.5}$
$t_{0.6}$
$t_{0.7}$
$t_{0.8}$
$t_{0.9}$
$t_{.995}$
3 · IDNTP
2 · IDNTP / INTERVAL
4 · IDNTP
$t_i = f \cdot t_{i-1}$

Fig.3.6 Key concentration points and respective time points for the redistribution of the time sampling points.

It is important to note that, although these key points are uniformly distributed along the concentration range $0 - c_{max}$, they are not as well distributed along the time range $t_{.005} - t_{.995}$. Therefore, to better represent the breakthrough curve, the time points should be distributed in such a way that the resulting concentrations associated with them are distributed as uniformly as possible within the range $0 - c_{max}$. This is done in two steps.

The first step is to calculate the time that corresponds to each of the eleven key concentration points. Because the estimated breakthrough curve is given in a discrete form, these time values must be interpolated. The interpolation procedure assumes that a function of the type,

$$\frac{c}{c_{max}} = erfc\left(\frac{A}{\sqrt{t - B}}\right) \tag{3.8}$$

where A and B are fitting parameters and *erfc* is the error function, could be fitted to any pair of consecutive points.

In the second step, a variable number of time points is logarithmically distributed within each interval between the key concentration points, according to the special pattern shown in Figure 3.6. This procedure requires a minimum of 23 time points and the total number of time points (NTP), that is user defined for the second stage, is automatically adjusted to be a multiple of 23. Beyond the time range, three and six extra points are, respectively, added for $t < t_{.005}$ and $t > t_{.995}$. Their distribution follows a geometric progression, based on the internal interval that is closest to the limits of the time range. If the number of discretized steps for the input functions is greater than hundred, then the limits for the time range are substituted for $t_{\Delta c/2}$ and $t_{1-\Delta c/2}$ and the new time range will contain the old one.

Now, concentrations can be reevaluated at these new time points, following the same procedure that was used in the prediction stage. The last part in the correction stage is to define the time each future discretized concentration step will happen, when this curve becomes the input function for the next segment. The times t_1^*, t_i^* and t_n^*, corresponding, respectively, to the concentration levels $\varepsilon_1 \Delta c$, $i\Delta c$ and ($1 - \varepsilon_2 \Delta c$.), are interpolated from the breakthrough curve with the aid of equation (3.8). The time associated with each future discretized concentration step is then calculated (refer to Figure 3.3). For the first and last step, the times are, respectively, given by $\tau_1 = t_1^*$ and $\tau_n = t_n^*$. For the intermediate steps, the time is given by:

$$\tau_i = \frac{1}{2}\left(t_{i-1}^* + t_i^*\right) \qquad (3.9)$$

At a node level, calculations are finished and this procedure continues for all the nodes. The final part is reporting of the results. All the input functions for the segments are stored and may be conveniently retrieved for the calculation of the spatial distribution of concentration in the network.

3.4 Verification of the Transport Model

The modelling approach is verified using two different tests. In the first, the numerical results are compared to the results of an analytical solution for the problem of transport down a single fracture subject to diffusion into the matrix (Tang et al., 1981). In the second test a simple fracture network was considered for which the analytical solution could be calculated by hand in order to verify the mass distribution procedure at the intersections.

3.4.1 Single Fracture Problem

The accuracy of the numerical solution is dependent on the number of concentration steps (NC) that discretizes the input function. The finer this discretization, the better the accuracy. Another parameter that influences the accuracy is the number of time points (NTP) used to evaluate the breakthrough curve at the segment end. If few time points are used, then the breakthrough curve may not be well described and the consecutive discretization of this curve, as the input for the next segment, may carry extra cumulative errors that degenerates the solution.

This test considers the effects of both NC and NTP on the overall accuracy of the numerical solution. The simplified case of no-dispersion is used for most of the simulations, but a few examples also include dispersion in the fracture.

The single fracture problem is described by the following parameters: $V = 1.0\text{x}10^{-5}$ m/s, $2b = 1.0\text{x}10^{-4}$ m, $\theta = 0.01$, $R_f = 1.0$, $R_m = 1.0$, $\lambda = 0.0$ and $L = 250.0$ m. Two different values for the effective matrix diffusivity, $D_m = 1.0\text{x}10^{-10}$ and $D_m = 1.0\text{x}10^{-12}$ m^2/s, are used so as to present a diversity of possible behaviours. The smaller diffusion coefficient leads to advection dominated flow, while the other one leads to diffusion dominated flow . Numerically, the single fracture is represented by twenty-five equal fracture segments ($L_i = 10.0$ m). This arrangement provides a test of the error involved with the increasing number of discrete convolution integrals evaluated.

In the simulations, six different values were used for NC, 25, 50, 100, 200, 500, 700, and two for NTP, 25 and 50. In Figure 3.7 the general trend of the numerical solution for the simplified case of no-dispersion is analyzed for the lower discretization level of the input function, NC = 25 and NTP = 25. Each curve represents the

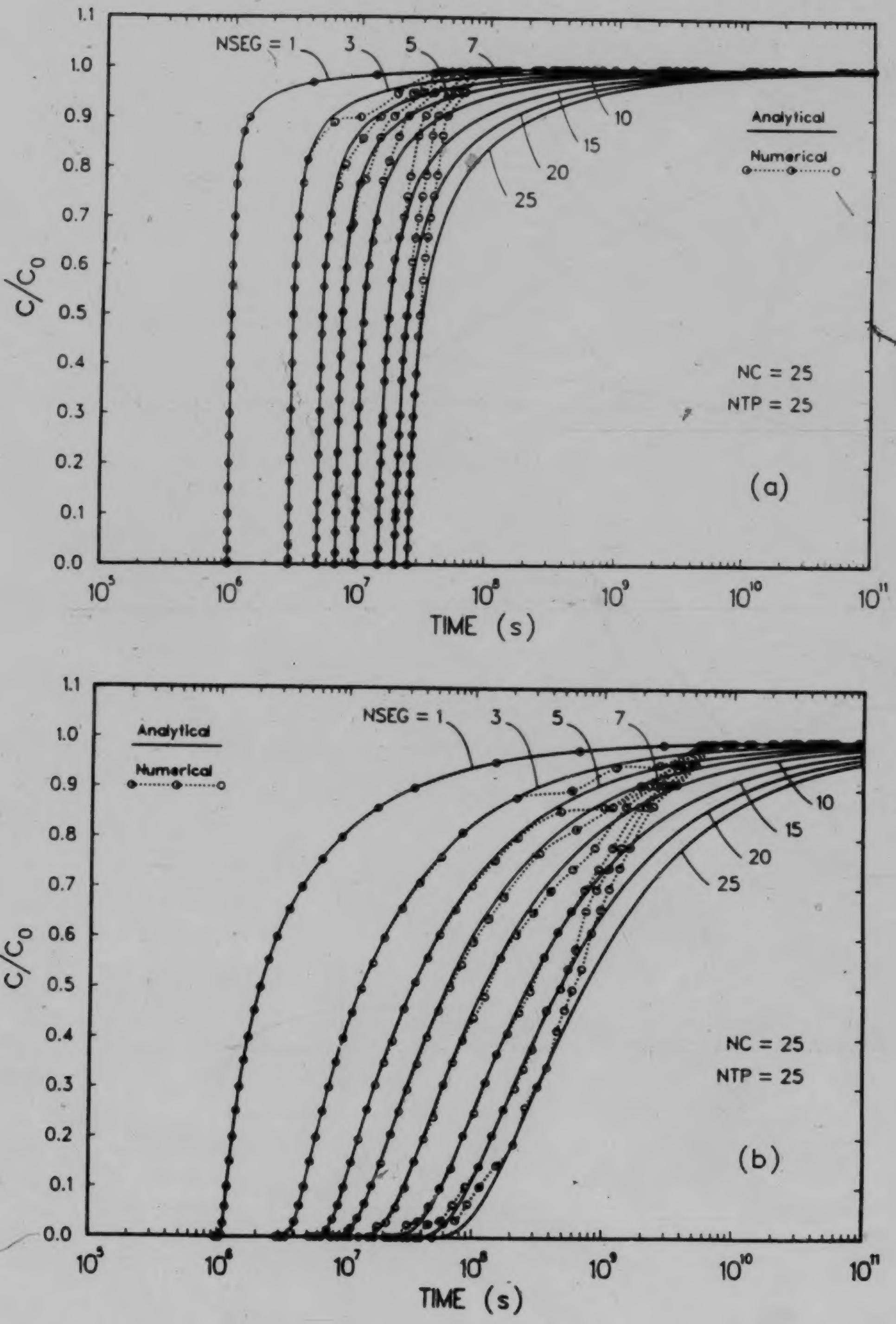

Fig. 3.7 Breakthrough curves obtained at the end of different segments, for a linear succession of segments. (a) advection dominated. (b) diffusion dominated.

breakthrough curve for different number of segments. At the end of the first segment (NSEG = 1), the numerical solution is exact, because the input function is given by the unit step function. As successive breakthrough curves are calculated, the accuracy of the solution deteriorates. This behaviour is the same for both the advection and diffusion dominated cases. It is interesting to note that, although the results are very poor for the tail of the breakthrough curves, they are amazingly good for the early part of the curves.

Figure 3.8 presents a summary of the breakthrough curves obtained for the twenty-fifth segment, considering different values for NC. It is clear that as NC increases, so does the accuracy of the numerical solution. Errors smaller than 2% are achieved for NC ≥ 500, for both the advection and diffusion dominated cases.

The number of time points, however, is not as important as NC. If NC is small, as in Figure 3.7, the increase in NTP may even degrade the accuracy, as shown in Figure 3.9. In this case NTP was doubled, but small plateaus (two or more points close together along the same horizontal line) appeared and the accuracy was no better. This is a typical indication that the number of discretization steps is small and must be increased. For large values of NC, the increase in NTP only slightly improves the accuracy, as shown in Figures 3.10 and 3.11 for both the advection and diffusion dominated cases.

This behaviour can be explained by considering the nature of the errors involved in the numerical approximations. These errors are due to the discretization of the input function and the interpolation of the discrete breakthrough curve. For the cases described above, the discretization errors dominate over the interpolation errors, causing NC to substantially increase before NTP has to do so. The initial number of time points, 25, was sufficient to give a good description of the breakthrough curves, but, as NC increases, the

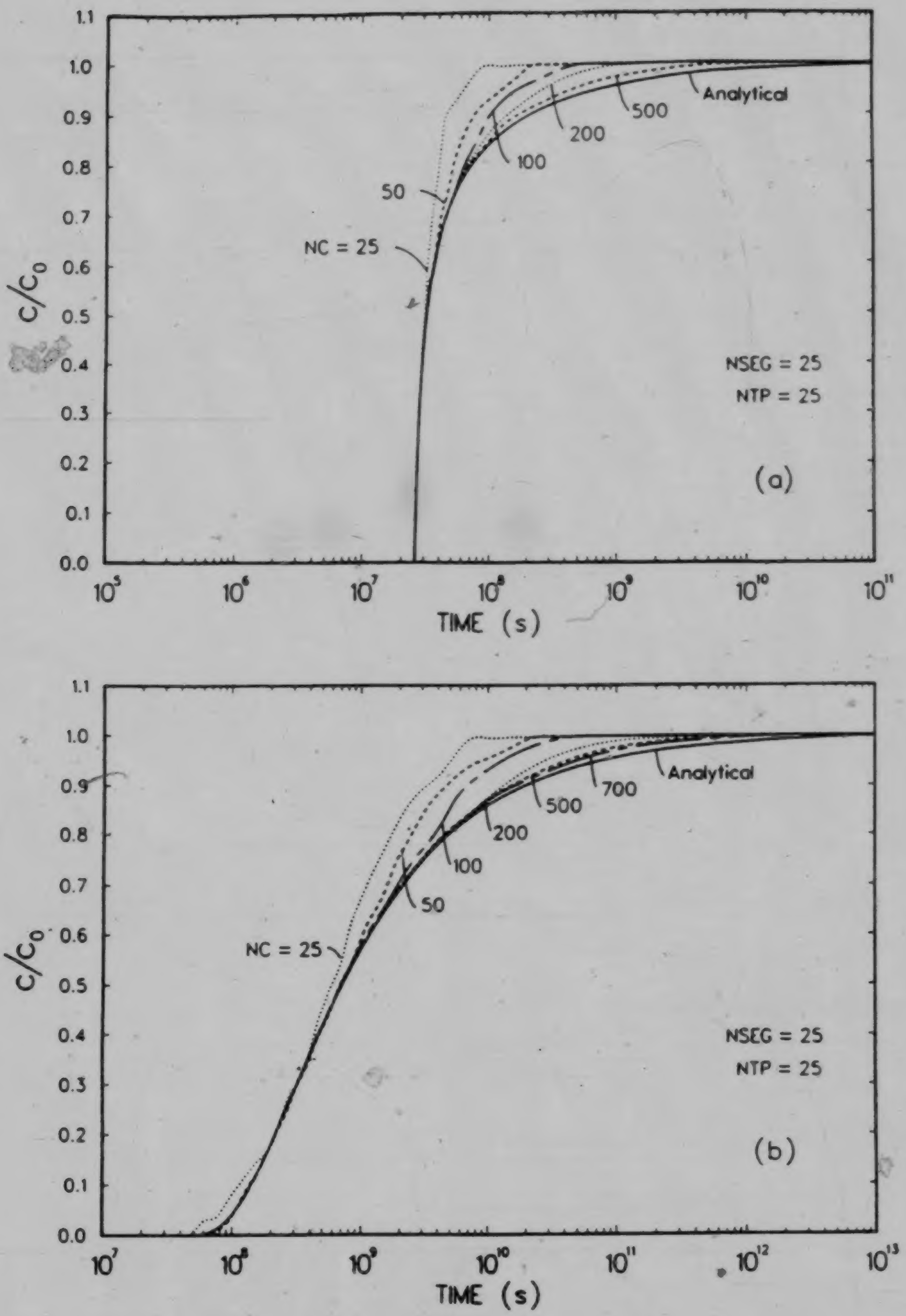

Fig. 3.8 Influence of the number of discretized concentration steps (NC) on the accuracy of the numerical solution for the breakthrough curve at the end of the last segment. (a) advection dominated. (b) diffusion dominated.

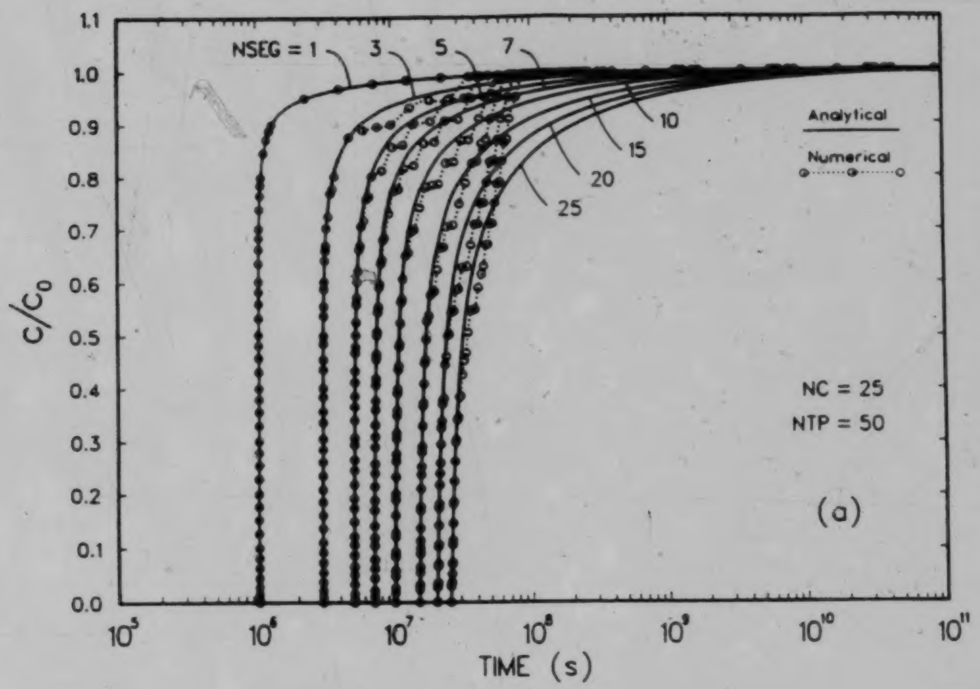

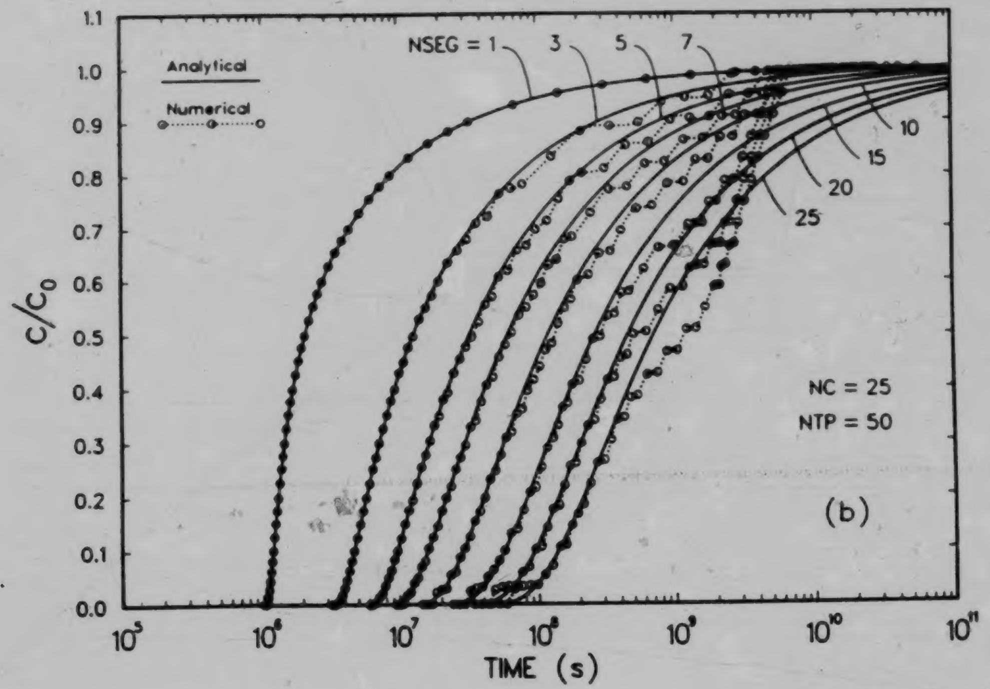

Fig. 3.9 Breakthrough curves obtained at the end of different segments, for a linear succession of segments. (a) advection dominated. (b) diffusion dominated.

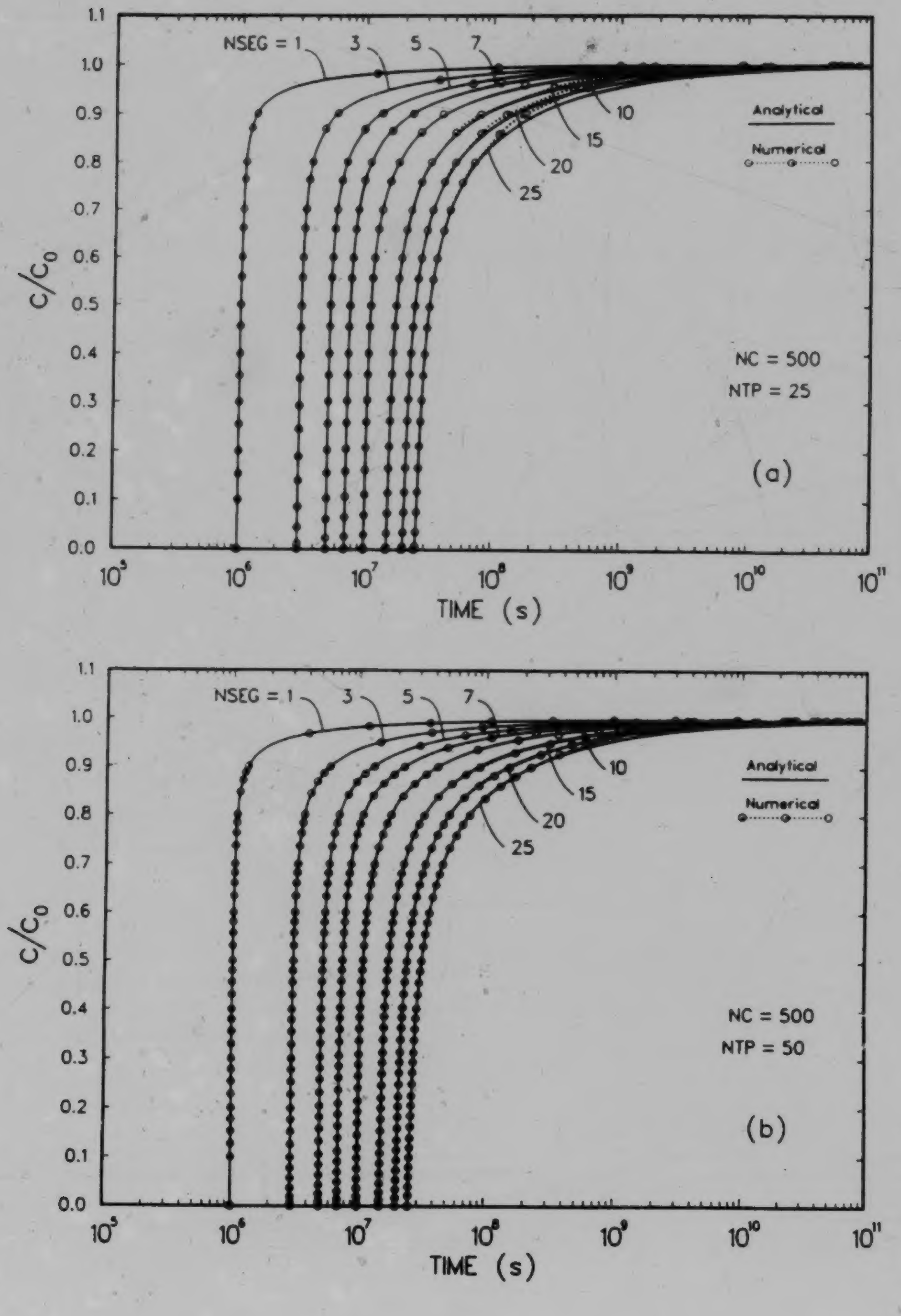

Fig. 3.10 Influence of the parameter NTP on the accuracy of the numerical solution for NC = 500. Advection dominated.

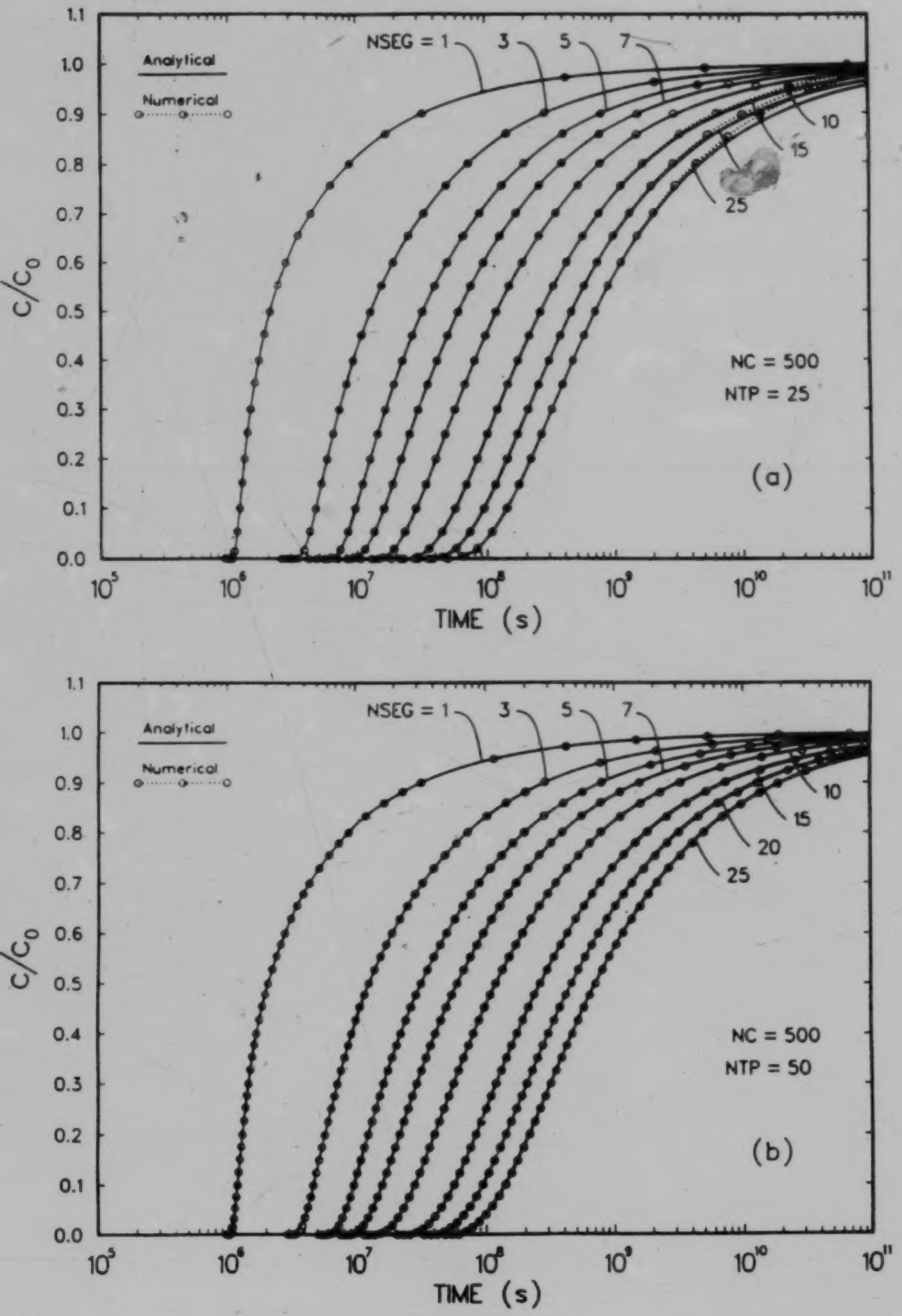

Fig. 3.11 Influence of the parameter NTP on the accuracy of the numerical solution for NC 500. Diffusion dominated.

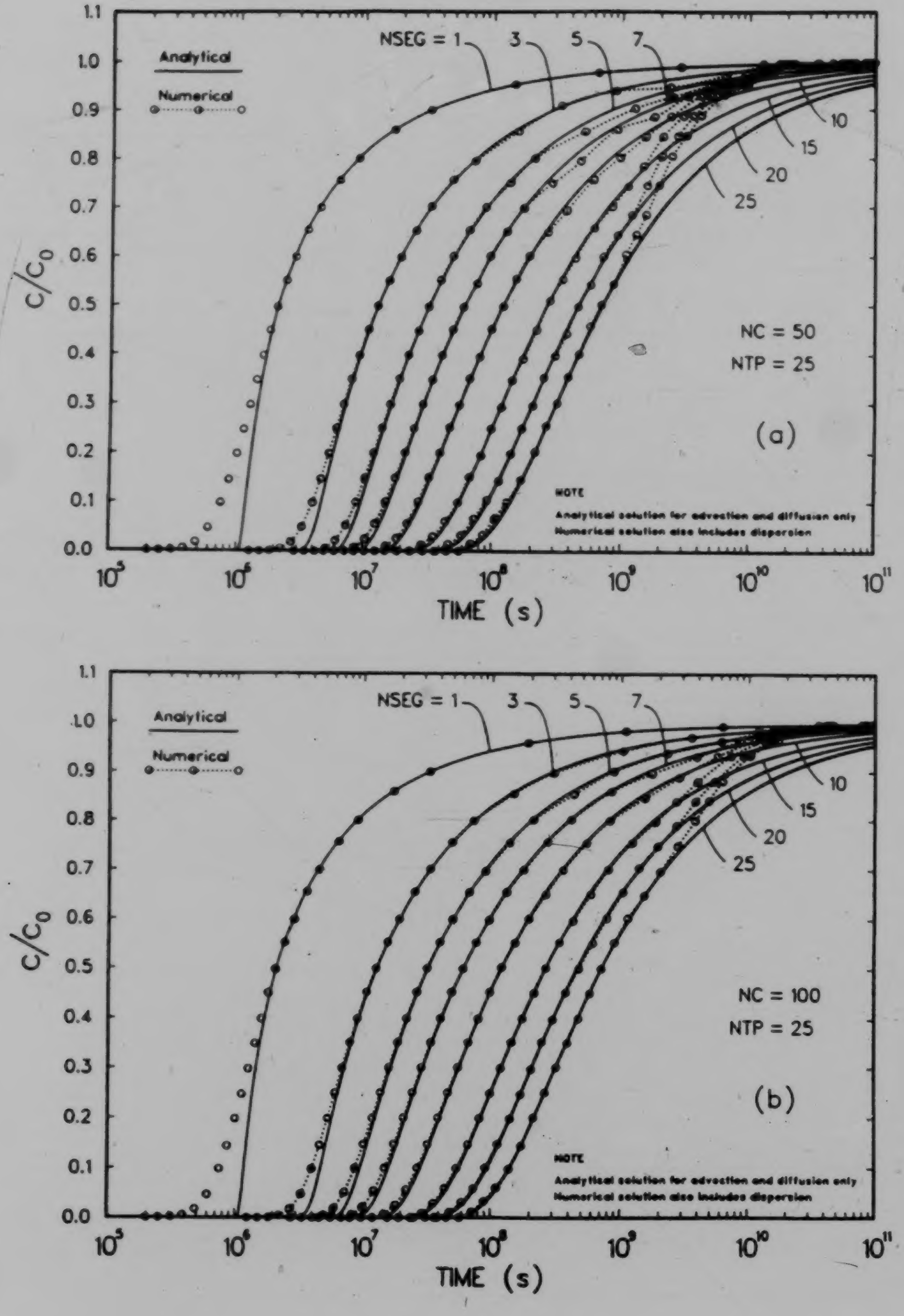

NOTE
Analytical solution for advection and diffusion only
Numerical solution also includes dispersion

Fig. 3.12 Verification of the accuracy of the numerical solution when dispersion in the fracture is also considered. Results obtained for the diffusion dominated case.

discretization errors may become comparable with the interpolation errors, making it necessary to also increase NTP in order to improve accuracy.

Dispersion in the fracture can be considered without any difficulty. The inclusion of dispersion does not alter the numerical procedure, but only changes the unit step response function. In this case, the response function (eq. 2.11) is not closed and numerical integration has to be performed for the evaluation of concentration, introducing additional computing time. The simulations considered only the diffusion dominated case. A value of 1.0 m was assumed for the dispersivity, resulting in **Pe** = 10 , for each individual segment. Two values were considered for NC, 50 and 100, and only one for NTP, 25. Figure 3.12 compares the numerical results with the analytical solution for the no-dispersion case. This comparison shows that, as the overall Peclet number increases, the general solution approaches the simplified no-dispersion solution. The numerical behaviour, however, is independent of the processes involved and the errors show the same trends described for the no-dispersion case.

3.4.2. Fracture Network Problem

In the second test, a simple fracture network was considered, in order to verify that the code adequately handled the mass distribution at the intersections. Both mixing models are considered. Figure 3.13 shows the network along with the basic data and the major features related to each mixing model. The derivation of the analytical solution for this case follows the procedure outlined in section 2.4 and is described in detail in Appendix A.

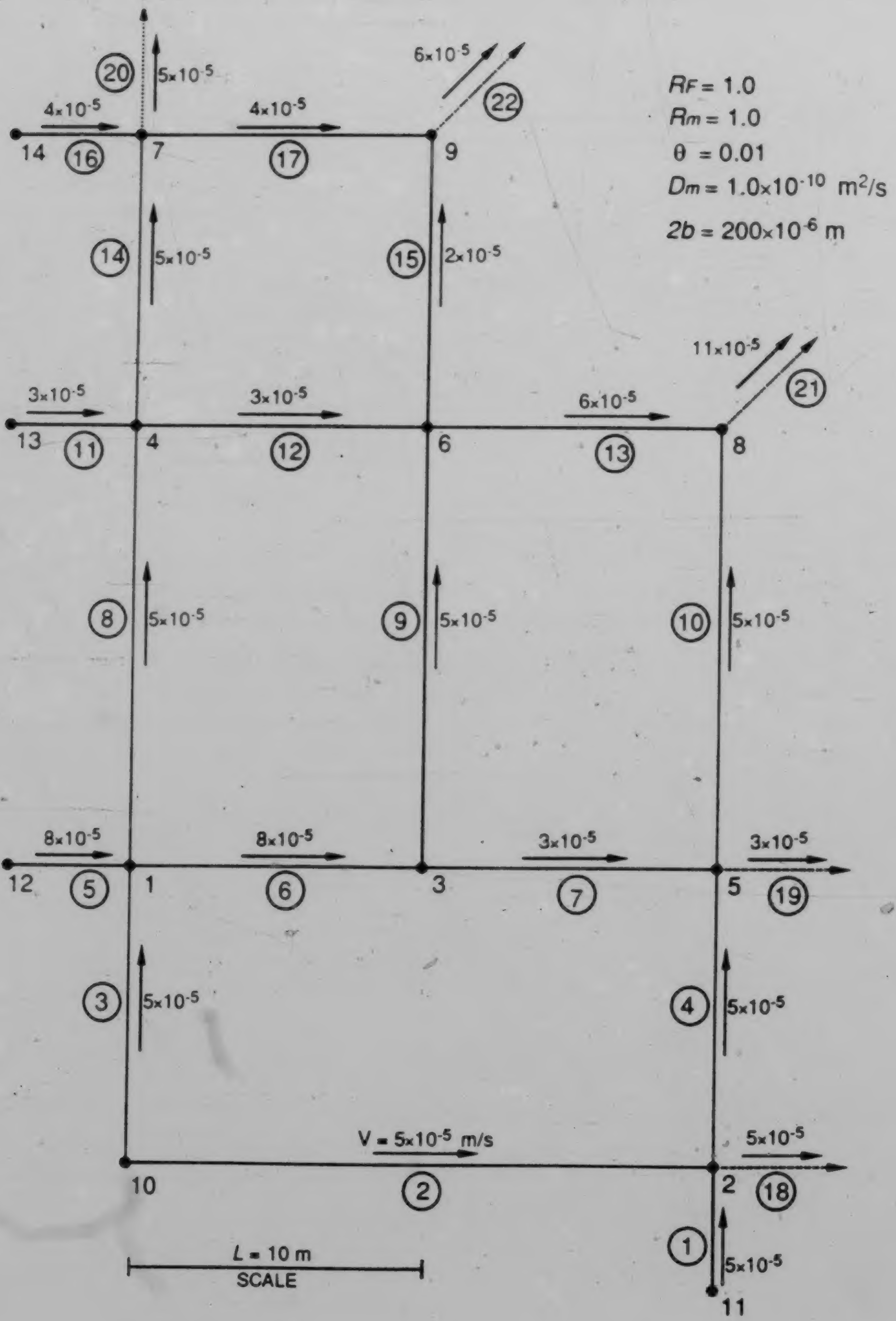
20
5×10-5
6×10-5
22
4×10-5
4×10-5
14
16
7
17
9
RF = 1.0
Rm = 1.0
θ = 0.01
Dm = 1.0×10-10 m2/s
2b = 200×10-6 m
14
5×10-5
15
2×10-5
11×10-5
21
3×10-5
3×10-5
6×10-5
13
11
4
12
6
13
8
8
5×10-5
9
5×10-5
10
5×10-5
8×10-5
8×10-5
3×10-5
3×10-5
12
5
1
6
3
7
5
19
3
5×10-5
4
5×10-5
V = 5×10-5 m/s
5×10-5
10
2
2
18
L = 10 m
SCALE
1
5×10-5
11

Fig. 3.13 Fracture network and fracture parameters used to verify the accuracy of the model for a general network.

Mass is assumed to be injected continuously at node 10. By analyzing Figure 3.13, it is possible to see that mass will show up in all five exits, nodes 2, 5, 7, 8 and 9, for the complete mixing model, but it will appear in only two exits, nodes 5 and 8, for the streamline routing model.

The simulations considered two values for NC, 25 and 100, and one for NTP, 25. Figure 3.14 and 3.15 show the results for both the complete mixing and the streamline routing models. The agreement between the numerical results and the analytical solution is very good, even for NC = 25. In this case, the farthest exit is only four segments away from the source and the numerical errors are not significative to affect the solution. For NC = 100, the agreement is excellent for both approaches. It is interesting to note that the redistribution of time points, as previously described, gives a good representation of the breakthrough curves.

From the numerical point of view, this method has advantages over other methods: only two parameters are responsible for the overall accuracy of the model and the numerical convergence seems to be independent of the physical parameters. It is dependent only upon the number of segments, i.e., upon the number of the convolution integral evaluations.

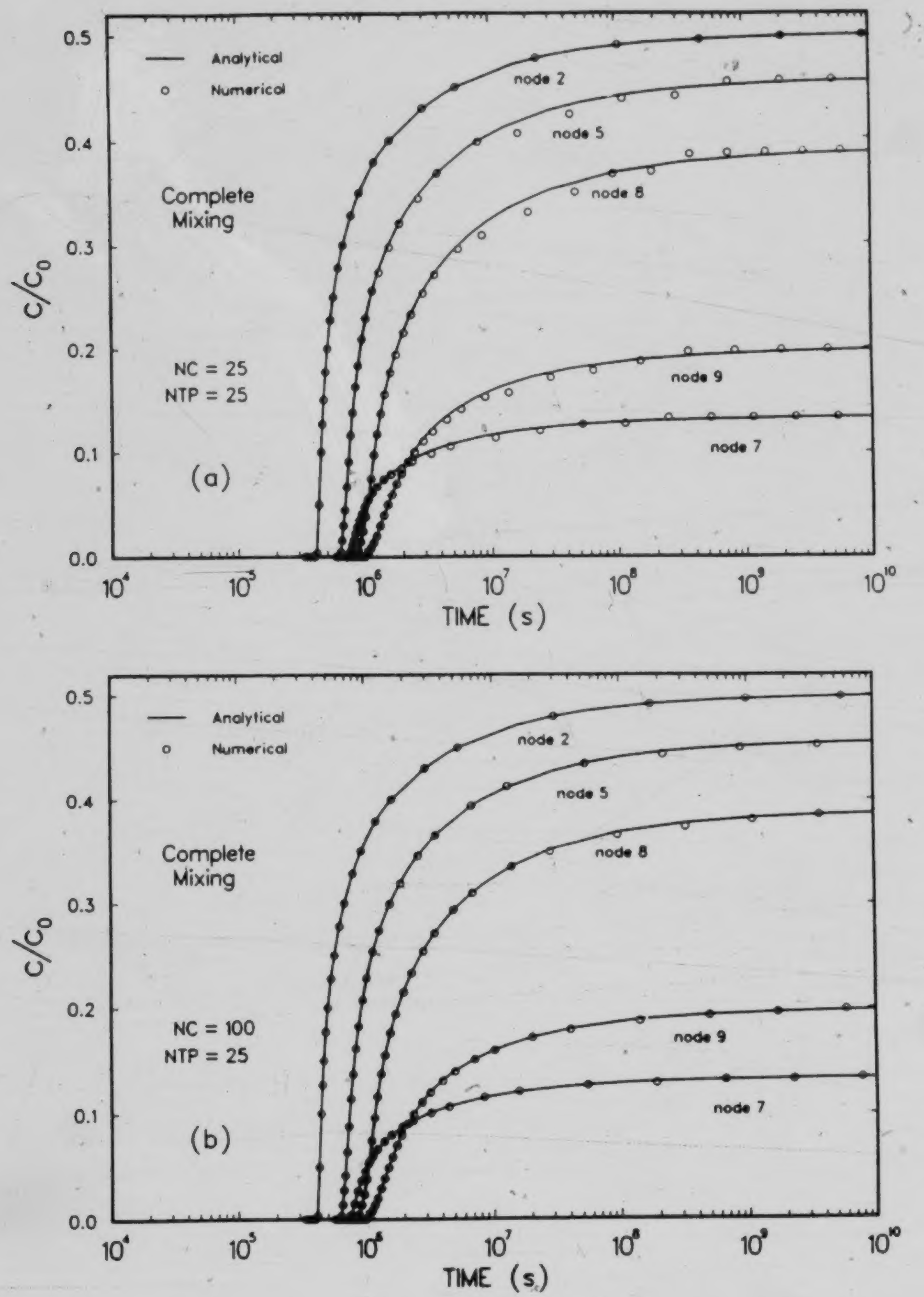

Fig. 3.14 Breakthrough curves obtained at all exit nodes showing the influence of the parameter NC on the accuracy of the numerical solution. Complete mixing model for mass distribution at intersections.

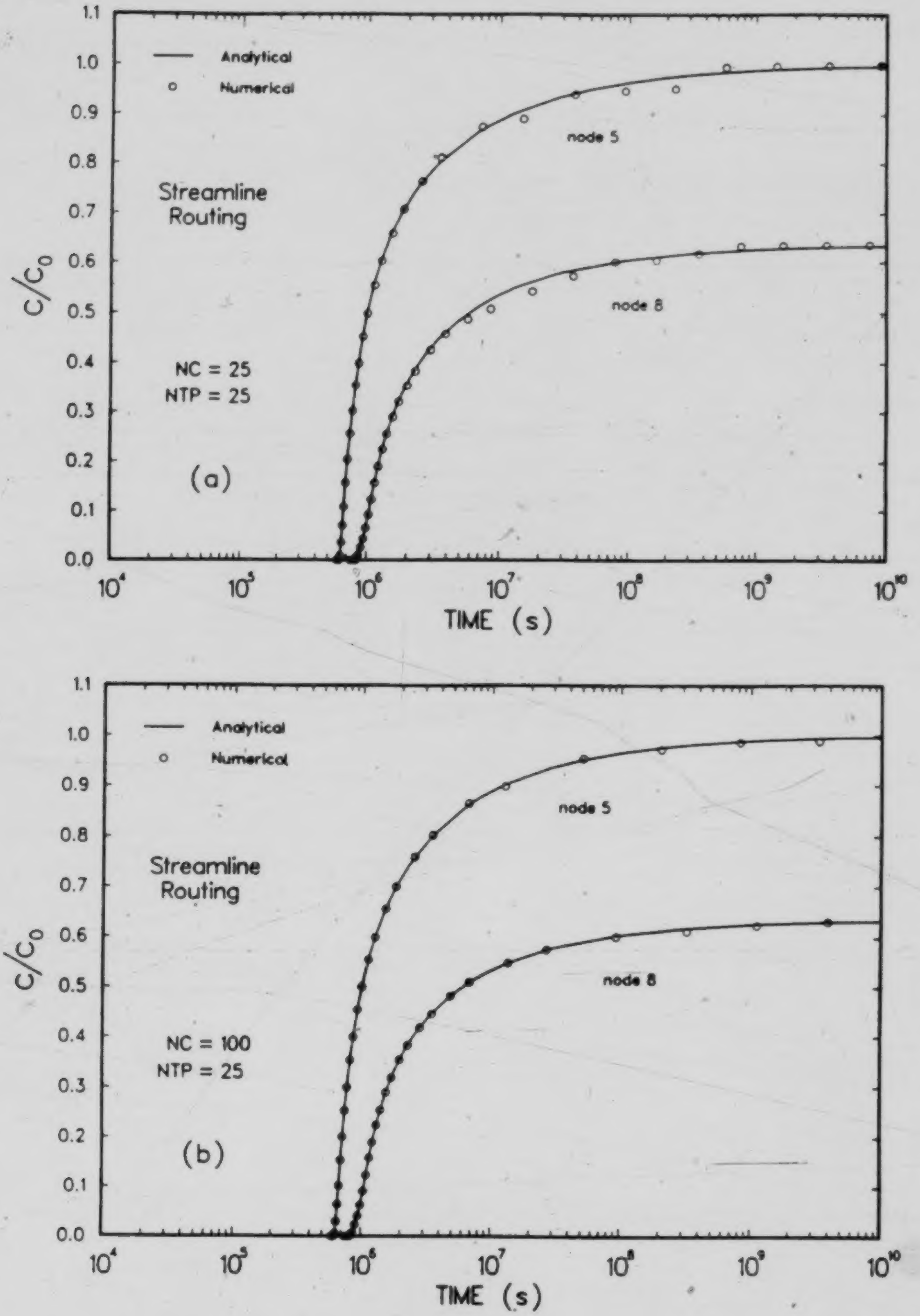

Fig. 3.15 Breakthrough curves obtained at all exit nodes showing the influence of the parameter NC on the accuracy of the numerical solution. Streamline routing model for mass distribution at intersections.

3.4.3 Discussion

The parameter NC is directly related to the discretization of the breakthrough curve. Therefore, the overall accuracy improves with increasing NC. The parameter NTP, in contrast, has a lesser degree of influence. In general, it is necessary to have a sufficient and well distributed number of points to evaluate the output breakthrough curve. When NC is increased, it may be also necessary to increase NTP, in order to make the interpolation errors comparable with the discretization errors of the input function.

An interesting feature of this model concerns the high accuracy obtained for the early part of the breakthrough curves. This is important for many situations, where low levels of solutes can be extremely toxical (Rasmuson et al., 1982).

4. APPLICATIONS OF THE TRANSFER FUNCTION MODEL

The mass transport model that has been developed provides an efficient way to examine mass transport processes in fractured rock systems. Discrete fracture networks are characterized by the many possible paths that mass can follow within the network. The particle tracking technique, for instance, takes this concept explicitly into account (Schwartz et al., 1983; Smith and Schwartz, 1984). The response of the system is the result of a series of mass contributions due to all different paths that convey mass to a particular sampling point. In some cases, distinct steps may be present on the breakthrough curves, as a clear indication of a path contribution. In other cases, a smooth curve may be obtained. The important fact is that, in any case, the response of the system is strongly dependent on the flow field developed in the network.

It is with this perspective that three issues are addressed here: (1) the influence of intersection mixing models on the overall response of discrete fracture systems; (2) the effects of diffusion into matrix on the overall response of discrete fracture networks; and (3) the mass transport behaviour for a two well system in discrete fracture networks.

These applications consider only advection and diffusion into the matrix. If necessary, adsorption on both fracture and matrix surfaces and radioactive decay can be readily implemented by substituting the appropriate values into the simplified unit step response function (Eq. 2-12). Dispersion in the fracture can also be considered, but the general unit step response function (Eq. 2.11) has to be used. For large travel distances, however, the effects of dispersion become less important due to the counteraction of diffusion into the matrix, as shown in section 3.4.1, and both response functions give equivalent results.

4.1 The Influence of the Intersection Mixing Models on the Overall Response of Discrete Fracture Systems

The complete mixing model and the streamline routing model represent two end-member models to partition mass at intersections. Few attempts have been made to compare both models under realistic flow conditions. Krizek et al. (1973) have compared these models under two different flow conditions: (a) regionally uniform radial flow and (b) injection into a regionally uniform flow field. They concluded that both mixing models give similar results and there was no advantage in using the more complex streamline routing model. Hull et al. (1987) used a model similar to the one described by Krizek et al. (1973), but also considered diffusion at the intersection. In their simulations, Hull et al. (1987) considered a regionally uniform flow field with no disturbance due to the introduction of the contaminant. Their results showed that different mixing models produced different effects on the distribution of the contaminant in the fracture network.

A basic difference between the simulations of Krizek et al. (1973) and Hull et al. (1987), besides diffusion at the intersection, is related to the simulated flow field conditions. There are two basic types of mass injection: active and passive (Raven et al. 1988). In the first one, the mass is pumped into the system with a high radial flow component, as in Krizek et al.'s experiments. In the second type of injection, mass is introduced without disturbing the original flow field, as in Hull et al.'s experiment. The question that arises is whether different flow fields could explain the apparently contradictory results.

To investigate whether or not the consideration of the flow field is important for the selection of the intersection mixing model, two sets of numerical experiments are carried out. In the first set, a regional flow field is set up, while in the second a convergent-divergent flow field is defined by a system of two wells (one recharging and the other pumping). These two flow field situations represent extremes of natural conditions.

4.1.1 Regionally uniform flow field.

Within a rectangular domain 300 x 600 m, a regionally uniform flow field was established by assigning constant head at all four boundaries, as described in section 3.2. The hydraulic gradient is parallel to the smaller side and has a value of 1/15.

Three fracture geometries were considered, as shown in Figure 4.1. For the first two cases, infinite fractures from two orthogonal sets, oriented at +45° and –45° in relation to the x-direction, are uniformly distributed within the domain. In case 1 the fracture network is sparse, with a fracture spacing $\Delta l_1 = 127.3$ m, while in case 2 the network is dense with a spacing $\Delta l_2 = 23.1$ m. The third case is derived from the second by removing some fracture segments, in order to decrease the degree of connectivity. In all, six trials were conducted, where variations in fracture aperture and direction of the hydraulic gradient were also taken into account. The matrix porosity is $\theta = 0.01$ and the effective diffusion coefficient is $D_m = 1.6\times10^{-10}$ m^2/s. Table 4.1 summarizes the data for each trial.

Continuous source(s) of mass was/(were) located at the nodes closer to the midpoint of the left boundary. For this particular source arrangement the geometry of the fracture network is such that the mass does not exit through the top or bottom boundaries, thus, preventing undesirable boundary effects.

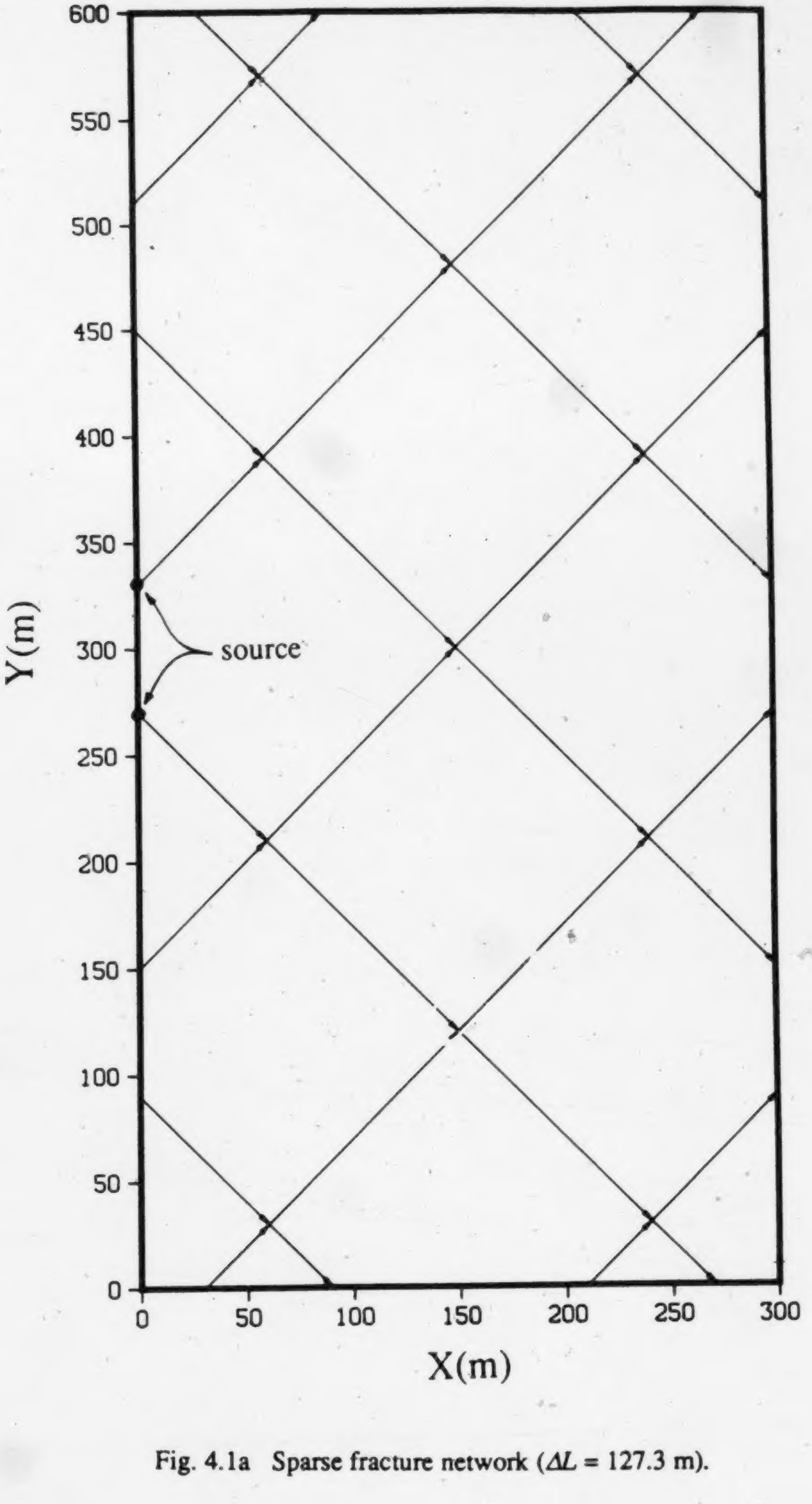
Y(m)
X(m)
source
0
50
100
150
200
250
300
350
400
450
500
550
600
0
50
100
150
200
250
300

Fig. 4.1a Sparse fracture network (ΔL = 127.3 m).

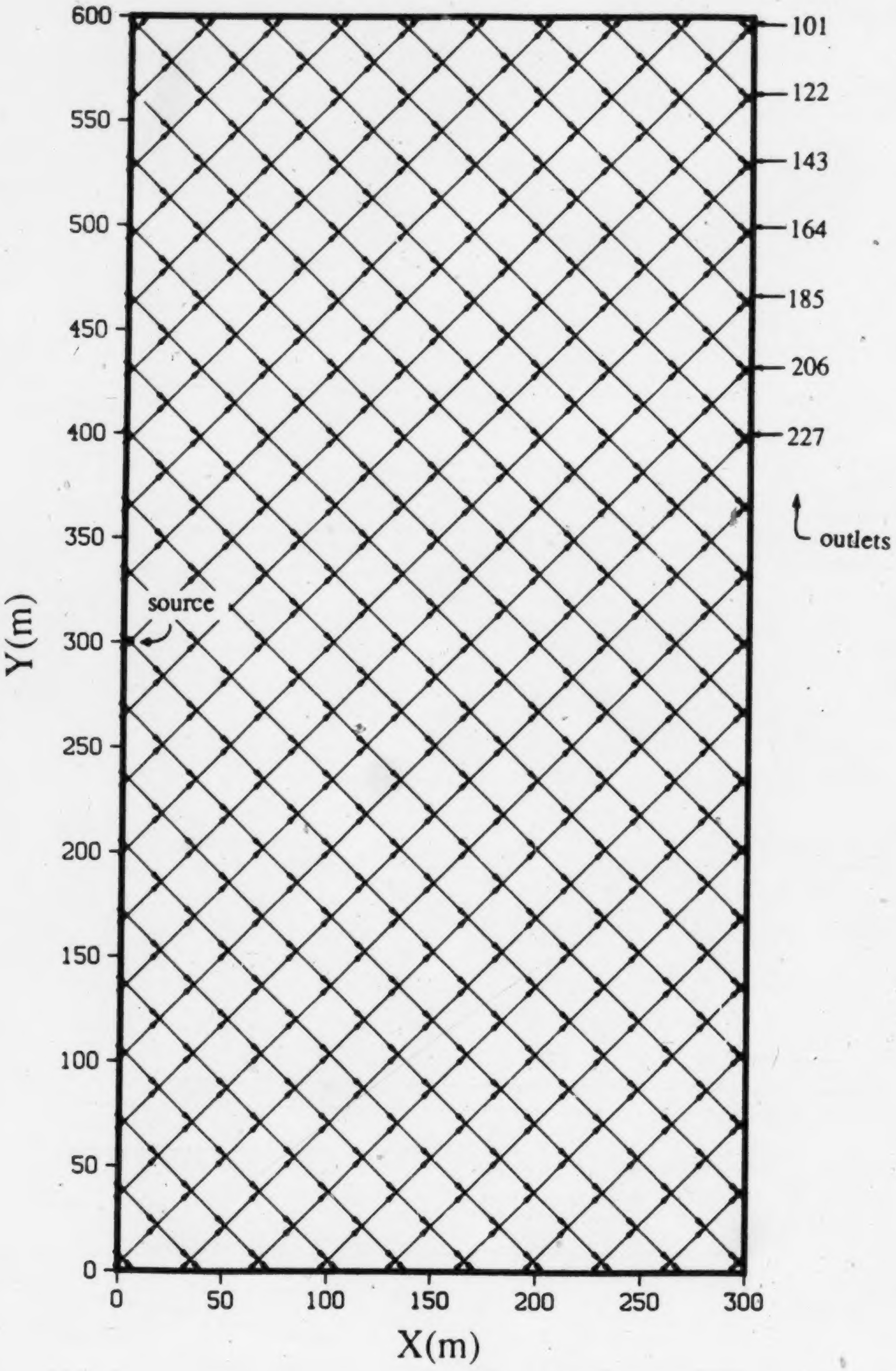
600
550
500
450
400
350
300
250
200
150
100
50
0
Y(m)
0
50
100
150
200
250
300
X(m)
source
101
122
143
164
185
206
227
outlets

Fig. 4.1b Dense fracture network (ΔL = 23.1 m).

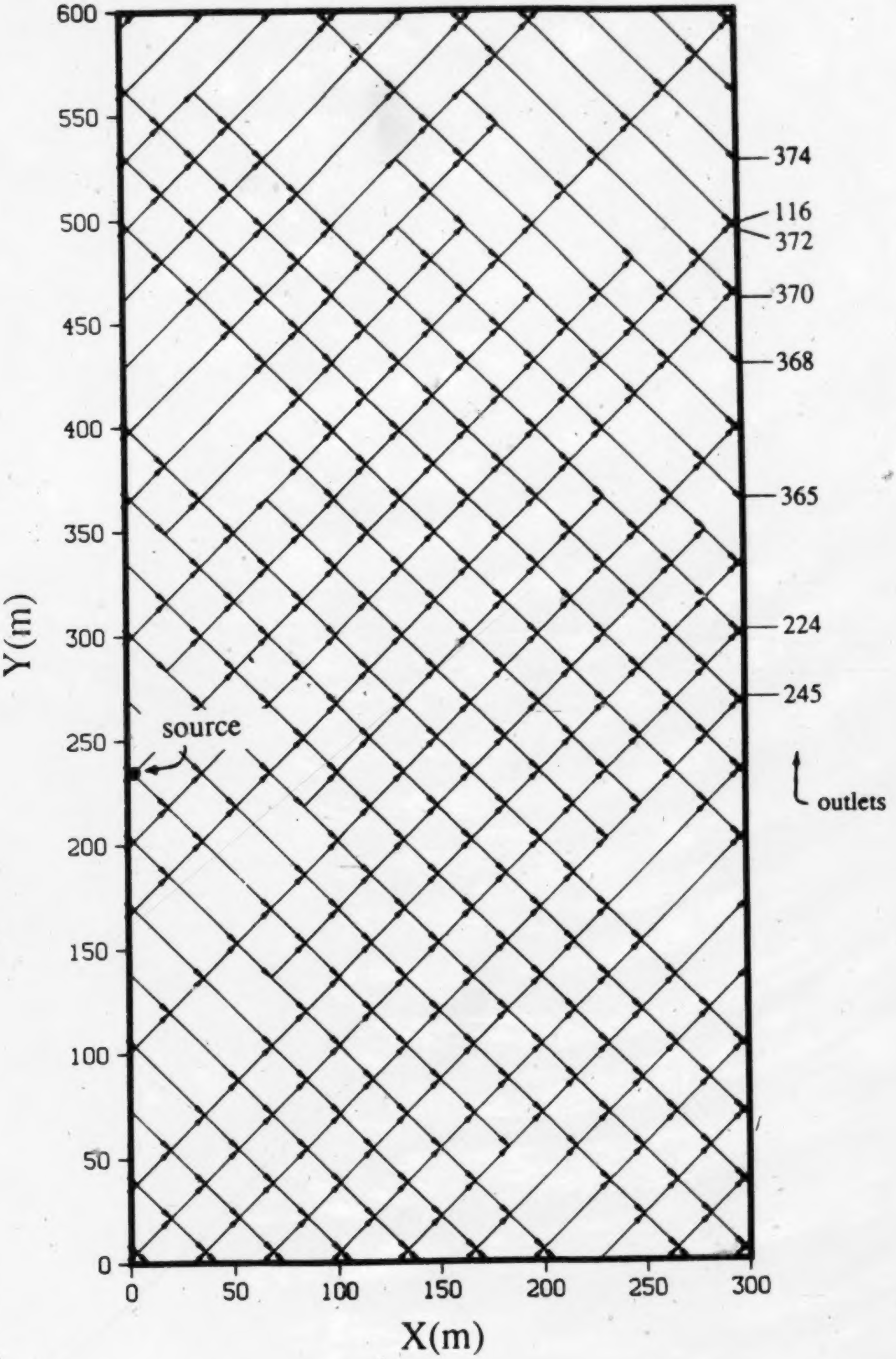
600
550
500
450
400
350
300
250
200
150
100
50
0
Y(m)
0
50
100
150
200
250
300
X(m)
source
374
116
372
370
368
365
224
245
outlets

Fig. 4.1c Incomplete fracture network (ΔL = 23.1 m).

Table 4.1 Data used for the regionally uniform flow field case

Fracture geometry	Trial number	∇h angle	Aperture mean (μm)	C_v
sparse	1	0°	200	0.0
dense	2	0°	200	0.0
dense complete	3	34°	200	0.0
	4	34°	200	1.0
dense incomplete	5	34°	200	0.0
	6	34°	200	1.0

The effects of the different intersection mixing models on the mass transport are compared at the exit boundary through the analysis of both the breakthrough curves and the transverse distribution of the maximum concentration. Figure 4.2 presents the results for trials 1 and 2, regarding the transverse distribution of the maximum concentration. In both trials, the streamline routing model has allowed mass to exit through only two exits, while the complete mixing model has led mass to several exits. It is interesting to note that, in trial 2, the complete mixing model leads to a bell shaped distribution for the maximum concentration.

Figure 4.3 compares the normalized (with respect to the maximum concentration) breakthrough curves obtained at the centerline outlets for trial 2. Both mixing models give equivalent results. In Figure 4.4 the normalized breakthrough curves for the complete mixing model are compared for all the outlets. Again, all the breakthrough curves coincide and the same is true for the streamline routing model. These results are consequence of the regular fracture geometry that leads to the same velocity and residence time for every fracture segment. In these particular trials, where the exit boundary is perpendicular to the regional hydraulic gradient, all outlets have the same residence time distribution. The

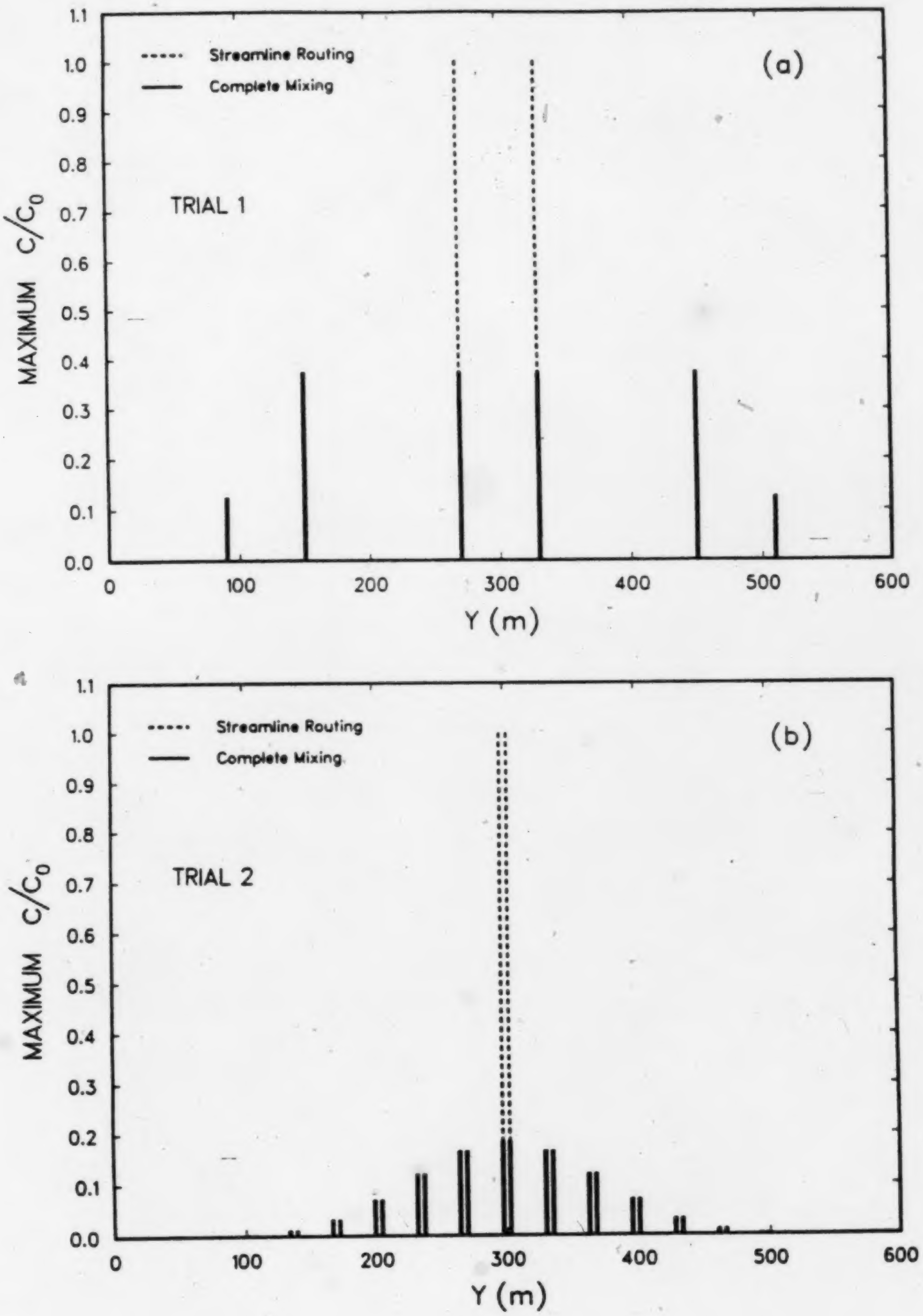

Fig. 4.2 Maximum relative concentration distribution at the exit boundary for trials 1 and 2.

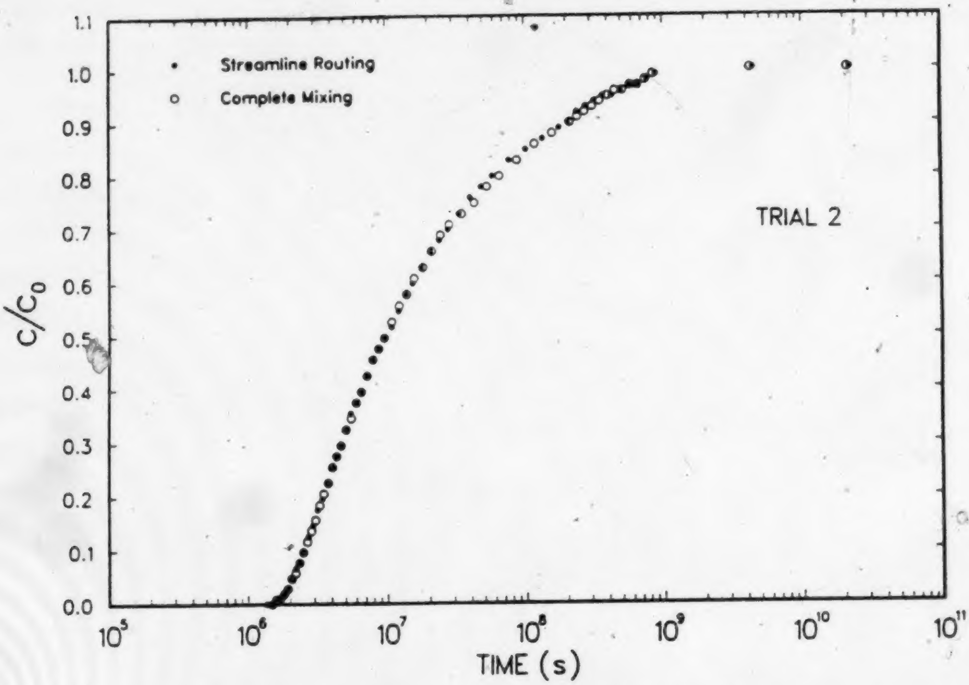

Fig.4.3 Comparison of the effects of the mixing models on the normalized breakthrough curves for the centerline outlets (x=300m, y=300m).

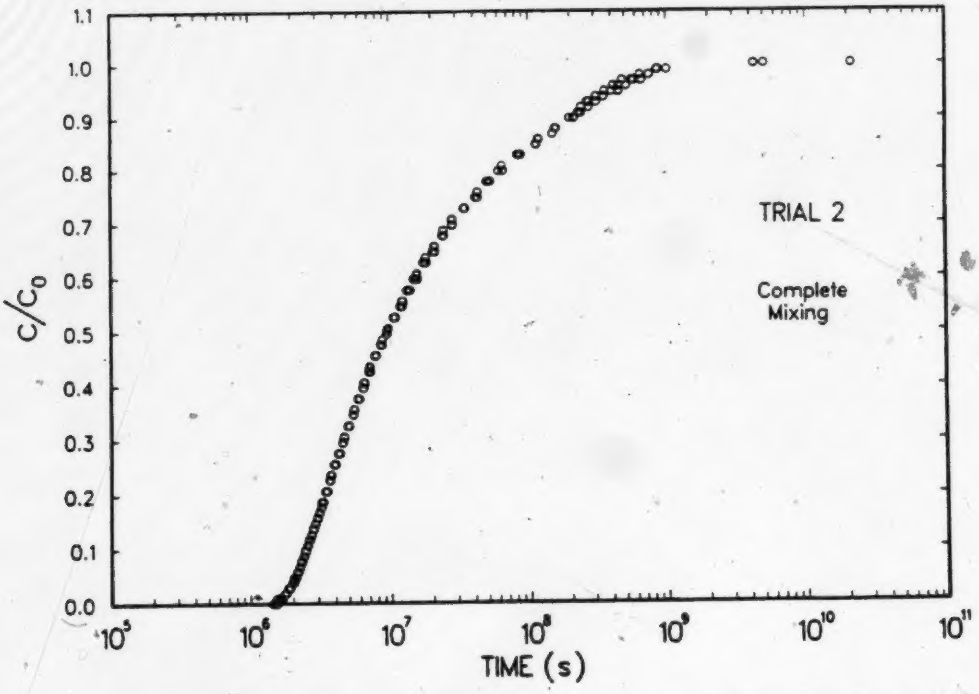

Fig.4.4 Comparison of the normalized breakthrough curves for all outlets at the exit boundary (x=300m)

different mixing models affect the overall response of the system only in the maximum concentration.

The particular flow field imposed over the network, in which velocities are the same for both fracture sets, exaggerates the behaviour of the streamline routing model. The contaminant is confined to only two paths along the centerline and there is absolutely no lateral spreading. The maximum concentration at the outlet is exactly the same as the inlet. The complete mixing model, on the other hand, spreads mass continually. Each intersection represents a mixing opportunity that dilutes the mass. The overall degree of mixing is controlled by the density of intersections: the higher the density, the higher the spreading and the lower the maximum attainable concentration.

Trials 3 to 6 were designed to systematically introduce more realistic characterization of the fracture system. These include variation of the hydraulic gradient direction, variation in the aperture distribution and variation on the degree of connectivity.

In trial 3, the orientation of the hydraulic gradient was changed to 34° in relation to the x-direction. For a network with constant fracture aperture, the velocity in one fracture set is roughly five times greater than the other set. Figure 4.5a shows that the peak of maximum concentration moved to the right. Both mixing models give similar results, but the streamline routing model gives a higher peak and a smaller lateral dispersion [note that concentrations in Figure 4.5a should be regarded as discrete points, as shown in Figure 4.2; the broken lines are just a visual aid for identification]. Figures 4.5b and 4.5c shows the breakthrough curves for some outlets, while Figure 4.5d shows the equivalent normalized breakthrough curves. Because the hydraulic gradient direction was changed, the normalized breakthrough curves for the outlets no longer coincide. Both mixing models, however, give identical results for the normalized breakthrough curves at the same outlet.

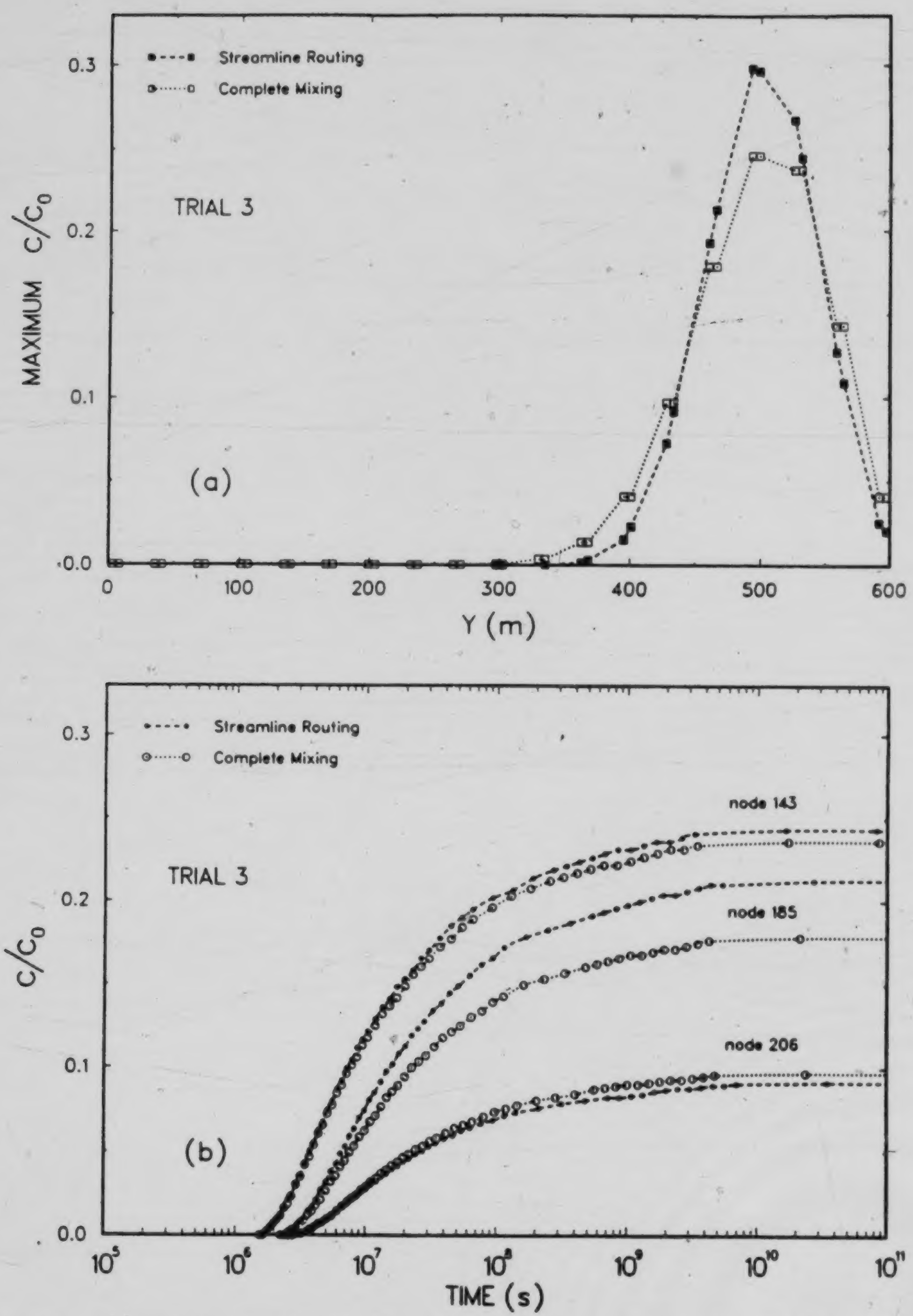

Fig. 4.5 Complete network with ∇h at 34° and uniform aperture distribution
(a) Maximum concentration distribution at exit boundary.
(b) Selected breakthrough curves at exit boundary.

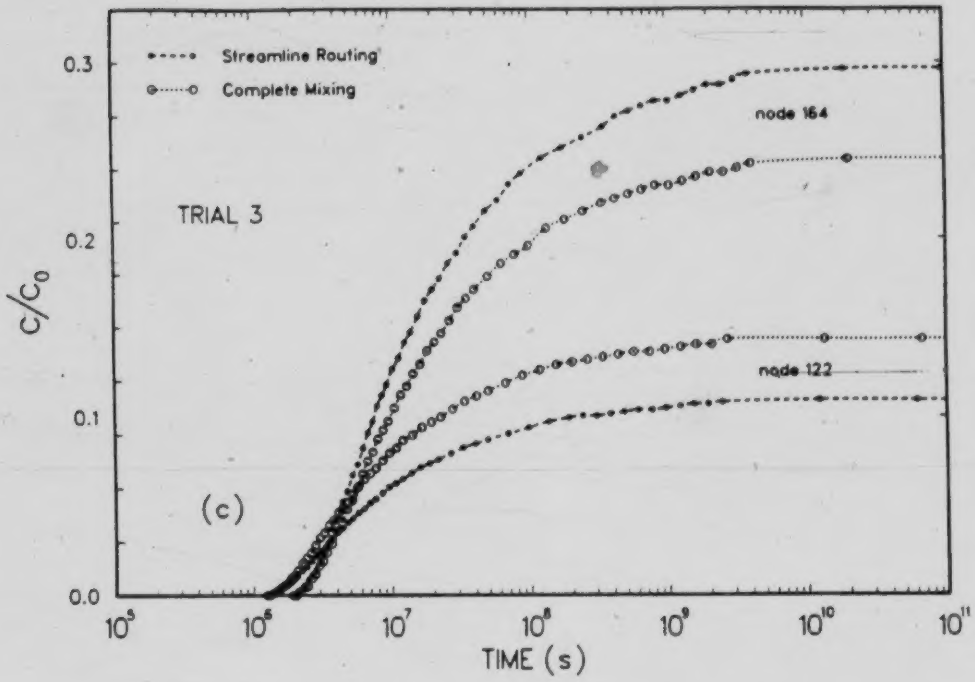

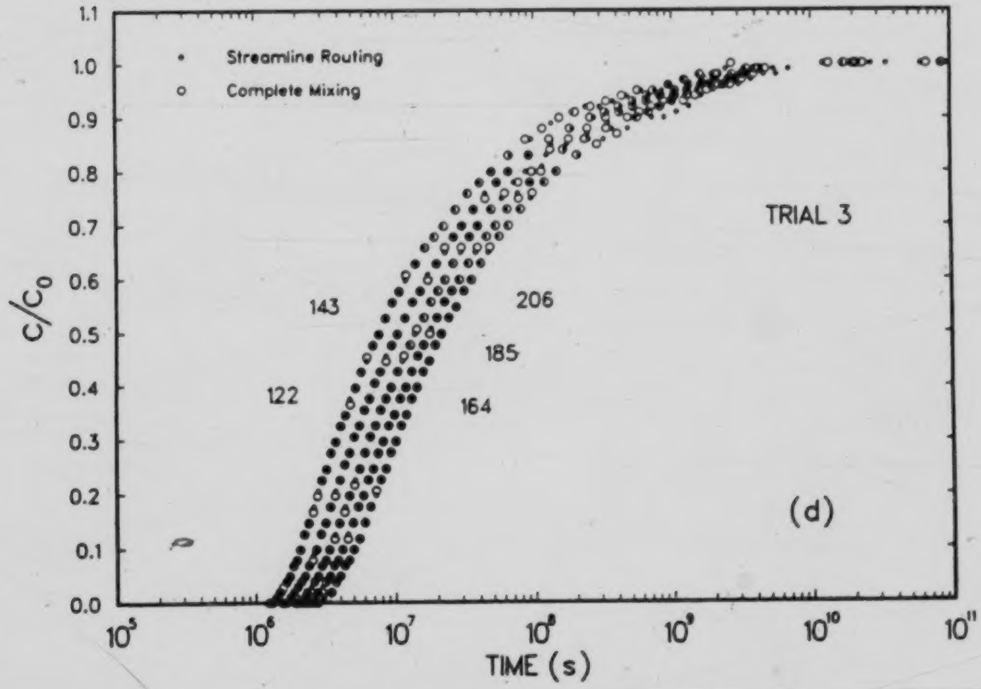

Fig. 4.5 Complete network with ∇h at 34° and uniform aperture distribution
(c) Selected breakthrough curves at exit boundary.
(d) Correspondent normalized breakthrough curves.

Again, the effect of the different mixing models is manifested only on the maximum concentration.

Trial 4 extended trial 3 to include variability in the fracture aperture. Apertures are sampled from a log-normal distribution with mean equal to 200 μm and coefficient of variation (C_v) equal to 1.0. Figure 4.6a presents the distribution of maximum concentration at the exit boundary. These results show that the effects of the complete mixing model are felt over the entire exit boundary, while the effects of the streamline routing are restricted to one third of the outlets. In general, a detailed comparison of the breakthrough curves for the mixing models (Figures 4.6b and 4.6c) shows a range in behaviour. At outlet 122, for instance, both approaches yield almost identical breakthrough curves. The concentration step that occurs at time 2×10^7 s is a clear indication of the contribution of a slower flow path. At outlets 143 and 164 different breakthrough curves are obtained for different mixing models. At outlet 143 both breakthrough curves start at the same time, but soon they take different directions: the streamline routing leads to a steeper curve than does the complete mixing. This result implies that the streamline routing paths coincide with the faster paths. At outlet 164 this is not the case, at least in the very beginning: the streamline routing produces later mass arrivals than the complete mixing. The complete mixing model introduced mass into higher velocity pathways, but the same procedure leads later to a lower rate of concentration increase and, consequently, to a lower maximum concentration, because the mass was inappropriately dispersed or mixed into other channels.

Trials 5 and 6 analyze a fracture network that is not fully connected (Figure 4.1c). For equivalent conditions, the removal of fracture segments decreases the available flow paths and increases the resistance of the network to the fluid flow. Under the same hydraulic gradient, the discharge through the network decreases, increasing the residence time.

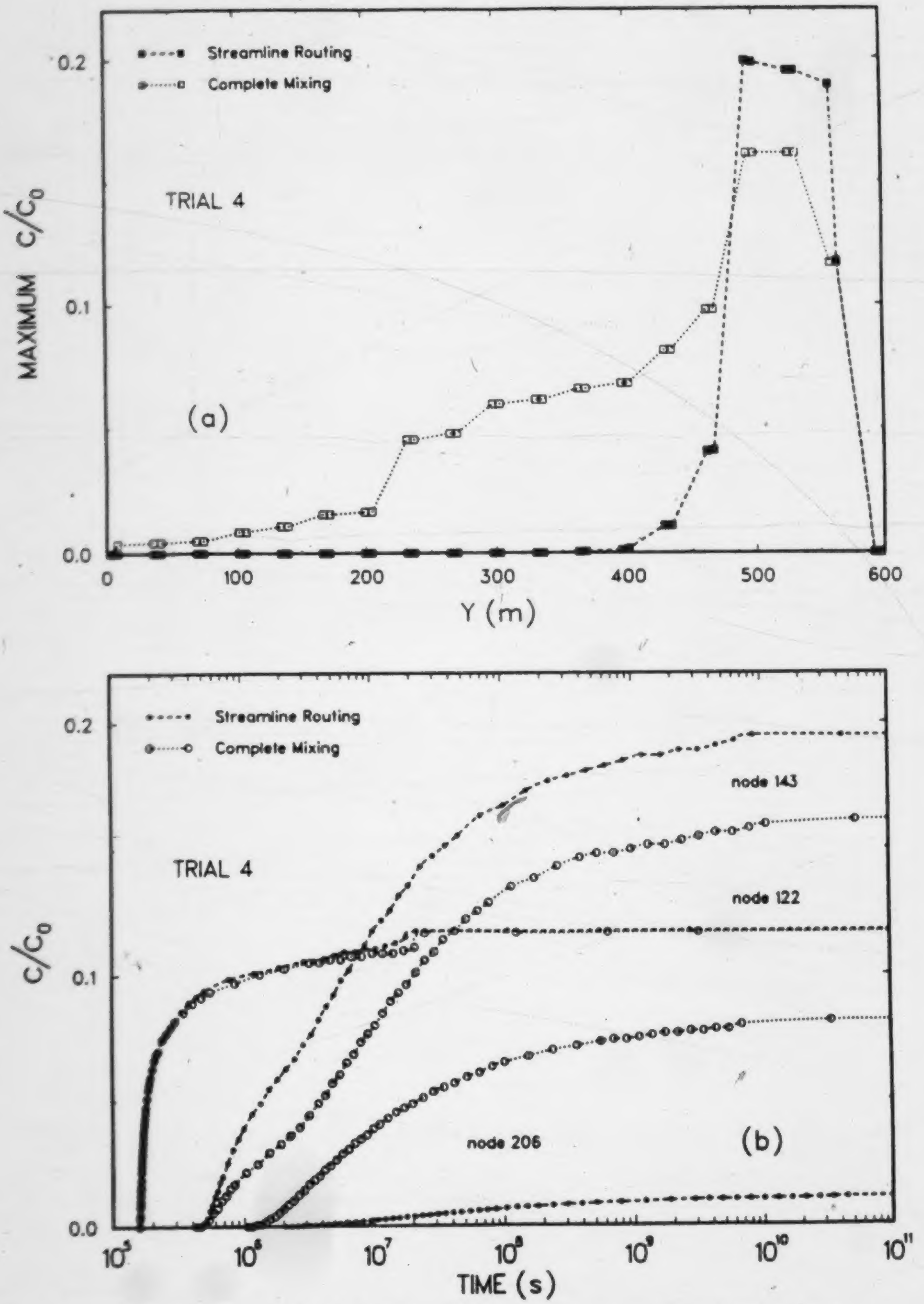

Fig. 4.6 Complete network with ∇h at 34° and random aperture distribution
(a) Maximum concentration distribution at exit boundary.
(b) Selected breakthrough curves at exit boundary.

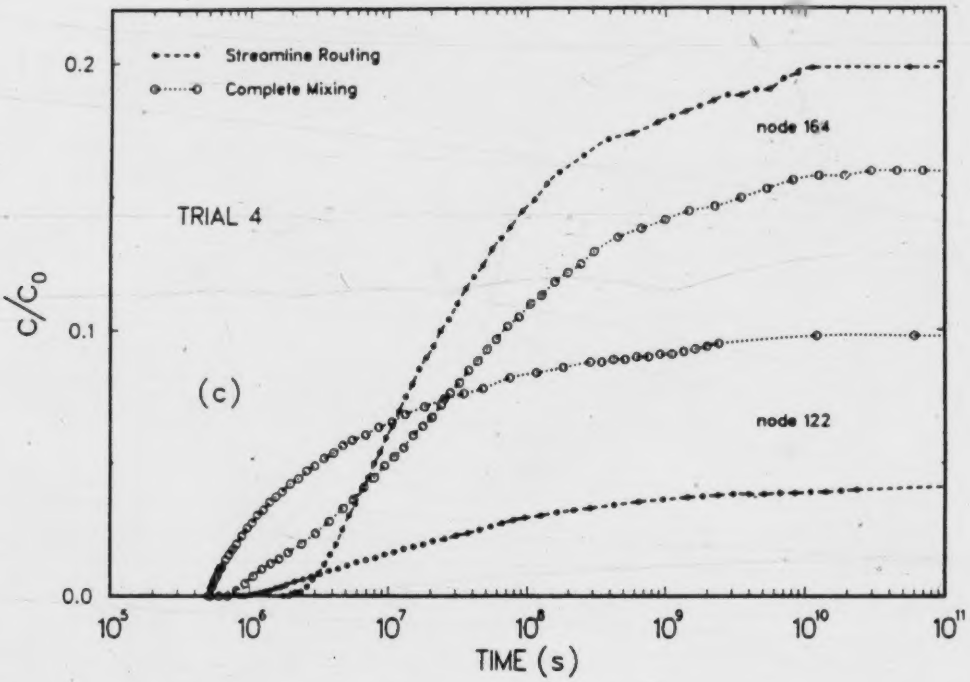

Fig. 4.6 Complete network with ∇h at 34° and random aperture distribution
(c) Selected breakthrough curves at exit boundary.

Trial 5 assumes constant fracture aperture and is comparable to trial 3. The distributions of maximum concentration (Figure 4.7a) are similar for both mixing models, though the streamline routing model produces a larger peak. The corresponding breakthrough curves (Figure 4.7b and 4.7c) show a smooth increase in concentration, without any significant steps.

The lack of connectivity affects the breakthrough curves at the outlets in two ways. First, because there are fewer paths that lead to a specific outlet, the residence time for the contributing paths may not vary significantly, resulting in a smooth breakthrough curve. Second, the fewer paths offer fewer mixing opportunities that restrict spreading and promote a higher maximum concentration at the outlets, when compared to trial 3.

Trial 6 introduces variability in the fracture aperture and it is comparable to trial 4. Figure 4.8a shows the distribution of maximum concentration at the exit boundary. The streamline routing promotes larger maximum concentrations and reduces lateral spreading, as compared to the complete mixing model. Curiously, the reduction in connectivity has increased substantially the maximum concentration at the outlets, when compared to the results of other trials. This behaviour is consistent for both mixing models, and is related to the fact that the aperture distribution and the smaller degree of connectivity created a system that is self contained for that particular source point and allows little interaction with fluids from other inlets. As a consequence, the concentrations are higher and some outlets even have a concentration comparable to the source concentration. Figure 4.8b and 4.8c show the corresponding breakthrough curves. Because few paths contribute to the breakthrough curves, the effect of different mixing models is felt mainly on the maximum concentration. Trial 6 is a good example of what could be expected when mass reaches impervious boundaries in a system.

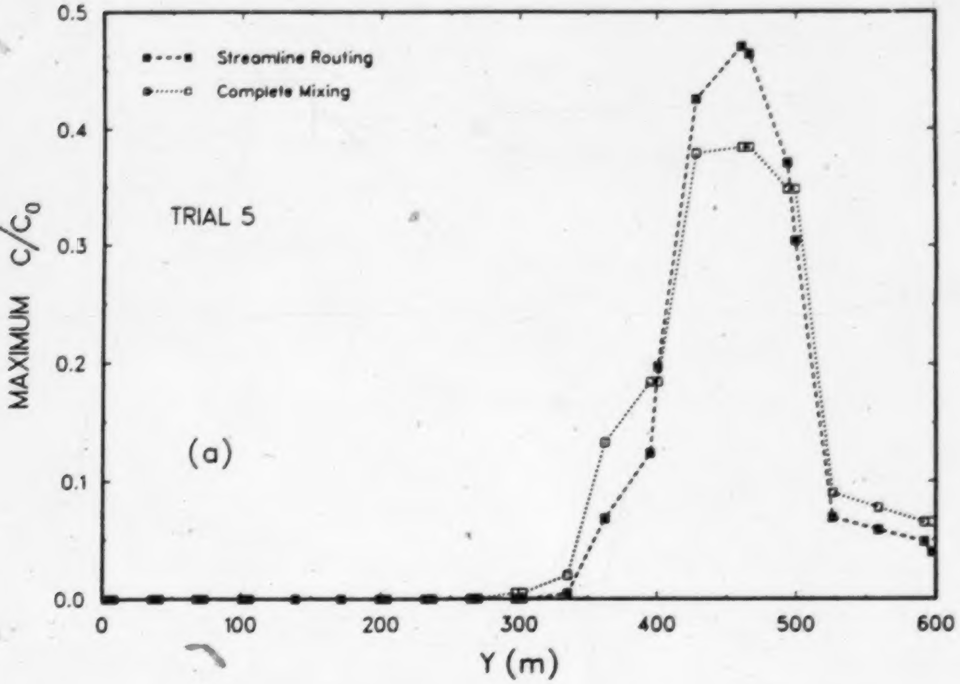

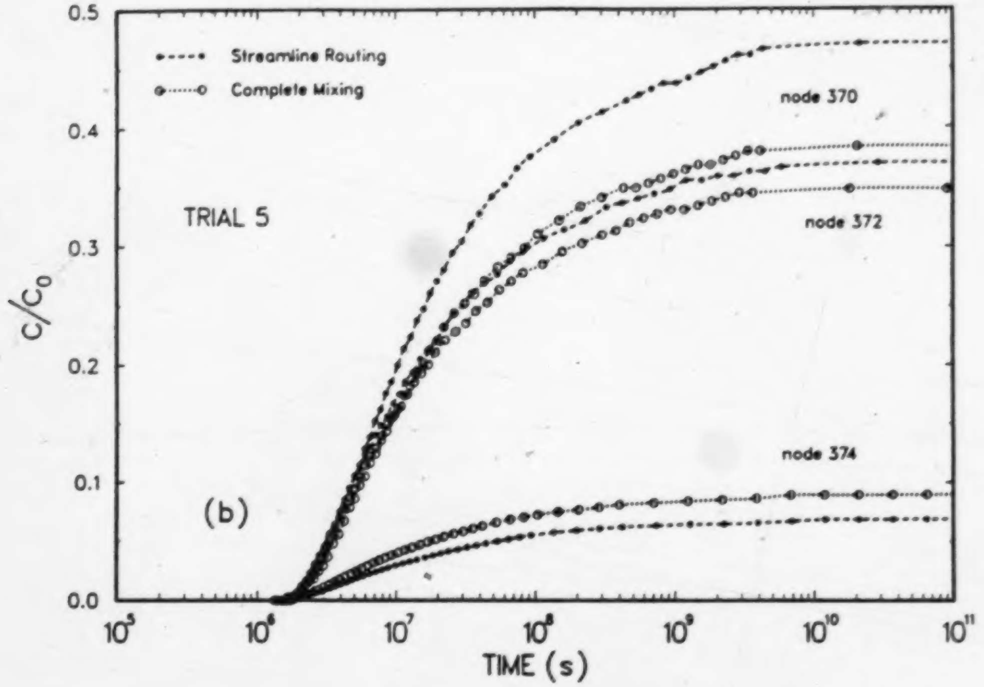

Fig. 4.7 Incomplete network with ∇h at 34° and uniform aperture distribution
(a) Maximum concentration distribution at exit boundary.
(b) Selected breakthrough curves at exit boundary.

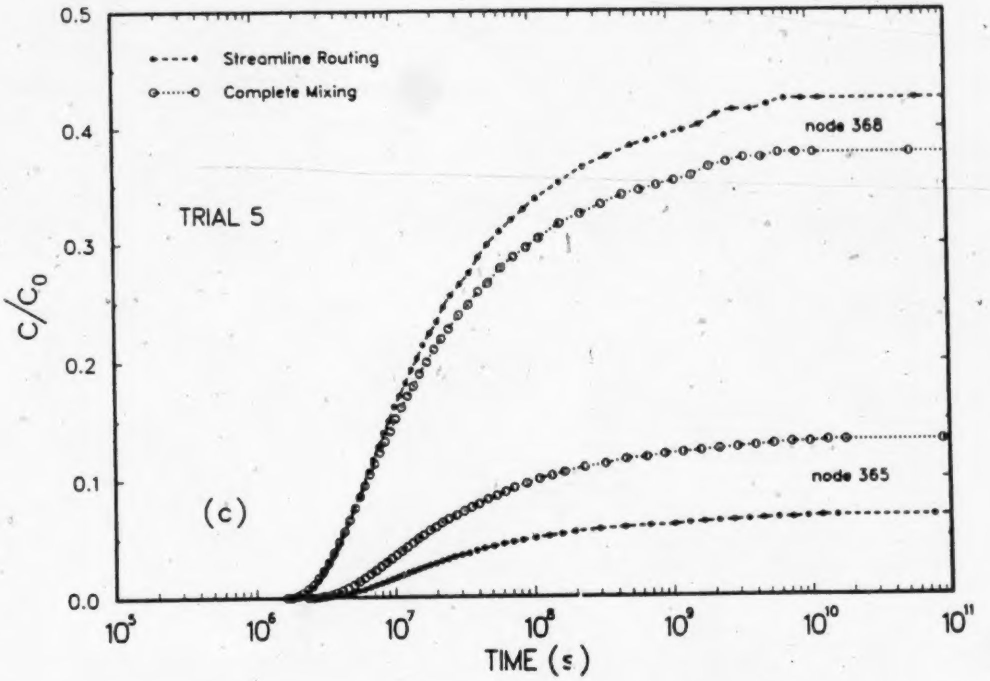

Fig. 4.7 Incomplete network with ∇h at 34° and uniform aperture distribution (c) Selected breakthrough curves at exit boundary.

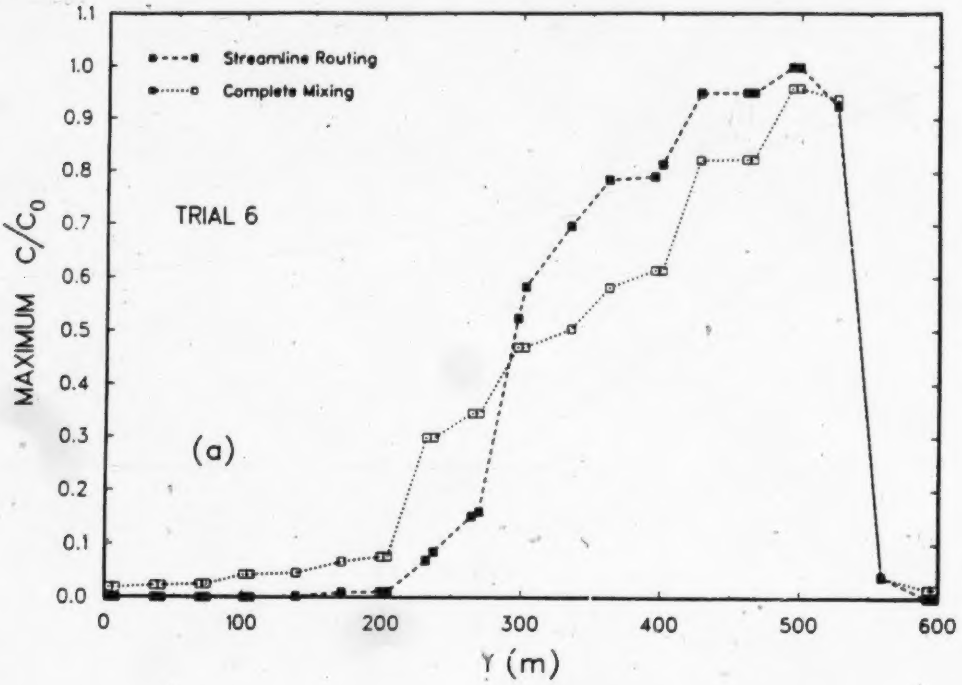

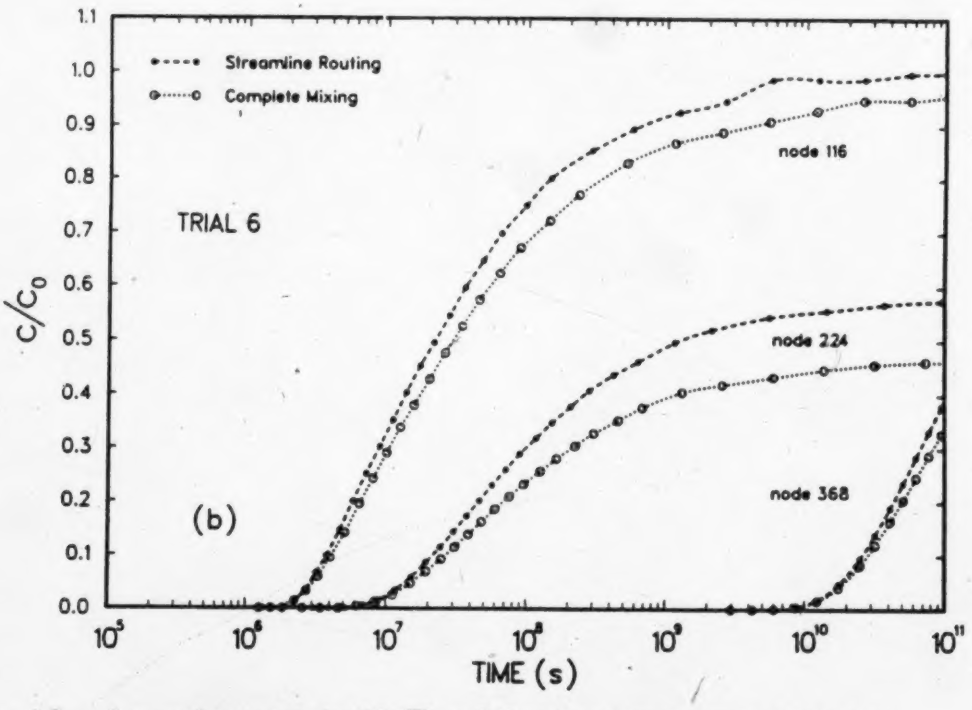

Fig. 4.8 Incomplete network with ∇h at 34° and random aperture distribution
(a) Maximum concentration distribution at exit boundary.
(b) Selected breakthrough curves at exit boundary.

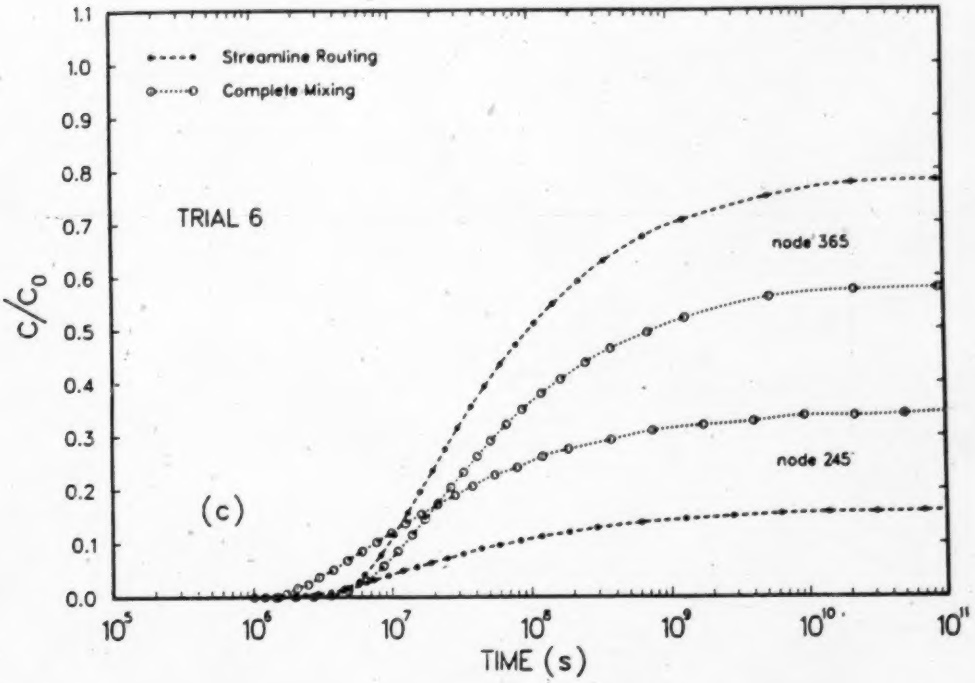

Fig. 4.8 Incomplete network with ∇h at 34° and random aperture distribution (c) Selected breakthrough curves at exit boundary.

These results show that mass transport in discrete networks subject to uniform regional flow field depends on the mixing model adopted for partitioning mass at intersections. In general, the effect of the complete mixing model is to spread mass over a large area, with consequent lower maximum concentrations. The effect of the streamline routing model, in contrast, is to confine mass to a few paths resulting in higher concentrations.

4.1.2 Regionally divergent-convergent flow field

The second group of simulations is based on a regionally convergent-divergent flow field created by a system of two wells. The domain is square with two orthogonal fracture sets that are parallel to the sides. Infinite fractures are distributed within the domain with a regular spacing of 20 m. Two well locations are defined at fracture intersections close to the center of the domain (Figure 4.9).

The steady-state flow pattern generated by the two well system, one recharging and the other pumping, is a function of the boundary conditions. Constant hydraulic heads are prescribed along the boundaries with values corresponding to the no flow equilibrium situation prevailing before the wells start working. For the flow pattern created by a well doublet, care must be taken to assure that boundary effects do not intrude on the solution. The key consideration is the size of the region surrounding the wells. In general, it must be expected that part of the injected fluid will leave through the boundaries and that an equivalent proportion of native fluid will be mixed in the pumped well. Ideally the boundaries should be far away to avoid flux crossing them. Numerical limitations, however, require a finite boundary.

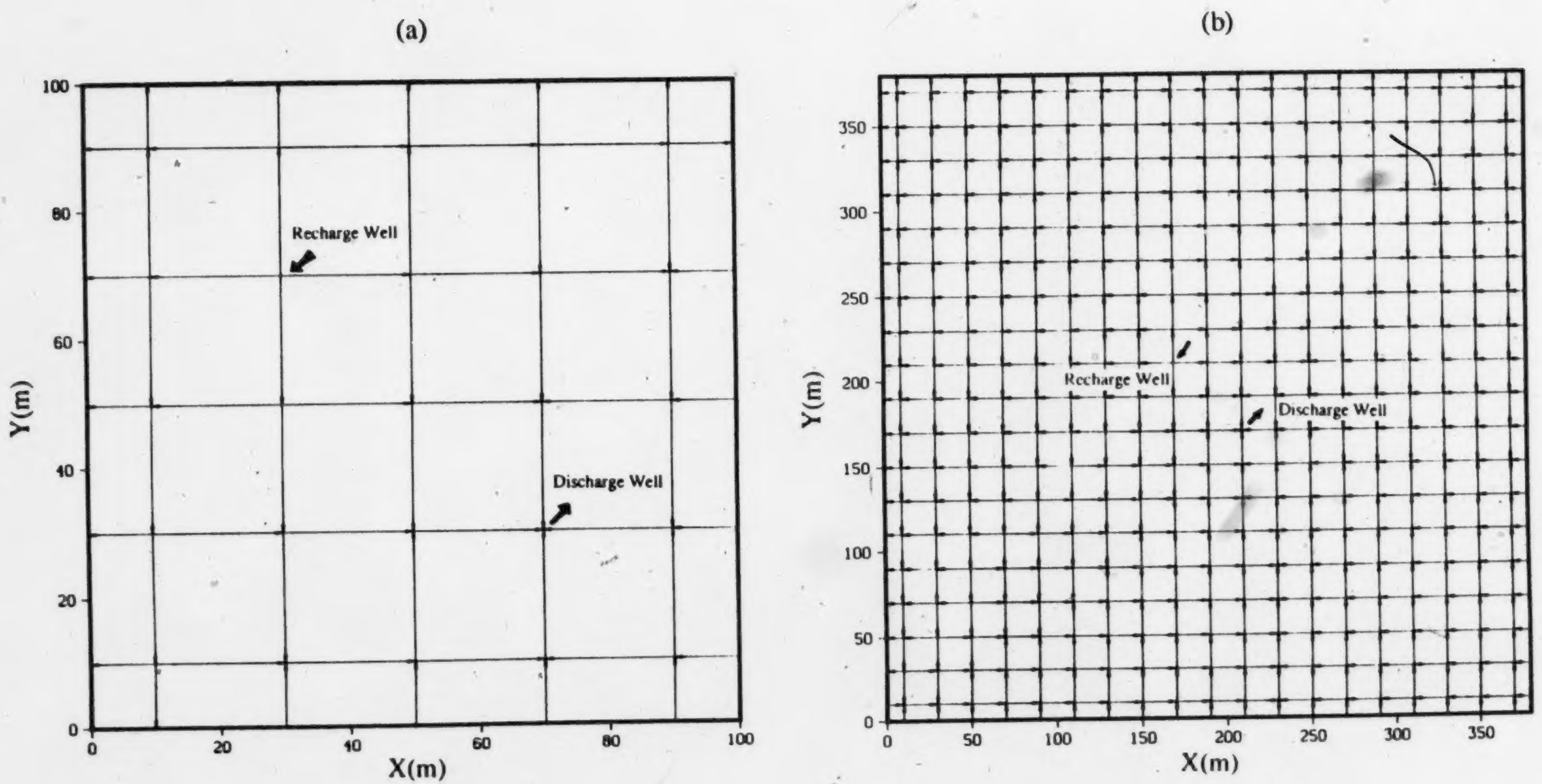
(a)
(b)
Recharge Well
Discharge Well
Y(m)
X(m)
0
20
40
60
80
100
0
50
100
150
200
250
300
350

Fig. 4.9 Fracture networks for the two-well system, showing the direction of the groundwater movement. (a) 100 m x 100 m. (b) 380 m x 380 m.

a) Definition of a suitable region size

The influence of the region size on the flow pattern and consequently on the mass transport can be assessed through the analysis of both the recovery parameter and the breakthrough curves at the pumping well. The recovery represents the maximum concentration at the pumping well, for a continuous injection of fluid with unit concentration. Four different region sizes were considered: 100x100m, 180x180m, 380x380m and 500x500m. The injected/pumped discharge was maintained at constant rate of 3.128×10^{-5} m³/s/m for all cases.

After the flow equation was solved and the flow field defined, the recovery was calculated as the relation between the boundary recharge and the total withdrawn discharge. These values are shown in Table 4.2. For areas larger than 380x380m the recovery starts to increase very slowly and the possible benefits gained by a better representation of the flow field may be offset by the cost of obtaining them.

Table 4.2. - Recovery for different region sizes.

Region size (m)	Boundary recharge (m³/s/m)	Recovery (%)
100x100	1.872×10^{-5}	0.401
180x180	1.118×10^{-5}	0.643
380x380	0.545×10^{-5}	0.825
500x500	0.415×10^{-5}	0.867

The corresponding breakthrough curves at the pumping well are compared in Figure 4.10. As the region size increases, additional flow paths become available and the maximum concentration, or the recovery, increases, but its increase has a natural time delay associated with it, producing a long tail for the breakthrough curve. In this example, advection dominates and the tail is a result of the delays along slow flow paths and not of diffusion into matrix. Diffusion into matrix, in fact, only smooths the steps (refer to section 4.2.1).

The first tracer arrival also depends on the region size. As it increases, the first arrival happens earlier and with higher concentration. This is due to the extra resistance of new fractures in the network that force an increase in the head difference between the two wells to drive the same discharge through the network. Consequently, the velocities along the shortest flow paths increase, increasing the mass flux and the tracer concentration at the pumping well. These differences start to become negligible for areas larger than 380x380m.

For this particular example, the analysis of both the recovery parameter and the breakthrough curves suggest that 380x380m can be considered as a workable region size. Anything larger than this seems to add very little information, even for the tail of the breakthrough curve.

It is important to note that the fracture system considered has open boundaries and that the only hydraulic stresses imposed on the system are due to the two-well discharge/ recharge pattern. As a consequence, the maximum concentration at the pumping well, or the recovery, is independent of the intersection mixing model considered. It is a function only of the region size, as a simple mass balance can show (vide Table 4.2).

b) Comparison of the mixing models

The effects of the two different approaches for dealing with mass distribution at intersections can now be evaluated. Based on a region size of 380x380m, regularly spaced

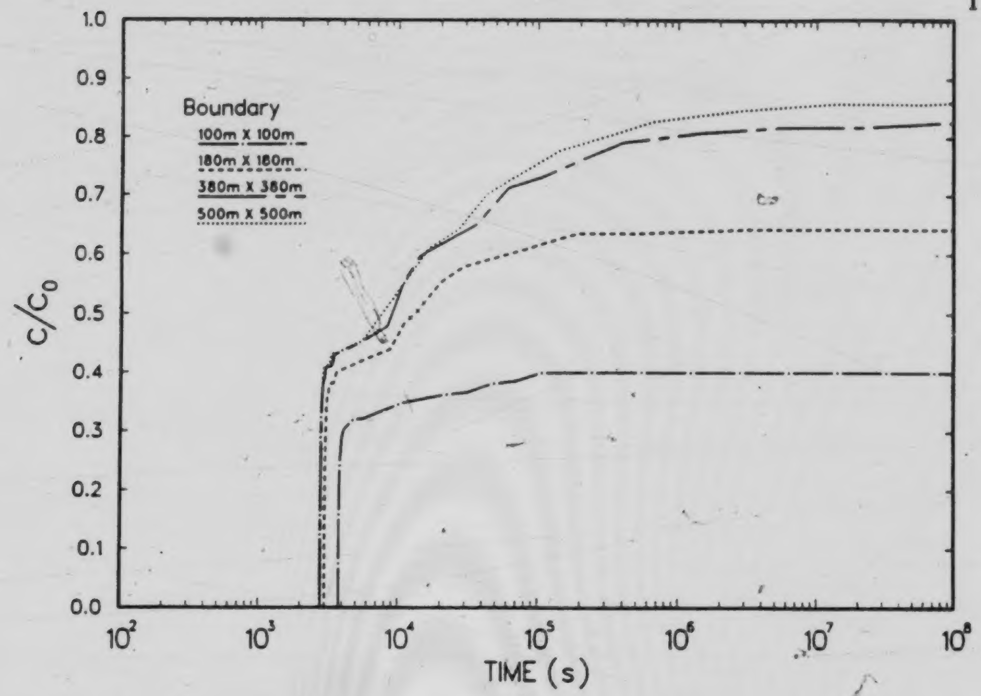

Fig. 4.10 Breakthrough curves at the pumping well for different region sizes (complete mixing model).

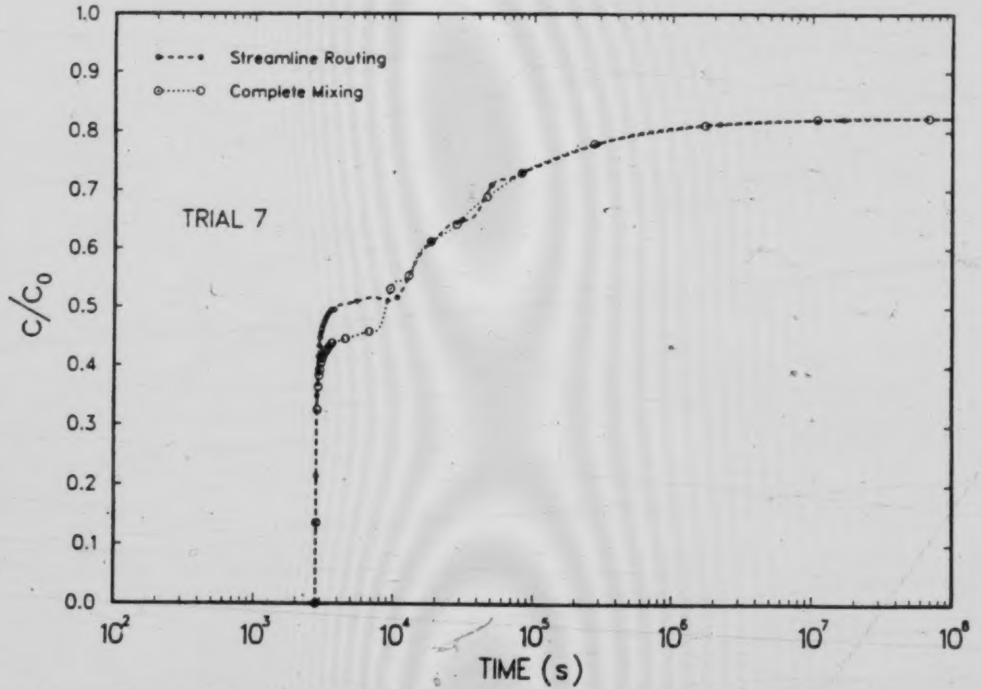

Fig. 4.11 Comparison of the effects of the mixing models on the breakthrough curves at the pumping well (Trial 7).

and randomly generated fracture geometries were considered (Figures 4.9b and 4.14, respectivily). For both geometries, three different trials consider both uniform and random aperture distribution. For all trials, the mean fracture aperture is 200 μm, the matrix porosity is 0.01, the matrix effective diffusion coefficient is 1.6×10^{-10} m^2/s and the well recharge/discharge is 3.128×10^{-5} m^3/s/m. Table 4.3 lists for each trial the respective coefficient of variation for the aperture distribution.

Table 4.3 Coefficients of variation for the aperture distribution.

Fracture geometry	Trial #	C_v	Realization #
	7	0.0	
uniformly distributed	8	0.5	1
		0.5	2
	9	1.0	1
		1.0	2
	10	0.0	
randomly distributed	11	0.5	1
		0.5	2
	12	1.0	1
		1.0	2

The results obtained for trial 7 are shown in Figure 4.11. The two mixing models produce very similar breakthrough curves. Basically, the effect of the streamline routing model is to increase the concentration of the first arrival in relation to that of the complete mixing model. The steps in the breakthrough curves represent contributions from different flow paths. Many steps, however, have small magnitude and their contributions may not be noticeable, except for a slight waviness in the tail of the curves.

The different paths explain the differences due to the two mixing models. The streamline routing does not disperse mass at the intersections and the concentration that enters the faster path is higher, giving a higher value for the first arrival. The complete mixing, on the other hand, allows mass to enter slow paths and it takes longer for this mass to reach the pumping well, resulting in a delay for the respective increase in concentration. The same reasoning, however, can justify an inverse situation, where the complete mixing could lead to a higher concentration than the streamline routing (vide Figure 4.19b). It is important to note that the maximum concentration at the pumping well is independent of the intersection mixing models considered. As pointed out previously, the maximum concentration is a function of only the region size, which controls the relative difference between the well and boundary recharges.

Trials 8 to 12 show the influence of aperture and network variability on the effects of the mixing models. Trials 8 and 9 both involve a geometrically uniform fracture network with two realizations per trial, in which the aperture varied. The coefficient of variation for trial 8 is $C_v = 0.5$, while for trial 9 it is $C_v = 1.0$. The results are shown in Figures 4.12 and 4.13. In all four realizations the breakthrough curves show almost identical results for both mixing models.

Trials 10 to 12 have considered an example of a random fracture geometry (Figure 4.14). In trial 10 the fracture apertures are constant, while in trials 11 and 12 they are random and follow the scheme discussed for trials 8 and 9. The results are presented in Figures 4.15 to 4.17. The breakthrough curves, again, exhibit the same shape for both mixing models.

The introduction of randomness in both fracture aperture and geometry has the tendency to offset the differences due to the different mixing models. However, the results

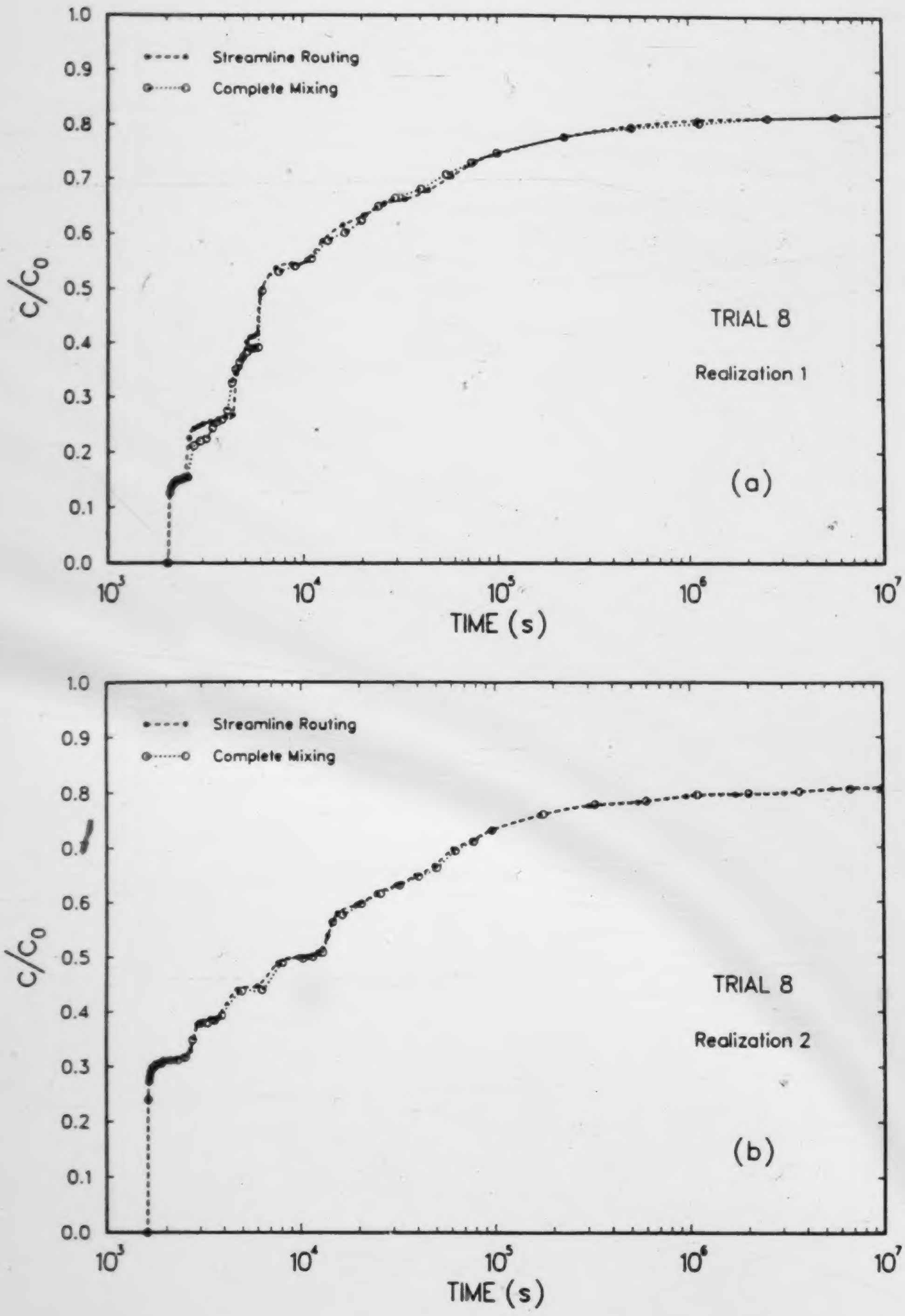

Fig. 4.12 Comparison of the effects of the mixing models on the breakthrough curve at the pumping well for Trial 8.

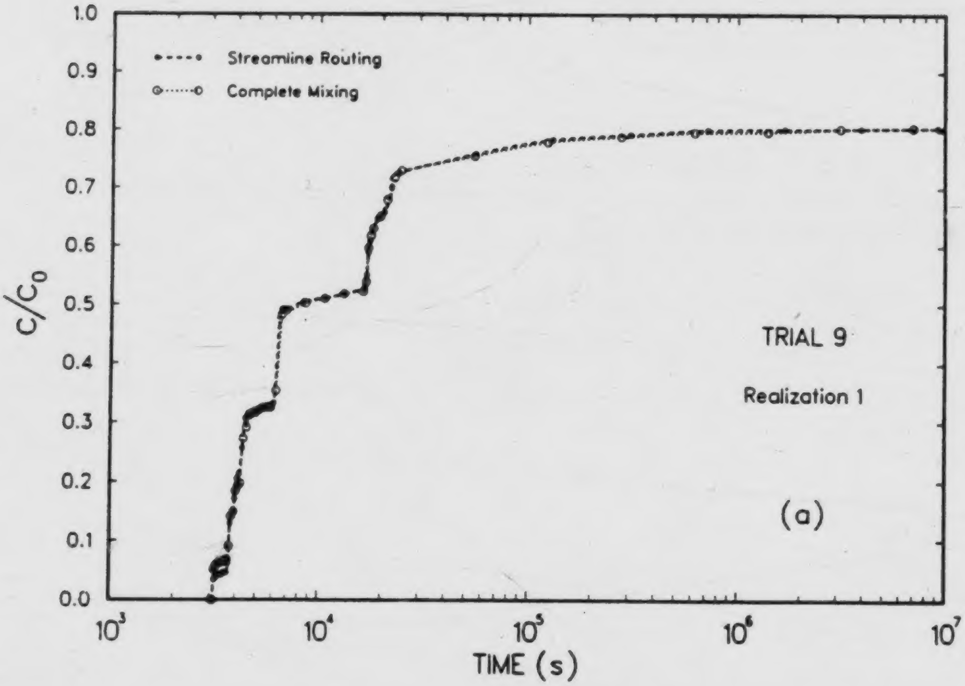

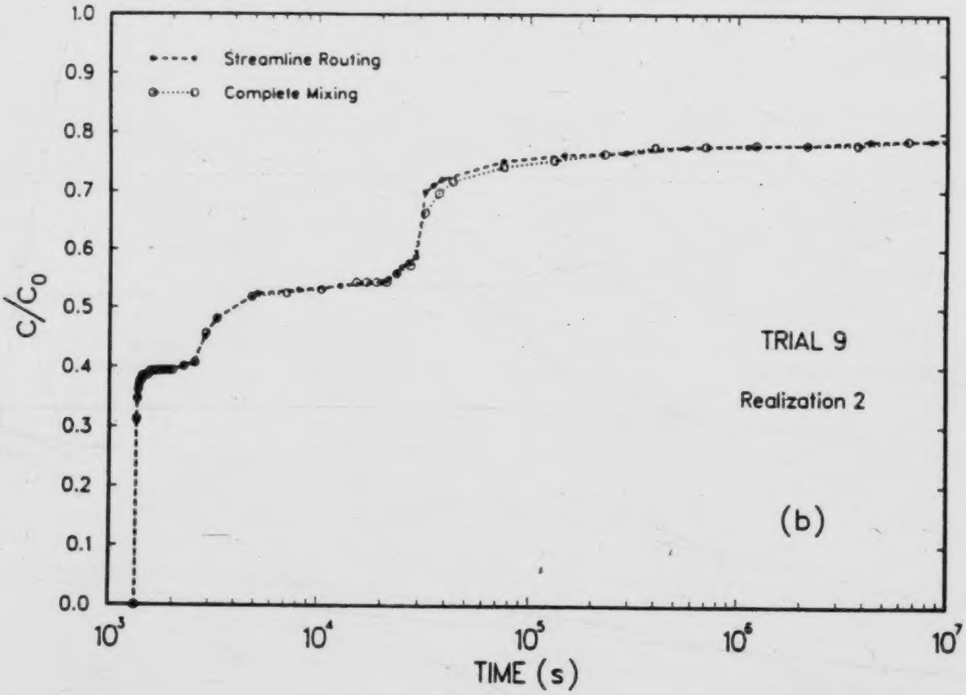

Fig. 4.13 Comparison of the effects of the mixing models on the breakthrough curve at the pumping well for Trial 9.

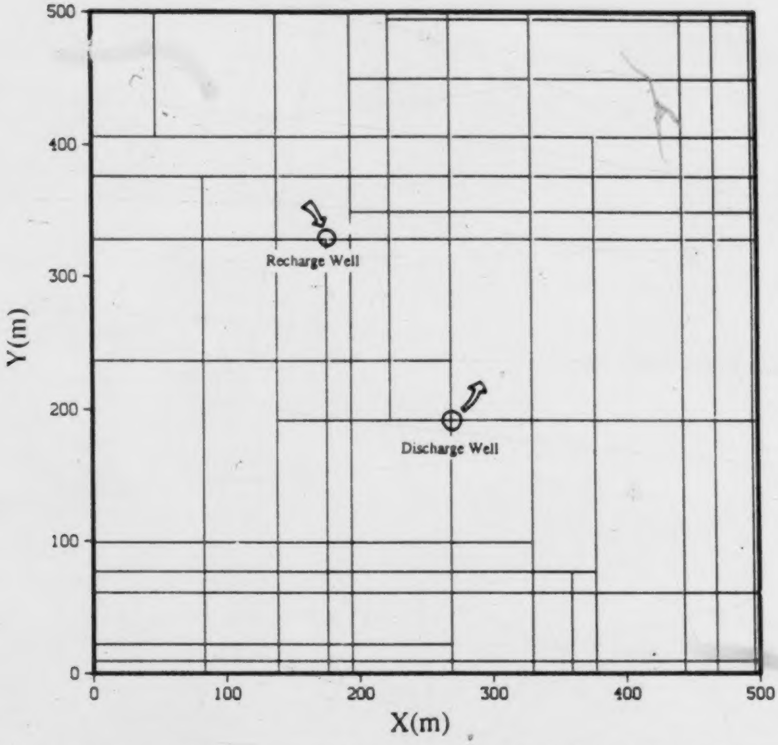
Recharge Well
Discharge Well
Y(m)
X(m)
0
100
200
300
400
500

Fig. 4.14 Random fracture network, considering variations in both fracture position and fracture length.

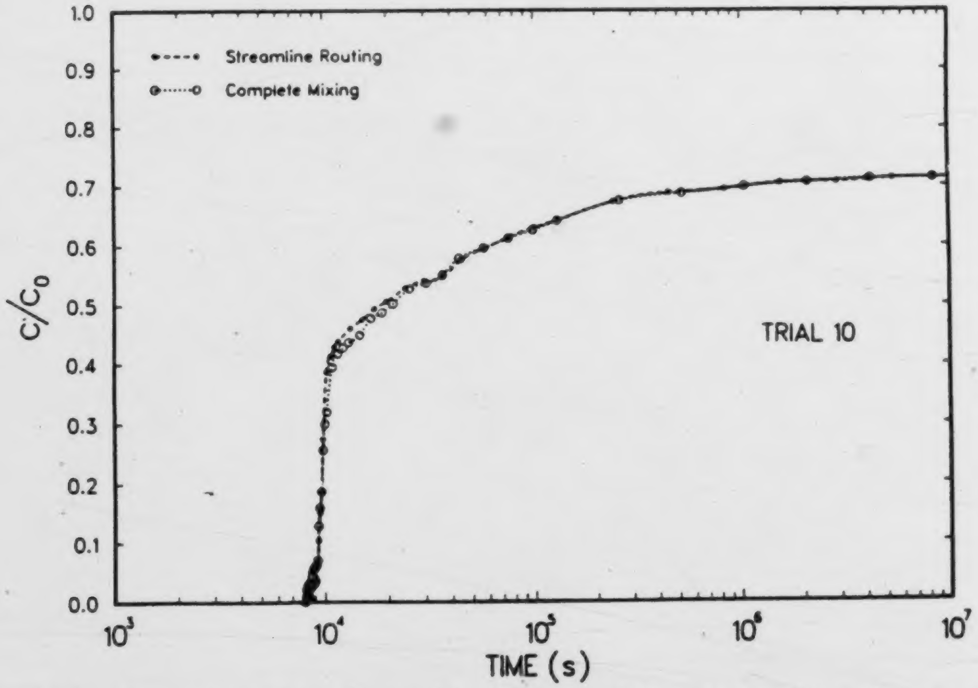

Fig. 4.15 Comparison of the effects of the mixing models on the breakthrough curve at the pumping well for Trial 10.

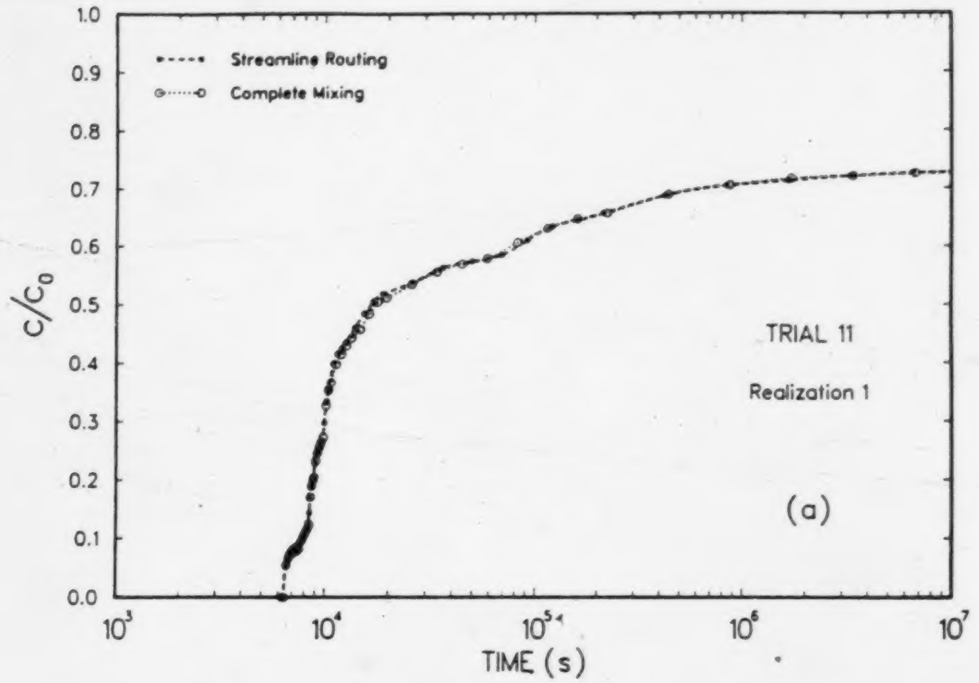

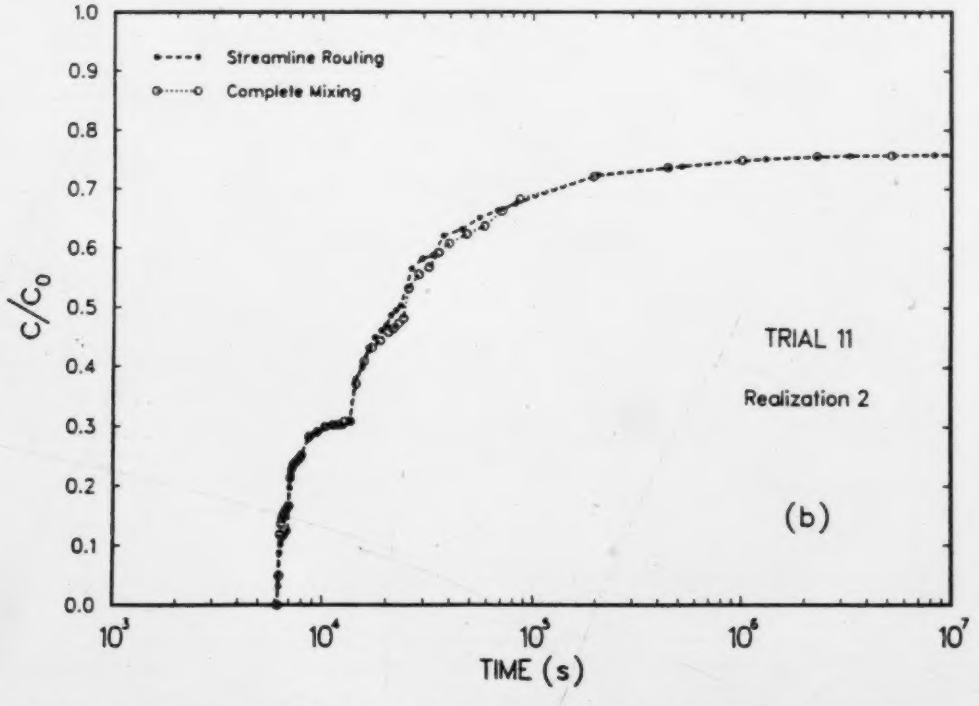

Fig. 4.16 Comparison of the effects of the mixing models on the breakthrough curve at the pumping well for Trial 11.

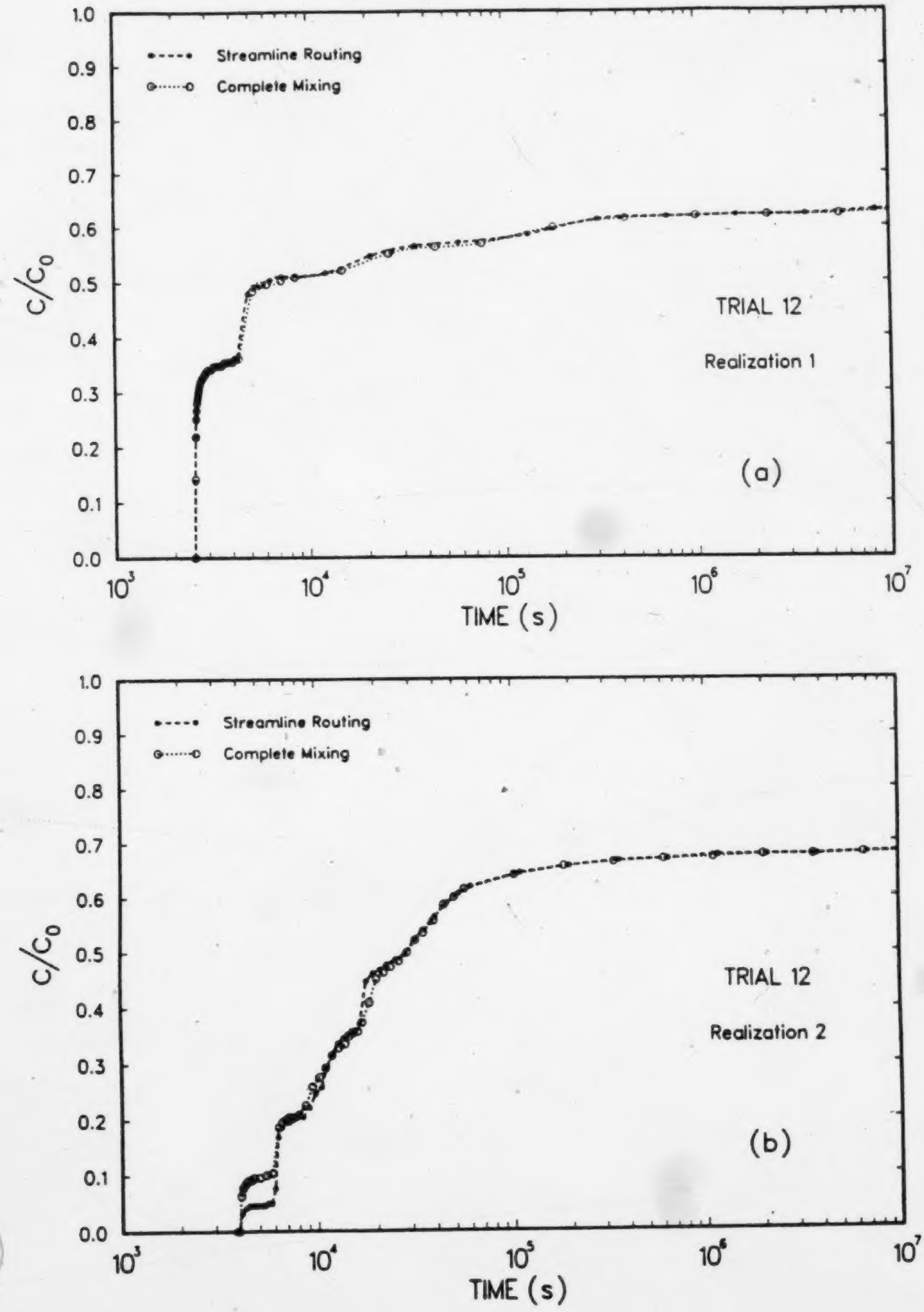

Fig. 4.17 Comparison of the effects of the mixing models on the breakthrough curve at the pumping well for Trial 12.

analyzed indicate that both mixing models yield similar breakthrough curves for a convergent-divergent flow field.

4.1.3 Discussion of results

The effects of the different intersection mixing models on the overall response of the fracture system are strongly dependent on the flow field conditions. In the case of the two well system, the two mixing models give essentially the same results. However, for the regional uniform flow field the different mixing models lead to different results.

The explanation for this flow dependent behaviour is related to the possible flow patterns at an intersection (Figure 4.18). In section 2.3.1 it was shown that only one, of four possible flow patterns at a fourway intersection, would yield different equations for the different mixing models: the continuous intersection (Figure 4.18d).

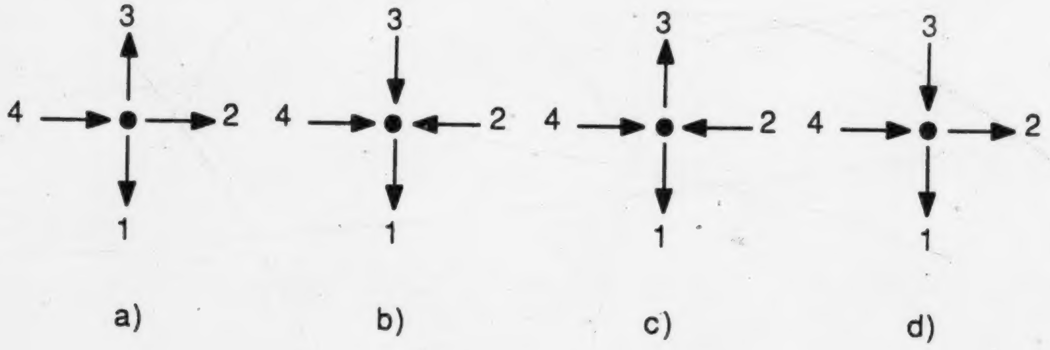

Figure 4.18 Possible flow patterns at a fourway intersection.

In a complex fracture system, all four intersection flow patterns are present. If patterns a), b) or c) predominate, then both mixing models would yield similar breakthrough curves at the same location, but if pattern d) dominates, then the different mixing models would, in general, yield different breakthrough curves. To establish whether the response of the system is affected by the different mixing models, it is necessary to estimate which intersection flow patterns are predominant for a given flow field and also the pattern of mass partitioning at successive intersections.

The two experiments mentioned in the beginning of section 4.1 provide good opportunity to verify these principles and explain why their results seemed to be contradictory.

/

Consider, initially, the fracture systems analyzed by Krizek et al. (1973) and reproduced in Figure 4.19. These systems consist of a rectangular region with two impervious boundaries (opposite sides), two constant head boundaries and an injection well at the center. The fractures, represented by the parallel plate model, have constant aperture and constant spacing. In the first case, the two head boundaries have the same value and the flow field generated by the injection well is symmetrical and only two types of flow patterns develop at the intersections, either type (a) or type (d), as defined in Figure 4.18. For flow patterns type (a), one inlet - three outlets, both mixing models give the same results. For flow pattern type (d), two inlets - two outlets, the different mixing models should give different results. This, however, is not the case for this particular situation. The regular fracture network, with constant aperture and spacing, leads to a radial symmetry in the flow field. Consequently, the two incoming discharges at a type (d) intersection are equal and, moreover, so are the concentrations. For this particular arrangement, the concentration leaving an intersection would be the same for both mixing models. The two different mixing models might give different results only if the flow field were asymmetric.

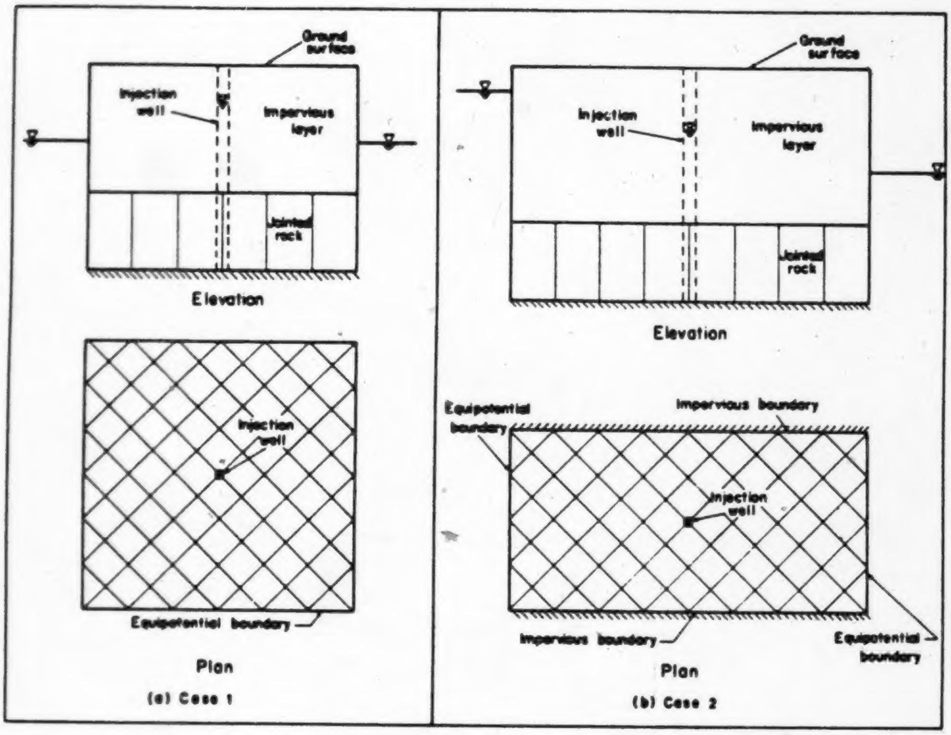
Ground surface
Injection well
Impervious layer
Jointed rock
Elevation
Injection well
Equipotential boundary
Plan
(a) Case 1
Ground surface
Injection well
Impervious layer
Jointed rock
Elevation
Equipotential boundary
Impervious boundary
Injection well
Impervious boundary
Equipotential boundary
Plan
(b) Case 2

Fig. 4.19 Fracture networks considered by Krizek et al. (1973).

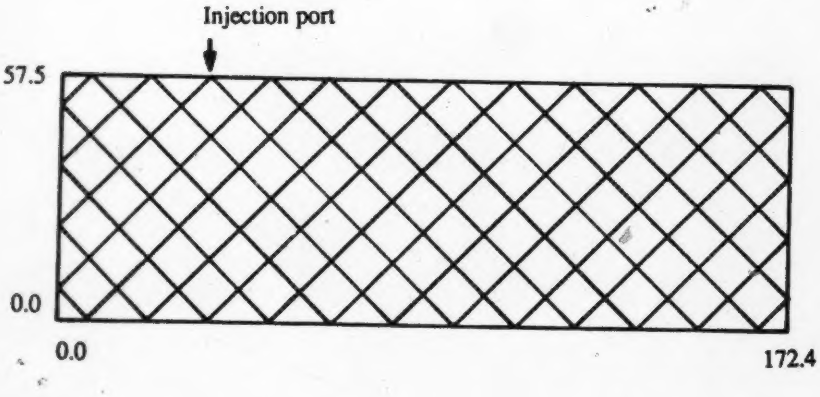
Injection port
57.5
0.0
0.0
172.4

Fig. 4.20 Fracture network considered by Hull et al. (1987).

In the second case the two constant head boundaries have different values (Figure 4.19b), creating a uniform flow field. If the head in the injection well coincides with that of the uniform flow, there is no disturbance of the uniform flow field and the injection is named passive. If, on the other hand, the head in the well is greater than the natural head, the injection is named active and the resultant flow field is a superposition of a simple uniform flow with a simple radial flow, that results in some backflow. Krizek et al. analyzed in detail the active injection of contaminant that generates an expanding plume. Inside the plume the flow pattern at the intersection was mainly type (a), while at the border it was type (b). This situation led to equivalent overall results for both mixing models.

Krizek et al. (1973), based on the above results, concluded that the different mixing models would not affect significantly the mass transport in discrete fracture network. Their generalization, however, was precipitate and should not be extended to different flow field configurations.

The experiments by Hull et al. (1987) considered only passive injection of contaminant. Their equally spaced, equal aperture fracture network is reproduced in Figure 4.20. The hydraulic gradient is parallel to the x-axis and the velocities are the same for both fracture sets. This type of problem is similar to the case analyzed in section 4.1.1, except for the source position. What controls the mass spreading is the type of mixing that occurs at the plume border, as it develops. The intersection pattern at the border is type (d), with only one inlet carrying mass. This pattern of flow accentuates the differences for the two mixing models. Just as an example, consider that mass arrives at the intersection through inlet number 3 (Figure 4.18d). Because flow is laminar and the discharges for both inlets are equal, the streamline routing model will take mass only to outlet number 2 with no dilution of concentration. The complete mixing model, in contrast, will take mass to both outlets with a 50% dilution in concentration, inducing, consequently, a larger spreading than the streamline routing model.

The apparent contradiction between the results of Krizek et al. (1973) and Hull et al. (1987) is, therefore, due to the different flow field configurations. For regular fracture networks, the differences are evident for regionally uniform flow field, but they become negligible for convergent/divergent flow fields.

These results have shown that different mixing models may lead to different system responses. The choice of an appropriate mixing model, however, should not be based on the response of the system, which is strongly dependent on the flow field, but rather on a careful analysis of the physics of mass transport at intersections.

4.2 The Effects of Diffusion into Matrix on the Overall Response of Discrete Fracture Networks

Diffusion into the matrix has already been shown to provide an important control on mass transport in fractured rocks (e.g., Neretnieks, 1980; Grisak and Pickens, 1980; Tang et al., 1981). Two examples are presented in this section to emphasize the influence of matrix diffusion in a fracture network and also to highlight some of the capabilities of the numerical model developed in this study. The first example considers a simple network with regular geometry, but variable fracture aperture. The second example considers a complex network with four fracture sets. Both analyses use the streamline routing model for mass distribution at intersections.

4.2.1 Regular fracture network

This example presents a reevaluation of trial 4, analyzed in section 4.1.1, by considering different diffusion coefficients. The fracture network, as shown in Figure 4.1b, consists of regularly spaced, infinite fractures with variable aperture, which derive from a log-normal distribution with mean 200 μm and coefficient of variation 1.0. The hydraulic gradient has a value of 1/15, with a direction of 34° in relation to the x-axis. The rock matrix porosity is 0.01 and two different diffusion coefficients have been considered: 1.6×10^{-10} and 1.6×10^{-12} m^2/s.

The original results presented in Figure 4.16 and reproduced in Figure 4.21a were based on a diffusion coefficient $D_m = 1.6\times10^{-10}$ m^2/s, which corresponds to the diffusive properties of tritium in a porous matrix with a tortuosity value of 0.1 (Tang et al., 1981).

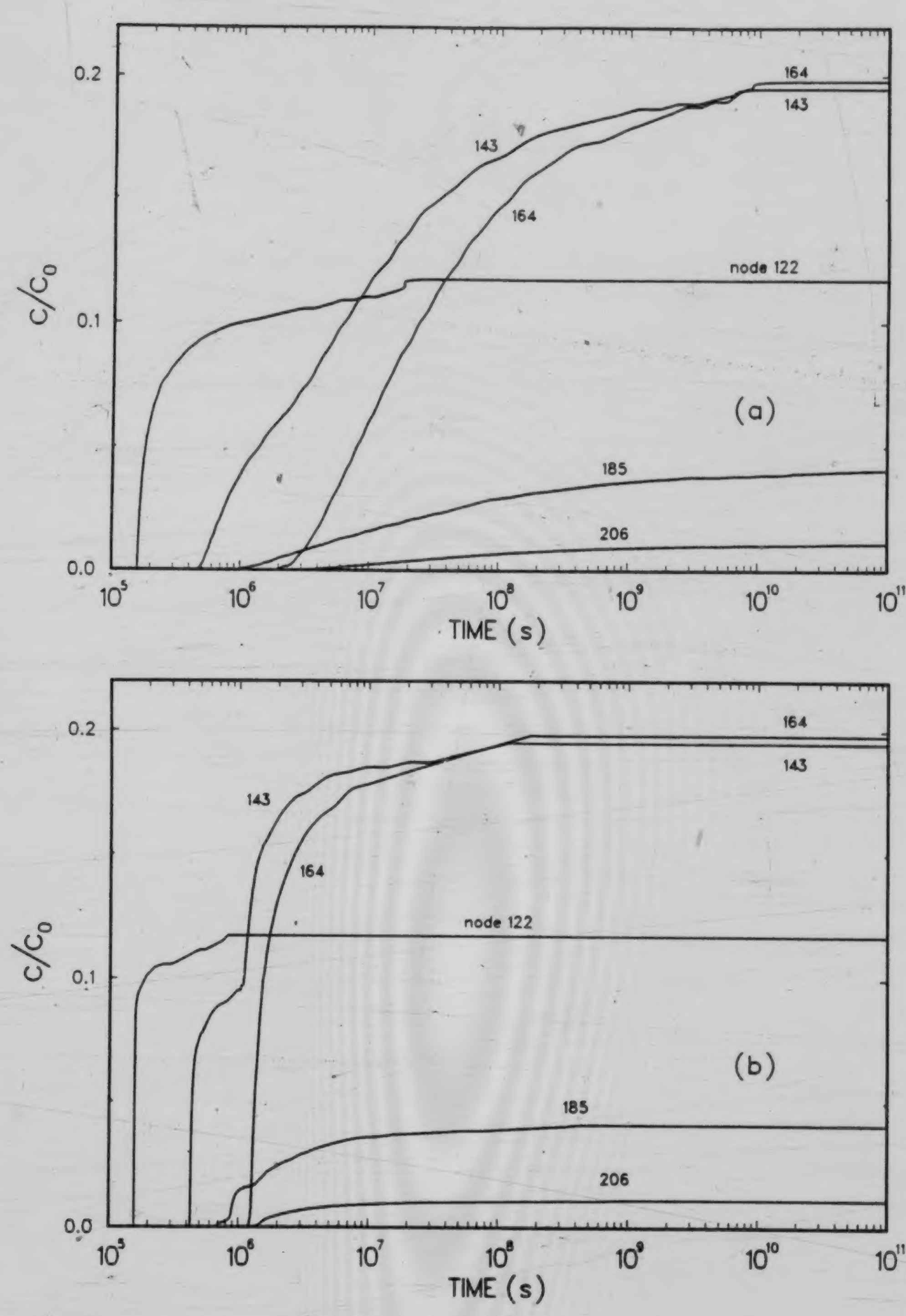

Fig. 4.21 Effect of the diffusion coefficient on the breakthrough curves for the network analyzed in Trial 4. (a) $D_m = 1.6\times10^{-10}$ m^2/s. (b) $D_m = 1.6\times10^{-12}$ m^2/s

The breakthrough curves span over a large time period and there is no evidence of concentration steps, in contrast to other situations analyzed in section 4.1.1.

When the diffusion coefficient decreases, there is a significant change in the shape of the breakthrough curves (Figure 4.21b). They become steeper with a few noticeable concentration steps and maximum concentration is obtained earlier than before. The breakthrough curve for outlet 143, for instance, presents a well defined contribution for a slower path. The smooth transition between the two almost vertical limbs is due to diffusion into the matrix. If advection were the only transport process, the breakthrough curves would be a succession of steps. Diffusion into matrix smooths these steps, which may disappear completely for high diffusion rates (vide section 4.3)

4.2.2 Complex fracture network

Following the procedure outlined in section 3.1, fractures from four different sets are generated over a square region 500 m x 500 m. Two factors control the final network geometry: the density and length of the fractures. The fracture density varies from set to set, but within a set the spacing between fractures is held constant. The fracture length is assumed to be a random variable, with exponential distribution, in order to produce variability in the geometry. The mean fracture length is constant for all sets, but the truncation factor, as defined by Schwartz et al. (1983), varied among sets. The fracture apertures are constant for a given fracture set. A summary of the relevant data for fracture generation is presented in Table 4.4. The resultant fracture network is shown in Figure 4.22.

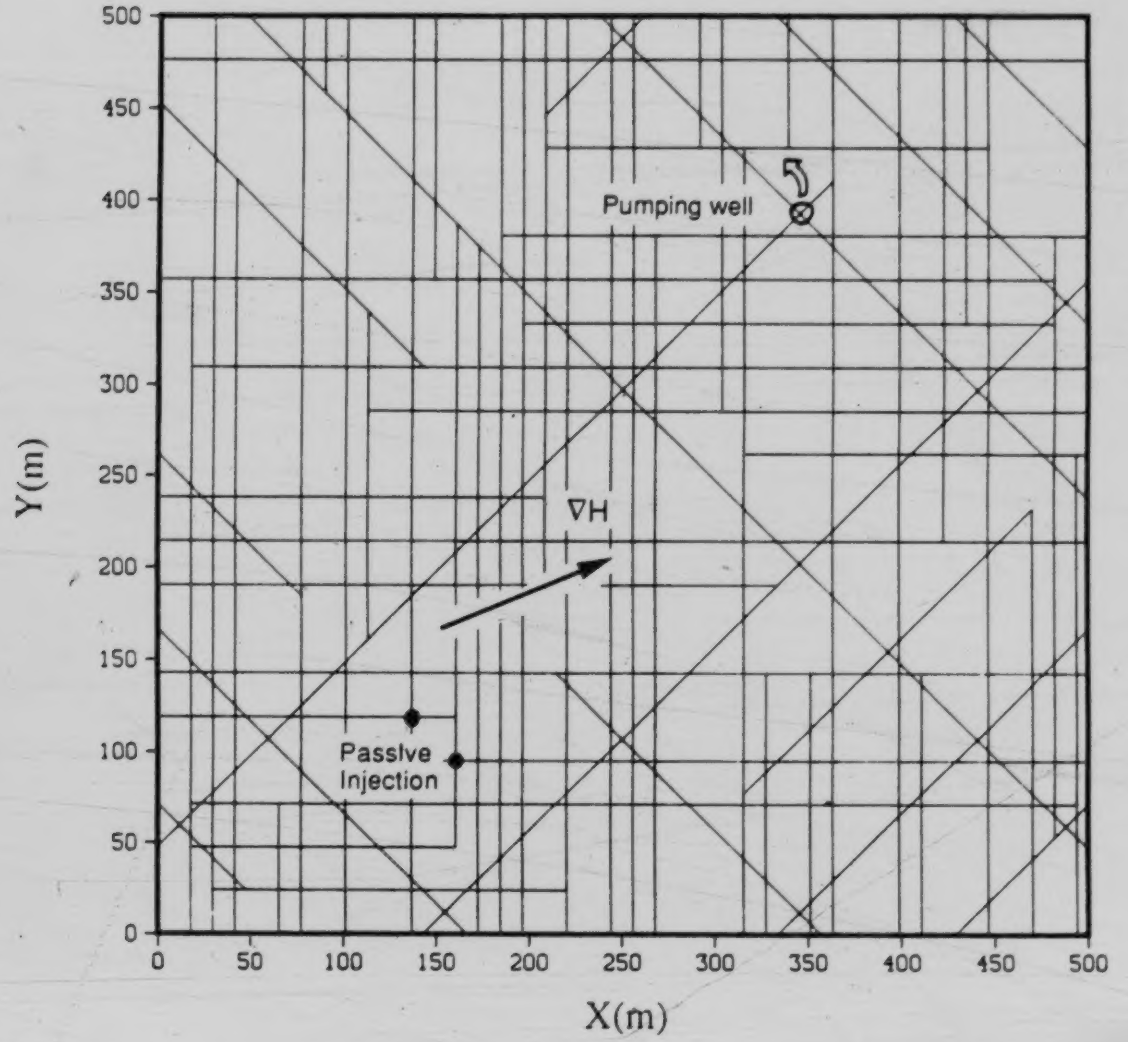
Y(m)
X(m)
0
50
100
150
200
250
300
350
400
450
500
Pumping well
∇H
Passive Injection

Fig. 4.22 Complex fracture network, showing the positions of the pumping well and the injection nodes.

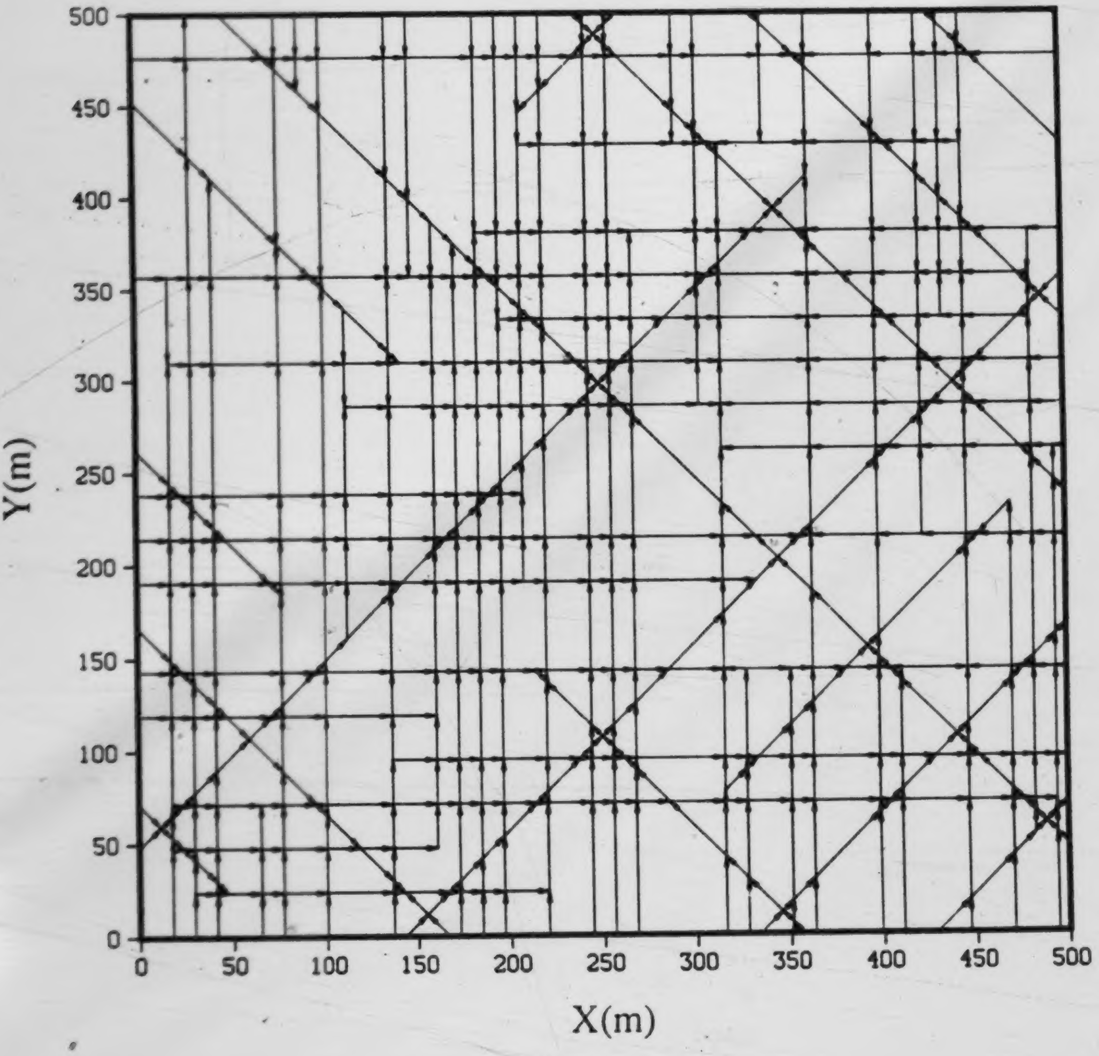

Fig. 4.23 Correspondent flow field obtained for the complex fracture network.

Table 4.4 Data used for fracture generation

Set	Angle	Truncation factor	Spacing (m)	Aperture (μm)
1	135°	0.40	67.34	250
2	45°	0.40	67.34	200
3	0°	0.25	23.82	100
4	90°	0.20	11.91	150

The flow conditions within the fracture network are defined by the combined effect of a pumping well and a regionally uniform flow field. The well is located at the intersection of two fractures (Figure 4.22), with a pumping rate of 1.0×10^{-6} $m^3/s/m$. The regional hydraulic gradient has a value of 1/500 and is oriented at 22.5° in relation to the x-direction. The resultant flow pattern is shown in Figure 4.23.

The mass transport through the fracture network is primarily dependent on the distribution of velocities within the network. Different flow conditions imply in different transport characteristics for a discrete network. The parameters related to the rock matrix, porosity and effective diffusion coefficient, are assumed to be constant throughout the rock. A value of 1% is assigned to porosity, while three different values are considered for the effective diffusion coefficient, 1.6×10^{-10}, 1.6×10^{-12}, and 1.6×10^{-14} m^2/s.

The accuracy of the mass transport simulations was verified by running a few tests with different NC values. Since NTP does not significantly influence the solution, as discussed earlier, its value has been set to 50. Figure 4.24 shows the breakthrough curves for three NC values, 100, 200 and 400. The results show that the numerical solution converges as NC increases. The value NC = 200 gives results comparable to NC = 400 and it has been adopted for the calculations.

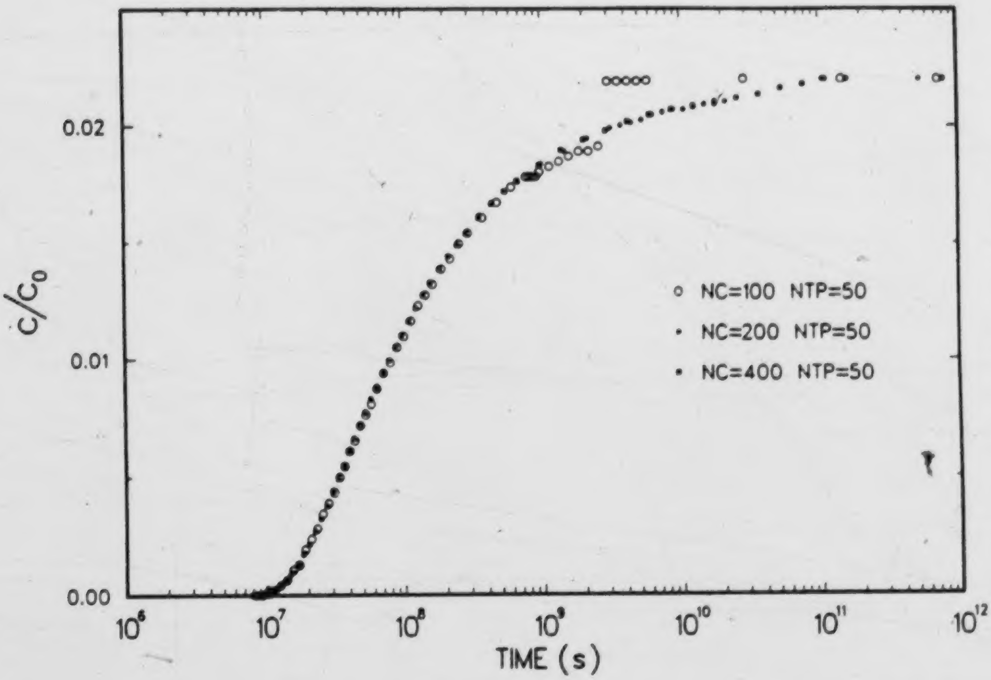

Fig. 4.24 Verification of the numerical model accuracy for the complex fracture network.

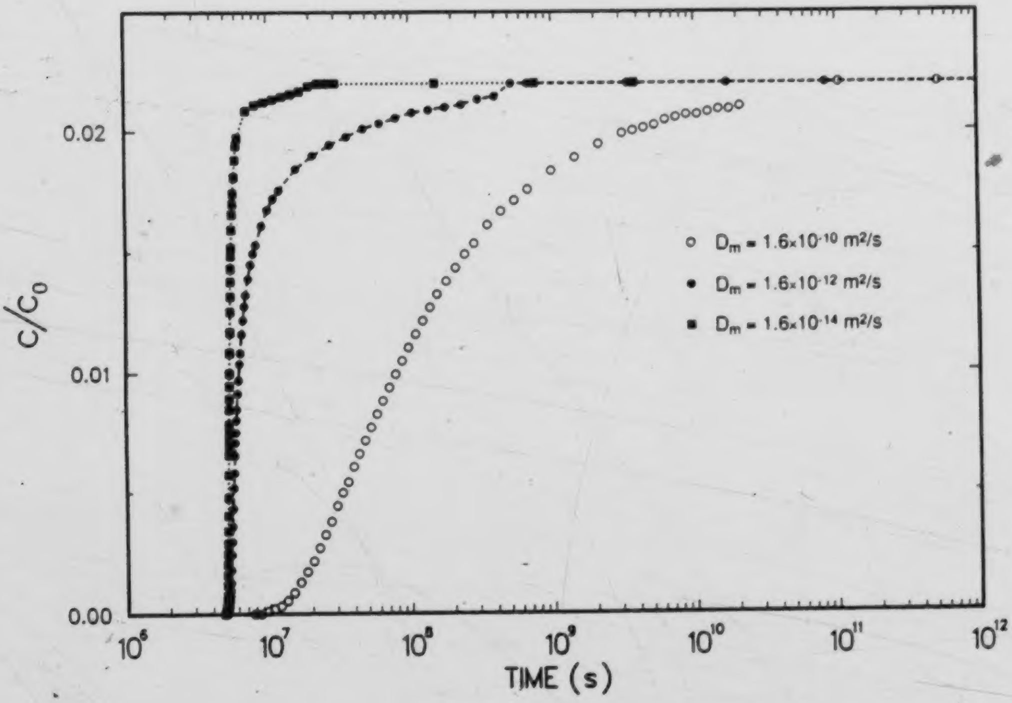

Fig. 4.25 Effect of the diffusion coefficient on the breakthrough curves obtained at the pumping well for the complex fracture network.

The pumping well provides a convenient point of convergence for the mass released into the system. By analyzing the breakthrough curves at the discharge well, the influence of diffusion into matrix can be assessed.

The results for the three different diffusion coefficients are presented in Figure 4.25. The breakthrough curves are, again, very distinct, showing that the influence of matrix diffusion is significant. As this coefficient decreases, advective transport dominates, becoming eventually piston-like. No concentration steps are evident in the breakthrough curves, even for the smallest diffusion coefficient.

4.2.3 Discussion

Diffusion into matrix is essentially a slow, time dependent process that becomes important when large times are involved (Neretnieks, 1980). The interesting point about these examples is the relatively short period of time it takes for the first signs of mass to show up at the sampling points.

For small diffusion coefficients, the first mass arrival is representative of mass transport by advection only. For the regular network, the first arrivals are in the range 2 to 15 days (Figure 4.21), while it is about 58 days for the complex network (Figure 4.25). If advection were considered the only mechanism for transport, the breakthrough curves, for both examples, could be almost completely developed within 120 days. This time frame is relatively short for groundwater movement. For example 1, with an average path length of 180 m, it implies in velocities in the range 15 - 90 m/day For example 2, the average length would be 380 m, implying in velocities of the order of 6.5 m/day.

The two examples show that, even in relatively active flow systems, diffusion into matrix does play an important role in retarding the contaminant arrival. The controlling parameters are well expressed in the dimensionless number δ, developed in section 2.5.1, which is defined as

$$\delta = \frac{\theta (R_m D_m)^{0.5}}{b R_f} \left(\frac{R_f L}{V} \right)^{0.5} \tag{4.1}$$

Considering no adsorption, the only parameters independent of the flow field are matrix porosity and diffusion coefficient. The influence of the later on mass transport has already been analyzed and attention is now focused on the matrix porosity. Its role is related to mass storage in the porous matrix. If, for example, the porosity increases, the storage increases, increasing the mass transfer from fracture to matrix and, consequently, reducing the concentration in the fracture. Rocks of low porosity and high confining pressures have porosity in the range 0.1% to 1% (Neretnieks, 1980). The results previously presented in this section were based on a value of 1%, which is the upper end of the range.

If, for example, $\theta = 0.001$ and $D_m = 1.6 \times 10^{-10}$ m^2/s , the results would be equivalent to the case where $\theta = 0.01$ and $D_m = 1.6 \times 10^{-12}$ m^2/s (same δ number for the two pairs of values). Consequently, as it can be seen in Figure 4.25, diffusion into matrix would still be important.

4.3 Mass Transport Behaviour for a Two Well System in Discrete Fracture Networks

In general, injection/withdrawal testing has been used to collect information about mass transport in fractured and porous media (Raven et al., 1988; Novakowski, 1988; Jensen, 1983; Fossum, 1982) The interpretation of the resulting data is not a simple matter and is dependent on the correct selection of a model that represents the physics of mass transport. Because the mass transport in fracture networks is complex in nature, the interpretation of field tests is difficult and often simplified models are used. In many situations, a one-dimensional model has been adopted, based on the assumption that the fracture system could be represented either as a single fracture or as a system of parallel fractures. The transport parameters have actually been estimated by fitting the chosen model to the available data. Although this procedure allows one to obtain numerical values for the parameters, these estimates are only as good as the assumptions involved in the selection of the model.

It is in this context that the model developed in this study finds a useful application. By analyzing mass transport at the fracture scale, this model provides a powerful tool that can be used to verify many of the assumptions underlying the current models used in the interpretation of field tests. Three major issues, concerned with the overall response of the system, are addressed here: (1) the influence of different paths within the fracture network; (2) the effects of different injection conditions; and (3) the effects of different fracture densities. These three points are all interrelated and they have been separated only for simplicity. The influence of matrix diffusion is implicitly considered as the analysis progresses.

In this section, mass transport is analyzed by means of the analytical procedure described in section 2.4. It becomes feasible, because the fracture networks are relatively simple.

4.3.1 Distinct paths within fracture networks

The mass transport in a fracture network is strongly dependent on the flow field developed within the network. In a two well tracer test, the flow field is divergent near the injection well and convergent near the withdrawal well. In between, there is a transition zone where the flow might be close to uniform. It is common practice to have both the injection and withdrawal rates the same. In the subsequent analysis, the streamline routing model has been adopted as the mixing model for partitioning mass at fracture intersections.

Because of the discrete character of the network, mass moves through the fractures and several paths may conduct the tracer from the injection well to the withdrawal well. Each path is a combination of several fracture segments and each has a characteristic residence time. The breakthrough curve at the withdrawal well represents the contributions of all the paths that convey the tracer to the withdrawal well. In many instances, the contributions of several paths are clearly defined in the breakthrough curve. Figure 4.26 shows a simple fracture network with variable fracture aperture, while Figure 4.27 shows the corresponding breakthrough curve at the withdrawal well.

A simple inspection of the breakthrough curve shows that at least four different path contributions can be identified. In fact, there are nine paths that convey the tracer from the injection well to the withdrawal well, but many of them contribute very little. All possible paths are listed in Table 4.5, arranged in the order of arrival, and the relative contribution of

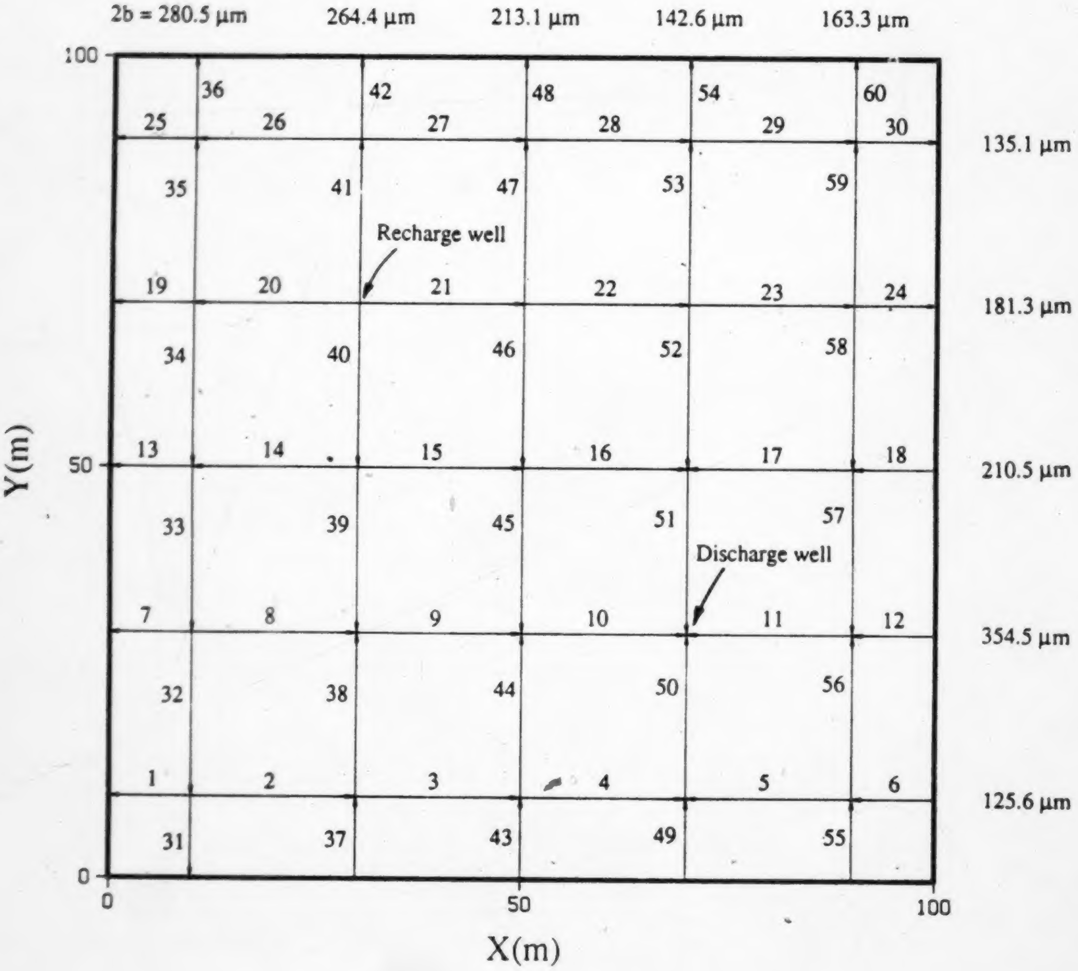
2b = 280.5 µm
264.4 µm
213.1 µm
142.6 µm
163.3 µm
135.1 µm
181.3 µm
210.5 µm
354.5 µm
125.6 µm
Recharge well
Discharge well
Y(m)
X(m)
0
50
100
1
2
3
4
5
6
7
8
9
10
11
12
13
14
15
16
17
18
19
20
21
22
23
24
25
26
27
28
29
30
31
32
33
34
35
36
37
38
39
40
41
42
43
44
45
46
47
48
49
50
51
52
53
54
55
56
57
58
59
60

Fig. 4.26 Hypothetical regular fracture network, showing the different apertures for each fracture and the position of the wells.

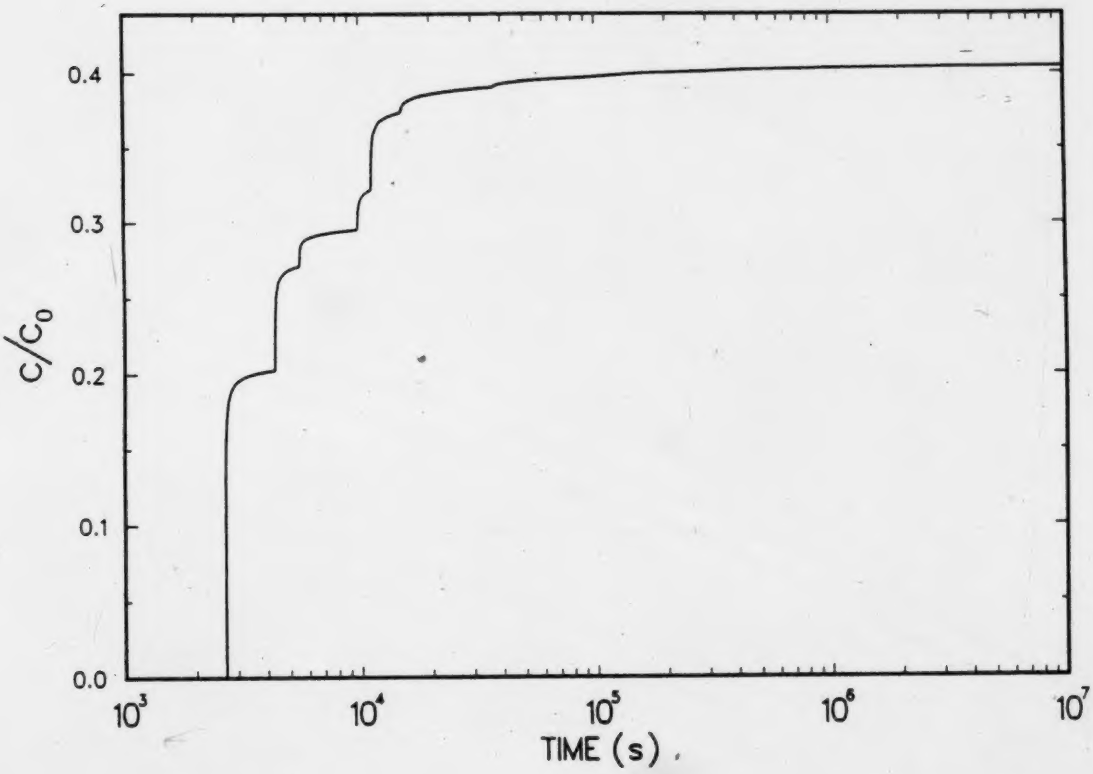

Fig. 4.27 Breakthrough curve obtained at the pumping well for a continuous injection.

each one to the breakthrough curve is shown in Figure 4.28. In the following paragraphs, an analytical procedure is developed to evaluate the elementary breakthrough curves for each path and it is shown how they can affect the breakthrough curve.

Table 4.5 Sequence of segments for each path.

Path	sequence of segments
1	40 39 9 10
2	40 15 45 10
3	21 46 45 10
4	21 46 16 51
5	40 14 33 8 9 10
6	21 22 52 51
7	21 22 23 58 57 11
8	21 22 23 58 17 51
9	40 14 33 32 2 38 9 10

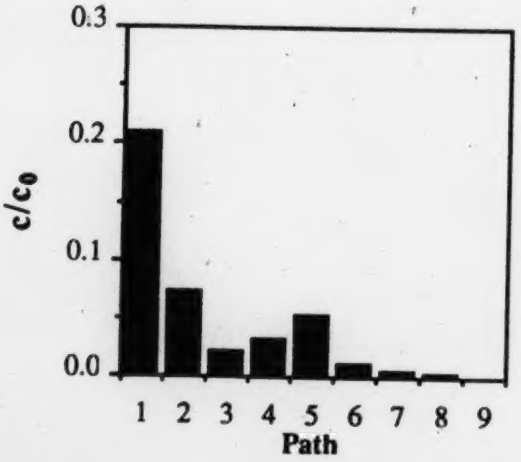

Figure 4.28 Relative contribution of the the different paths.

In this analysis only advection and matrix diffusion are considered, because of the simplicity of the corresponding unit step response function that does not require the evaluation of the convolution integral (as discussed in section 2.4).

The unit step response function (eq. 2.12) takes then the form,

$$c = erfc\left[\frac{A}{(t-B)^{0.5}}\right] \quad \text{in the Real domain} \qquad (4.2)$$

or

$$C = \frac{1}{s} exp\left[-\left(A\, s^{0.5} + B\, s\right)\right] \quad \text{in the Laplace domain} \qquad (4.3)$$

where A and B are defined by equation (2.35), i.e.

$$A = \frac{\theta (R_m D_m)^{0.5} L}{Vb}$$

$$B = \frac{R_f L}{V}$$

The application of the convolution theorem to a fracture network, as shown in section 2.4 and Appendix A, leads to a response function for each path of the form

$$c_j = (c_{max})_j\, erfc\left[\frac{A_j^T}{\left(t - B_j^T\right)^{0.5}}\right] \qquad (4.4)$$

where

$$A_j^T = \sum_{i=1}^{n_j} A_i$$

$$B_j^T = \sum_{i=1}^{n_j} B_i$$

n_j is the number of segments in the path j, $(c_{max})_j$ represents the percentage of the tracer that follows path j, and the subscript i refers to individual segments along path j. The breakthrough curve at the withdrawal well (the response of the system) is obtained by adding the contributions of all paths that arrive at the well,

$$c^T = \sum_{j=1}^{n_{paths}} c_j \tag{4.5}$$

At steady state (t → ∞), c^T is equivalent to the recovery at the withdrawal well. Table 4.6 lists the parameters $(c_{max})_j$, A_j^T, B_j^T, for each path given in Table 4.5 The relative importance of each path is given by the $(c_{max})_j$ factor, as shown in Figure 4.28. The parameter A_j^T conveys information related to matrix diffusion, while B_j^T represents the advective residence time for the path.

Table 4.6 Parameters for each path shown in Table 4.5

Path number	$(c_{max})_j$	A_j^T [$s^{1/2}$]	B_j^T [s]
1	0.20905	1.106	2661.1
2	0.07294	2.400	4331.3
3	0.02039	3.243	5522.2
4	0.03180	6.517	9768.8
5	0.05247	4.819	11206.
6	0.01121	12.38	14997.
7	0.00383	27.31	36826.
8	0.00211	63.03	96677.
9	0.00086	186.8	298476.
TOTAL	0.40467		

The solution for each path can be thought as a solution of an equivalent single fracture that contains, intrinsically, the contributions of several fracture segments. Different paths, in general, are represented by different equivalent single fractures. But the paths are not completely independent of each other: they share several fracture segments among themselves. The final response of the system is therefore very site specific and it depends on the relative magnitude of the path breakthrough curves.

As the number of fracture segments and intersections increase, the likelihood of different paths having similar parameters increases. The tendency is to increase the number of paths and reduce the relative importance of each one. The overall response of the system becomes complex due to the combination of many individual breakthrough curves and a single fracture model is not appropriate anymore, but a multi-fracture model is not feasible to implement either, because thousands or millions of individual paths may be present in the solution. The response of the system, therefore, represents the transport behaviour in a region around the two wells. Its size is a function of the hydraulic stress being applied. Most important of all, the transport behaviour cannot be dissociated from the velocity field generated by the hydraulic boundaries. For instance, data obtained from a two well tracer test with a discharge/recharge pattern will yield different parameters from data obtained from a two well tracer test with a passive injection or passive withdraw, because the flow field generated is different for each of the three situations. The resulting paths followed by the tracer are different for each situation and so will be the respective transport parameters, because different fractures are being sampled in each situation.

For the case shown in Figure 4.26, one path is responsible for 50% of the total mass transport to the withdrawal well. From 9 paths that convey tracer to the withdrawal well, 95% of the tracer is taken by five paths, while 5% is taken by four slow paths. In fact, the bulk of the transport is localized in the region between the two wells, what could be called direct paths, and only a small percentage take a longer path. It should be recalled, however, that the size of the region surrounding the wells plays an important role in defining the tail of the breakthrough curve, because longer paths take longer times to reach the withdrawal well.

This results suggest that most of the transport in a two well tracer test is probably restricted to the region between the two wells and care must be taken when extrapolating the data beyond that region. If the fractures are sufficiently dense, such that a REV can be contained within the two wells, then it is possible that variations in the positioning of the wells do not significantly affect the breakthrough curves at the withdrawal well.

Parameters derived from the breakthrough curve depend on the model assumed for mass transport. An important point is that fracture or fracture segment data are not possible to obtain. The data reflects the behaviour of individual paths and not of individual segments or fractures.

4.3.2 Effects of different injection conditions

The interpretation of a two well tracer test may be also dependent on the way the tracer is introduced into the fracture system. The example considered in Figure 4.26 assumes a continuous injection of tracer, but many tests are performed using an instantaneous injection. Theoretically, the response due to an instantaneous injection is just the time derivative of the response due to a continuous injection and both types of injection should yield the same estimate for the transport parameters, but this may not be the case.

Consider the same fracture system depicted in Figure 4.26, but now also subjected to an instantaneous mass injection. The responses at the withdrawal well due to both types of injection are illustrated in Figure 4.29. The flow field generated is relatively fast and the contribution of each path is characterized by either a step, in the case of continuous injections, or a spike, in the case of instantaneous injection. Both steps and spikes occur at the same time. It is interesting to note that only four spikes can clearly be identified in the Figure, from a total of 9 spikes. The breakthrough curves for the continuous injection, however, allows more steps to be identified. The magnitude of the spikes decrease very fast for the slower paths and they become negligible when compared to the first tracer arrival. By considering a log-scale for the concentration, all spikes can be seen (Figure 4.30). It is, however, questionable whether field measurements could achieve the necessary precision to identify all the steps. The identification of slower paths becomes more difficult, when a slower, and more realistic, velocity field is considered. The residence time of the injected mass increases and effects due to diffusion into the matrix becomes important.

In the second case analyzed, the velocities in the fractures have been reduced by a factor of 100, by considering a corresponding reduction in the injection/withdrawal rates. Although this reduction in rates alters the magnitude of the flow velocity in the fracture, it does not alter its relative distribution in the fracture network and the flow paths are maintained. The breakthrough curves obtained for both types of injection are shown in Figure 4.31 For the continuous injection, the steps have been smeared out and the breakthrough curve becomes an almost smooth curve. The contributions of slower paths can still be identified by the presence of slight discontinuities in the breakthrough curves. However, in a real field experiment, where observations are discrete in nature, the steps could probably be associated with experimental errors and, most likely, a unique smooth curve would be drawn for the interpretation of the data. For the instantaneous injection, a similar behaviour is observed. Instead of spikes, a two peak, smooth curve is obtained. Basically, only the two fastest paths can be identified in this curve. Diffusion into the matrix has united all spikes into a single curve, making it hard to distinguish different paths. With the previous knowledge of the position of the spikes (from Figure 4.30), it is

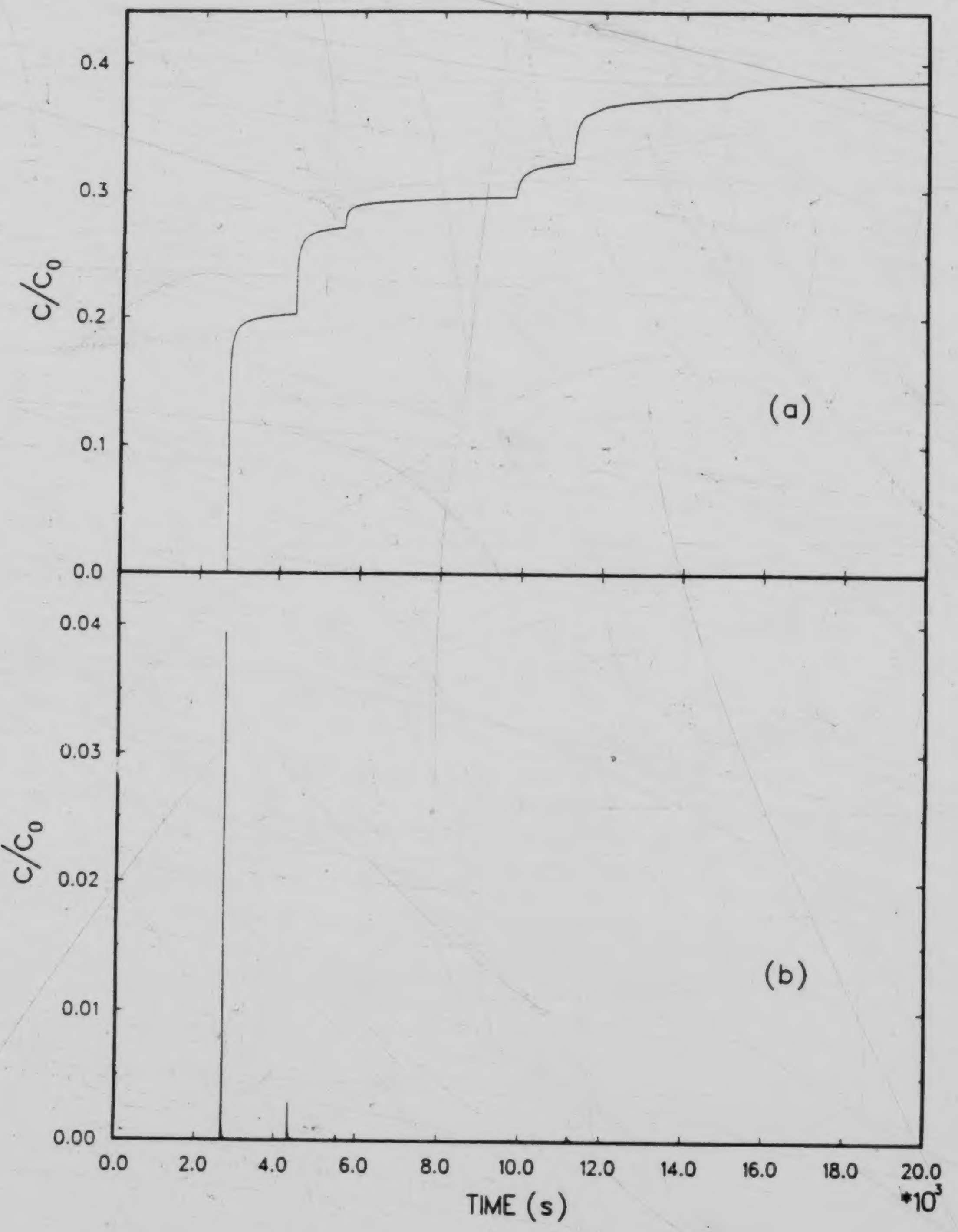

Fig. 4.29 Breakthrough curves obtained at the pumping well, for a injection/ withdrawal rate $Q = 3.128\times10^{-5}$ m^3/s/m. (a) continuous injection. (b) instantaneous injection.

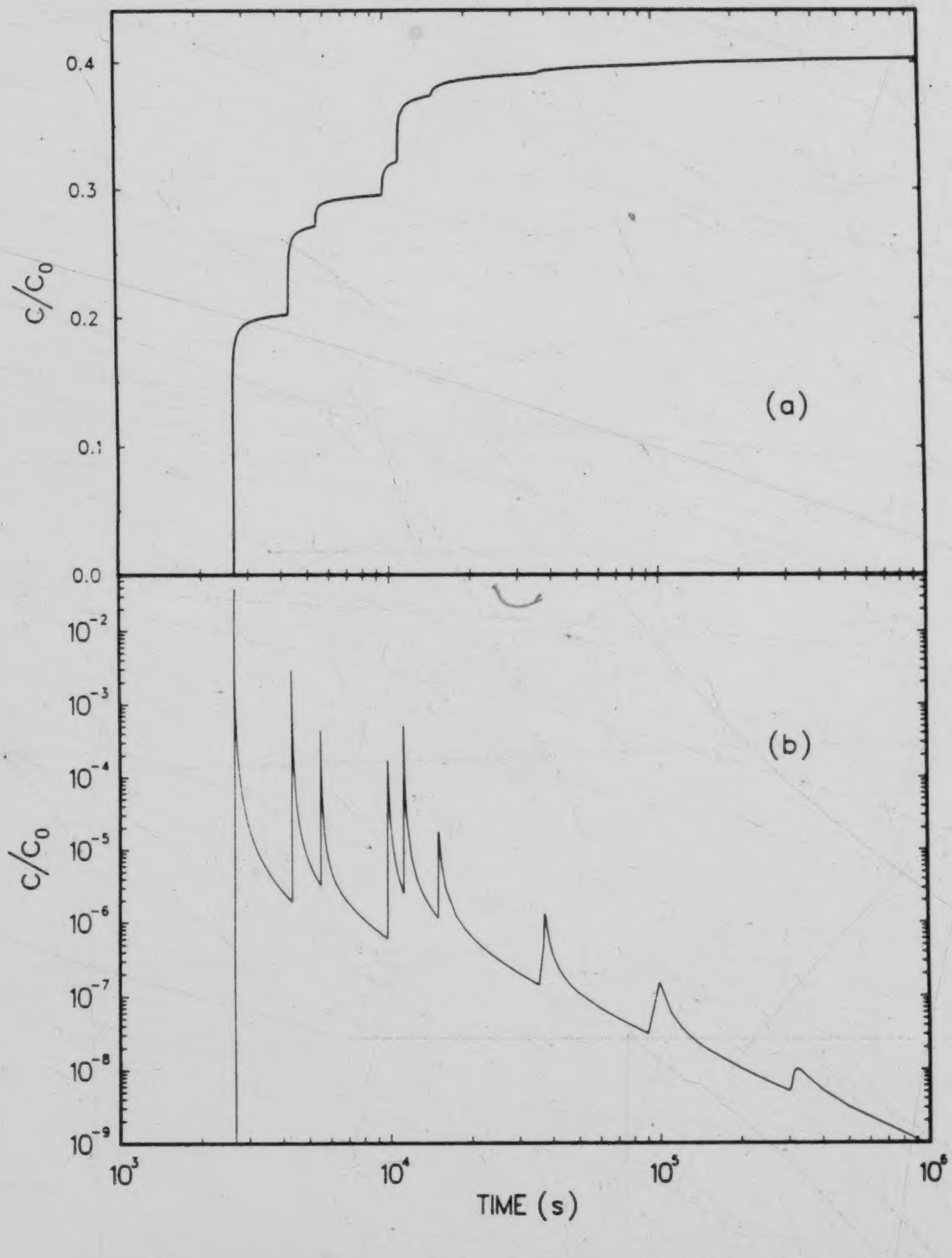

Fig. 4.30 Breakthrough curves obtained at the pumping well, for a injection/ withdrawal rate $Q = 3.128 \times 10^{-5}$ m^3/s/m. (a) continuous injection. (b) instantaneous injection.

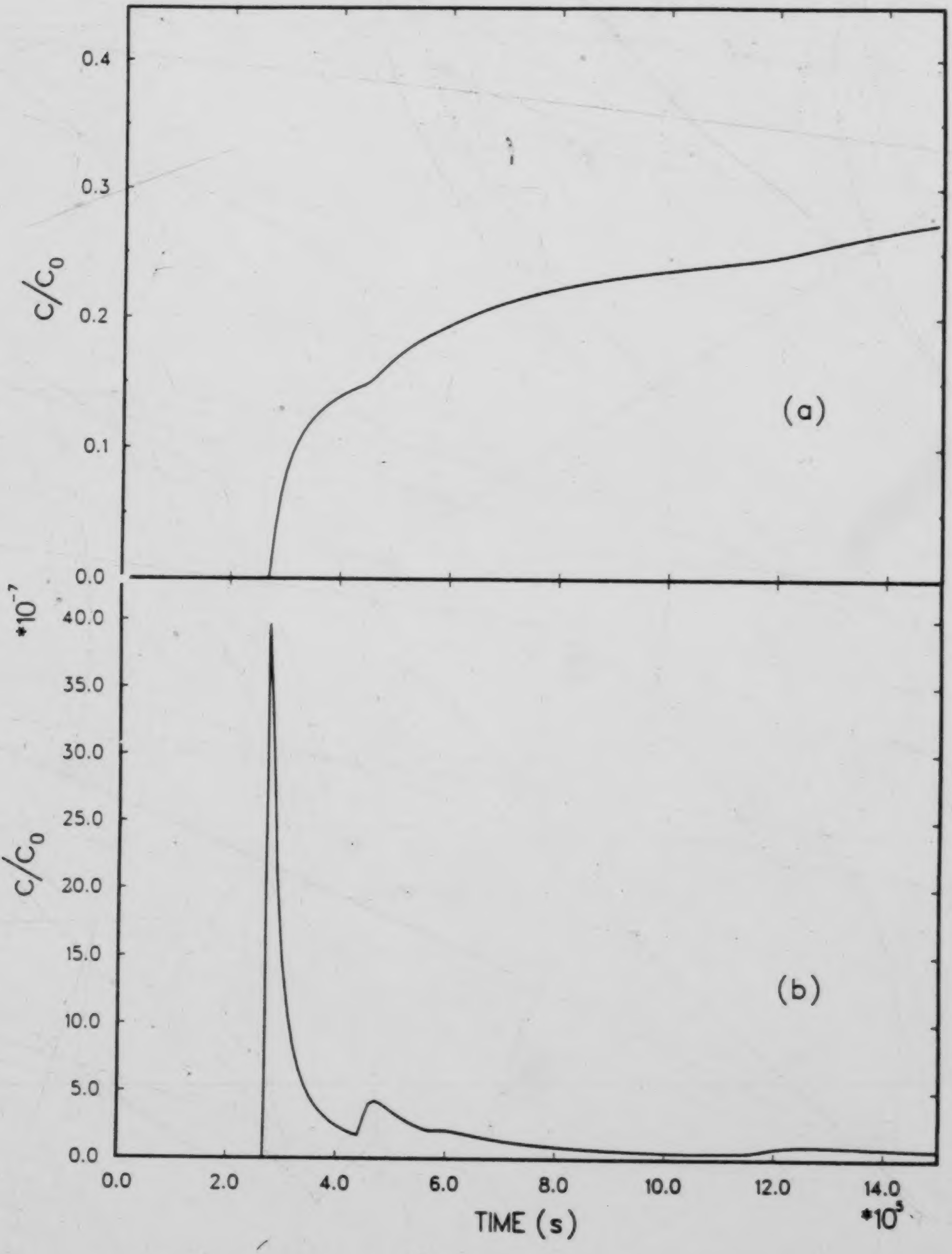

Fig. 4.31 Breakthrough curves obtained at the pumping well, for a injection/ withdrawal rate $Q = 3.128\times10^{-7}$ m³/s/m. (a) continuous injection. (b) instantaneous injection.

possible to recognize the contribution of different paths that only produce a slight waviness in the curve. Again, experimental data may show equivalent variations due to experimental errors and contributions of different paths would go unnoticed. A further decrease in the well discharges would allow more time for diffusion and the evidence of the second path would disappear (Figure 4.32).

If the results for any of the above cases were obtained in the field for an instantaneous injection, it is possible that only the first path contribution would be considered for the estimation of transport parameters. The small magnitude of all other path contributions could not be detected or could even be mistaken for background noise. In this case, any parameter estimated from the test would be representative of only one path. Broader-scale extrapolations under this circumstances would be misleading.

In general, the contribution of individual paths are better defined in the breakthrough curve under conditions of continuous rather than instantaneous injection. The later procedure would provide small values of concentration, which are likely to be misinterpreted in actual tests. If the definition of paths is important, then a fast flow field inducing primarily advective transport is recommended.

The important issue, however, is the realization that mass is transported along different paths which may sample different fractures. In general, the fastest paths are the ones that contribute most to the breakthrough curve. But they do not represent any average for the rock in between the two wells, neither for a single fracture, but rather a definite combination of several fracture segments for a specific flow field condition.

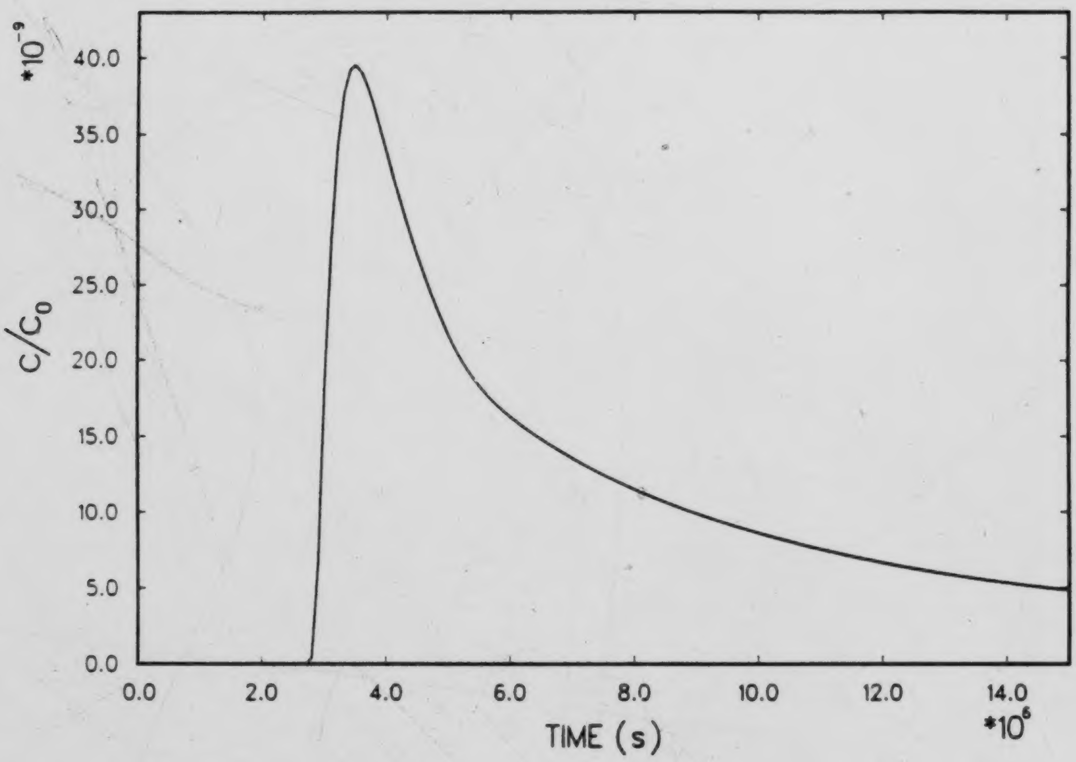

Fig. 4.32 Breakthrough curve obtained at the pumping well, for a injection/ withdrawal rate $Q = 3.128\times10^{-8}$ m^3/s/m. Instantaneous injection.

4.3.3 Effects of different fracture densities

The density of the fracture network plays an important role in defining mass transport. Generally, a greater density of fractures increases the number of intersections and fracture segments, increasing, consequently, the number of paths followed by mass from a source point to a particular sampling point. As a result, the relative contribution of each path to the breakthrough curve decreases.

To verify the influence of fracture density on mass transport between a pair of wells, three fracture networks with different densities have been considered. The network consists of two orthogonal sets of fractures, with the position, length and aperture of individual fractures assumed to be random. The three fracture networks are successively generated, such that a higher density network contains all the fractures from a previous sparse network. This is achieved by considering additional fractures for each new stage in generation. The parameters describing each successive group of fractures are shown in Table 4.7, while Figures 4.33 to 4.35 show the generated networks. This procedure ensures that any higher density network generated preserves the original fractures and the position of the wells, allowing a fair comparison of breakthrough curves from the different networks.

Table 4.7 Data used for generation of fracture networks with different densities.

Set	Fract. per set	Angle	Mean Length (m)	Trunc. Factor	Aperture Mean (μm)	Aperture C_V
1	25	0°	550	0.4	200	1.0
2	25	90°	550	0.4	200	1.0
3	23	0°	550	0.1	200	1.0
4	23	90°	550	0.1	200	1.0
5	17	0°	550	0.1	200	0.5
6	17	90°	550	0.1	200	0.5

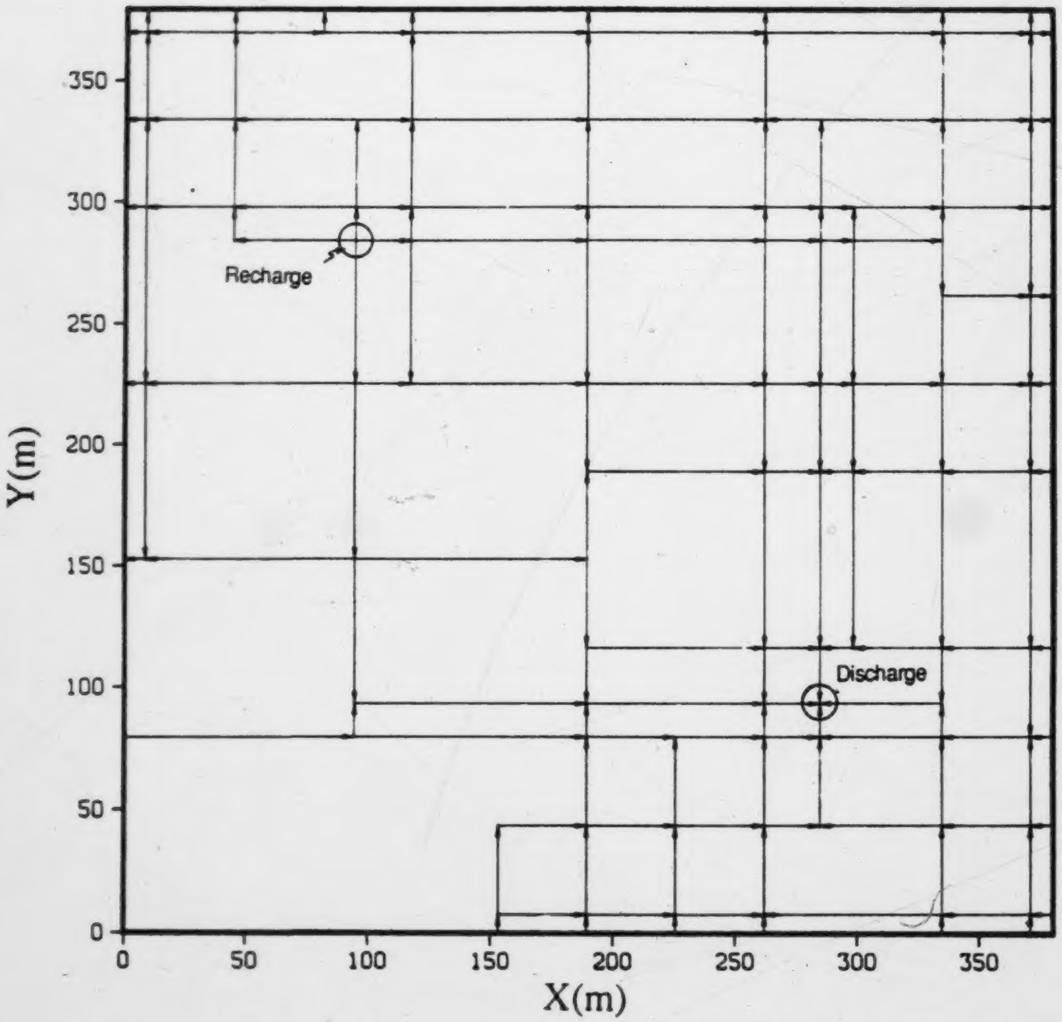

Fig. 4.33 Sparse fracture network, showing the position of the wells and the flow field obtained.

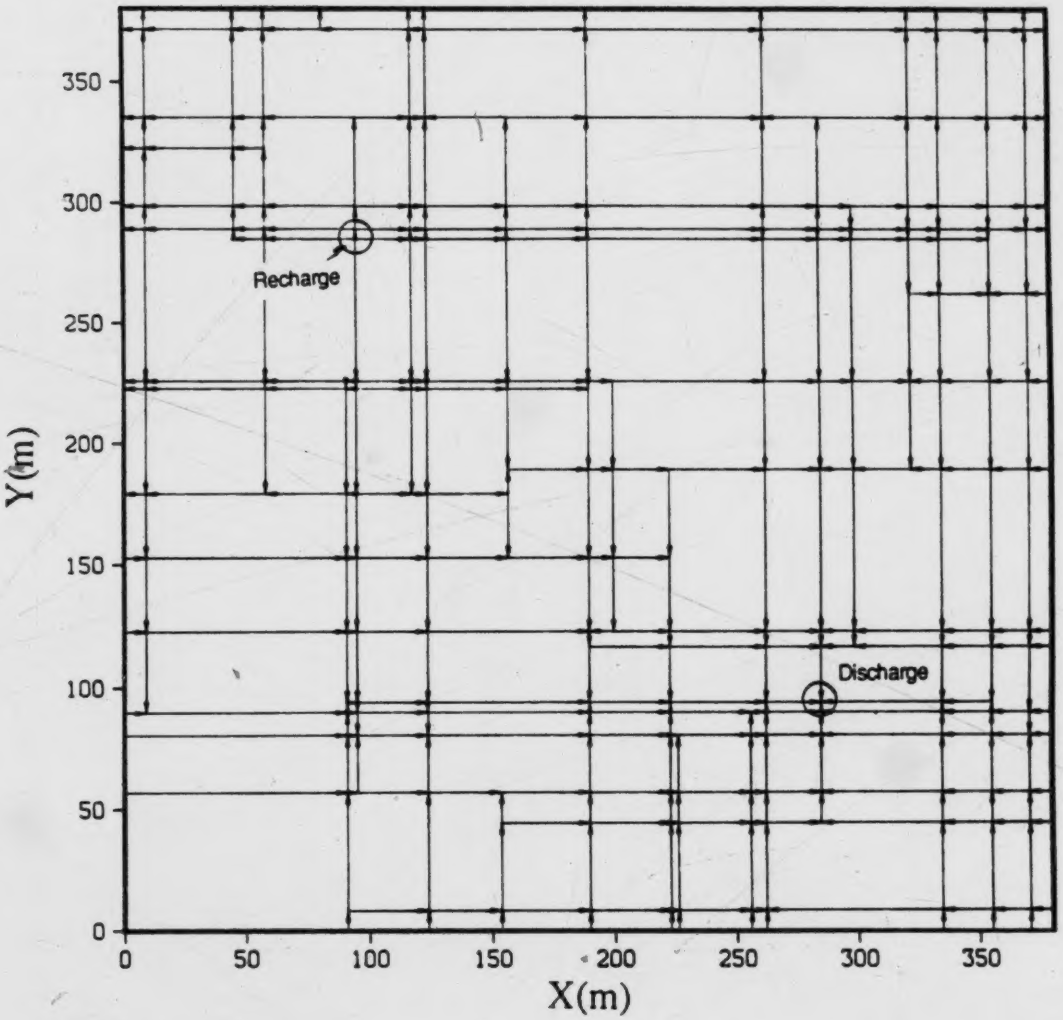
Recharge
Discharge
Y(m)
X(m)
0
50
100
150
200
250
300
350

Fig. 4.34 Intermediate fracture network, showing the position of the wells and the flow field obtained.

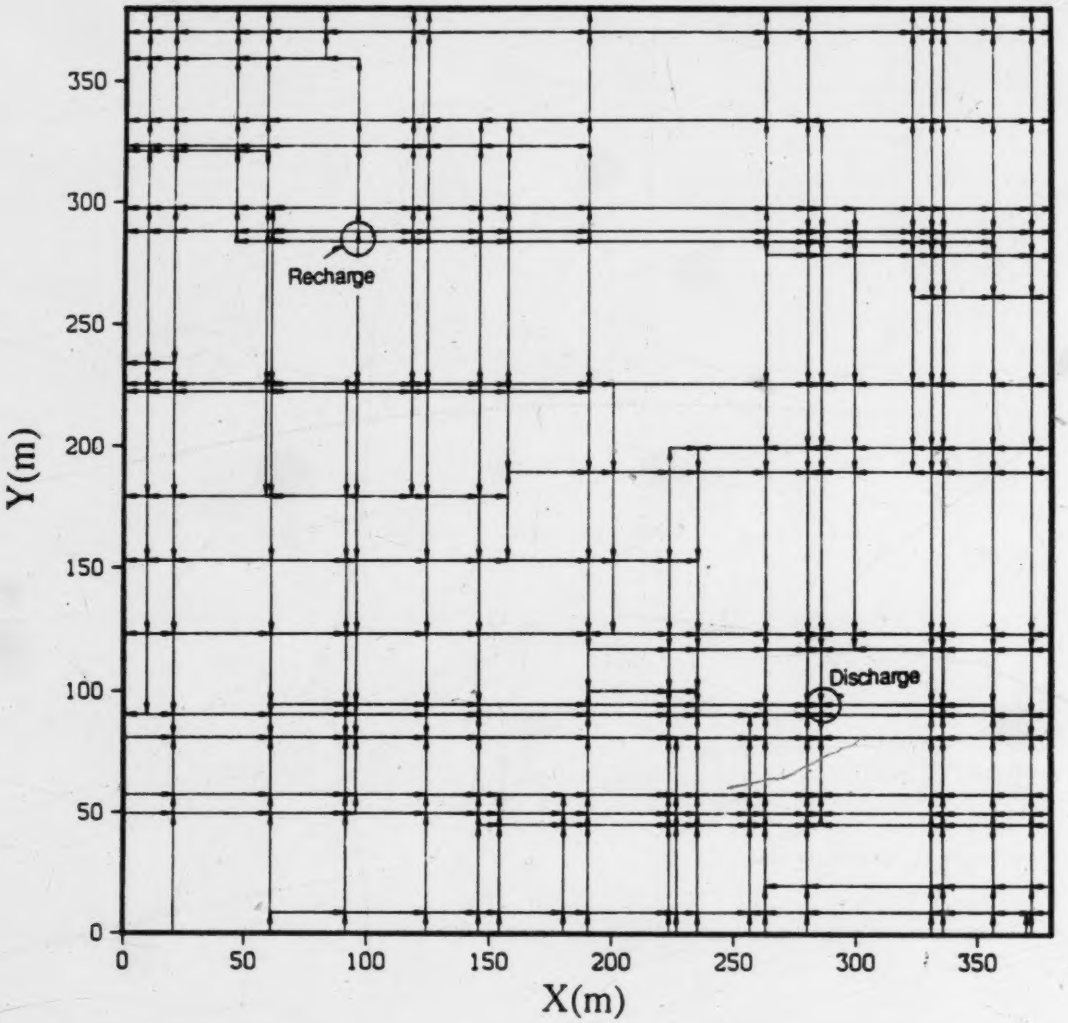
Recharge
Discharge
Y(m)
X(m)
0
50
100
150
200
250
300
350

Fig. 4.35 Dense fracture network, showing the position of the wells and the flow field obtained.

The relative small size of these networks, as already mentioned, is suitable for an analytical treatment, instead of the numerical simulation. The advantage of the analytical solution is to better represent the breakthrough curve for the instantaneous injection, that, otherwise, would have to be obtained by numerical differentiation of the simulated breakthrough curve for a continuous injection. As discussed in Chapter two, the number of time points (NTP) used to evaluate the breakthrough curve for a continuous injection does not have to be large to represent it well. Its time derivative, however, may be poorly represented in predominantly advective cases, because few points may not adequately define the concentration steps present in the breakthrough curve. The resultant impulse response may show an erroneous lower magnitude for the concentration.

The increase in fracture density shows an incredible increase in the total number of distinct paths from the injection well to the withdrawal well. For the sparse network there are only 37 paths, for the intermediate density network, 4527 paths and for the high density network, 61344 paths. For higher fracture density networks the analytical solution becomes impractical, because of the large number of paths that would have to be evaluated.

Continuous Injection

The results for the continuous injection case are plotted in Figures 4.36 and 4.37. Figure 4.36 shows the breakthrough curves for all three networks, considering only transport by advection. The increase in fracture density increases the number of flow paths within the network and the resistance to flow decreases. Consequently, the recovery increases significantly and a long tail develops, as already discussed in section 4.1.2.

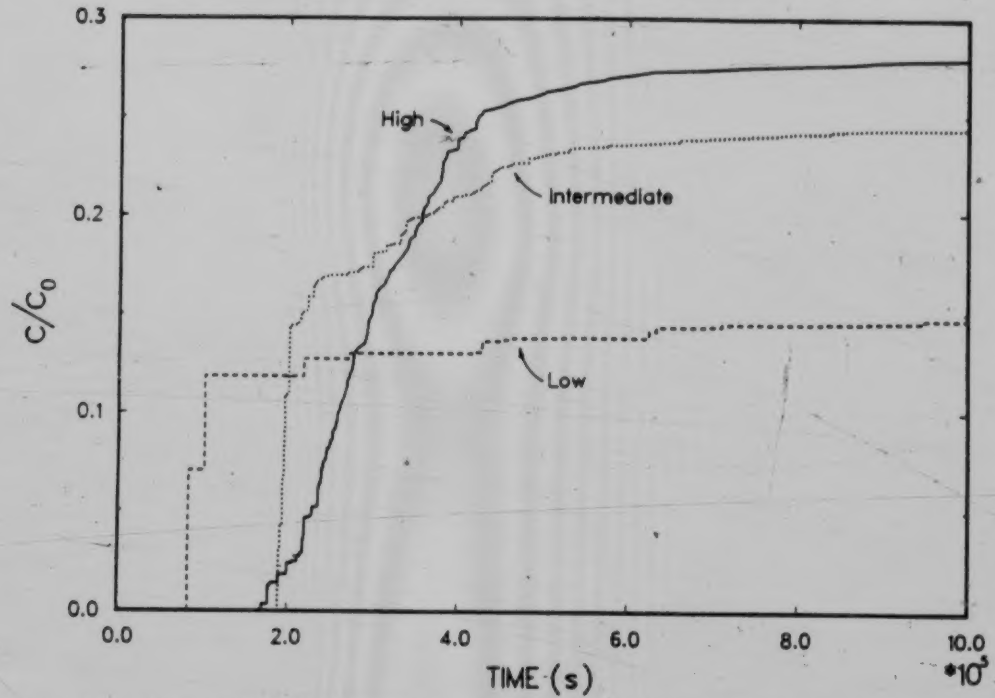

Fig. 4.36 Effect of different fracture densities on the mass transport by advection only (D_m = 0.0). Breakthrough curves obtained at the pumping well for a continuous injection.

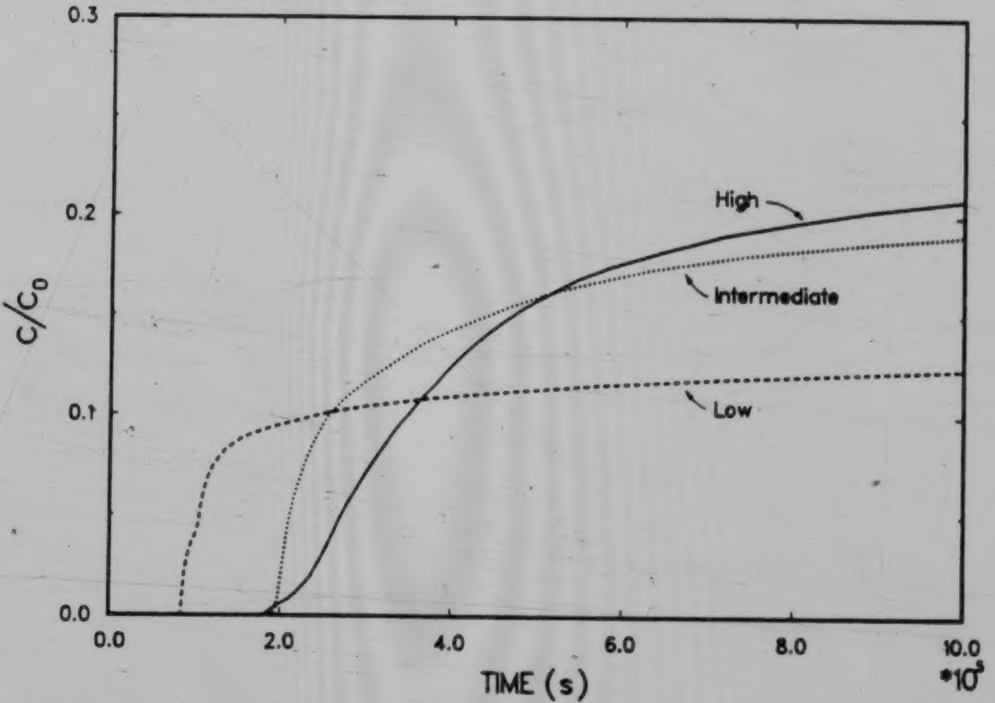

Fig. 4.37 Effect of different fracture densities on the mass transport when diffusion into the matrix is significant ($D_m = 1.6\times10^{-10}$ m²/s). Breakthrough curves obtained at the pumping well for a continuous injection.

The breakthrough curves show distinct concentration steps, due to the contribution of different paths. For the sparse network, for example, two steep steps bring almost 80% of the total mass recovered by the withdrawal well. As the fracture density increases, the number of the concentration steps increase, but their magnitude decreases and the breakthrough curve tends toward an S-shaped curve, reflecting some dispersion in the arrival of mass. The dispersion, however, cannot be said to be Gaussian, because of the long tail.

Figure 4.37 shows the equivalent set of breakthrough curves for a diffusion coefficient $D_m = 1.6\times10^{-10}$ m^2/s . As already discussed, the influence of diffusion is significant. There is a large retardation in the arrival of mass and the concentration steps have been smeared out.

Instantaneous injection

Figure 4.38 presents the impulse responses for all three networks, considering mainly advection ($D_m = 1.6\times10^{-14}$ m^2/s). The contribution of each path now becomes evident. As the fracture density increases, the number of spikes increases, but their magnitude decreases. It is possible to say that the density of spikes increases with increasing fracture density, leading eventually to a smooth continuous peaked curve.

Diffusion into matrix has a very interesting effect on the behaviour of the breakthrough curves. Because mass is stored in the porous matrix, as a consequence of diffusion, the peak concentration of each spike is reduced and the equivalent mass is spread in between spikes, in exactly the same way as a flood wave is attenuated through a reservoir. The spikes become eventually united, forming a single curve, as shown in Figures 4.39 to 4.41.

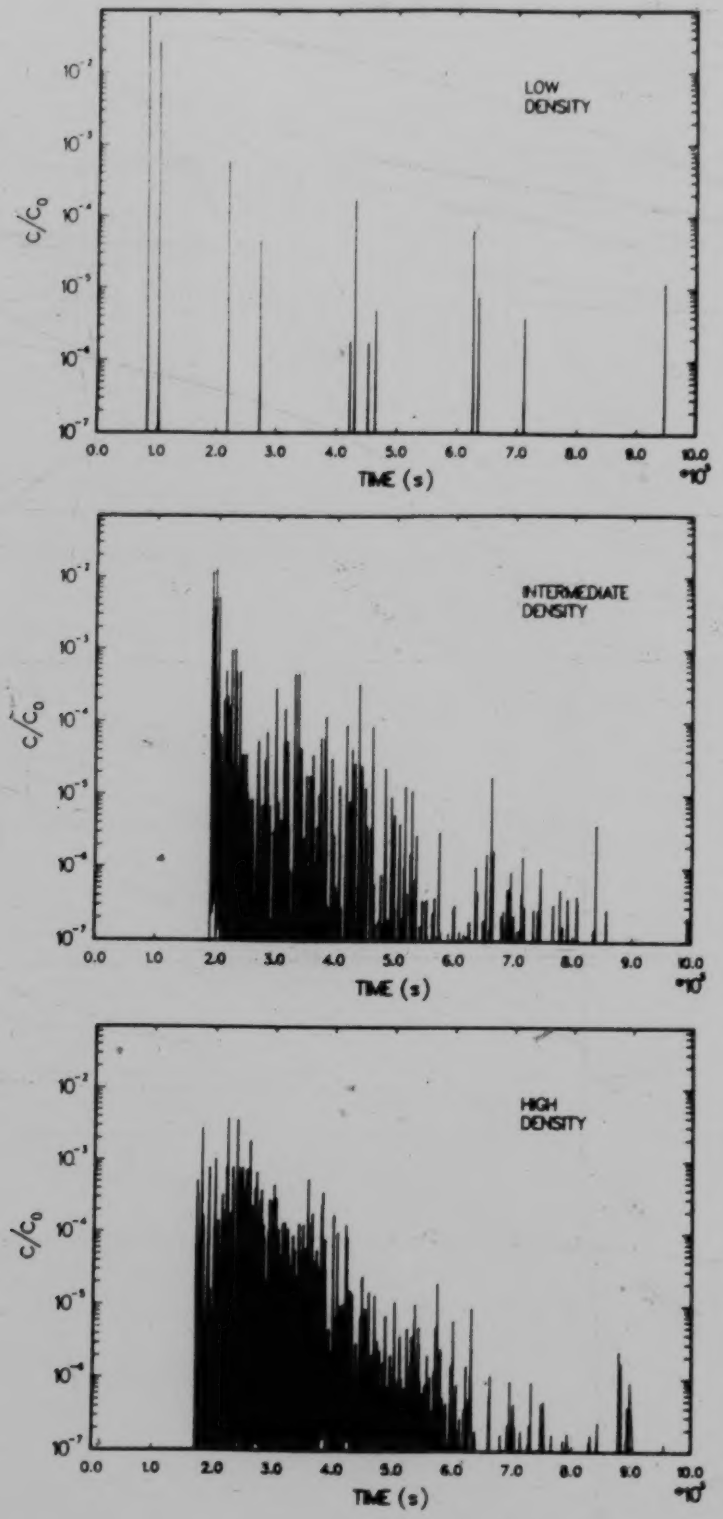

Fig. 4.38 Effect of different fracture densities on the breakthrough curve at the pumping well, for an instantaneous injection. ($D_m = 1.6\times10^{-14}$ m^2/s).

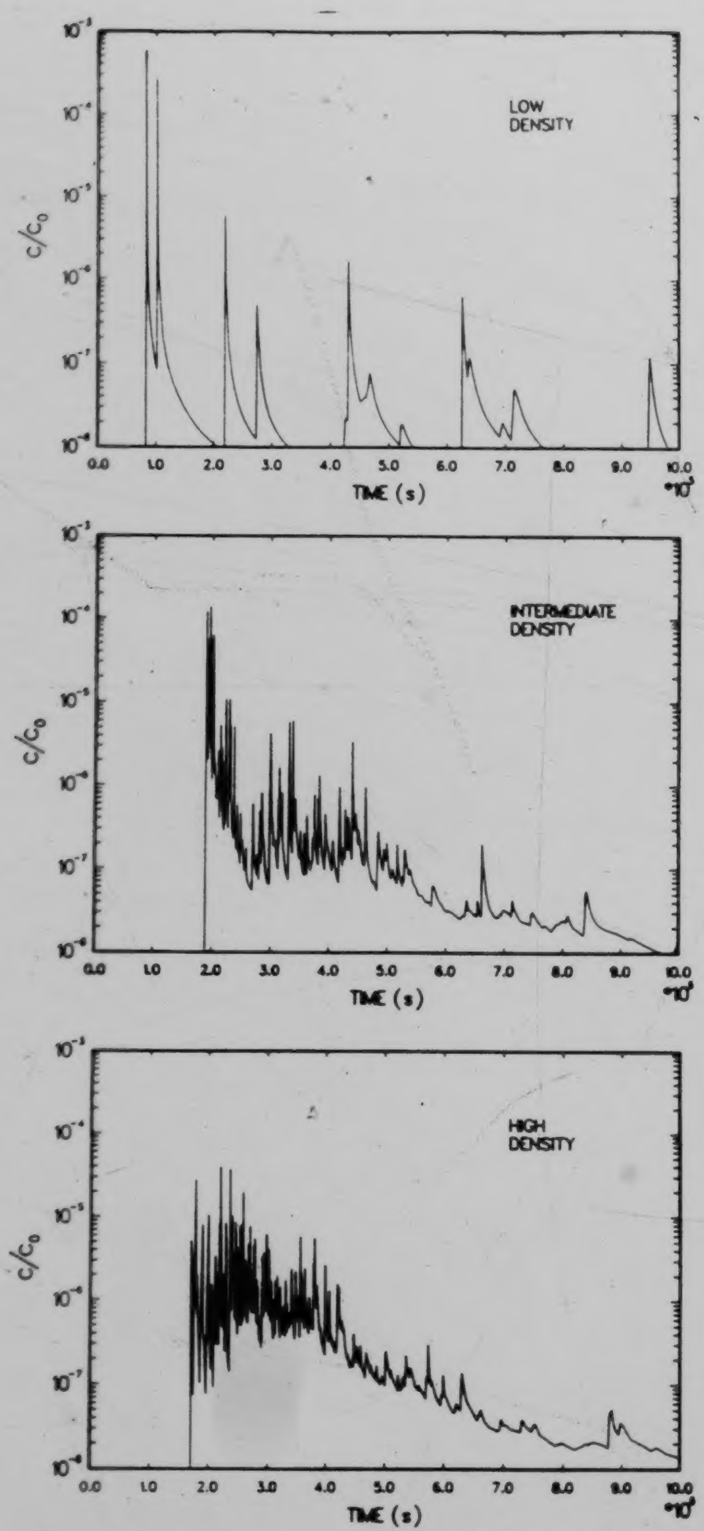

Fig. 4.39 Effect of different fracture densities on the breakthrough curve at the pumping well, for an instantaneous injection. ($D_m = 1.6 \times 10^{-12}$ m^2/s).

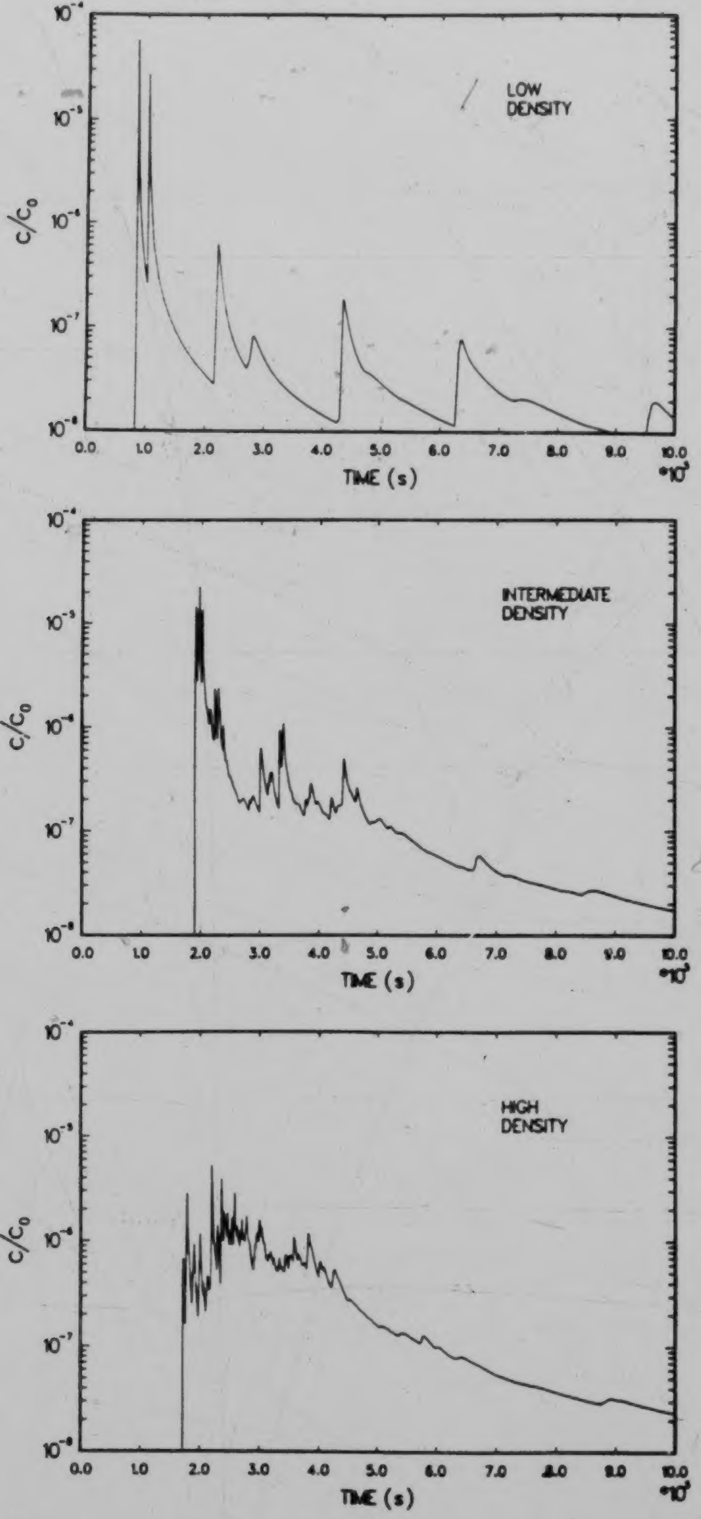

Fig. 4.40 Effect of different fracture densities on the breakthrough curve at the pumping well, for an instantaneous injection. ($D_m = 1.6\times10^{-11}$ m^2/s).

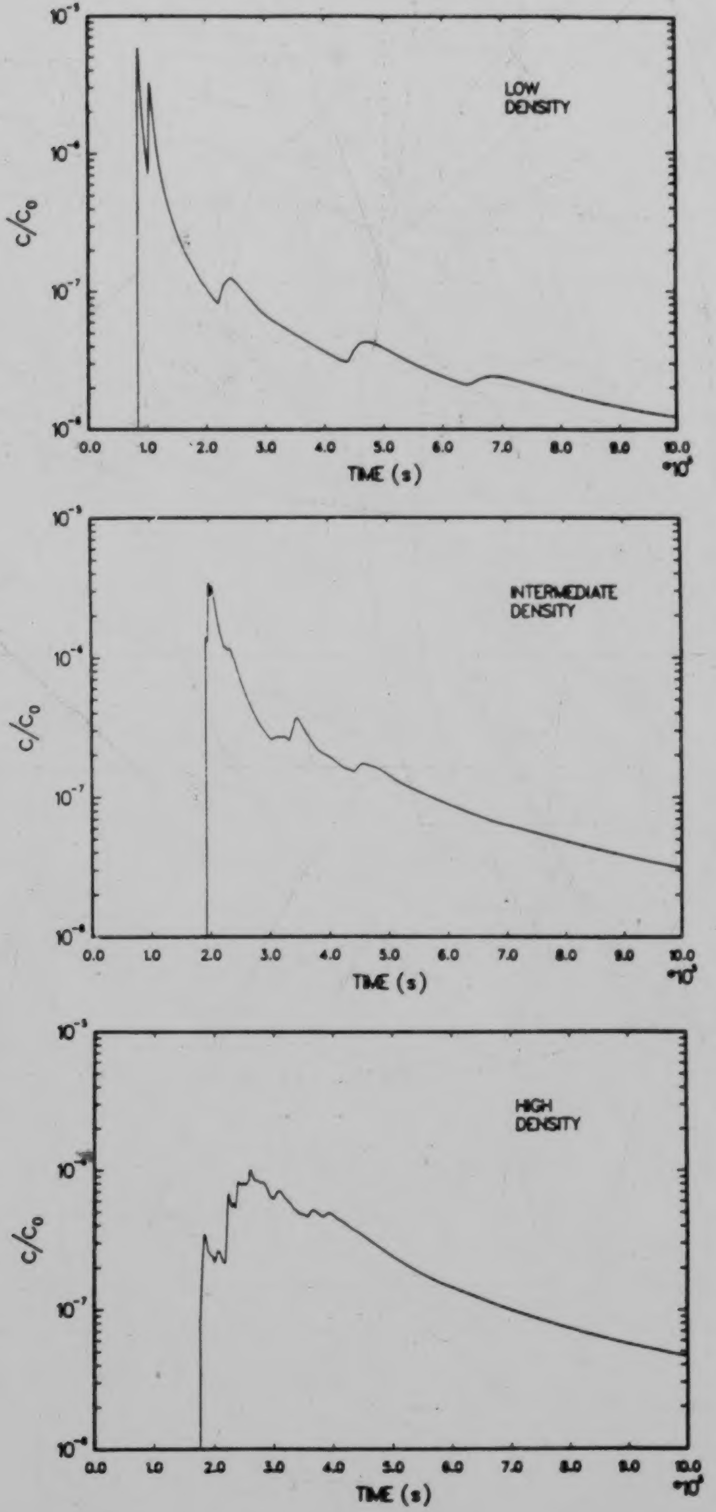

Fig. 4.41 Effect of different fracture densities on the breakthrough curve at the pumping well, for an instantaneous injection. ($D_m = 1.6 \times 10^{-10}$ m²/s).

The increase in fracture density enhances the development of a single curve by providing higher surface area for diffusion and, consequently, higher storage volume for the mass transported that help regulate the mass flow. An additional effect is due to the increase in density of the spikes, that offers the possibility of fitting an average curve to the data points, when interpretation is due.

4.3.4 Discussion

It has been shown in this section that mass transport in discrete fractured networks is strongly dependent on the flow paths developed within the network. The flow paths are dependent on the network geometry and also on the flow stresses imposed over the network. As a consequence, tracer tests are restricted to the region in between the source and the particular sampling point and also on the flow conditions under which the test was performed. Because of the discrete character of the flow paths, the breakthrough curves obtained may be representative of only a few paths and extrapolations for other sampling points or different flow field configurations should be avoided.

The instantaneous injection test, when compared to the continuous injection test, may be more susceptible of not revealing most of the information regarding different flow paths. A reason for this is the inherent small magnitude of the spikes that may be mistaken for background noise. Another reason is diffusion into matrix that may decrease even more the magnitude of the spikes and, at the same time, spread mass in between them, leading eventually to a single smooth curve.

A high fracture density may also lead to single smooth curves, because of the increase in the number of flow paths that decreases the magnitude of the spikes. The resultant response curve does not represent any particular flow path, but rather a combination of flow paths in a particular region. Each flow path may sample many fracture segments and different paths may share many segments. As fracture densities increases, each path samples more segments and also shares more segments with other paths. Consequently, the likelihood of different paths yielding similar transport characteristics also increases. The response curves, therefore, are the result of the complex interaction of many paths, being characteristic of the region in between the two wells. If diffusion into matrix is important, the breakthrough curve will show an additional smearing (Figure 4.42).

In these cases, it becomes very difficult to extract information for single paths from the breakthrough curves. A possible approach for interpretation is to define a transfer function that characterizes mass transport between the two wells. The transfer function, however, is dependent on the site being tested and also on the flow field configuration. If the fracture density is large enough such that it is possible to define a representative elementary volume (REV), then the transfer function could be used for predictive purposes in adjacent areas, provided that a similar region size and flow field configuration characterizes that area. Fossum (1982), for instance, has applied these concepts to geothermal reservoirs. He studied the influence of a re-injection well on a producer well, to verify how much water from the injection well would reach the production well. The definition of a transfer func-tion works well, because the parameters obtained are not used for other pairs of wells.

A two well test is, therefore, dependent on the position of the wells, on the type of the test (continuous x instantaneous, passive x active) and on the flow field generated by the test. The interpretation of the test results must take these factors into account. The parameters obtained do not represent an average for the fractured system surrounding the wells, but a specific test dependent combination of parameters. The objectives of the test should be very clear, because results from one test may differ completely from other tests and the parameters obtained may not be used for different flow conditions.

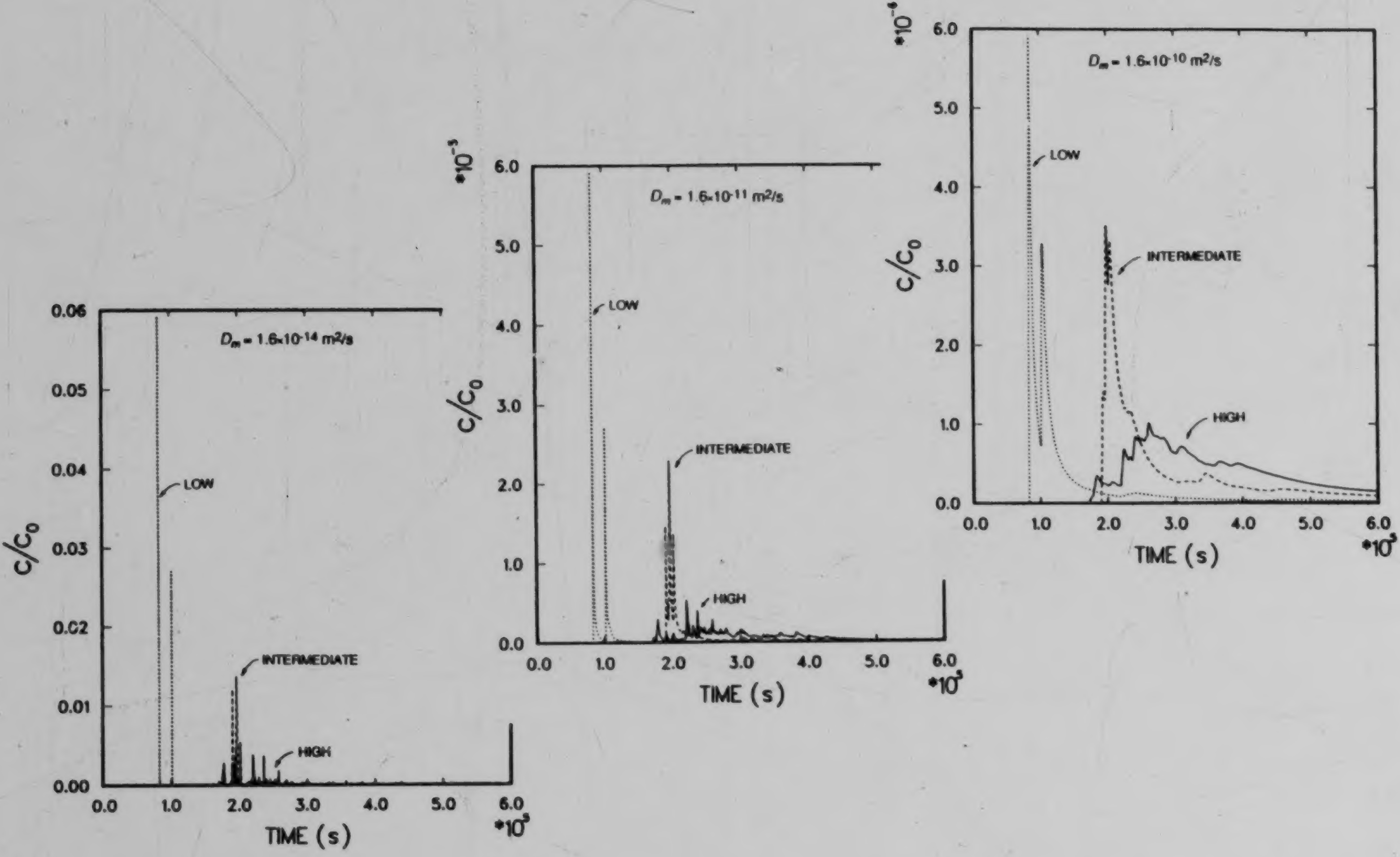

Fig. 4.42 Combined effect of different fracture densities and diffusion coefficients on the breakthrough curves obtained for an instantaneous injection.

5. CONCLUSIONS

This work has analyzed the problem of mass transport in discrete fracture networks. One of the main objectives of this work was to develop a numerical model that could actually take the process of diffusion into matrix into account for complex fracture networks.

The development of this model is based on systems analysis. The complex fracture network is regarded as a single system with multi-input and multi-output points. At a smaller scale, the system is characterized by two components: the fracture segments and the fracture intersections. In this model, it is assumed that the mass transport behavior for each of these components is known and can be expressed by appropriate transfer functions or indicial admittance functions. Given the organization of the components within the network and the multi-input load or excitation, the response of the system at different output points can be calculated by the orderly application of the convolution integral to each component. The systems approach also enables one to derive analytical solutions for simple fracture networks.

For the intersection component, the only process involved is the distribution of the incoming mass among the outgoing outlets and the transfer functions are easily obtained. For the fracture component, the transfer functions depend on the transport processes considered and they become more complex. Tang et al.(1981) showed that solutions for mass transport in a single fracture can be divided into two groups: with dispersion in the fracture and without it. The resultant transfer function for the no-dispersion case is relatively simple, being given in a closed form. The transfer function for the dispersion case, in contrast, involves an infinite integration.

One of the major numerical advantages of this model is that it does not require discretization of either the matrix or the fracture. The discretization is done in a larger scale by considering the fracture segments.

This model proved to be extremely valuable in analyzing the behavior of mass transport in discrete fracture networks. Three applications have been conducted with this model. The first one looked at the influence of two mixing models on the response of the fracture system; the second showed how important diffusion into matrix is; and the third analyzed a system of two wells, showing the importance of paths, injection types and fracture densities on the overall response of a system.

The major conclusions of this work can be summarized as:

1. The systems approach provides a powerful tool for analyzing mass transport in discrete fractured networks. All transport processes can be incorporated into the model by considering appropriate transfer functions for the fracture. In the same way, different mixing models for the fracture intersection can be taken into account.

2. The model can efficiently handle heterogeneous systems, where rock-related properties such as porosity, retardation coefficient, diffusion into the matrix and fracture aperture vary spatially.

3. An important feature of this model is that it can compute exceedingly low concentrations accurately, whereas other numerical models cannot, due to numerical dispersion, etc. This is important for many organic compounds that have drinking water standards in the PPB range ($c/c_0 \approx 10^{-5} - 10^{-6}$).

4. In discrete fracture networks, mass is transported along different paths which sample different fractures. Different observational points may show completely different breakthrough curves as a result of different paths. The flow paths are dependent on the network geometry and on the flow stresses imposed over it. As a consequence, the overall response of the system is strongly dependent on the flow field developed in the network.

5. Another factor that influences the definition of the paths for mass transport is how mass is partitioned at fracture intersections. The selection of the appropriate mixing model, however, should be based on the physics underlining mass transport in the intersection and not on the overall response of the system.

6. Breakthrough curves are the result of the contributions of many individual flow paths that convey mass from a source to a particular sampling point. These paths can be idealized as a system of parallel fractures, each with different parameters.

7. The increase in fracture density in the network provides additional paths for mass transport. The magnitude of each path contribution decreases and the breakthrough curves become smoother, presenting eventually no indication of path contributions.

8. The way mass is introduced into the fracture system, i.e. continuously or instantaneously, may make it more difficult to identify the path contributions. For sparse fracture networks, continuous injection provides breakthrough curves with distinct concentration steps that clearly identify the path contributions. The instantaneous injection yields several concentration spikes for each path contribution, but their relative magnitude is small and not cumulative, what makes them hard to identify, unless high sensitive concentration measurements are possible. In dense fracture networks, the number of paths may be large and the path contributions become difficult to identify.

9. Tracer tests conducted in fractured rocks should be interpreted with care. The test is site dependent, flow dependent, and, in general, does not represent any average for the region surrounding the site. If the velocities in the fractures are high enough, the identification of the major path contributions can be done. However, this will give no information regarding the physical characteristics of individual fractures, because the effects of several fractures have been combined into a single path. Different well arrangements may yield significantly different transport parameters due to the different paths that conduct mass to each well. Moreover, mass transport is strongly dependent on the flow field and the parameters obtained from a tracer test with a certain flow pattern may not be applicable to field situations where the flow field is different.

10. The type of the mass injection may also affect the interpretation of the data. Continuous injection provides, in general, a better record of the path contributions because of the cumulative character of the breakthrough curves. Instantaneous injection, in contrast, leads to a series of spikes which may not be all identified due to their small magnitude. In many instances, the breakthrough curves obtained for an instantaneous injection may show the contributions of only a few fast paths and the transport parameters obtained may not represent the actual transport in the site.

11. Diffusion into matrix has a definite influence on mass transport in regional systems, as already shown by other researchers, and it may also affect significantly the results of tracer tests, especially if instantaneous injection is considered. In general, the effects of matrix diffusion are to retard the mass arrival and to smooth the breakthrough curve, making it difficult to identify the path contributions. When instantaneous injection is considered, the role of matrix diffusion is similar to the role of a reservoir in attenuating a flood wave. In fact, matrix diffusion is the process that makes matrix storage available for the mass being transported. Its effect is to reduce the magnitude of the spikes, by taking

mass into storage, and to spread mass in between spikes, by releasing mass from storage. The breakthrough curves become eventually a continuous smooth curve, with no signs of the discrete spikes. Interpreting such a curve could be misleading, if one is not aware of the transport processes involved. The breakthrough curve represents the response of the system to a series of processes that can no longer be uniquely identified. The choice of a single or multiple fracture model to interpret the data may yield transport parameters that do not characterize at all the physics of mass transport in the network. These models are, in fact, tentative transfer functions that poorly describe the mass transport between the two wells. In being transfer functions, these models are restricted to the type of test performed and cannot be dissociated from the flow field, making extrapolations completely unrealistic. Since the fracture network is, in fact, unknown, a better procedure would be to assume a general transfer function, as given by the response at the sampling points, and verify its variability from point to point and among different flow field conditions. If the fracture density is high enough, it may be possible to obtain a transfer function that independs on the position of the sampling points and, less likely, on the type of flow field. One thing, however, is certain: standard tracer tests are unable to obtain parameters for a single fracture.

12. The coding of the model developed is not optimized and there are several ways to increase the efficiency and the accuracy of the model. Loss of accuracy is, basically, caused by the poor representation of the calculated breakthrough curve, which, in turn, affects its discretization. Future work may consider improving the accuracy of the model by better distributing the time sampling points for the calculation of the breakthrough curves, especially at the tail.

13. Studies on error propagation in the model could also be included in future works. Once a good representation is obtained for the breakthrough curves, the major source of errors is given by the discretization of the input function for each segment. By feeding the model with the resultant error distribution due to the discretization of the input breakthrough curve, it is possible to analyze how the errors are propagated. It may be speculated, for instance, that the errors at the beginning of the breakthrough curve are dissipated in the transfer process and that the errors at the tail are amplified. Such an analysis could lead to more efficient algorithms.

REFERENCES

Ahlstrom, S.W., H.P. Foote, R.C. Arnett, C.R. Cole, and S.J. Serne, Multicomponent mass transport model: Theory and numerical implementation (discrete-parcel-random walk version), Rep. BNWL-2127, Battelle Pac. Northwest Lab., Richland, Wash., 1977.

Barenblatt, G.I., I.P. Zheltov, and I.N. Kochina, Basic concepts in the theory of seepage of homogeneous liquids in fissured rocks [strata], *Soviet Applied Mathematics and Mechanics (PMM)*, 24(5), 852-864, 1960.

Barker, J.A., Laplace transform solutions for solute transport in fissured aquifers, *Adv. Water Resour.*, 5, 98-104, 1982.

Bear, J., *Dynamics of Fluids in Porous Media*, Elsevier, New York, 764pp., 1972.

Berkowitz, B. and C. Braester, The effect of channeling on solute transport behavior in fractured hard rocks, Proceedings, 4th Canadian-American Conference on Hydrology of Fractured Rocks, Banff, Canada, June 1988.

Bibby, R., Mass transport of solutes in dual-porosity media, *Wat. Resour. Res.*, 17(4), 1075-1081, 1981.

Bridges, M.C., Presentation of fracture data for rock mechanics, Proceedings, Australian and New Zealand Conference on Geomechanics, nº 2, 144-148, Institute of Engineering of Australia, Brisbane, 1975.

Castillo, E., G.M. Karadi, and R.J. Krizek, Unconfined flow through jointed rock, *Water Resour. Bull. Amer. Water Resour. Assoc.*, 8(2), 266-281, 1972.

Coats, K.H. and B.D. Smith, Dead-end pore volume and dispersion in porous media, *Soc. Pet. Eng. J.*, 73-84, 1964.

Cohen, B.L., The disposal of radioactive nuclear wastes from fission reactors, *Scientific American*, 236(6), 21-31, June 1977.

Cruden, D.M., Describing the size of discontinuities, *Int. J. Rock Mech. Min. Sci. Geomech. Abstr.*, 14, 133-137, 1977.

Edwards, A.L., TRUMP: A computer program for transient and steady state temperature distribution in multidimensional systems, Rep. UCRL 14754, rev. 3, Natl. Tech. Inf. Serv., Springfield, Va, 1972.

Endo, H.K., J.C.S. Long, C.R. Wilson, and P.A. Witherspoon, A model for investigating mechanical transport in fracture networks, *Wat. Resour. Res.*, 20(10), 1390-1400, 1984.

Fossum, M.P., Tracer analysis in fractured geothermal reservoir: field results from Wairakey, New Zealand, Stanford Geothermal Program, Rep. SGP-TR-56, Stanford University, Stanford, Ca, 123 pp., 1982.

Freeze, R.A. and P.A. Witherspoon, Theoretical analysis of regional groundwater flow: 2. Effect of water table configuration and subsurface permeability variation, *Wat. Resour. Res.*, 3(2), 623-634, 1967.

Fryar, A.E. and P.A. Domenico, Analytical inverse modeling of regional-scale tritium waste migration, *J. Contam. Hydrol.*, 4, 113-125, 1989.

Gale, J., Assessing the permeability characteristics of fractured rocks, Spec. Publ. Geol. Soc. Am., 189, 163-181, 1982.

Germain, M.-S. D., Contaminant migration in fractured porous media: Modelling and analysis of advective-diffusive interaction. Ph.D. Thesis, Univ. of Waterloo, 166 pp., 1988.

Grisak, G.E. and J.F. Pickens, Solute transport through fractured media: 1. The effect of matrix diffusion, *Wat. Resour. Res.*, 16(4), 719-730, 1980.

Grisak, G.E. and J.F. Pickens, An analytical solution for solute transport through fractured media with matrix diffusion, *J. Hydrol.*, 52, 4757, 1981.

Gureghian, A.B. and G. Jansen, One-dimensional analytical solutions for the migration of a three-member radionuclide decay chain in a multilayered geologic medium, *Wat. Resour. Res.*, 21(5), 733-742, 1985.

Herrera, I. and R. Yates, Integrodifferential equations for systems of leaky aquifers and applications: 3. A numerical method of unlimited applicability, *Wat. Resour. Res.*, 13(4), 725-732, 1977.

Himmenblau, D.M. and K.B. Bischoff, *Process Analysis and Simulation*, John Wyley & Sons, 348 pp., 1968.

Hopkirk, R.J. and D.J. Gilby, A method for modelling the transport of nuclides in fissured rock with diffusion into the solid matrix, NAGRA, Bade, Switzerland, Rep. NTB 83-06, 1984.

Hull, L.C. and K.N. Koslow, Streamline routing through fracture junctions, *Wat. Resour. Res.*, 22(12), 1731-1734, 1986.

Hull, L.C., J.D. Miller, and T.M. Clemo, Laboratory and simulation studies of solute transport in fracture networks, *Wat. Resour. Res.*, 23(8), 1505-1513, 1987.

Huyakorn, P.S., B.H. Lester, and J.W. Mercer, An efficient finite element technique for modelling transport in fractured porous media: 1. Single species transport, *Wat. Resour. Res.*, 19(3), 841-854, 1983a.

Huyakorn, P.S., B.H. Lester, and J.W. Mercer, An efficient finite element technique for modelling transport in fractured porous media: 2. Nuclide decay chain transport, *Wat. Resour. Res.*, 19(5), 1286-1296, 1983b.

Huyakorn, P.S., B.C. Jones, and P.F. Andersen, Finite element algorithms for simulating three-dimensional groundwater flow and solute transport in multilayer systems, *Wat. Resour. Res.*, 22(3), 361-374, 1986.

Jensen, C.L., Matrix diffusion and its effect on the modelling of tracer returns from the fractured geothermal reservoir at Wairakei, New Zealand, Stanford Geothermal Program, Rep. SGP-TR-71, Stanford, Ca, December 1983.

Jeppson, R.W., *Analysis of flow in pipe networks*, Ann Arbor Science Pub. Inc., Ann Arbor, 164pp., 1976.

Johns, R.A., C.E. Fox and R.N. Horne, Solute transport in a fractured laboratory core: experimental results and interpretation using the matrix diffusion model, Proceedings, 4th Canadian-American Conference on Hydrology of Fractured Rocks, Banff, Canada, June 1988.

Jury, W.A., Simulation of solute transport using a transfer function model, *Wat. Resour. Res.*, 18(2), 363-368, 1982.

Jury, W.A., G. Sposito, and R.E. White, A transfer function model of solute transport through soil: 1. Fundamental concepts, *Wat. Resour. Res.*, 22(2), 243-247, 1986.

Krizek, R.J., E. Castillo, and G.M. Karadi, Theoretical study of dispersion in a fractured rock aquifer, *J. Geophys. Res.*, 78(3), 558-573, 1973.

Lever, D.A. and M.H. Bradbury, Rock-matrix diffusion and its implications for radionuclide migration, *Mineralogical Magazine*, 49, 245-254, 1975.

Long, J.C.S., J.S. Remer, C.R. Wilson, and P.A. Witherspoon, Porous media equivalents for networks of discontinuous fractures, *Wat. Resour. Res.*, 18(3), 645-658, 1982.

Long, J.C.S., P. Gilmour, and P.A. Witherspoon, A model for steady fluid flow in random three-dimensional networks of disc-shaped fractures, *Wat. Resour. Res.*, 21(8), 1105-1115, 1985.

Marsily, G. de, Flow and transport in fractured rocks: Connectivity and scale effect. *in* Hydrogeology of Rocks of Low Permeability, International Association of Hydrogeologists, Tucson, Arizona, pp. 267-277, 1985

Marsily, G. de, *Quantitative Hydrogeology, Groundwater Hydrology for Engineers*, Academic Press Inc., Orlando, Florida, 440pp., 1986.

McGillem, C.D. and G.R. Cooper, *Continuous and Discrete Signal and System Analysis*, Holt, Rinehart and Winston, 418 pp., 1984.

Mercer, J.W. and C.R. Faust, Geothermal reservoir simulation: 3. Application of liquid- and vapor-dominated hydrothermal modeling techniques to Wairakey, New Zealand, *Wat. Resour. Res.*, 15(3), 653-671, 1979.

Moench, A.F., Double-porosity models for a fissured groundwater reservoir with fracture skin, *Wat. Resour. Res.*, 20(7), 831-846, 1984.

Moreno, L. and A. Rasmuson, Contaminant transport through a fractured porous rock: impact of the inlet boundary conditions on the concentration profile in the rock matrix, *Wat. Resour. Res.*, 22(12), 1728-1730, 1986.

Mollard, J.D., Fracture lineament research and applications on the western Canadian plains, *Can. Geotech. J.*, 25, 749-767, 1988.

Narasimhan, T.N. and K. Pruess, MINC: an approach for analyzing transport in strongly heterogeneous systems, Proceedings, NATO Advanced Research Workshop on Advances in Analytical and Numerical Groundwater Flow and Quality Modelling (ed. E. Custodio, A. Gurgui and J.P. Lobo Ferreira), 375-391, June 1987.

Narasimhan, T.N., Multidimensional numerical simulation of fluid flow in fractured porous media, *Wat. Resour. Res.*, 18(4), 1235-1247, 1982.

Neretnieks, I., Diffusion in the rock matrix: An important factor in radionuclide retardation?, *J. Geophys. Res.*, 85, 4379-4389, 1980.

Neretnieks, I., A note on fracture flow dispersion mechanisms in the ground, *Wat. Resour. Res.*, 19(2), 364-370, 1983.

Neretnieks, I., Transport in fractured rocks, Proc. IAH, 17th International Congress, Tucson, Arizona, USA, January 1985.

Neretnieks, I., H. Abelin, L. Birgersson, L. Moreno, A. Rasmuson, and K. Skagius, Chemical transport in fractured rock, Advances in Transport Phenomena in Porous Media, ed. J. Bear and M.Y. Corapcioglu, Martinus Nijhoff Publishers, Dordrecht, 473-550, 1987

Neretnieks, I. and A. Rasmuson, An approach to modelling radionuclide migration in strongly varying velocity and block sizes along the flow path, *Wat. Resour. Res.*, 20(12), 1823-1836, 1984.

Noorishad, J. and M. Mehran, An upstream finite element method for solution of transient transport equations in fractured porous media, *Wat. Resour. Res.*, 18(3), 588-596, 1982.

Novakowski, K.S., Comparison of fracture aperture widths detrmined from hydraulic measurements and tracer experiments, Proceedings, Fourth Canadian/American Conference on Hydrogeology: Fluid Flow, Heat Transfer and Mass Transport in fractured Rocks, Banff, Canada, 1988

Novakowski, K.S., G.V. Evans, D.A. Lever, and K.G. Raven, A field example of measuring hydrodynamic dispersion in a single fracture, *Wat. Resour. Res.*, 21(8), 1165-1174, 1985.

NRC, A study of the isolation system for geological disposal of radioactive waste, Board on Radioactive Waste Management, National Research Council, National Academy Press, Washington, D.C., 1983.

Ogata, A. and R.B. Banks, A solution of the differential equation of longitudinal dispersion in porous media, U.S. Geol. Surv. Prof. Paper 411-A, 7pp., 1961.

Pankow, J.F., R.L. Johnson, J.P. Hewetson, and J.A. Cherry, An evaluation of contaminant migration patterns at two waste disposal sites on fractured porous media in terms of the equivalent porous media (EPM) model, *J. Contam. Hydrol.*, 1, 65-76, 1986.

Philip, J.R., The fluid mechanics of fracture and other junctions, *Wat. Resour. Res.*, 24(2), 239-246, 1988.

Price, N.J., The development of stress systems and fracture patterns in undeformed sediments, Proceedings, 3rd Congress of the Int. Soc. for Rock Mech., Denver, USA, 1974.

Rasmuson, A., Diffusion and sorption in particles and two-dimensional dispersion in a porous medium, *Wat. Resour. Res.*, 17(2), 321-328, 1981.

Rasmuson, A., Migration of radionuclides in fissured rock: Analytical solutions for the case of constant source strength, *Wat. Resour. Res.*, 20(10), 1435-1442, 1984.

Rasmuson, A., The effects of particles of variable size, shape and properties on the dynamics of fixed beds, *Chem. Eng. Sci.*, 40(4), 621-629, 1985a.

Rasmuson, A., The influence of particle shape on the dynamics of fixed beds, *Chem. Eng. Sci.*, 40(7), 1115-1122, 1985b.

Rasmuson, A. and I. Neretnieks, Exact solutions of a model for diffusion in particles and longitudinal dispersion in packed beds, *AIChE J.*, 26(4), 686-690, 1980.

Rasmuson, A. and I. Neretnieks, Migration of radionuclides in fissured rock: The influence of micropore diffusion and longitudinal dispersion, *J. Geoph. Res.*, 86(B5), 3749-3758, 1981.

Rasmuson, A., T.N. Narasimhan and I. Neretnieks, Chemical transport in a fissured rock: Verification of a numerical model, *Wat. Resour. Res.*, 18(5), 1479-1492, 1982.

Rasmuson, A. and I. Neretnieks, Radionuclide migration in strongly fissured zones: the sensitivity to some assumptions and parameters, *Wat. Resour. Res.*, 22(4), 559-569, 1986.

Raven, K.G., K.S. Novakowski, and P.A. Lapcevic, Interpretation of field tracer tests of a single fracture using a transient solute storage model, *Wat. Resour. Res.*, 24(12), 2019-2032, 1988.

Robertson, J.B., Digital modeling of radioactive and chemical waste transport in the Snake River Plain aquifer at the National reactor testing station, Idaho, U.S. Geol. Surv. open file report IDO-22054, 41pp., 1974.

Robinson, J.W., Connectivity, flow and transport in network models of fractured media, Ph.D. Thesis, Oxford Univ., London, 1984.

Robinson, J.W. and J.E. Gale, A laboratory and numerical investigation of solute transport in discontinuous fracture systems, Proceedings, 4th Canadian-American Conference on Hydrology of Fractured Rocks, Banff, Canada, June 1988.

Ross, B. and C.M. Koplik, A new numerical method for solving the solute transport equation, *Wat. Resour. Res.*, 15(4), 949-955, 1979.

Rouleau, A., A stochastic particle transport model based on directional statistics of flow through fracture networks, Proceedings, NATO Advanced Research Workshop on

Advances in Analytical and Numerical Groundwater Flow and Quality Modelling (ed. E. Custodio, A.Gurgui and J.P. Lobo Ferreira), 393-406, 1987.

Rowe, R.K. and J.R. Booker, Modelling of contaminant movement through fractured media with parallel fractures, *Num. Meth. in Geomech.*, 855- 862, 1988.

Skagius, K. and I. Neretnieks, Porosities and diffusivities of some nonsorbing species in crystalline rocks, *Wat. Resour. Res.*, 22(3), 389-398, 1986.

Schwartz, F.W., L. Smith, and A.S. Crowe, A stochastic analysis of macroscopic dispersion in fractured media, *Wat. Resour. Res.*, 19(5), 1253-1265, 1983.

Schwartz, F.W. and L. Smith, A new continuum approach for modeling dispersion in fractured media, Proceedings, IAH Symposium on Hydrogeology of Rocks of Low Pearmeability, Tucson, Arizona, USA, January 1985.

Schwartz, F.W. and L. Smith, A continuum approach for modelling mass transport in fractured media, *Wat. Resour. Res.*, 24(8), 1360-1372, 1988.

Smith, L. and F.W. Schwartz, An analysis of the influence of the fracture geometry on mass transport in fractured media, *Wat. Resour. Res.*, 20(9), 1241-1252, 1984.

Smith, L., C. Mase, F.W. Schwartz, and D. Chorley, A numerical model for transport in networks of planar fractures, Proceedings, IAH Symposium on Hydrogeology of Rocks of Low Pearmeability, Tucson, Arizona, USA, 666-675, January 1985a.

Smith, L., C. Mase, and F.W. Schwartz, A stochastic model for transport in networks of planar fractures, Proceedings, IAHR Symposium on the Stochastic Approach to Subsurface Flow, Montvillargnne, France, June, 1985b.

Snow, D.T., Anisotropic permeability of fractured media, *Wat. Resour. Res.*, 5(6) 1273-1289, 1969.

Snow, D.T., The frequency and apertures of fractures in rock, *Int. J. Rock. Mech. Min. Sci.*, 7, 23-40, 1970.

Stein, R. and R. Yeats, Hidden earthquakes, *Scientific American*, 260(6), 48-57, June 1989.

Stephanopoulos, G., *Chemical Process Control, an Introduction to Theory and Practice*, Prentice-Hall, 1984.

Strang, G., *Introduction to Applied Mathematics*, Wellesley-Cambridge Press, Wellesley, MA, 758 pp., 1986.

Streeter, V.L. and E.B. Wylie, *Fluid Mechanics*, McGraw-Hill Ryerson, 562 pp., 1981.

Sudicky, E.A. and E.O. Frind, Contaminant transport in fractured porous media: Analytical solutions for a system of parallel fractures, *Wat. Resour. Res.*, 18(6), 1634-1642, 1982.

Sudicky, E.A. and E.O. Frind, Contaminant transport in fractured porous media: Analytical solution for a two-member decay chain in a single fracture, *Wat. Resour. Res.*, 20(7), 1021-1029, 1984.

Sudicky, E.A., The Laplace transform Galerkin technique: a time continuous finite element theory and application to mass transport in groundwater, *Wat. Resour. Res.*, 25(8), 1833-1846, 1989a.

Sudicky, E.A., The Laplace transform Galerkin technique for large scale simulation of mass transport in discretely fractured porous formations, paper presented at the AGU 1989 Fall Meeting, San Francisco, Ca; abstract in EOS, 70(43), p. 1082, 1989b.

Tang, D.H., E.O. Frind, and E.A. Sudicky, Contaminant transport in fractured porous media: An analytical solution for a single fracture, *Wat. Resour. Res.*, 17(3), 555-564, 1981.

Taylor, G.I., Dispersion of soluble matter in solvent flowing slowly through a tube, *Proc. Royal Soc.*, London, Ser. A., 219, 186-203, 1953.

van Genuchten, M.T., D.H. Tang and R. Guénelon, Some exact solutions for solute transport through soils containing large cylindrical macropores, *Wat. Resour. Res.*, 20(3), 335-346, 1984.

White, R.E., J.S. Dyson, R.A. Haigh, and W.A. Jury, A transfer function model of solute transport through soil: 2. Illustrative applications, *Wat. Resour. Res.*, 22(2), 248-254, 1986.

Wilson, C.R. and P.A. Witherspoon, Flow interference effects at fracture intersections, *Wat. Resour. Res.*, 12(1), 102-104, 1976.

Witherspoon, P.A., J.S.K. Wang, K. Iwai, and J.E. Gale, Validity of cubic law for fluid flow in a deformable rock fracture, *Wat. Resour. Res.*, 16(6), 1016-1024, 1980.

Wylie, C.R., Jr., *Advanced Engineering Mathematics*, McGraw-Hill, 3rd ed., 813 pp., 1966.

APPENDIX A - ANALYTICAL SOLUTIONS FOR A SIMPLE FRACTURE NETWORK

This section describes the derivation of analytical solutions for mass transport through simple fracture networks. Both mixing approaches for distributing mass at intersections are considered. The solutions are derived in the Laplace domain, using the convolution theorem, equation (2.9), for the segments and continuity for the intersections, as explained in section 2.4. For the simplified case of no-dispersion analytical solutions are also presented in the Real domain.

A.1 Analytical Solutions in the Laplace Domain

The fracture network layout, including all the basic data, is presented in Figure A.1. At time $t \leq 0$ the concentration is zero everywhere. At $t = 0$, the concentration is suddenly raised to a level c_0, at node 10. The Laplace transform of the step function is given by c_0/s. Capital letters identify the Laplace transforms.

a) Complete Mixing Approach

In the complete mixing approach the concentration is the same for every segment leaving the intersection, or node. The breakthrough curves are then associated with the nodes. In the following equations $F_{i,j}$ represents the Laplace transform of the unit step response function for the segment between nodes i and j, with flux in the direction $j \rightarrow i$. The mass partitioning coefficient at the node, $\eta_{i,j}$, represents the percentage of the total incoming discharge to node i that comes from node j and it can be expressed as,

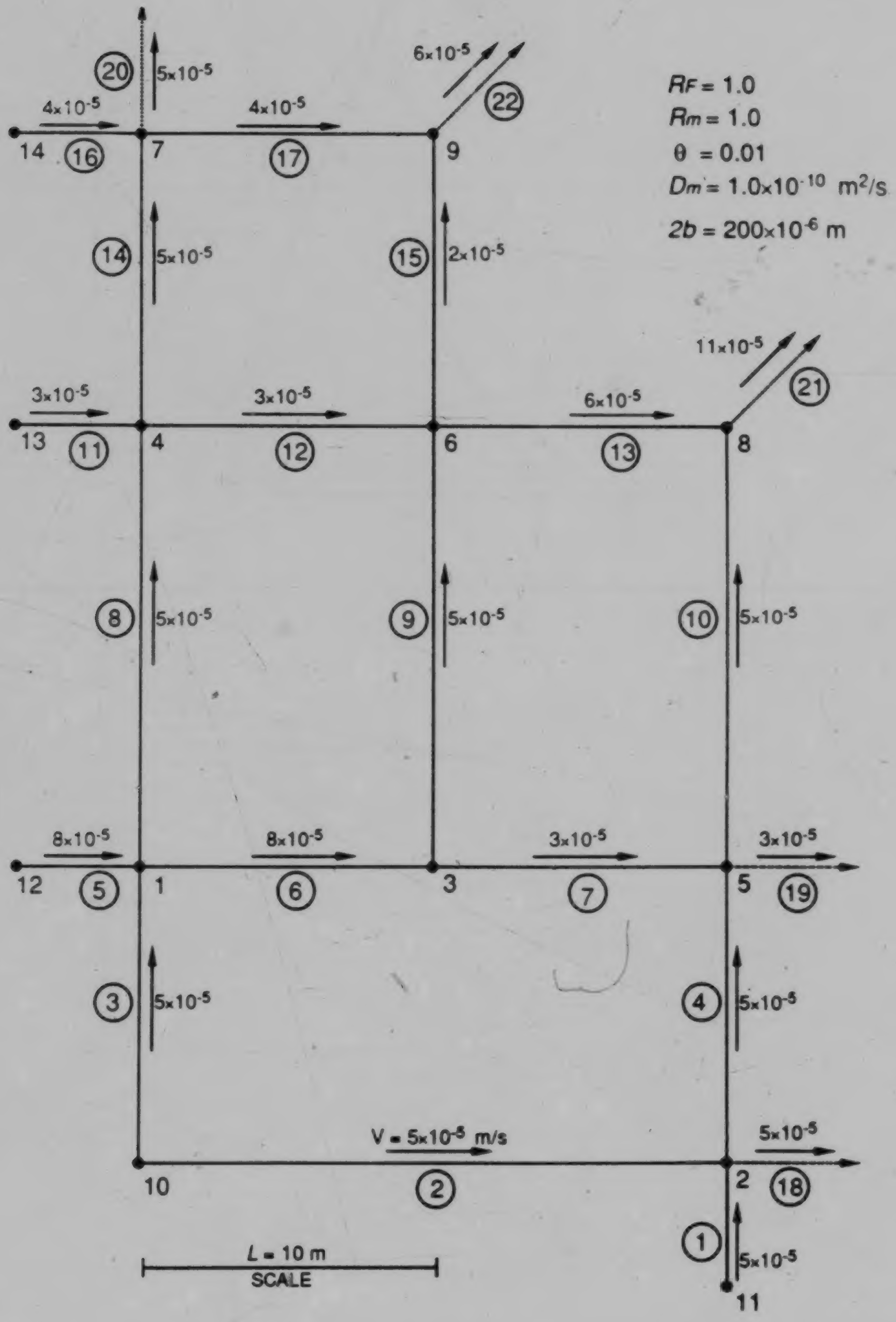

RF = 1.0
Rm = 1.0
θ = 0.01
Dm = 1.0x10-10 m2/s
2b = 200x10-6 m
⑳
5x10-5
6x10-5
㉒
4x10-5
4x10-5
14 ⑯ 7 ⑰ 9
⑭ 5x10-5
⑮ 2x10-5
11x10-5
㉑
3x10-5
3x10-5
6x10-5
13 ⑪ 4 ⑫ 6 ⑬ 8
⑧ 5x10-5
⑨ 5x10-5
⑩ 5x10-5
8x10-5
8x10-5
3x10-5
3x10-5
12 ⑤ 1 ⑥ 3 ⑦ 5 ⑲
③ 5x10-5
④ 5x10-5
V = 5x10-5 m/s
5x10-5
10 ② 2 ⑱
① 5x10-5
11
L = 10 m
SCALE

Fig. A1 Fracture network and fracture parameters used to calculate the analytical solution.

$$\eta_{i,j} = \frac{Q_{i,j}}{\sum_{j=1}^{n} Q_{i,j}} \qquad \text{(A.1)}$$

where n is the total number of incoming segments.

At node 1, there are two incoming segments and the distribution coefficients are calculated as

$$\eta_{1,10} = \frac{Q_{1,10}}{Q_{1,10} + Q_{1,12}} = 0.3846$$

$$\eta_{1,12} = \frac{Q_{1,12}}{Q_{1,10} + Q_{1,12}} = 0.6154$$

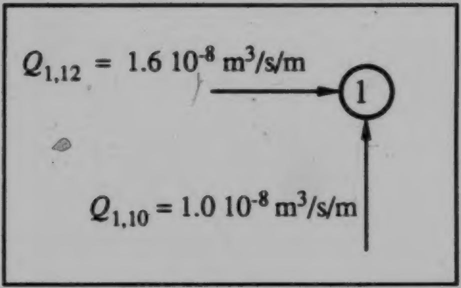
$Q_{1,12}$ = 1.6 10^{-8} m^3/s/m
1
$Q_{1,10}$ = 1.0 10^{-8} m^3/s/m

Since only one segment carries tracer to node 1, the breakthrough curve at node 1 is given by

$$C_1 = \eta_{1,10} \frac{c_0}{s} \left(F_{1,10} \cdot s \right) \qquad \text{(A.1)}$$

where c_0/s is the Laplace transform of the concentration step input c_0 and $F_{1,10}$ is the Laplace transform of the unit step response function for the segment between nodes 1 and 10.

For node 2 the mass transfer is similar. The partitioning coefficients are given by

$$\eta_{2,10} = \frac{Q_{2,10}}{Q_{2,10} + Q_{2,11}} = 0.5$$

$$\eta_{2,11} = \frac{Q_{2,11}}{Q_{2,10} + Q_{2,11}} = 0.5$$

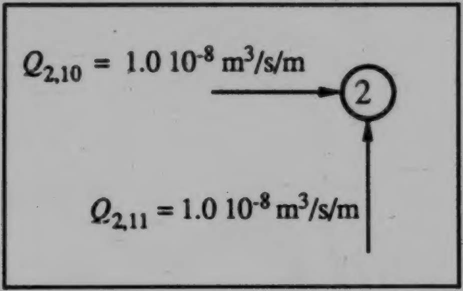
$Q_{2,10}$ = 1.0 10^{-8} m^3/s/m
2
$Q_{2,11}$ = 1.0 10^{-8} m^3/s/m

and the breakthrough curve at node 2 is given by

$$C_2 = \eta_{2,10} \frac{c_0}{s}\left(F_{2,10} \cdot s\right) \tag{A.2}$$

At node 3 there is only one incoming segment and the partitioning coefficient, $\eta_{3,1}$, is equal to one. The breakthrough curve at node 3 is, then, given by,

$$C_3 = \eta_{3,1}\, C_1\left(F_{3,1} \cdot s\right) = \left(\eta_{3,1}\, \eta_{1,10}\, c_0\right) \cdot \left(F_{3,1}\, F_{1,10}\right) \cdot s \tag{A.3}$$

where C_1 is the breakthrough curve at node 1, which becomes the input function for the segment between nodes 1 and 3.

At node 4, the mixing is similar to node 1 and the breakthrough curve is given by

$$C_4 = \eta_{4,1}\, C_1\left(F_{4,1} \cdot s\right) = \left(\eta_{4,1}\, \eta_{1,10}\, c_0\right) \cdot \left(F_{4,1}\, F_{1,10}\right) \cdot s \tag{A.4}$$

At node 5, there are two incoming segments and both carry tracer. The partitioning coefficients are given by

$$\eta_{5,2} = \frac{Q_{5,2}}{Q_{5,2} + Q_{5,3}} = 0.625$$

$$\eta_{5,3} = \frac{Q_{5,3}}{Q_{5,2} + Q_{5,3}} = 0.375$$

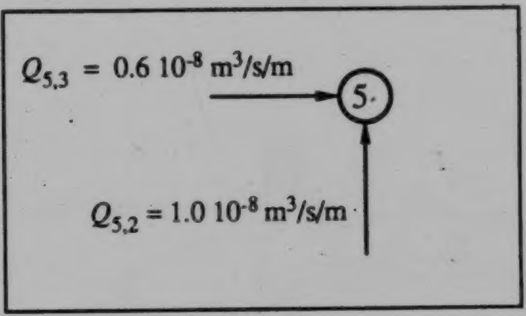
$Q_{5,3}$ = 0.6 10^{-8} $m^3/s/m$
5
$Q_{5,2}$ = 1.0 10^{-8} $m^3/s/m$

and the breakthrough curve is given by

$$C_5 = \eta_{5,2}\, C_2\left(F_{5,2} \cdot s\right) + \eta_{5,3}\, C_3\left(F_{5,3} \cdot s\right) \tag{A.5a}$$

which represents the transferred incoming breakthrough curves from nodes 2 and 3, weighed in relation to the incoming discharges. Expanding the previous calculated breakthrough curves C_2 and C_3, one obtains

$$\begin{aligned} C_5 &= (\eta_{5,2}\,\eta_{2,10}\,c_0)\cdot(F_{5,2}\,F_{2,10})\cdot s\ + \\ &\quad (\eta_{5,3}\,\eta_{3,1}\,\eta_{1,10}\,c_0)\cdot(F_{5,3}\,F_{3,1}\,F_{1,10})\cdot s^2 \end{aligned} \tag{A.5b}$$

This procedure is then repeated for all nodes, yielding the following equations:

$$\begin{aligned} C_6 &= \eta_{6,3}\,C_3\left(F_{6,3}\cdot s\right) + \eta_{6,4}\,C_4\left(F_{6,4}\cdot s\right) \\ &= (\eta_{6,3}\,\eta_{3,1}\,\eta_{1,10}\,c_0)\cdot(F_{6,3}\,F_{3,1}\,F_{1,10})\cdot s^2\ + \\ &\quad (\eta_{6,4}\,\eta_{4,1}\,\eta_{1,10}\,c_0)\cdot(F_{6,4}\,F_{4,1}\,F_{1,10})\cdot s^2 \end{aligned} \tag{A.6}$$

$$\begin{aligned} C_7 &= \eta_{7,4}\,C_4\left(F_{7,4}\cdot s\right) \\ &= (\eta_{7,4}\,\eta_{4,1}\,\eta_{1,10}\,c_0)\cdot(F_{7,4}F_{4,1}\,F_{1,10})\cdot s^2 \end{aligned} \tag{A.7}$$

$$\begin{aligned} C_8 &= \eta_{8,5}\,C_5\left(F_{8,5}\cdot s\right) + \eta_{8,6}\,C_6\left(F_{8,6}\cdot s\right) \\ &= (\eta_{8,5}\,\eta_{5,2}\,\eta_{2,10}\,c_0)\cdot(F_{8,5}\,F_{5,2}\,F_{2,10})\cdot s^2\ + \\ &\quad (\eta_{8,5}\,\eta_{5,3}\,\eta_{3,1}\,\eta_{1,10}\,c_0)\cdot(F_{8,5}\,F_{5,3}\,F_{3,1}\,F_{1,10})\cdot s^3\ + \\ &\quad (\eta_{8,6}\,\eta_{6,3}\,\eta_{3,1}\,\eta_{1,10}\,c_0)\cdot(F_{8,6}\,F_{6,3}\,F_{3,1}\,F_{1,10})\cdot s^3\ + \\ &\quad (\eta_{8,6}\,\eta_{6,4}\,\eta_{4,1}\,\eta_{1,10}\,c_0)\cdot(F_{8,6}\,F_{6,4}\,F_{4,1}\,F_{1,10})\cdot s^3 \end{aligned} \tag{A.8}$$

$$\begin{aligned} C_9 &= \eta_{9,6}\,C_6\left(F_{9,6}s\right) + \eta_{9,7}\,C_7\left(F_{9,7}\cdot s\right) \\ &= (\eta_{9,6}\,\eta_{6,3}\,\eta_{3,1}\,\eta_{1,10}\,c_0)\cdot(F_{9,6}\,F_{6,3}\,F_{3,1}\,F_{1,10})\cdot s^3\ + \\ &\quad (\eta_{9,6}\,\eta_{6,4}\,\eta_{4,1}\,\eta_{1,10}\,c_0)\cdot(F_{9,6}\,F_{6,4}\,F_{4,1}\,F_{1,10})\cdot s^3\ + \\ &\quad (\eta_{9,7}\,\eta_{7,4}\,\eta_{4,1}\,\eta_{1,10}\,c_0)\cdot(F_{9,7}\,F_{7,4}\,F_{4,1}\,F_{1,10})\cdot s^3 \end{aligned} \tag{A.9}$$

b) Streamline Routing Approach

In the streamline routing approach, concentrations are associated with the segments, rather than nodes. In this way, the input breakthrough curve is associated with the segment. In the following equations, F_i represents the Laplace transform of the unit step response function for the i^{th} segment and $\eta_{i,j}$ represents the percentage of the total incoming discharge to segment i, that comes from segment j. The solutions derived are based on equation (2.14) for the segments and equations (2.17) to (2.20) for the intersections.

At node 10, the tracer is introduced as a step function with magnitude c_0. Due to the routing process, the tracer is now restricted to fewer paths. At node 1 the partitioning coefficients are given by

$$\eta_{6,3} = \frac{Q_5}{Q_6} = 0.625$$

$$\eta_{6,5} = \frac{Q_6 - Q_5}{Q_6} = 0.375$$

$$\eta_{8,3} = 1.0$$

$$\eta_{8,5} = 0.0$$

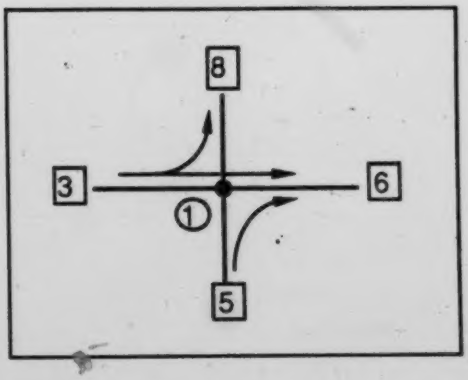

The breakthrough curve entering segment 6 is given by

$$C_6 = \eta_{6,3} \cdot (C_3 \, F_3 \, s) + \eta_{6,5} \cdot (C_5 \, F_5 \, s) \tag{A.11a}$$

Since C_5 is identically null and C_3 is the step function with magnitude c_0/s, equation (A.11a) becomes

$$C_6 = \eta_{6,3} \, C_3 \, F_3 \tag{A.11b}$$

For node 2, the partitioning coefficients are given by

$$\eta_{4,1} = 0.0$$

$$\eta_{4,2} = 1.0$$

$$\eta_{18,1} = 1.0$$

$$\eta_{18,2} = 0.0$$

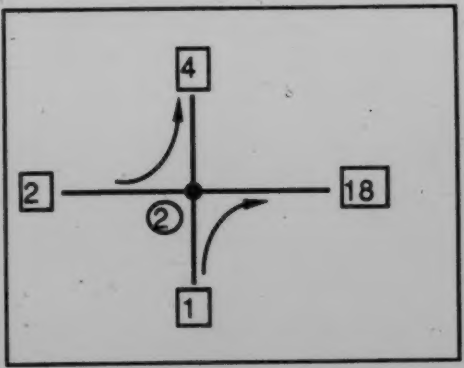

and the breakthrough curve entering segment 4 is given by

$$C_4 = \eta_{4,2}\, c_0\, F_2 \tag{A.12}$$

Following the same procedure, the other breakthrough curves are given by

$$\begin{aligned} C_7 &= \eta_{7,6} \cdot (C_6\, F_6\, s) \\ &= (\eta_{7,6}\, \eta_{6,3}) \cdot (F_6\, F_3) \cdot s \end{aligned} \tag{A.13}$$

$$\begin{aligned} C_9 &= \eta_{9,6} \cdot (C_6\, F_6\, s) \\ &= (\eta_{9,6}\, \eta_{6,3}) \cdot (F_6\, F_3) \cdot s \end{aligned} \tag{A.14}$$

$$\begin{aligned} C_{10} &= \eta_{10,4} \cdot (C_4\, F_4\, s) \;+\; \eta_{10,7} \cdot (C_7\, F_7\, s) \\ &= (\eta_{10,4}\, \eta_{4,2}) \cdot (F_4\, F_2) \cdot s \;+ \\ &\quad (\eta_{10,7}\, \eta_{7,6}\, \eta_{6,3}) \cdot (F_7\, F_6\, F_3) \cdot s^2 \end{aligned} \tag{A.15}$$

$$\begin{aligned} C_{19} &= \eta_{19,4} \cdot (C_4\, F_4\, s) \\ &= (\eta_{19,4}\, \eta_{4,2}) \cdot (F_4\, F_2) \cdot s \end{aligned} \tag{A.16}$$

$$\begin{aligned} C_{13} &= \eta_{13,9} \cdot (C_9\, F_9\, s) \\ &= (\eta_{13,9}\, \eta_{9,6}\, \eta_{6,3}) \cdot (F_9\, F_6\, F_3) \cdot s^2 \end{aligned} \tag{A.17}$$

$$\begin{aligned} C_{21} &= \eta_{21,10} \cdot (C_{10}\, F_{10}\, s) \;+\; \eta_{21,13} \cdot (C_{13}\, F_{13}\, s) \\ &= (\eta_{21,10}\, \eta_{10,4}\, \eta_{4,2}\, c_0) \cdot (F_{10}\, F_4\, F_2) \cdot s^2 \;+ \\ &\quad (\eta_{21,10}\, \eta_{10,7}\, \eta_{7,6}\, \eta_{6,3}\, c_0) \cdot (F_{10}\, F_7\, F_6\, F_3) \cdot s^3 \;+ \\ &\quad (\eta_{21,13}\, \eta_{13,9}\, \eta_{9,6}\, \eta_{6,3}\, c_0) \cdot (F_{13}\, F_9\, F_6\, F_3) \cdot s^3 \end{aligned} \tag{A.18}$$

All other segments present no variation in the concentration.

A.2 Analytical Solutions in the Real Domain

The procedure described in the previous section is applicable to both the general and the simplified no-dispersion case. For the simplified case, the multiplication of the Laplace transforms of the unit step response functions leads to a summation of the function arguments, as shown in section 2.4. The solution in the Real domain is then obtained by a linear combination of the unit step response functions, with appropriate substitution of the parameters. However, for the general case this is not possible and the inversion of the Laplace transform must be carried out either analytically or numerically.

Assuming no radioactive decay, the unit step response function in the Real domain, for the simplified no-dispersion solution, may be written as:

$$c = erfc\left[\frac{A}{(t-B)^{0.5}}\right] \tag{A.19}$$

where the parameters A and B are defined as

$$A = \frac{\theta (R_m D_m)^{0.5} L}{V b} \tag{A.20a}$$

$$B = \frac{R_f L}{V} \tag{A.20b}$$

The final solution in the Real domain, for each node, can be obtained by the appropriate summation of the parameters A and B and by the multiplication of the equivalent partitioning coefficients, as explained in section 2.4.

a) Complete Mixing Approach

The solutions for the complete mixing approach are summarized in Table A.2, based on the parameters listed in Table A.1.

Table A.1 Values of the parameters A, B and η for the network shown in Figure A.1 (Complete mixing approach).

Node	Partitioning Coefficients	Parameter A ($s^{1/2}$)	Parameter B (s)
1	$\eta_{1,10} = 0.3846$	$A_{1,10} = 100.0$	$B_{1,10} = 200\,000$
2	$\eta_{2,10} = 0.5000$	$A_{2,10} = 200.0$	$B_{2,10} = 400\,000$
3	$\eta_{3,1} = 1.0000$	$A_{3,1} = 62.5$	$B_{3,1} = 125\,000$
4	$\eta_{4,1} = 0.6250$	$A_{4,1} = 150.0$	$B_{4,1} = 300\,000$
5	$\eta_{5,2} = 0.6250$ $\eta_{5,3} = 0.3750$	$A_{5,2} = 100.0$ $A_{5,3} = 166.7$	$B_{5,2} = 200\,000$ $B_{5,3} = 333\,333$
6	$\eta_{6,3} = 0.6250$ $\eta_{6,4} = 0.3750$	$A_{6,3} = 150.0$ $A_{6,4} = 166.7$	$B_{6,3} = 300\,000$ $B_{6,4} = 333\,333$
7	$\eta_{7,4} = 0.5556$	$A_{7,4} = 100.0$	$B_{7,4} = 200\,000$
8	$\eta_{8,5} = 0.4545$ $\eta_{8,6} = 0.5455$	$A_{8,5} = 150.0$ $A_{8,6} = 83.3$	$B_{8,5} = 300\,000$ $B_{8,6} = 166\,667$
9	$\eta_{9,6} = 0.3333$ $\eta_{9,7} = 0.6667$	$A_{9,6} = 250.0$ $A_{9,7} = 125.0$	$B_{9,6} = 500\,000$ $B_{9,7} = 250\,000$

Table A.2 Solutions in the Real domain for the breakthrough curves at each node (Complete mixing approach)

$\frac{c_1}{c_0} = 0.3846\cdot erfc\left[\frac{100}{\sqrt{t-200000}}\right]$	$\frac{c_2}{c_0} = 0.5000\cdot erfc\left[\frac{200}{\sqrt{t-400000}}\right]$
$\frac{c_3}{c_0} = 0.3846\cdot erfc\left[\frac{162.5}{\sqrt{t-325000}}\right]$	$\frac{c_4}{c_0} = 0.2404\cdot erfc\left[\frac{250}{\sqrt{t-500000}}\right]$
$\frac{c_5}{c_0} = 0.3125\cdot erfc\left[\frac{300}{\sqrt{t-600000}}\right] +$ $0.1442\cdot erfc\left[\frac{329.2}{\sqrt{t-658333}}\right]$	$\frac{c_6}{c_0} = 0.2404\cdot erfc\left[\frac{312.5}{\sqrt{t-625000}}\right] +$ $0.0901\cdot erfc\left[\frac{416.7}{\sqrt{t-833333}}\right]$
$\frac{c_7}{c_0} = 0.1336\cdot erfc\left[\frac{350}{\sqrt{t-700000}}\right]$	
$\frac{c_8}{c_0} = 0.1420\cdot erfc\left[\frac{450}{\sqrt{t-900000}}\right] +$ $0.0656\cdot erfc\left[\frac{479.2}{\sqrt{t-958333}}\right] +$ $0.1311\cdot erfc\left[\frac{395.8}{\sqrt{t-791667}}\right] +$ $0.0492\cdot erfc\left[\frac{500}{\sqrt{t-1000000}}\right]$	$\frac{c_9}{c_0} = 0.0801\cdot erfc\left[\frac{562.5}{\sqrt{t-1125000}}\right] +$ $0.0300\cdot erfc\left[\frac{666.7}{\sqrt{t-1333333}}\right] +$ $0.0890\cdot erfc\left[\frac{475}{\sqrt{t-950000}}\right]$

Note: time in seconds

b) Streamline Routing Approach

The solutions for the streamline routing approach are summarized in Table A.4, based on the parameters listed in Table A.3.

Table A.3 Values of the parameters A, B and η for the network shown in Figure A.1 (Streamline routing approach)

Segment #	Partitioning Coefficient	Parameter A [$s^{1/2}$]	Parameter B [s]
1	–	50.0	100 000
2	–	200.0	400 000
3	–	100.0	200 000
4	$\eta_{4,2} = 1.0$ $\eta_{4,1} = 0.0$	100.0	200 000
5	–	31.25	62 500
6	$\eta_{6,3} = 0.625$ $\eta_{6,5} = 0.375$	62.5	125 000
7	$\eta_{7,6} = 1.0$	166.7	333 333
8	$\eta_{8,5} = 1.0$ $\eta_{8,3} = 0.0$	150.0	300 000
9	$\eta_{9,6} = 1.0$	150.0	300 000
10	$\eta_{10,7} = 0.6$ $\eta_{10,4} = 0.4$	150.0	300 000
11	–	83.3	166 667
12	$\eta_{12,8} = 1.0$ $\eta_{12,11} = 0.0$	166.7	333 333
13	$\eta_{13,9} = 0.833$ $\eta_{13,12} = 0.167$	83.3	166 667
14	$\eta_{14,8} = 0.4$ $\eta_{14,11} = 0.6$	100.0	200 000
15	$\eta_{15,12} = 1.0$ $\eta_{15,9} = 0.0$	250.0	500 000

16	–	62.5	125 000
17	$\eta_{17,14} = 1.0$ $\eta_{17,16} = 0.0$	125.0	250 000
18	$\eta_{18,1} = 1.0$ $\eta_{18,2} = 0.0$	–	–
19	$\eta_{19,4} = 1.0$ $\eta_{19,7} = 0.0$	–	–
20	$\eta_{20,14} = 0.2$ $\eta_{20,16} = 0.8$	–	–
21	$\eta_{21,10} = 0.4545$ $\eta_{21,13} = 0.5455$	–	–
22	$\eta_{22,15} = 0.3333$ $\eta_{22,17} = 0.6667$	–	–

Table A.4 Solutions in the Real domain for the breakthrough curves at selected nodes. (Streamline routing approach)

$\frac{c_4}{c_0} = 1.0000 \cdot erfc\left[\frac{200}{\sqrt{t-400000}}\right]$	$\frac{c_6}{c_0} = 0.6250 \cdot erfc\left[\frac{100}{\sqrt{t-200000}}\right]$
$\frac{c_7}{c_0} = 0.6250 \cdot erfc\left[\frac{162.5}{\sqrt{t-325000}}\right]$	$\frac{c_9}{c_0} = 0.6250 \cdot erfc\left[\frac{162.5}{\sqrt{t-325000}}\right]$
$\frac{c_{13}}{c_0} = 0.5208 \cdot erfc\left[\frac{312.5}{\sqrt{t-625000}}\right]$	$\frac{c_{19}}{c_0} = 1.0000 \cdot erfc\left[\frac{300}{\sqrt{t-600000}}\right]$
$\frac{c_{10}}{c_0} = 0.4000 \cdot erfc\left[\frac{300}{\sqrt{t-600000}}\right] +$ $0.3750 \cdot erfc\left[\frac{329.2}{\sqrt{t-658333}}\right]$	$\frac{c_{21}}{c_0} = 0.1818 \cdot erfc\left[\frac{450}{\sqrt{t-900000}}\right] +$ $0.1704 \cdot erfc\left[\frac{479.2}{\sqrt{t-958333}}\right] +$ $0.2841 \cdot erfc\left[\frac{395.8}{\sqrt{t-791667}}\right]$

Notes: (1) time in seconds.
(2) all other breakthrough curves are identically null